# SPATIAL VARIABILITY OF THERMAL PROPERTIES IN RECLAMATION COVER SYSTEMS

A Thesis Submitted to the College of

Graduate Studies and Research

In Partial Fulfillment of the Requirements

For the Degree of Doctor of Philosophy

In the School of Environment and Sustainability

University of Saskatchewan

Saskatoon

By

Lindsay Keith Tallon

Permission to Use

In presenting this thesis in partial fulfilment of the requirements for a Postgraduate degree from the University of Saskatchewan, I agree that the Libraries of this University may make it freely available for inspection. I further agree that permission for copying of this thesis in any manner, in whole or in part, for scholarly purposes may be granted by the professor or professors who supervised my thesis work or, in their absence, by the Head of the Department or the Dean of the College in which my thesis work was done. It is understood that any copying or publication or use of this thesis or parts thereof for financial gain shall not be allowed without my written permission. It is also understood that due recognition shall be given to me and to the University of Saskatchewan in any scholarly use which may be made of any material in my thesis.

Requests for permission to copy or to make other use of material in this thesis in whole or part should be addressed to:

Head of the School of Environment and Sustainability

University of Saskatchewan

Saskatoon, Saskatchewan (S7N 5C8)

## ABSTRACT

Soil cover systems are an integral part of a mine reclamation program and are increasing in area. Knowledge of temperatures and thermal properties in the cover system provide important information regarding the energy balance, thermal regime, as well as preliminary insight into soil water content. Cover system temperatures and thermal properties are measured at a small number of vertically intensive profiles. Current methods do not provide any information as to the spatial variation of temperatures and thermal properties at scales other than the point scale. The objective of this study was to investigate the spatial scaling of thermal properties in reclamation cover systems. A distributed temperature sensing (DTS) system was installed in three cover systems of various textures and configurations. Semivariogram analysis demonstrated that on a 40 m slope consisting of mineral soil over sand (Site #1) soil temperatures did not exhibit any spatial structure, due to the presence of vegetation. A 100 m cover system comprised of a structureless sand (Site #2) was confirmed to be spatially uniform through semivariogram analysis. Semivariograms at Site #2 displayed secondary structure that corresponded to the 65 m plateau and 35 m slope. Site #3 consisted of a uniform peat and a 2% slope. Spatial structure was non-existent at Site #3 and was attributed to the unique thermal properties of peat that magnified the effect of microtopography on the surface energy balance. A method to estimate apparent thermal inertia (ATI) using DTS measurements at the soil surface was developed. Apparent thermal inertia was found to be less uncertain than the current standard apparent thermal diffusivity. The ATI method was determined to be the preferred method as it was related to soil water content and not prone to estimation errors due to imprecise depth measurement. The spatial scaling properties of a 236 m cover system (Site #3) were investigated using estimations of ATI. Measurements

were taken every meter along the transect for bulk density, elevation, air-dried thermal conductivity and air-dried volumetric heat capacity. The dominant scale of variation in ATI was not related to physical or thermal properties, which tended towards the 3 m scale (bulk density and thermal conductivity) or the 108 m and field scale trend (elevation and volumetric heat capacity). The dominant scale of variation in ATI shifted between 30 m and the field scale trend and was related to water content as represented by the soil matric potential. A dry cover system tended to homogenize thermal property distribution, leading to a dominance of the 108 m and field scale trend. Wetter days led to a shift to the 30 m scale, with intermediate days showing a mix in scale dominance. Information on thermal property spatial scaling properties of cover systems can be used to optimally design monitoring systems that measure at the same scale as that which the cover is performing. Characterizing the spatial variability of the system will lead to better cover system designs and ultimately a more sustainable system.

## ACKNOWLEDGMENTS

I would like to acknowledge the support and guidance of my supervisors, Drs. Lee Barbour and Bing Si. Dr. Barbour challenged me to be better than I thought I was, for which I am thankful. Dr. Si has advised me throughout my entire academic career, and I am eternally grateful for his mentorship. I hope to show my gratitude by passing on what I've learned. I appreciate the assistance of my advisory committee, Drs. Warren Helgason, Angela Bedard-Haughn, Carey Simonson, and Charles Maule. Your input was of great help, and it is only to my detriment that I didn't take greater advantage of your combined experience.

I am deeply indebted to Mike O'Kane and O'Kane Consultants. This research program would not have been possible without the support and encouragement of Mike, and the help and mentorship of Dave Christensen, Mark Phillip, Sophie Kessler, and Brian Ayres. Financial support for this work was funded through an NSERC Industrial Postgraduate Scholarship collaboration with O'Kane Consultants. Additional funding was provided by the School of Environment and Sustainability, the College of Agriculture and Bioresources, and the department of Soil Science.

Graduate studies wouldn't be the same if it weren't for the shared experiences of fellow students and friends. I'm richer for having friends like the Soil Physics crew, Clare, Henry, Asim, and especially Martin and Melissa. Thank you.

I owe everything to my family. I could not have done this work without the love and support of my wife, Monique. You're everything to me, and you were the only thing keeping me going at times. Finally to Finn. You bring me joy and perspective, and I can't thank you enough. I'm thankful every day that I have you both.

Dedication

This work is dedicated to Finn and the one I haven’t met.

I did this for you. Anything I can do, you can do better.

TABLE OF CONTENTS

page

## LIST OF TABLES

## LIST OF FIGURES

# 1.0 INTRODUCTION

Genuine attempts to move the mining industry toward sustainability require addressing the deleterious effects that mining can have on the landscape (Costa and Scoble, 2006). As interim stewards of the land on which the mine operates, it is incumbent upon a mine to develop a closure plan that seeks to remediate any negative effects the mine may have had on the surrounding environment. Unsaturated soil cover systems are an integral component of mine closure operations. A successful cover system will reintegrate the decommissioned mine into the landscape while serving to reduce contamination of surrounding surface and groundwater sources to the extent possible. Verification of success of the cover system requires extensive monitoring to ensure closure objectives are being achieved.

Reclamation objectives typically center on limiting the interaction of water and oxygen with the mine waste underlying the cover system. Performance of the cover system depends on optimizing the balances of water and energy into, through, and out of the system. The water balance is optimized when evaporation of water at the surface, transpiration from plants, and the amount of water the soil can store is maximized, thereby limiting the amount of water available to drainage into the waste material. The energy balance is optimized when the net balance of incoming and outgoing radiation at the soil surface is partitioned between sensible heat, ground heat, and evaporation, with the goal of maximizing the removal of water through evaporation.

Monitoring of cover systems is carried out with a suite of sensors to monitor certain components of the water and surface energy balances, such as water content, matric potential, soil temperature, and meteorological conditions such as air temperature, wind speed, humidity, and net radiation. It is common practice to establish a small

number of monitoring locations within the cover profile, similar to the configurations reported in O'Kane et al. (1998) and Tallon et al. (2011). Monitoring data are then used as inputs into one-dimensional numerical models to further understand the processes governing performance (Bohnhoff et al., 2009).

While dataloggers allow for collection of temporally intensive datasets, the measurements are confined to a small number of intensively instrumented vertical profiles. However, the distance over which values from the monitoring profiles are correlated to each other cannot be determined using a single point source measurement. Therefore, the true performance of the cover system at the field scale is not known. Assuming all points in a cover system behave in a similar fashion to a central monitoring station may be acceptable for small scale field trials of less than a hectare in area. Current reclamation projects can range from tens to hundreds of hectares in area, and it is only by examining the spatial variability of the cover system at a range of spatial scales that we begin to fully understand the behavior of the system (Grayson et al., 1997). Our understanding of cover system dynamics is incomplete without a rigorous examination of the spatial scaling of the properties and processes at work within the system. The current research program looks to address the paucity of data related to how cover systems perform on scales other than the typically monitored point scale.

Soil physical, hydraulic, and thermal properties vary in both space and time (Si, 2008; Parent et al. 2006). The heterogeneity associated with these properties leads to variability in associated processes such as infiltration, evaporation, transpiration, runoff and percolation. How the physical, hydraulic, and thermal properties are distributed will determine the eventual patterns of soil water across the cover system. These patterns can

persist temporally, and have been found to be related to soil texture and topographical indices (Vachaud et al., 1985; Tallon and Si, 2004, Biswas and Si, 2011a,b,c,d). Spatial patterns of soil water exist because water is distributed in response to certain physical and meteorological controls. Grayson et al. (1997) found that during periods of drying the connection between adjacent locations is lost, and the organization of soil water will be controlled by local factors such as texture and vegetation. During wet periods when water is actively redistributing, patterns will be organized by non-local controls, such as the topography at upslope locations (Grayson et al., 1997). The patterns in soil water that arise in response to climatic forcing will in turn alter the water and energy dynamics across the landscape. Furthermore, differential patterns of water and energy dynamics across the landscape can lead to scaling effects, where processes that are dominant at one scale may not be commensurate at another scale (Vereecken et al, 2007). While studies characterizing the spatial variability of soil properties and processes are numerous in natural systems, similar studies in cover systems are limited (Mapfumo et al., 2006; Kelln et al., 2008; Leatherdale et al., 2012).

Cost and technological constraints have precluded a detailed understanding of the spatial variability of soil water and cover system response to climatic forcing. Measuring water content on the scales necessary to investigate spatial variability is difficult and expensive (Minacapilli et al, 2009). An ideal measurement system for characterizing spatial variability in soil would optimize the scale triplet (Western and Blöschl, 1999). That is, measurements would cover the maximum spatial extent while minimizing the spacing and optimizing the support of the measurement. By optimizing the scale triplet, both large scale trends and small scale variability can be characterized (Si et al., 2008).

Distributed temperature sensing (DTS) is a technology that measures temperatures along a fiber optic cable at very high spatial and temporal frequencies. The technique uses a high powered laser reader to interrogate an optical fiber every meter at distances of up to 10 to 15 km. Backscattered light from the incident laser pulse provides accurate and precise readings of temperature by exploiting the Raman effect (Tyler et al., 2009). Distributed temperature sensing systems have been recently applied to many natural science problems including stream hydrology (Selker et al, 2006a,b; Westhoff et al., 2007; Vogt et al., 2010), aquifers (Henderson et al., 2009), municipal sewers (Schilperoort et al, 2009; Hoes et al., 2010), atmospheric boundary layers (Thomas et al., 2011), soil water content (Sayde et al., 2010) and soil thermal properties (Rutten et al., 2010; Steele-Dunne et al., 2010; Krzeminska et al., 2011). The technique is ideally suited to investigations of spatial variability because of the inherent ability to measure over large extents at high spatial resolutions.

Soil water content or soil water storage has been the primary focus for spatial variability investigations in general, and cover system performance studies in particular. Although not studied to the extent of soil water content, soil temperatures are an important state variable and examining soil temperatures represents a promising means of characterizing the spatial variability of a system (Mohanty et al., 1998; Steele-Dunne et al., 2010). Soil temperatures vary in response to energy inputs and thermal properties, and are related to soil water content through the surface energy balance. Soil temperatures and thermal properties are important variables to characterize as they are indicative of the local energy balance, the distribution of thermal properties, and serve to characterize the soil thermal regime. An additional benefit to investigating soil

temperatures is the relationship between thermal properties, soil temperatures, and soil water content (Arya, 2001). The interaction of soil temperatures and water content has been recognized by others and has recently been applied to studies of the spatial distribution of soil water using DTS systems (Rutten et al., 2010; Steele-Dunne et al., 2010; Krzeminska et al., 2011).

There is a dearth of studies examining the spatial variability of thermal properties in reclamation cover systems. A characterization of the spatial scaling properties of cover systems stands as an important gap in our current understanding of cover system performance. Distributed temperature sensing represents an ideal tool for investigating spatial variability given the large spatial extents and high spatial resolutions of which the system is capable of measuring. Soil temperatures and thermal properties are an important variable in cover system performance. Characterizing the spatial scaling properties of soil temperatures and thermal properties in cover systems will allow for important insights into how the systems perform at a range of spatial scales. Therefore, the overall objective of this research was to investigate the spatial variability of soil thermal properties in reclamation cover systems.

The research program was broken into three individual studies that would cohesively integrate the research program under the primary objective. The objective of the first study was to investigate the utility of a DTS system for use in mining applications and to perform a preliminary analysis of soil temperature spatial variability. Three cover systems representing three different soil textures and cover configurations were instrumented with a DTS system. Preliminary geostatistical analysis provided insights into the spatial scaling of the cover system thermal regime. The objective of the

second study was to develop a simple method to estimate soil thermal properties using soil temperatures for use in spatial variability investigations. Current methods for estimating thermal properties suffer from problems related to non-uniqueness and high uncertainty. A method using apparent thermal inertia was introduced and an uncertainty analysis was performed for a comparison to the more common approach of estimating apparent thermal diffusivity. Finally, the objective of the third study was to characterize the spatial scaling properties of thermal properties in a recently constructed reclamation cover system. Using the lessons from the first two studies, the third study investigated the dominant scales of thermal property variation and how that variability changed with changes in soil water content. In summary, the first study examined the application of distributed temperature sensing to the mining industry; the second study developed an improved method for estimating soil thermal properties using high resolution temperature measurements; and the third study integrated the previous findings to examine the spatial scaling properties of soil thermal properties in cover systems.

# 2.0 LITERATURE REVIEW

## 2.1 Vadose Zone Dynamics

Unsaturated cover systems rely on vadose zone dynamics to achieve reclamation objectives. The vadose zone is most broadly defined as the zone of geologic media between the land surface and the regional water table (Hillel, 1998). This simple definition belies the critical importance the vadose zone has in mediating physical, biological, and chemical processes on a global scale. The vadose zone acts as a repository of water and nutrients for terrestrial plants and as a habitat for myriad living organisms (Brady and Weil, 2007). Although soil water only represents ~0.05% of the global hydrological cycle (Robinson et al., 2008), the vadose zone acts as the principal control on partitioning meteoric water between surface and ground water reservoirs, and consequently, as a pathway for contaminants to drinking water supplies (Brady and Weil, 2007). Finally, the vadose zone serves to mediate global energy cycling through the phase change of water and energy transport processes, (Campbell, 1977). Water is the unifying control that is central to every biological, chemical, and hydrological process occurring in the vadose zone. As such, the dynamics of water in the vadose has been, and will continue to be, an intensively researched subject.

Cover system performance is ultimately controlled by the partitioning of water and energy between soil and the atmosphere. Performance of the system is enhanced when energy and water are partitioned such that drainage, D, is minimized and evaporation, E and plant transpiration, T, are maximized. A growing season water balance can be for a soil cover can be defined as follows:

$$P = E + T + \mathrm{D} + R + I + \Delta S \qquad [2.1]$$

where P is precipitation, R is runoff at the soil surface, I is interflow within or between soil layers in the subsurface, and ΔS is change in water storage (all units in L).

**2.2 Soil Water Movement**

The movement of water in cover systems is governed by the potential energies of the system (Selker, 1999). The primary components of the hydraulic potential gradient in unsaturated soils are gravitational, matric, and osmotic (Hillel, 1998). Given that soil is a three phase system, partially water-filled flow paths can be described by capillary theory, and is given by Poisseuille's Law:

$$Q = \left(\frac{\pi r^4}{8\eta}\right)\left(\frac{\Delta P}{\Delta L}\right) \quad [2.2]$$

where Q is the flow rate through a capillary tube ($cm^3\ s^{-1}$) that has a radius r (cm), η is the viscosity of the fluid, ΔP is the pressure change along the tube and ΔL is the tube length (Hillel, 1998).

Poisseuille's Law quickly becomes inadequate to describe water flow in soils as it does not account for irregularities in the soil system, such as flow path tortuosity and pore size distribution. On a macroscopic level, these irregularities are integrated into the total gradient of the system as captured by Darcy's Law:

$$q = -k\left(\frac{\Delta \mathrm{H}}{\Delta \mathrm{z}}\right) \quad [2.3]$$

where q is the water flux density ($m^3\ m^{-2}\ s^{-1}$), Δz is the change in elevation (m), and ΔH (m) includes the sum of matric, osmotic, gravitational, and hydrostatic pressure heads.

The hydraulic conductivity of an unsaturated soil is a function of the matric potential, or negative pressure, of the system. The matric potential, in turn, will depend on the water content of the soil. The relationship of the two is known as the soil water characteristic curve. It is this

unique phenomenon of decreasing hydraulic conductivity with increasing matric potential that controls vadose zone dynamics and differentiates the field of study from that of saturated systems (Hillel, 1998).

### 2.3 Vadose Zone Energy Interactions

The upper boundary of the cover system responds to climatic forcing, and represents the boundary across which mass and energy will be exchanged between cover system and the atmosphere (Ochsner, et al., 2006). The primary input of energy into the cover system is solar radiation, and temperatures within the cover will vary in response to exchanges in radiant, thermal, and latent energy exchange (Hillel, 1998). Cover system temperatures and thus thermal regimes are established depending on soil thermal properties. Due to the strong relationship between soil water and temperature, the soil thermal regime either governs or strongly influences most physical, biological, and chemical processes taking place in the vadose zone. Soil temperature can have an influence on microbial communities, and thus has implications for nutrient cycling (Paul, 2007). For example, cycling of global soil carbon stocks are influenced by temperature, and if researchers are to predict future carbon dynamics, soil thermal regimes must be understood (Buchan, 2001). Soil water dynamics and temperature are closely linked, and knowledge of soil thermal regimes will aid in the understanding of water movement through soil (Buchan, 2001). It is through determining the variation of soil temperature in time and space that researchers will fully gain a better understanding of soil physical processes of energy and mass exchange with the atmosphere and subsurface (Hillel, 1998).

### 2.4 Energy Interactions in Soil

Radiation input and loss from the surface is governed by the temperature of the sun and the soil, and is described using the Stefan-Boltzman Law (Hillel, 1998). The total energy emitted by a body is proportional to the absolute temperature of the body and is given by:

$$J_t = \varepsilon \sigma T^4 \quad [2.4]$$

where $J_t$ (W $m^{-2}$) is the total energy emitted by the body integrated over all wavelengths, ε is the emissivity coefficient, which equals unity for a perfect emitter, and σ is a constant

The specific wavelength of the radiation being emitted by a body at a certain temperature is given by Wien's Law (Hillel, 1998):

$$I(\lambda) = 2900/T \quad [2.5]$$

where I(λ) (μm) is the wavelength of maximal radiation intensity.

It is clear from equations 2.4 and 2.5 that there will be little overlap between the emission wavelengths of soil, where T ranges from 258 to 300 K, and the sun, where T = 6000 K. Therefore, incoming and outgoing radiation from the soil surface is typically classed as short wave (range in I(λ) of < 0.3 to 0.7 μm) and long wave (range in I(λ) of 3 to 50 μm). The sum of short wave radiation (positive) and long wave radiation (negative) is referred to as net radiation, $R_n$ ($Wm^{-2}$).

The net radiation input at the soil-atmosphere interface is balanced by energy outputs as given by the surface energy balance (Sauer, 2002):

$$R_n - G_0 = LE + H \quad [2.6]$$

where $G_0$ (W $m^{-2}$) is the heat flux density at the soil surface, and LE (W $m^{-2}$) and H (W $m^{-2}$) are latent and sensible heat fluxes, respectively.

Energy that has not been partitioned into LE or H then becomes available for changing the temperature of the soil. The ground heat flux, G (W $m^{-2}$), will determine the soil temperature in response to the thermal properties of the soil and volumetric water content. When examining the flow of heat through soil, the three key thermal properties of soil are (i) thermal conductivity (λ; W $m^{-1}$ $K^{-1}$), which describes the soil's ability to transmit heat; (ii) volumetric heat capacity (J

$m^{-3}$ $K^{-1}$) is the product of specific heat, c (J $kg^{-1}$ $K^{-1}$) and soil bulk density, ρ (kg $m^{-3}$) and describes the soil's ability to store heat; and (iii) thermal diffusivity ($\alpha = \lambda/\rho c$; $m^2$ $s^{-1}$), which describes the rate of transmission of temperature change within the soil (Bristow, 2002). Volumetric heat capacity is defined as:

$$C_v = f_s\rho_s c_s + f_w\rho_w c_w + f_a\rho_a c_a \quad [2.7]$$

where f denotes the volume fraction of the soil (s), water (w), and air (a) components (de Vries, 1975). Note that $f_w$ is equivalent to volumetric water content, $\theta_v$, ($cm^3$ $cm^{-3}$). Typical values for λ and $C_v$ of air, water, and an average of soil minerals at 10 °C are given in Table 2.1 (Hillel, 1998).

Table 2.1 Typical values of λ and $C_v$ of air, water, and soil minerals (average) at 10 °C.

| Component | λ ($Wm^{-1}K^{-1}$) | $C_v$ (J $m^{-3}$ $K^{-1}$) |
|---|---|---|
| Air | 0.025 | $1.25 \times 10^3$ |
| Water (liquid) | 0.57 | $4.2 \times 10^6$ |
| Soil minerals | 2.9 | $2.0 \times 10^6$ |

## 2.5 Measurement of Soil Thermal Properties

Research into the thermal properties of soil has led to important insight into their effect on mass and energy transfers within the vadose zone. Soil hydraulic properties vary with temperature (Hopmans and Dane, 1986b) and soil thermal properties vary as a function of water content, density, and temperature (Hopmans and Dane, 1986a; Campbell et al., 1994). A common techniques for measuring soil thermal properties *in situ* are heat pulse methods, where transient temperature responses to a known input of energy are measured. Heat pulse methods can include single probe heat pulse methods (de Vries, 1963) and dual probe heat pulse (DPHP) methods

(Campbell et al., 1991). The DPHP method has been refined to measure thermal diffusivity, heat capacity, and conductivity (Bristow et al., 2002), heat flux (Ochsner et al., 2007), soil water flux (Hopmans et al., 2002; Mori et al., 2005), soil water content and electrical conductivity (Mori et al., 2003), and snow density (Liu and Si, 2008). The classic equation upon which most heat pulse methods are based was described by Carslaw and Jaeger (1959). Temperature change at a radial distance r from an infinitely long line heat source in a homogeneous, isotropic, isothermal porous medium of infinite extent, resulting from a heat pulse of duration $t_0$ is given as (Kluitenberg et al., 1993):

$$\Delta T_1(r,t) = \frac{-q'}{(4\pi\lambda)} Ei\left(\frac{-r^2}{4\alpha t}\right); \qquad 0 < t \leq t_0 \qquad [2.8]$$

$$\Delta T_2(r,t) = \frac{q'}{(4\pi\lambda)}\left\{Ei\left(\frac{-r^2}{4\alpha(t-t_0)}\right) - Ei\left[\frac{-r^2}{4\alpha t}\right]\right\} \qquad t > t_0$$

where ΔT is the change in temperature (K), t is time (s) , r is distance from the line source (m), q' is the finite quantity of heat liberated by the line source (J $m^{-1}$ $s^{-1}$), and -*Ei*(-x) is the exponential integral.

**2.6 Soil Heat Transfer**

There are generally four modes of energy transfer in the soil: radiation, conduction, convection, and latent transfer. Heat transfer in a soil cover system will occur primarily via conduction. Conduction occurs when energy is transferred in response to temperature gradients between two units of mass in which there is no bulk motion (Incropera and DeWitt, 1996). Heat conduction is given by Fourier's law and is analogous to Darcy's law (Eq. 2.3):

$$q = -\lambda \frac{dT}{dx} \qquad [2.9]$$

where q (W $m^{-2}$) is the heat flux per unit area, λ is the thermal conductivity (W $m^{-1}$ $K^{-1}$), and dT⁄dx is the thermal gradient.

Fourier's law allows us to represent the temperature distribution through time within soil resulting from heat flux at the surface using the heat flux equation (Jury et al., 1991):

$$\frac{\partial T}{\partial t} = \alpha \frac{\partial^2 T}{\partial z^2} \quad [2.10]$$

where, t is time (s), T temperature (K), α apparent thermal diffusivity ($m^2$ $s^{-1}$), and z depth (m). Energy is primarily conducted through soil via water and solids; therefore, the rate at which a given soil can conduct heat will be influenced by water content, bulk density, and mineral properties (de Vries, 1963; Figure 2.1). Diffusion of a temperature wave through the soil profile is controlled by α. The relationship between temperature and soil water content is nonlinear due to an internal maximum in the α vs. $\theta_v$ relationship (Figure 2.2). As such, soil temperature profiles or determination of α do not uniquely define $\theta_v$ owing to the nonlinear relationships, but are still appropriate for inferring relative wetness (Steele-Dunne et al. 2009).

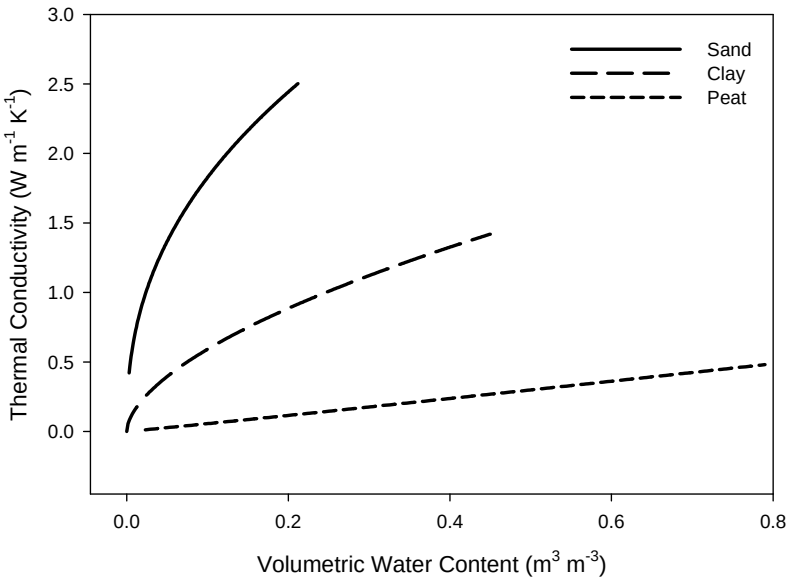


Figure 2.1. Thermal conductivity of three different soil types as a function of volumetric water content. (After de Vries, 1963).

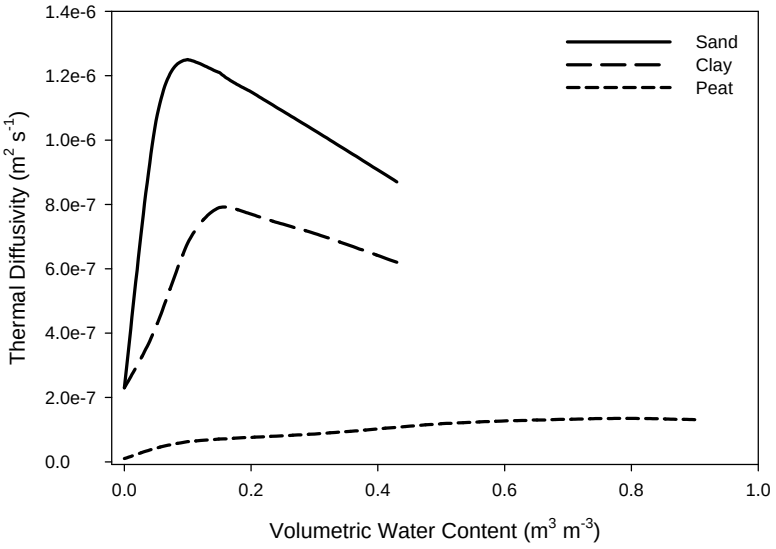


Figure 2.2 Thermal diffusivity of three different soil types as a function of volumetric water content. (After de Vries, 1963).

Temperature distributions within soil resulting from a heat flux at the surface can be represented in a number of ways. Assuming a one-dimensional, homogeneous semi-infinite solid with a constant surface heat flux boundary condition where:

$$T(x, O) = T_i \quad [2.11]$$

$$-\lambda\, \partial T/\partial x|_{x=0} = q_0 \quad [2.12]$$

the temperature distribution within the soil becomes (Incropera and DeWitt, 1996):

$$T(x,t) - T_i = \frac{2q_0(\alpha t/\pi)^{1/2}}{\lambda} \exp\left(\frac{-x^2}{4\alpha t}\right) - \frac{q_0 x}{\lambda} \text{erfc}\left(\frac{x}{2\sqrt{\alpha t}}\right) \quad [2.13]$$

where erfc is the complimentary error function.

Temperature profiles can also be determined as a function of depth and time based on the phase shift and amplitude decay of the surface temperature wave. For a periodic input, the temperature distribution at any depth and time can be described by (Campbell, 1977):

$$T(z,t) = \bar{T} + A_0 e^{-z/D} \sin(\omega t - z/D) \quad [2.14]$$

where $\bar{T}$ is the average surface temperature (K), $A_0$ is the amplitude of the surface temperature fluctuation, z(m) is the depth below the surface, ω is the angular frequency of the oscillation, given by $2\pi/\tau$, where τ is the period of oscillation, and

$D = (2\alpha/\omega)^{\frac{1}{2}}$ is the damping depth (m).

Horton and Wierenga (1983) used temperature observations near the soil surface to determine both α and G by applying a Fourier series, denoted as the Harmonic method. Given the following boundary conditions:

$$T(0,t) = \bar{T} + \sum_{n=1}^{M} A_{on} \sin(n\omega t + \phi_{on}) \quad [2.15]$$

$$T(\infty, t) = \bar{T} \quad [2.16]$$

the thermal diffusivity is solved implicitly from:

$$T(z,t) = \bar{T} + \sum_{n=1}^{M} \left\{ A_{on} \exp\left(-z\sqrt{n\omega/2\alpha}\right) \sin\left(n\omega t + \phi_{on} - z\sqrt{n\omega/2\alpha}\right) \right\} \quad [2.17]$$

and the soil heat flux at all depths and all times is solved using the thermal diffusivity

$$G(z,t) = \sum_{n=1}^{M} \left\{ A_{on} c\sqrt{n\omega\alpha} \exp\left(-z\sqrt{n\omega/2\alpha}\right) \sin\left[n\omega t + \phi_{on} + (\pi/4) - z\sqrt{n\omega/2\alpha}\right] \right\} \quad [2.18]$$

where M is the number of harmonics, c the volumetric heat capacity of the soil (J $m^{-3}$ $K^{-1}$), and $A_{on}$ and $\varphi_{on}$ are the amplitude and phase angles of the nth harmonic for the upper boundary, respectively.

Soil temperatures change in response to thermal properties and the ground heat flux, G. As such, time series of soil temperature changes can be used to estimate thermal properties and the flux of energy through the soil. Diurnal changes in soil temperature can be approximated as a sum of periodic sine waves. Horton and Wierenga (1983) found that analyzing harmonics temperature waves at two depths can provide a more accurate estimate of apparent thermal diffusivity than other methods that did not incorporate a consideration of harmonics. The extension of using the harmonic method to estimate apparent thermal diffusivity is to then estimate the soil heat flux. A harmonic method to estimate G has been found to be successful in measuring soil heat flux in both homogeneous, and nonhomogeneous soils (Horton and Wierenga, 1983, Nassar and Horton, 2002), and in arid desert regions (Heusinkveld et al., 2004). The Force Restore method, first proposed by Bhumralkar (1975) uses temperature measurements in a thin upper layer of soil and the average soil temperature to estimate $G_0$. The Force Restore

method has been reported to accurately reproduce heat flux data (Liebethal and Foken, 2007, Gao et al., 2008) and is best suited to application in numerical modeling (Liebethal and Foken, 2007). Others have used surface temperature measurements as a basis for determining the evaporative state of a soil (Santanello and Friedl, 2003; Oliver et al., 1987; Fuchs and Hadas, 1972), or the thermal inertia. Thermal inertia ($TI = \sqrt{\lambda C_v \omega}$ [J m$^{-2}$ K$^{-1}$ s$^{-1/2}$]) is a measure of the resistance to temperature change (Murray and Verhoef, 2007). An interesting application of thermal inertia was presented by Verhoef (2004) who looked to provide a truly remote estimation of $G_0$ without using *in situ* measurements. Assuming that LE is effectively zero at night, and under no-wind conditions, H should be close to zero as well. In that case, $G_0$ and $R_n$ are the dominant components of the SEB. Under clear-sky conditions, $R_n$ is primarily composed of long-wave emitted radiation and can be estimated with the soil surface temperature. The change in overnight soil surface temperature was first formulated by Brunt (1932) as:

$$T(t,0) = \frac{G[4\alpha(t-t_0)]^{1/2}}{\lambda \pi^{1/2}} \quad [2.19]$$

Verhoef (2004) recognized that under the assumption of low LE and H, measurement of $R_n$ would allow for an estimate of apparent thermal inertia (ATI) as:

$$ATI = \frac{2|R_n| \cdot \sqrt{\Delta t}}{\Delta T_s \cdot \sqrt{\pi}} \quad [2.20]$$

where $R_n$ is the overnight net radiation measured at the soil surface, $\Delta t$ (s) is the time between sunset and sunrise taken from the point at which solar radiation readings pass through zero, and $\Delta T_s$ is the change in surface temperature between sunset and sunrise.

**2.7 Cover Systems**

Engineered soil covers have become the accepted method of controlling drainage into underlying wastes for mine sites and landfills (Albright et al., 2006). Although the particular

mode of action may differ, cover systems are generally designed to limit the ingress of uncontaminated water or oxygen into the underlying material. In this way, cover systems have traditionally been designed as a means of isolating the waste material with the surrounding environment.

The goal of conventional engineered cover systems is to limit water or oxygen ingress into the underlying waste by employing a barrier system. Barrier systems usually consist of a resistive layer of lower hydraulic conductivity (Albright et al., 2006a; Albright et al., 2006b; Albright et al., 2004), or employ materials that act as a barrier to oxygen ingress, thus limiting the production of acidic oxidation products (Weeks and Wilson, 2005). A major drawback of conventional barrier systems is the tendency for the performance of the barrier materials to decrease over time, relative to what was designed. Decreased performance usually occurs through increasing hydraulic conductivity of the barrier material (Albrecht and Benson, 2001; and Albright et al., 2003). In some cases, hydraulic conductivity has been reported to increase by 750 (Albright et al., 2006) to 1000 times (Albright et al., 2006). In the case of Albright et al. (2006) the decrease in performance occurred within two to four years; much less than the design life of 30 years specified for waste containment facilities.

An alternative to using barrier layers to prevent meteoric water from percolating below cover systems is to exploit vadose zone processes. By relying on a combination of plant transpiration and evaporation from the soil surface, water can be removed from the soil before it becomes available for percolation. Evapotranspirative (ET) covers have recently been used in the mining and waste storage industry (McGuire, et al., 2009; Blight and Fourie, 2005; Albright, et al., 2004; Hauser, et al., 2001; Khire, et al., 1997). However, due to their relatively recent acceptance by regulators and stakeholders, unsaturated cover systems have not been monitored

long enough to make conclusive statements on their performance. Scanlon et al. (2005) asserted that ET covers would be an effective tool in the waste containment industry for semi-arid and arid locations, although that assertion has been challenged by Gee et al. (2006) who noted that in some semiarid sites, ET covers did not perform as well as capillary barrier systems or resistive barriers. However, for areas where the bulk of precipitation arrives during summer when plants are active, ET covers should be effective in achieving reclamation objectives (Scanlon et al., 2006).

Monitoring to verify whether the cover system is performing as designed is important, irrespective of the type of cover system used. McGuire et al. (2009) monitored the performance of a full scale, 6.1 ha cover system, based on the amount of drainage that was collected in a large scale (0.9 m × 1.57 m dia.) lysimeter. Drainage through the ET cover system was negligible throughout the five years that comprised the study. It should be noted that validity of the results of the McGuire et al. (2009) study may not be entirely representative of actual field performance. Generalizations of performance were based entirely on drainage as the single performance parameter. Scanlon et al. (2005) cautioned against this approach as opposed to monitoring vadose zone processes comprehensively. In addition, the design of the lysimeter system could have led to an underestimation of drainage due to its configuration and location within the cover (O'Kane and Barbour, 2003). As well, although numerical model simulations predicted negligible drainage over the course of the study period, Bohnhoff et al. (2009) found that four popular modeling codes often could not predict percolation accurately. The study by Bohnhoff et al. (2009) found that all four codes under-predicted percolation, most likely due to difficulties in accounting for runoff and preferential flow. They concluded that cover modelers should closely scrutinize results to ensure predictions are reasonable.

### 2.7.1 Cover System Energy Interactions

Energy balances at the soil-atmosphere interface are of keen interest to the reclamation scientist. Evaporation of water stored in the cover system is the principle upon which unsaturated soil covers are based, as water that is evaporated is no longer available to interact with waste material. Long-term monitoring of cover system evaporation will be critical in understanding the performance of the system (Carey, 2008). Determination of energy balances, of which evaporation is the central component, is as important to assessing long term cover system performance as a water balance (Saito and Simunek, 2009), yet due to measurement difficulty, is often estimated as the water balance residual (Blight et al., 2002).

Evaporation is a particularly difficult component of the water and energy balance to quantify, and is most accurately measured using micrometeorological techniques. Eddy covariance methods were used to determine the components of an energy balance and measure actual evapotranspiration (AET) on a fine textured cover system by Carey et al. (2005). They found that energy available for evaporation was consistently reduced over the measurement time frame, as the homogeneous nature of the surface material and high surface albedo reduced absorption of incoming radiation. The evolution of an energy balance for a developing cover system was studied by Carey (2008). It was found that for wet years, latent heat was the dominant flux, but was replaced by sensible heat as the dominant flux during dry years. For researchers to begin to explain the water and energy dynamics within cover systems, the spatial variation of evaporation must be determined. Researchers have a general understanding of the factors influencing evaporation, including soil water content, vegetation species and density, radiation, relative humidity, and wind speed among others, although how these factors interact to produce patterns of evaporation is less well understood (Hipps and Kustas, 2001).

Soil temperature profiles develop in response to the ground heat flux ($G_0$) component of the SEB, which in turn is a function of the partitioning of energy in the SEB. Soil heat flux is recognized as being an important component of the SEB, yet is one that is typically ignored or estimated (Heusinkveld et al., 2004). Over the course of a day, G is neither constant, nor negligible and can exhibit high variability in response to soil properties and vegetation (Kustas et al., 2000; Santanello and Friedl, 2003). When wet conditions are prevalent, the SEB will be dominated by the latent flux (Carey, 2008). High rates of atmospherically controlled (Stage 1) evaporation lead to a decrease in the ratio of $G_0$ to $R_n$ after a midmorning maximum, resulting in a lower amplitude temperature change, irrespective of soil type (Santanello and Friedl, 2003). During dry conditions, the SEB is soil controlled (Stage 2), and sensible flux is the dominant component of the SEB (Carey, 2008). When the soil is desiccated (Stage 3), the SEB is no longer soil controlled, and heat flux is essentially taking place in a two-phase system consisting of air and minerals. During the transition from Stage 1 to Stage 2 evaporation, $G_0$:$R_n$ is expected to increase, with G remaining positive later in the day relative to soils undergoing Stage 1 evaporation (Santanello and Friedl, 2003). Soils undergoing different stages of evaporation will exhibit characteristic temperature profiles, heat flux rates, and patterns of $G_0$:$R_n$. Differences in temperature profiles will be attributable to the differences in evaporation rates (Fuchs and Hadas, 1972). Thermal regimes can thus form the basis for examining patterns of water distribution within soil cover systems.

### 2.8 Spatial Variability

Water is distributed throughout a soil both spatially and temporally in response to properties and processes such as soil texture and density, vegetation, and topography, among others (Western and Blöschl, 1999; Gómez-Plaza et al., 2001). Temporal patterns exist within a field, and can be related to soil texture or topographical indices (Vachaud et al., 1985; Tallon and

Si, 2004). Spatial patterns of soil water exist because water will distribute in response to local and nonlocal controls (Grayson et al., 1997). Depending on what Grayson et al. (1997) referred to as the preferred state of the soil, the organization of soil water can be random, and controlled by local factors such as texture and vegetation, or patterns will be organized by non-local controls, such as the topography at upslope locations (Grayson et al., 1997). Our ability to characterize the spatial variation of soil water will be essential for efficient monitoring and modeling of the landscape, thereby leading to more sustainable cover system designs.

Describing the spatial variability of a landscape can provide powerful information as to the underlying processes that control patterns of soil water distribution. At its simplest, variability within the landscape can be described using basic statistical properties, such as the mean and variance, as well as higher moments, such as skewness and kurtosis. The distribution of the data can be described using the probability density function, to provide clues as to the underlying nature of the data.

However, if we are to understand how processes and properties vary in time and space, then we turn to geostatistics to understand the spatial or temporal continuity of natural phenomena (Isaaks and Srivastava, 1989). Soil properties often display patterns within the landscape, and these patterns can be a combination of variation at different scales (Si, 2008). Geostatistics examines the autocorrelation of the data to determine the spatial similarity of the underlying patterns. Having an understanding of the structure of spatial or temporal variability in a soil allows for better design of monitoring networks, proper data interpretation, and better assessments of simulation and uncertainty analyses (Si, et al., 2008). Semivariogram analysis is a widely used technique that exploits the phenomenon that two points that are close in space (or time) tend to be more similar than two distant points (Si et al., 2008). Semivariogram analysis

simply applies the concept of autocorrelation along with the mean and variance to examine at what separation distance a given measurement no longer carries any similarity to a neighboring measurement.

Semivariogram analysis was applied by Anctil et al. (2002) to examine near-surface water dynamics in an organic soil. It was found that water contents were not controlled by organic matter content; a finding that would not have been determined with traditional statistics. Petrone et al. (2004) examined semivariograms to find that wetting and drying of a cutover peatland was scale dependent, with different patterns forming depending on the wetness state of the study area. Semivariograms were also employed by Western et al. (2004) to examine the controls of soil water in four different catchments. In general, water content was controlled by soil processes operating at scales smaller than the topography, and was not related to vegetation. From the previous examples, it is seen that incorrect assumptions on the controlling processes of soil water can be made if the variability of those underlying processes is not properly examined.

Semivariogram analysis is limited in its ability to distinguish concurrent scales of variability. Spectral methods, including wavelet analysis, assist in identifying each dominant scale of variation by separating the total measurement variance into scale frequency components (Si, 2008). By transforming a dataset from the temporal or spatial domain to the frequency domain, identifying the dominant scales of variation becomes a simple matter of identifying frequency peaks (Si, 2008). Kachanoski and de Jong (1988) used spectral analysis to demonstrate that patterns in soil water content are a product of hydrological processes that operate at different spatial scales. Perfect and Carron (2002) applied spectral methods to reveal large scale variability driven by randomized fertilizer applications and antecedent tillage treatment. By using spectral analysis, not only can spatial structure be elucidated, but the method

provides straightforward means of assigning statistical significance and as a characterization tool for determining appropriate tools for further analysis (Si, 2008).

Although spectral analysis is useful in determining the dominant spatial scales of variability, the method does not provide any information as to where in space the processes are active. This is due to the fundamental assumption of stationarity; that the data do not contain a trend and that mean and variance are equal at all locations. Wavelet analysis deals with non-stationary data by decomposing the overall variations into different scales at each location. Thus, information on the spatial scale of processes operating at each location is determined. Wavelets were used by Wu et al. (2002) to determine both the dominant modes of spatial variation, and how they varied with respect to time. Wu et al. (2002) were able to demonstrate that the soil profile acts as a low pass filter for precipitation, where spectral peaks are dominated by low frequencies of greater than one year. It was found that drought signals will exhibit different temporal patterns than average climate years, and can propagate to 2 m below the surface. Lauzon et al. (2004) were also able to distinguish how watershed outflows are controlled by different depths within the soil profile. In their study of a French watershed, Lauzon et al. (2004) determined that surface soil layers contributed to high flows during precipitation events, subsurface soil depths close to 35 cm were responsible for production of outflow in the short term of 1 to 16 days, and depths of up to 115 cm were responsible for generating long term outflows. Without a demonstration of the coherency of variations in time and space, depth controls of outflow generation could not have been demonstrated by Lauzon et al. (2004). An excellent demonstration of the power of wavelet analysis in hydrological studies was provided by Parent et al. (2006). In their study, Parent et al. (2006) were able to partition spatial and temporal variability in soil water content into preferential bands, and describe how water content

depends on the duration and periodicity of precipitation events. Perhaps counter intuitively, Parent et al. (2006) showed that while 93% of the variation in rainfall occurred within 1 to 48 hours, only 15% of the variation in soil water content occurred in this same time frame. It was shown that water content only varies with the most important rainfall events, and that other climatic and soil controls were more determinant in controlling water content variations at that time scale. For time scales of 48 hours to 1 week, variations were mostly attributable to meteoric systems, while at scales of 1 to 2 weeks, variation in water content was soil controlled.

Wavelet analysis has proven to be effective at describing location specific scale effects (Si and Farrell, 2004; Yates et al., 2006; Biswas and Si, 2011a,b). Although wavelet analysis is useful for investigating non-stationary processes, the method depends on a mathematical function in the form of the mother wavelet. Thus, wavelets are necessarily subject compromises when selecting the appropriate mother wavelet for the analysis (Si, 2008). Empirical mode decomposition (EMD) is a promising technique that reveals detailed scale information that would otherwise remain obscured, doing so directly from the data (Huang et al., 1998). The EMD technique decomposes a spatial or temporal dataset into a finite and small number of intrinsic mode functions (IMF) in an iterative sifting process (Biswas and Si, 2011c). Biswas and Si (2011c) used EMD as the first step in applying Hilbert Spectral Analysis to examine scale specific controls on soil water storage in a non-level landscape. Elevation and organic carbon combined at the 80 to 100 m scale to account for over half of the total variance in soil water storage across a 576 m transect. Usowicz and Usowicz (2004) used EMD to examine the heat transfer regime at the soil-atmosphere interface. Net radiation and transient weather conditions were found to be the two main contributors to near surface soil temperature, and that high frequency changes in air

temperature were not transferred to the soil below due to higher thermal inertia in the soil (Usowicz and Usowicz, 2004).

### 2.8.1 Soil Temperature Variability

Soil temperatures vary in response to energy inputs and soil thermal properties. Thus, the distributions of temperatures across the landscape are reflective of the distribution of thermal properties and available energy. Soil temperature variability will decrease with depth as high frequency variations in radiation are effectively filtered by the overlying soil (Scharringa, 1976). The effect of decreasing variability with depth was shown by Anctil et al. (2008) who used wavelet analysis to demonstrate decreasing coherency between air temperatures and soil temperatures as depth increased. Amplitude damping and phase attenuation of the diurnal temperature wave increased with increasing depth for the entire year, except for winter when latent heat release caused a total divergence in coherency between air and soil temperatures. Temporal variability of soil temperatures will decrease at night during periods of cooling, and increase during daytime periods of radiation input (Mohanty et al., 1995; Mohanty et al., 1998). Temperature variability hysteresis can be attributed to the complex and non-linear interactions of of net radiation, air temperature, and surface wind (Mohanty et al., 1995; Mohanty et al., 1998).

Soil temperatures also vary laterally between points in the landscape. The spatial structure of soil temperatures has been found to be anisotropic depending on factors such as transect orientation and tillage operation (Vauclin et al., 1982; Mohanty et al., 1995). In agricultural systems, spatial autocorrelations of soil temperature have been reported to be up 7 m by Vauclin et al. (1982), and between 1.5 to 9 m depending on transect orientation (Mohanty et al., 1995). In forested systems, Bond-Lamberty et al. (2006) reported correlation lengths in soil temperature that ranged from 0 to 150 m. Increasing spatial structure was attributed to canopy closure and thick ground cover, which served to homogenize spatial variations in the incoming

solar radiation. Soil temperature variability is also subject to scale effects. Significant differences in spatial variability of soil surface temperature and the temperature measured at 5 cm were found to exist when comparing transects of 200m and 10 km in length (Xu et al., 2002). Spatial variations were explained by topography effects, vegetation patch type, and canopy structure.

Variability of soil temperatures will generally decrease with an increase in water content due to a homogenizing effect of water (Mohanty et al., 1998; Ashcroft and Gollan, 2013). However, the relationship between soil temperature and soil water content is not a direct correlation. A greenhouse study conducted showed soil temperature autocorrelations up to 15 m over a 55 m transect (Al-Kayssi, 2002). Although the greenhouse transect was homogenous in texture and was not subject to variability in surface boundary conditions, the distribution of temperatures was not homogenous. In fact, soil temperatures and water content were only cross correlated at distances up to 5 m. It was found that small scale variations in water content were sufficient to produce larger scale changes in temperature (Al-Kayssi, 2002). Although soil temperatures can be generally indicative of the variability of soil water, the correlation is not perfect and a consideration of the complex interactions leading to a given soil temperature are required (Bond-Lamberty et al., 2006).

### 2.8.2 Cover System Variability

Cover systems are typically designed as a one dimensional system. Design approaches are typically similar to that of Bohnhoff et al. (2009) and McGuire et al. (2009) where numerical simulations of a single model column are conducted to represent the entire system. As cover systems increase in size to hundreds of hectares in area, it may not be sufficient to assume that the performance of the entire cover behaves identically to that of a centrally located monitoring system. Homogeneous systems may in some cases contribute to low levels of spatial variability, as Kabwe et al. (2005) found with $CO_2$ flux on a uniform waste rock pile. However, the

uniformity may be the exception to the rule. Spatial heterogeneity in what has ostensibly been designed as a homogeneous system has been reported in the literature. Redistribution of water in sloping capillary break covers was investigated using numerical models by Aubertin et al. (2009). In their study it was found that increasing cover thickness would increase diversion length downslope. Conversely, Kelln et al. (2008) reported that spatial patterns of soil water during spring melt were not strongly related to topographic position. Instead, redistribution within the cover was attributed to textural heterogeneity; a finding that suggests that even during wet periods, it cannot be assumed that water will move in response to topography alone. At the same study areas, Leatherdale et al. (2012) reported that variability in moisture regimes were most likely due to heterogeneity imparted by local vegetation. Recently, Lu et al. (2011) demonstrated that flow regimes in unsaturated hillslopes depend on the wetting or drying state of a particular location to control the direction of water flow. Variably saturated conditions will therefore lead to complex flow patterns. As an indication of complex flow patterns in soil covers, Mapfumo et al. (2006) reported very high spatial dependencies of soil water, indicating high spatial heterogeneity. The spatial heterogeneity of soil water content was also attributed to small-scale heterogeneity in soil texture (Mapfumo et al., 2006).

### 2.9 Distributed temperature sensing

As cover systems increase in size, one of the main impediments to characterizing spatial variability is the large number of measurements needed, and the resultant labour requirements. The technique has been adapted from use in the oil and gas industry by users in the natural sciences to study streams (Selker et al, 2006; Westhoff et al., 2007; Vogt et al., 2010), aquifers (Henderson et al., 2009), municipal sewers (Schilperoort et al, 2009; Hoes et al., 2010), and atmospheric boundary layers (Thomas et al., 2011) among others. A DTS system measures temperature at many points in an optical fiber by measuring the backscatter and return time of an

incident laser pulse. The measurement is based on the Stokes and Anti-Stokes backscatter of the incident light in what is known as the Raman effect (Selker et al., 2006a; Tyler et al. 2009). The incident laser light will interact with the glass fiber molecules, which will emit light at both the Stokes and Anti-Stokes frequency. In the Stokes frequency, the backscattered light returns at a lower frequency and at the Anti-Stokes frequency, the backscattered light returns at a higher frequency than the incident laser pulse. As temperature increases over a given location in the fiber, the fraction of Anti-Stokes signal will increase relative to that of the Stokes signal. Therefore, the ratio of the Anti-Stokes to Stokes signals is temperature sensitive. The travel time of the incident laser pulse determines the spatial discrimination. Most commercial fibers have a two-way travel time of 10 ns $m^{-1}$ with the signal from any particular meter arriving over a 5 ns period (Tyler et al., 2009). The first and last 1 or 2 ns of the signal are trimmed in order to limit temperature distortions due to dispersion of light in the fiber (Tyler et al., 2009). Because of the trimming and very fast two-way travel time, the signal is inherently weak. Signals are integrated over a length of time in order to increase the signal strength. The temporal integration of the signal represents the major compromise with a DTS system; temperature precision is increased with longer integration times, while longer integration times necessarily result in a decrease in the sensitivity to short term temporal variations (Tyler et al., 2009).

Distributed temperature sensing systems have been applied to problems in soil science related to determination of thermal properties and the subsequent inference of water content from those properties. Early applications of using fibre optic technology for measurement of water content focused on internal angles of refraction and were limited to either micro-scale situations (Garrido et al., 1999; Fields et al., 2000) or situations where the probe was not directly in contact with soil (Alessi and Prunty, 1986). More recent uses of DTS systems for measuring soil water

content have utilized two main strategies: active heating and passive heating. Active heating methods involve generation of a heat pulse using the theory described by Campbell et al. (1991) and summarized in Eq. 2.8. In active heating, a stainless steel strength member is electrified to generate a heat pulse, making the cable itself the line heat source. Soil thermal properties are estimated based on the time required to dissipate the temperature rise resulting from a known input of energy. Passive methods rely on inversions of Fourier's law (Eq. 2.9) to infer water content from thermal diffusivity estimates. Thermal diffusivity is estimated based on the temperature responses in two sub-surface cables to diurnal radiative forcing.

Active heating methods were used by Weiss (2003) to discern changes in water content in a homogenous landfill cover soil. While the active heating method showed initial promise, it was unable to resolve 2% changes in water content below 0.06 $m^3$ $m^{-3}$, due to issues with the signal to noise ratio (Weiss, 2003). Using a similar heat pulse technique, Sayde et al. (2010) was able to accurately resolve water contents between 0.05 and 0.41 $m^3$ $m^{-3}$ in a laboratory column. Measurement uncertainty increased with increasing water content up to 0.046 $m^3$ $m^{-3}$ at the highest water contents (Sayde et al., 2010). The opposite relationship was reported by Ciocca et al. (2012) who found that water content was consistently underestimated at the drier end of the measurement range. Discrepancies between the DTS method and capacitance probes were less than 0.04 $m^3$ $m^{-3}$ at high water contents. Measurement discrepancies increased to 0.1 $m^3$ $m^{-3}$ at the dry end. The increased discrepancies were attributed to the time required for the temperature reading to become asymptotic in the less conductive dry soil (Ciocca et al., 2012).

Passive heating methods have also been investigated to determine the feasibility of inferring water content from estimates of apparent thermal diffusivity. Steele-Dunne et al. (2010) used temperatures from two cables at different depths to estimate thermal diffusivity. The estimated

value was then used to infer water content from an inversion of Fourier's law. The passive method was found to be insufficient in determining relative saturation due to the non-unique relationship between thermal diffusivity and soil water content. On cloudy days with low surface radiation inputs it was not possible to infer a single value of relative saturation from a diffusivity value for at least half of the dynamic range (Steele-Dunne et al., 2010). Uncertainty estimates covered the entire dynamic range (Steele-Dunne et al., 2010). Rutten et al. (2010) had a similar finding when trying to develop a numerical inversion technique for using DTS to quantify spatial variations in soil water content. The technique was not able to optimize the relationship between soil water content and soil temperature using thermal diffusivity (Rutten et al., 2010). A similar approach was used by Krzeminska et al. (2011) to examine the spatial distribution of water content in a landslide using passive techniques. Precise measurements of soil water content were not possible using an inversion of thermal diffusivity. However, Krzeminska et al. (2011) did suggest that the technique did show promise for qualitatively determining areas of varying soil wetness.

**2.10 Synopsis**

Soil cover systems are one of the most important components of a mine reclamation program. Not only do cover systems control the fate of the underlying contaminants, they also represent the surface expression of the project and will be the basis upon which the public forms an opinion of the reclamation program. Given the importance of cover systems to the overall success of a reclamation program, it is critical that the performance of the system is properly understood. Present methods of cover system performance monitoring involve intensively monitoring a soil profile in a limited number of locations for components of the water and energy balance. While current methods have their place, our understanding of how cover systems behave at a range of spatial scales remains deficient. The purpose of this research program is to

address the data gap associated with the spatial variability of cover system properties and processes.

Cover system performance is governed by climate, near surface meteorological conditions, and the physical properties of the cover material. The total performance of the system can be expressed through a water balance and the surface energy balance. While previous studies on cover system performance have focused on the mass balance of water in the soil, there is an opportunity to use high resolution temperature measurements to examine the spatial variability of soil temperature and thermal properties. Examining the spatial variability of temperatures and thermal properties of a cover system can provide insight into the distribution of physical properties and energy within the system. Examining soil thermal properties has the added benefit of being related to soil water content through the surface energy balance.

An emerging technology known as distributed temperature sensing allows for accurate and precise measurements of temperature at high spatial and temporal resolutions. The technology has previously been used in earth science applications, but has yet to be used to examine spatial variability of thermal properties in cover systems. The data gathered by a DTS system is ideally suited to studies of spatial variability. The data are collected over large spatial extents at small spatial spacing, thus allowing for an examination of both large scale trends and small scale variability. Many methods are available for investigating the spatial variability of temperature and thermal properties in reclamation cover systems. The simplest methods involve classical statistics using mean, variance, and the probability density function of the data. Semivariogram analysis applies these methods to determine the autocorrelation length of adjacent measurements. Spectral methods and wavelet analysis use the frequency domain to uncover the dominant spatial scales of variation. More sophisticated techniques such as Hilbert

spectral analysis and empirical mode decomposition can be used to reveal the hidden scales of spatial variability for both non-stationary and non-linear datasets.

Public acceptance of current and future mine reclamation programs will depend on how well the systems function and whether their design objectives are being achieved. Therefore, it is critical to understand the behavior of cover systems at all spatial scales. Examining the spatial scales of variability of thermal properties in cover systems will allow for a better understanding of the system as a whole through improved model inputs, better experimental designs, and proper data interpretation. The sustainability of the mining industry will depend on the efficacy of cover systems, which in turn will depend on a greater understanding of how the systems behave at all spatial scales.

# 3.0 HIGH RESOLUTION TEMPERATURE OBSERVATIONS TO DETECT SPATIAL STRUCTURE IN RECLAMATION SOIL COVER SYSTEMS

## 3.1 Preface

Rigorous investigations of the spatial variability of temperature in reclamation cover systems do not exist. A novel technology known as distributed temperature sensing (DTS) provides precise temperature measurements at high spatial resolutions and represents the ideal analytical tool for investigating spatial variability. A DTS system has not previously been installed into the unique field context of a mine reclamation cover system. What are the challenges associated with DTS installation? What is the nature of the dataset that a DTS system can provide, and can we describe spatial variability of cover system temperature at a basic level? Three cover systems were instrumented and analyzed as the first step in deploying DTS systems in the mining industry.

## 3.2 Introduction

Soil temperature is a key state variable in the soil energy balance. Temperature will determine the rates and directions of mass and energy fluxes to the atmosphere and govern evaporation and aeration of the soil (Hillel, 1998; Novak, 2005). Soil temperature has important implications for near surface hydrology and thermodynamics, chemical reactions, and rates of biological productivity. Characterizing the temporal and spatial variability of soil temperature can reveal important information on the distribution of underlying processes and properties present in soil.

Variations in soil temperature are reflective of both the thermal properties of the soil components as well as the partitioning of energy at the soil surface (Hillel, 1998). Energy at the soil surface is partitioned based on the radiation balance, atmospheric exchange processes near

the surface, and the presence of vegetation and microtopography (Arya, 2001). Latent heat is the primary consumer of energy in the surface energy balance, and as such, will strongly affect soil temperature (Shahraeeni and Or, 2011). Propagation of energy through the subsurface is the outcome of complex energy transfer processes and soil thermal and physical properties. The primary thermal properties of interest are the volumetric heat capacity and thermal conductivity; both of which are dominated by the volume of water present in the soil (Hillel, 1998).

The spatial distribution of temperature and how it changes with time can provide indications as to the variations in the surface energy balance and consequently the soil thermal properties at a specific location. Scharringa (1976) reported decreasing standard deviations of mean soil temperature with depth, while cautioning that temperature measured at one location is generally not sufficient for estimation of temperatures at other depths or locations. The implication of this finding is that soil temperature will vary from point to point, and that it is important to characterize the spatial structure of temperature within a field. Using semivariogram analysis Vauclin et al. (1982) examined the spatial structure of soil temperature within an agricultural field. Soil temperature measurements were found to be anisotropic depending on transect orientation, but were autocorrelated at distances up to 7 m and agreed well with the spatial structure of soil water content. Anisotropy in the spatial structure of soil temperature was also found by Mohanty et al. (1995) who demonstrated that spatial correlations could vary between 1.5 to 9 m, depending on transect orientation and tillage operation. A key finding of both Mohanty et al. (1995) and Mohanty et al. (1998) was the existence of hysteretic loops in the relationship between soil temperature variance and mean soil temperature. Lower loops of the hysteretic relationship were associated with nighttime and early morning cooling, while the upper loop corresponded to heating during the day. The cause of the hysteresis was attributed to

complex interactions of the spatio-temporal distribution of net radiation, air temperature, and near surface winds. Hysteretic relationships were found to be a universal feature of soil temperature variations, regardless of soil type, tillage, or microtopography and would decrease with an increase in field average water content, likely due to a homogenizing effect of water content (Mohanty et al., 1998). In forested systems, Bond-Lamberty et al. (2006) found that correlation lengths in soil temperature could range from non-existent to 150 m. Increased spatial structure in soil temperature was attributed to canopy closure and thick ground cover, which served to dampen spatial variations in incoming radiation. While not a perfect correlation, the above research demonstrates that soil temperature variations are indicative of local variations in soil water content and the surface energy balance and warrants further investigation.

Spatial and temporal variations in soil temperature are best measured over the largest extent possible with the smallest spacing to adequately capture variability at all scales (Blöschl and Grayson, 2000). Distributed temperature sensing (DTS) is an emerging technology that has recently been employed to measure soil temperature over large spatial extents with high spatial and temporal resolution (Tyler, 2009). A DTS system consists of a high intensity laser source that also acts as a detector, and a distributed sensor. In the case of a DTS system the distributed sensor is the fiber optic cable. A high intensity laser pulse is propagated along the fiber, most of which travels through the glass unimpeded. The backscattering that returns to the detector is comprised of three wavelength components: the wavelength of the incident light, a wavelength slightly above the incident light, and a wavelength slightly below the incident light. The latter two are the Stokes and Anti-Stokes wavelength bands, respectively. The ratio of the Stokes and Anti-Stokes bands is temperature sensitive and consequently can be used to measure the temperature of the cable at any particular location. Given that the velocity of light is constant, the

return time of the backscattered light allows for the determination of the location of the recorded temperature within the fiber. Therefore, for any given time, the temperature can be determined at discrete locations along the fiber. The fiber, which can extend to lengths of thousands of meters, can be interrogated at any time to obtain temperature measurements at spatial resolutions on the order of 1 m or better and measurement resolutions as high as 0.01 °C. The reader is directed to Selker et al. (2006a,b) and Tyler et al. (2009) for further descriptions of the technique and its applications.

Distributed temperature sensing has recently been employed in the earth sciences, primarily in the area of stream hydrology (Selker et al., 2006a,b). A developing area of application is in soil science, where DTS has been investigated for use in monitoring soil water content (Weiss, 2003; Steele-Dunne et al., 2010; Sayde et al., 2010), thermal properties in a clay-shale landslide (Krzeminska et al., 2011), and observing the spatio-temporal variability of surface energy exchanges (Rutten et al., 2010). The spatial distribution of soil temperatures were found to yield quantitative information on the local energy balance and heat partitioning (Krzeminska et al., 2011). Steele-Dunne et al. (2010) also found that variations in soil temperature are largely controlled by local soil water content, although the relationship between the two is insufficiently unique to yield precise estimates of water content from soil thermal properties.

A link exists between soil temperature and subsurface soil water content and surface evaporation. The relationship between temperature and water makes temperature an appealing subject of investigation, given the ease with which temperature can be measured relative to soil water content. Indeed, soil surface temperature has long been used as an indicator of soil water content or evaporation by the remote sensing field (Pratt and Ellyett, 1979; Price, 1980;

Cracknell and Xue, 1996; Scheidt et al., 2010) and in numerical modeling studies (Shahraeeni and Or, 2010; 2011). An area where the spatial distribution of evaporation and soil water content has not been explored yet is of particular relevance is in the mine reclamation industry. An entire subset of soil cover systems used in mine waste reclamation rely almost entirely on storing water in the soil matrix and releasing that water as evaporative demands permit (McGuire, et al., 2009; Blight and Fourie, 2005; Albright, et al., 2004; Hauser, et al., 2001; Khire, et al., 1997). Performance of the systems is based on the volume of water stored in the cover and the evaporation from the surface (Scanlon, 2005). Reclamation cover systems can cover areas from hundreds to thousands of square meters, yet performance is typically based on point source monitoring at a limited number of stations. Characterizing the structure of the temporal and spatial variability of soil temperature represents an appealing first step in examining the distribution of soil water content or zones of differing evaporation in reclamation cover systems.

The motivation for this study was to find a user friendly method of characterizing spatial variability of temperature in reclamation soil cover systems. Soil temperature is a variable that is easily and intensively measured in both time and space with a DTS system. The objectives of this study were to document the implementation of a DTS system in a range of cover system configurations, present the novel temperature datasets obtained for this application, and provide a preliminary characterization of the spatial structure of soil cover system temperature with respect to depth and time based on these observations.

## 3.3 Materials and Methods

### 3.3.1 Site Description

Three recently constructed reclamation soil covers over mine waste were instrumented with fiber optic cable as part of a field monitoring campaign. All three sites were located in the northern region of western Canada (Figure 3.1).

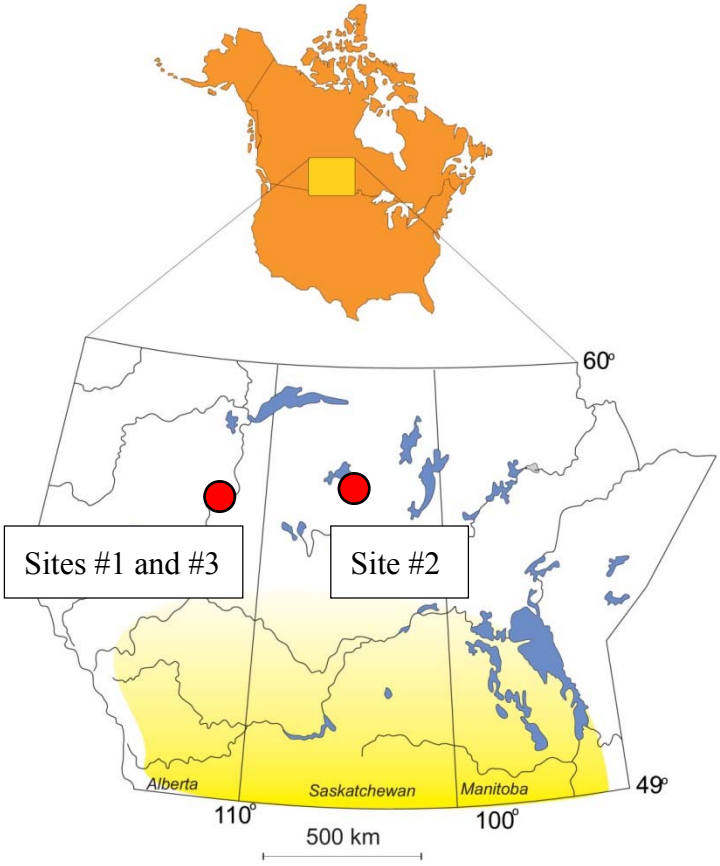


Figure 3.1. Map of western Canada with field site locations indicated.

Site #1 was located in the oil sands region of northern Alberta, Canada. The instrumented cover was part of the reclamation of a 240 ha tailings pond. The instrumented test cover was situated on a 40 m long, south facing 8% slope. The landform topography was created using waste tailings sand and was overlain by 1.2 m of clean densified tailings sand. The densified tailings sand was a byproduct of an industrial cyclone separation of tailings sand where the coarse material was used for the cover system. The surface layer of the cover system was 0.6 m of a mixture of mineral soil and peat that was incorporated during salvage (Figure 3.2). The cover was constructed in the summer of 2010 and seeded with a mix of barley and clover to aid in soil stabilization. Physical properties of the cover soils are given in Table 3.1.

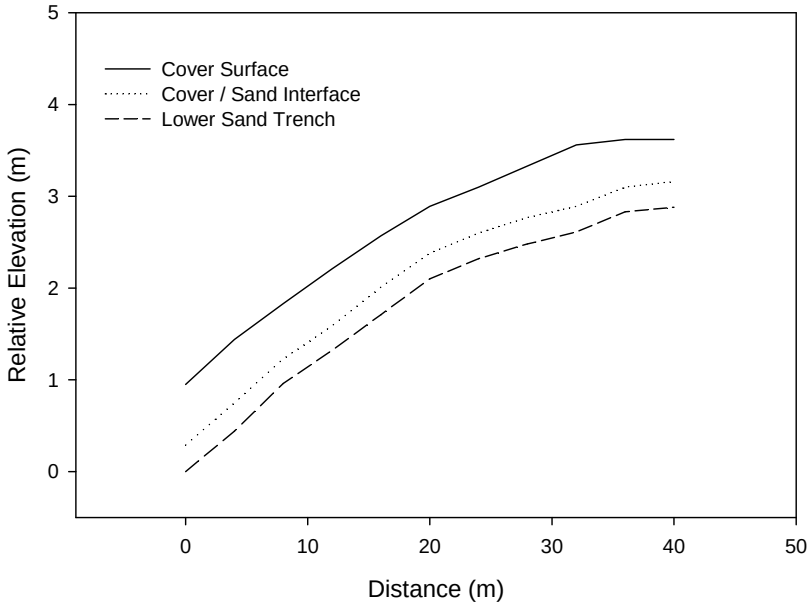

Figure 3.2. Cross section of the transect at Site #1 depicting material layers and thicknesses.

Table 3.1. Soil cover physical properties for the three study locations. Standard deviations (SD) are in parentheses.

| Site | Cover Material | Average Bulk Density (SD) | Average Sand Content | Average Silt Content | Average Clay Content |
|---|---|---|---|---|---|
| | | g $cm^{-3}$ | % | % | % |
| Site #1 | Peat / Mineral Mix | 0.8 (0.1) | 72.3 (4.3) | 27.4 (4.4) | 0.2 (0.2) |
| Site #1 | Sand | 1.6 (NA) | 94.0 (NA) | 5.0 (NA) | 1.0 (NA) |
| Site #2 | Sand | 1.4 (0.1) | 94.0 (2.0) | 5.7 (2.0) | 0.2 (0.3) |
| Site #3 | Peat | 0.6 (0.1) | | | |

Site #2 was located at a uranium mine in northern Saskatchewan, Canada, at a similar latitude to Site #1. The cover was constructed over waste rock in September of 2010 and consisted of a 1 ha plateau with a 2% north facing slope and a 35 m long, 25% south facing slope

(Figure 3.3). The cover consisted of a nominal thickness of 1 m of fine sand sourced from a local drumlin on the plateau, and similarly textured weathered sandstone on the slope (Table 3.1).

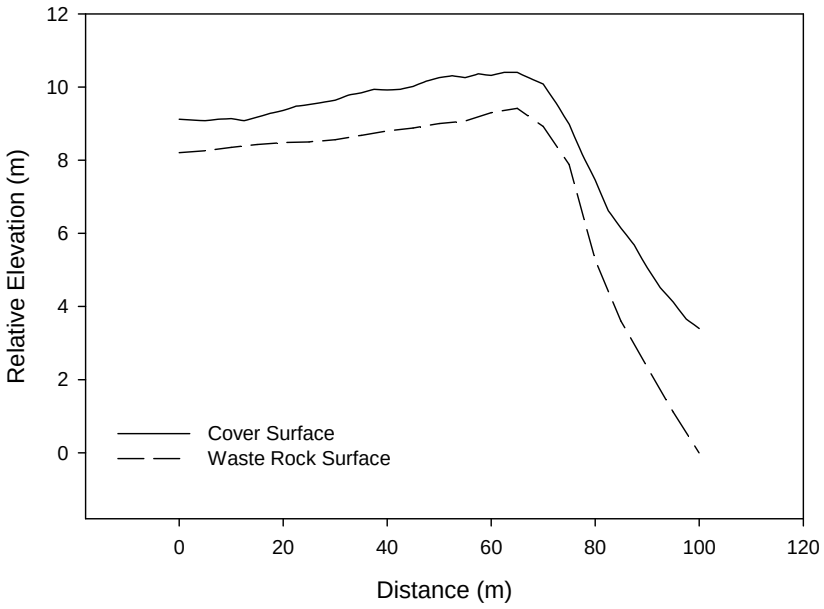


Figure 3.3. Cross section of the transect at Site #2 indicating the cover surface, and the base of the cover system at the waste rock surface.

The third site was located at an oil sands mine approximately 50 km north of Site #1. The site was part of a 50 ha study site comprised of thirty six 1 ha reclamation trial covers, constructed on an overburden dump consisting of lean oil sand that was not economical to mine. The DTS study site was focused on two of the 1 ha plots and was constructed from October, 2011 to May, 2012. The plots comprising Site #3 were adjoining west- and east-facing plots sloped at 2% to join at the peak and consisted of 70 cm of natural sand overlain by 30 cm of peat (Figure 3.4). Only the surface 30 cm of peat was instrumented with fiber optic cable.

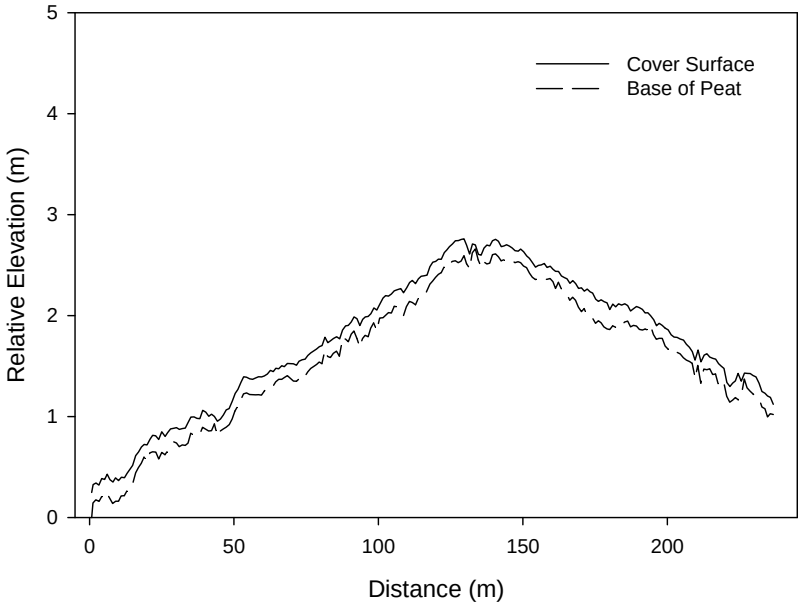


Figure 3.4. Cross section of the transect at Site #3 indicating the cover surface, and the base of the peat layer immediately overlying the sand layer.

The regional climate in which Sites #1 and #3 are located is classed as humid continental. According to thirty year climate normals, mean January and July air temperatures were -19 and + 17 °C, respectively, with mean annual precipitation of 456 mm (Carey, 2008). Site #2 is classed as a continental climate and thirty year climate normals indicated mean January and July air temperatures of -23 and +16 °C, respectively, with mean annual precipitation of 481 mm (Carey et al., 2005).

### 3.3.2 Experimental Set-Up

3.3.2.1 Distributed Temperature Sensing

The DTS system was a commercially available Oryx DTS-SR (Sensornet, UK). The Oryx is a field-deployable unit with a measurement range of up to 5000 m and manufacturer reported temperature resolutions as fine as 0.01 °C. The Oryx has a reported measurement resolution of 1

m and 2 m spatial resolution, defined as the fiber distance required to resolve 90% of a step change in temperature (Tyler et al., 2009). Temporal resolution is set at the discretion of the user, and is a compromise between increased signal quality with longer integration times, and the ability to capture temporal variations in temperature variations. The lowest practical temporal resolution is 30 s, but may result in a noisy, low precision measurement, when compared to a longer integration time that necessarily averages out small scale temporal variations.

The cable used at Sites #1 and #2 was the 5.5 mm diameter Sensornet DamSense cable (Sensornet, UK). DamSense cable consists of four optical fibers encased in a polyurethane jacket with a hard aramid yarn wrap for additional protection. The DamSense cable was chosen because it was a strong, flexible cable with no cable memory; ideal for laying directly on the soil surface. The temperature measurement range of the DamSense cable was reported as -55° to +85 °C. Brugg BRUclean BC150 (Brugg Cables, Switzerland) was installed at Site #3. BRUclean was also a strong, 7.5 mm diameter, four-fiber cable with the fibers encased in a gel-filled loose tube. The cable consists of a polyethylene outer sheath, glass yarn with water-blocking tape for additional strength and fiber protection and is suited to installing directly in the ground. The BRUclean 150 cables was chosen for similar reasons to the DamSense cable, where it was important that the cable be robust, yet have little memory to facilitate direct placement on the soil surface. Temperature measurement range of the BRUclean cable was reported as -20° to +60 °C.

3.2.3.2 Cable Installation

The procedure for installing the cable was the same at all three sites with some minor changes to reflect field conditions and cover configurations. In all cases, the cable was installed along a linear transect with a single length of cable being retraced along the length of the transect

at different depths. Nominal installation depths and the material in which they occur are given in Table 3.2. For Sites #1 and #2, a 2 m wide trench was excavated to 60 cm depth (Site #1) and 1 m depth (Site #2) using an excavator. An excavator was used rather than direct placement with a plough, as the choice of equipment at mine sites is often limited. At Site #3 a 15 cm wide trench was excavated to 30 cm by hand with a shovel (Site #3). Note that cable was only installed into the peat layer at Site #3. In the case of Site #1, which did not have a homogenous profile, care was taken to ensure no mixing of the peat /mineral layers with the underlying sand. Depths for Site #1 were chosen in order to monitor close to the material interface. Once the proper depth was reached, the trench bottom was surveyed so that final cable elevations are known. The cable was then buried and the excavated material was replaced to bring the trench up to the next prescribed depth. This procedure was continued until the trench was completely backfilled. A final length of cable was then laid on the soil surface and was covered with the minimum amount of soil to cover the cable with the *in situ* soil, and is referred to as the 0 cm depth. Site #3 had a final course of cable laid directly on the surface of the soil without a final cover to facilitate comparison of temperatures immediately above and at the soil surface. It is expected that Surface cable measurements would differ from the 0 cm cable. The Surface cable laid directly on the soil surface would be subject to direct exposure to short wave radiation during the day, and long wave radiation from the soil at night. Therefore, it is anticipated that the Surface cable measurements will be subject to increased temporal and temperature variability relative to the 0 cm cable. Typical installation times vary with transect length and depth, cover system texture, availability of heavy equipment, and availability of labour. For Site #1, the 40 m transect was instrumented by one person over three days using a shovel with assistance from an excavator. Site #2 had the 100 m transect instrumented by two people and an excavator over two days. The

236 m transect of Site #3 was excavated completely by hand by two people over two and a half days.

Table 3.2. Fiber optic cable installation depths.

| Site | Cable Depth (cm) | Cover Material |
|---|---|---|
| Site #1 | 0 | Peat / mineral mix |
| | 55 | Peat / mineral mix |
| | 65 | Sand |
| | 90 | Sand |
| Site #2 | 0 | Sand |
| | 10 | Sand |
| | 50 | Sand |
| | 90 | Sand |
| Site #3 | Surface | Exposed |
| | 0 | Peat |
| | 10 | Peat |
| | 15 | Peat |

A solar panel array that charged deep cycle batteries powered the Oryx, which was rated for 18 W during measurements, and 0.5 W when on standby. The solar system for Sites #1 and #2 had 210 W of solar power and 280 Ahr of battery capacity. The power system at Site #3 used 470 W of solar power and 245 Ahr of batter capacity. The solar power system also charged a peripheral laptop used for data collection.

3.2.3.3 Data Collection

Temperature measurements with a DTS system are calibrated by comparing a length of cable maintained at a constant temperature with an independent measurement. A length of cable 30 to 50 m long was reserved immediately adjacent to the Oryx reader at all three sites for calibration. The calibration length was placed inside a standard beverage cooler that was buried in the ground and then filled with ice water. The calibration bath was not constantly mixed, potentially introducing a source of calibration error. Independent calibration temperatures were

recorded using two PT-100 platinum thermistors. Calibrations were examined for both temporal and spatial sensitivity. The spatial repeatability, where a length of cable is held at a constant temperature was found to be ±0.16 °C. Temporal repeatability, where one point on the cable is measured at different times, averaged a standard deviation of ±0.04 °C. The measured sensitivities compare well with others (Ciocca et al., 2012). Following calibration the length of cable remained submersed in water to serve as an area of known thermal properties to aid in data interpretation.

Soil DTS data were collected every 20 minutes with a 60 s integration time. Data at Site #1 were collected from June 10 to July 16, 2011. Power supply issues resulted in the DTS system only being active during daylight hours from approximately 09:00 to 21:00 hrs. Therefore, data from Site #1 are only presented for daytime periods. Data were collected continuously at Site #2 from August 22 to 28, 2011 for the 0 and 10 cm depths. Measurements at the 50 and 90 cm depths at Site #2 were stopped on August 27, 2011. Data were continuously collected at Site #3 from July 2 to July 7, 2012. Data gaps were minimal for Sites #2 and #3, and were filled by simple linear interpolation. Missing data comprised less than 2% of the dataset.

### 3.2.4 Physical properties

Surface bulk density samples were collected every meter along the transect. Bulk soil samples were also collected at the same locations for particle size analysis for Sites #1 and #2 using a Horiba LA-950 particle size distribution analyzer (Horiba, Japan). Particle size analysis could not be conducted for Site #3 as the material was entirely composed of peat.

### 3.2.5 Data Analysis Methods

3.2.5.1 Semi-Variogram Analysis

The spatial structure of daily minimum and maximum temperatures along the transect at all depths was analyzed with semivariograms using standard methods (Isaaks and Srivastava, 1989; Cressie, 1991). Data from all measurement days were aggregated to make a single minimum and maximum temperature dataset for each site. Data were detrended using first order differencing to adhere to the assumption of a stationary dataset (Cressie, 1991). Data were grouped into bins at lags of up to 75% of the total spatial extent and the omnidirectional semivariogram, γ(h), was calculated using (Si et al., 2008):

$$\gamma(h) = \frac{1}{2N(h)} \sum_{k=1}^{N(h)} [T(x_k) - T(x_k + h)]^2 \quad [3.1]$$

where N is the number of pairs at lag distance, h, T(xk) measured soil temperatures at location xk and T(xk+h), the soil temperature at location xk increased by h lags. The semivariograms were normalized by dividing by the sample variance (Si et al., 2008).

Experimental semivariograms were fit with a spherical model (Isaaks and Srivastava, 1989):

$$\gamma(h) = c_0 + 1.5\frac{h}{\alpha} - 0.5\left(\frac{h}{\alpha}\right)^3 \quad [3.2]$$

where $c_0$ is the nugget, the extrapolated semivariance at lag = 0, and α is the range, the lag at which the semivariance reaches a plateau and becomes constant. In the spherical model the semivariance value at which the range is reached is known as the sill. A spherical model has the characteristics of being linear at small lag distances, and reaches a true range value (Schabenberger and Gotway, 2005). A nested spherical model was used to fit the data only

where there was evidence of a secondary range and sill (Goovaerts, 1997). Goodness of fit of the spherical model was judged based on both $R^2$ and the root mean squared error (RMSE):

$$RMSE = \sqrt{\frac{\sum_{i=1}^{n}(\hat{y}_i - y_i)^2}{n}} \quad [3.3]$$

where $y_i$ is the observed value for the ith observation and $\hat{y}_i$ is the predicted value.

3.2.5.2 Summary statistics

Mean, variance, and standard deviation were calculated for each semivariogram dataset. Spatial dependence was calculated as the ratio of the nugget variance to the sill variance, which gives a general indication of the degree to which there is spatial dependence. Spatial dependence values <25% indicate strong spatial structure, values between 25% and 75% indicate moderate structure, and values >75% indicate little to no structure at all (Si et al., 2008).

## 3.3 Results

### 3.3.1 Site #1

The monitoring period during the Site #1 investigation had consistently smooth net radiation profiles, indicating bright cloudless days and resulting in high air temperatures with little variation during the day (Figure 3.5). Average air temperature during the experiment was 19.2 °C with a total of 0.1 mm of rainfall occurring on July 15, 2011. Mean soil temperatures and variances recorded at the midpoint of the transect decreased with depth, yet standard deviations remained consistent at all depths (Table 3.3). Note that noise in the temperature measurements at depth in the soil were not expected, and suggest possible issues with calibration or signal attenuation. Percent sand content had higher standard deviations relative to that of soil temperatures, while standard deviation of bulk density was low (Table 3.3).

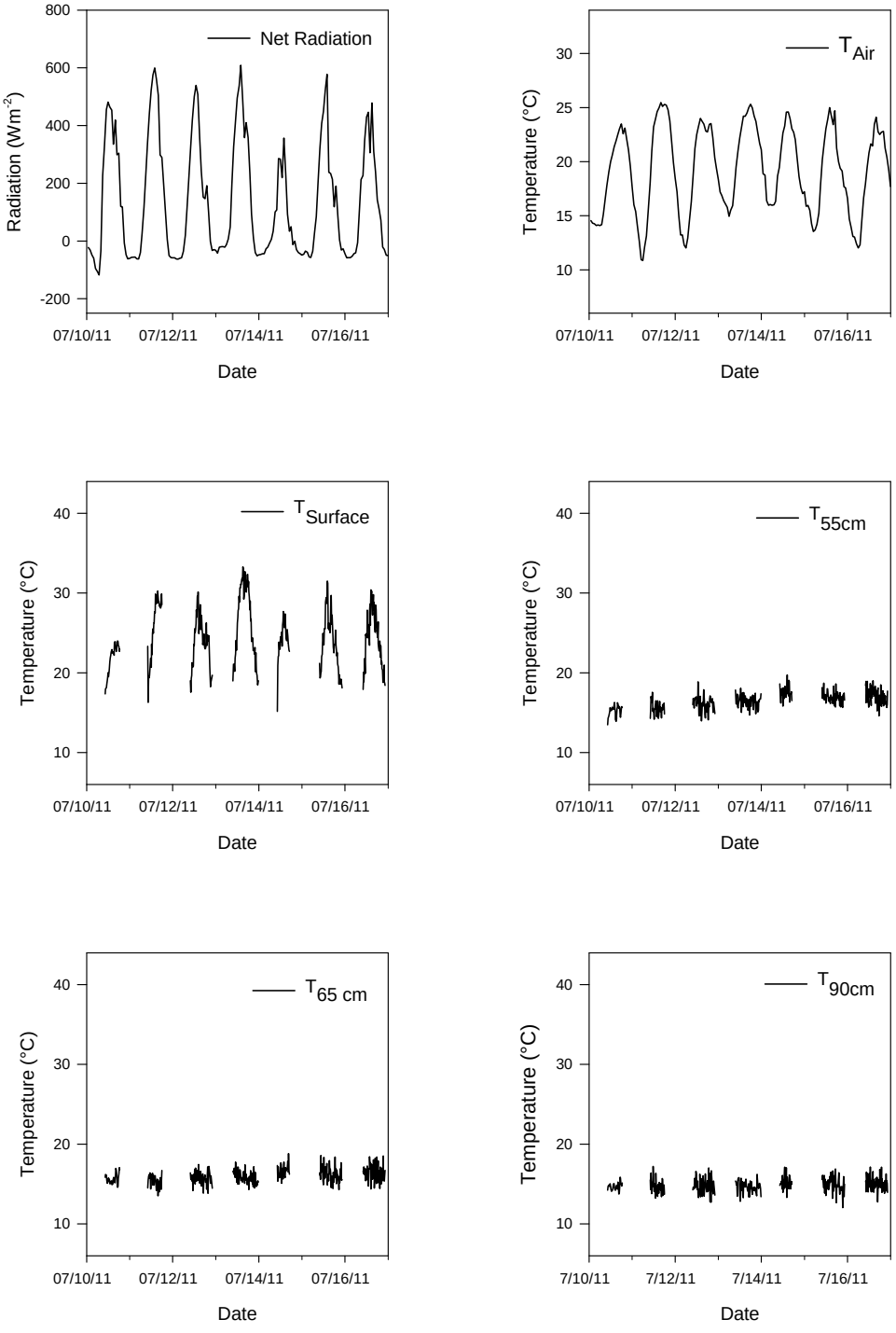


Figure 3.5. Net radiation, air temperature ($T_{air}$) and soil temperatures ($T_x$, where x = depth) measured at Site #1 during the field experiment.

Table 3.3. Summary statistics for Site #1 spatial temperature distributions.

| Depth (cm) | Min /Max - | Mean (°C) | Var. $(°C)^2$ | Std. Dev. (°C) |
|---|---|---|---|---|
| 0 | Max | 28.0 | 8.3 | 2.8 |
| 55 | Max | 16.7 | 1.6 | 1.3 |
| 65 | Max | 16.0 | 1.8 | 1.3 |
| 90 | Max | 14.9 | 2.1 | 1.4 |
| % Sand | - | 72.4 | 18.6 | 4.3 |
| Bulk Density | - | 0.8 | 0.0 | 0.1 |

Distributed daytime soil temperature data from DTS at Site #1 are given in Figure 3.6. Periods of missing data are represented by solid dark blue bars. Temperatures were greatest at the surface and decreased with increasing depth. The greatest qualitative degree of spatial variability in soil temperature occurred at the surface. These differences occurred both within a single day and between days. Within the same day, the first 25 m of the transect, which corresponded to the zone of greatest insolation due to transect aspect, reached higher temperatures and maintained higher temperatures relative to the lower slope position for a longer period (cf. Figure 3.1). Temperature variation between days corresponded closely to net radiation and air temperature (cf. Figure 3.5). Between days, the spatial pattern in soil temperature remained the same for all depths throughout the measurement period, indicating that the processes and properties leading to a certain temperature condition were not changing with time.

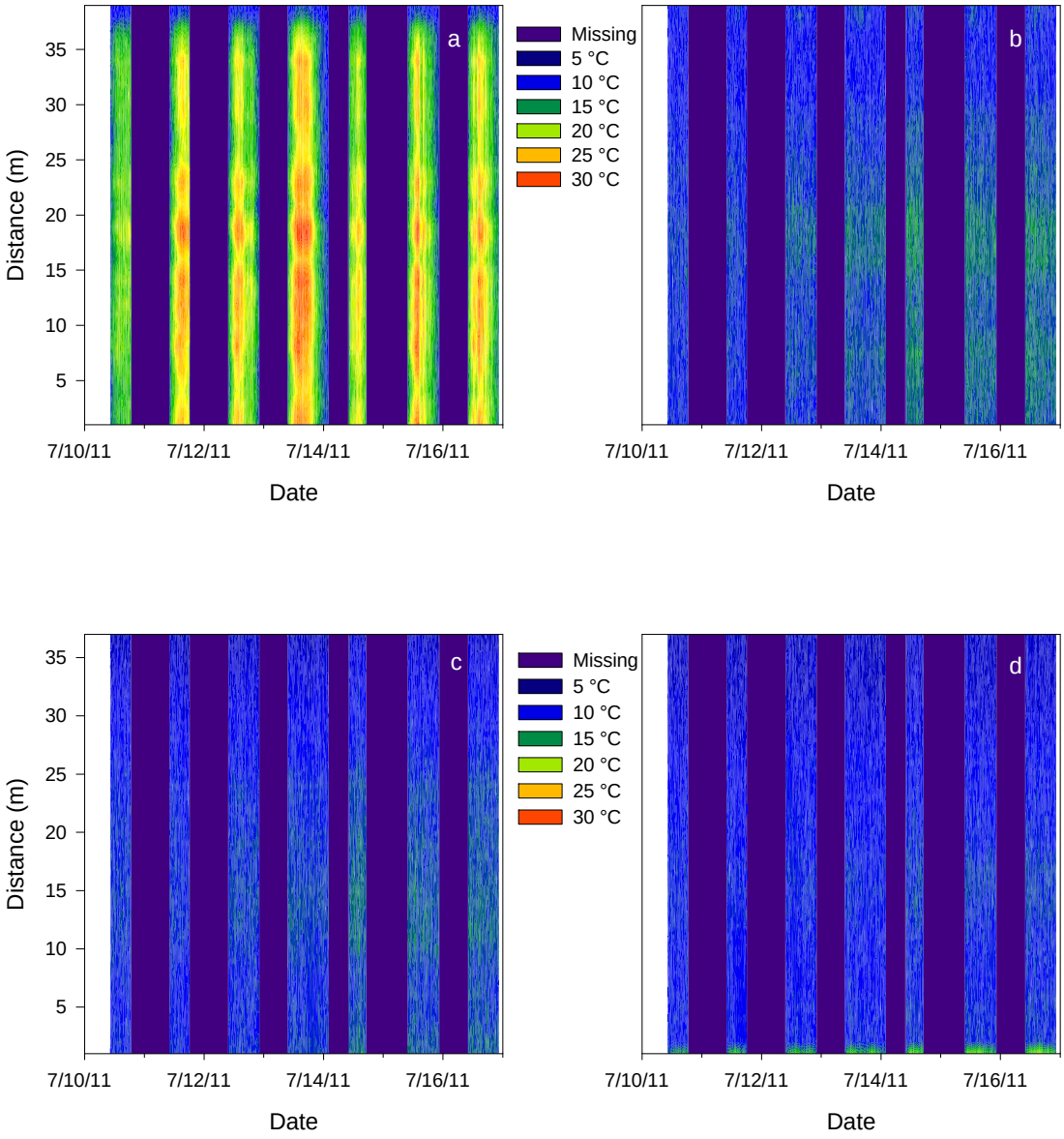


Figure 3.6. Distributed soil temperature values measured at a) 0, b) 55, c) 65, and d) 90 cm depths over the experimental period.

There was little spatial structure in maximum daily temperatures at Site #1, as evidenced by the near-zero sill, negligible range, and high spatial dependence for the 55, 65, and 90 cm depths (Figure 3.7). The exception was at 0 cm, which showed an initial short range of 5 m and a

secondary range of 16 m. Spatial dependence of surface soil temperatures was high at 98%, indicating that daily maximum temperatures values depend greatly on the location at which they were measured. Physical property semivariograms were not fit with a model as the shape of the estimated semivariogram did not lend itself to physical interpretation with a spherical model. However, qualitative analysis of sand content and bulk density was still possible (Figure 3.8). Sand content did not reach a sill within the lag distance measured, suggesting textural homogeneity across the transect. The estimated semivariogram for bulk density appeared to increase at the greatest lag distances. However, the low number of lag pairs available on a 40 m transect make interpretation of semivariogram trends difficult. Semivariogram analysis of bulk density was affected by measurement noise, as indicated by the diffuse semivariance values (Figure 3.8b).

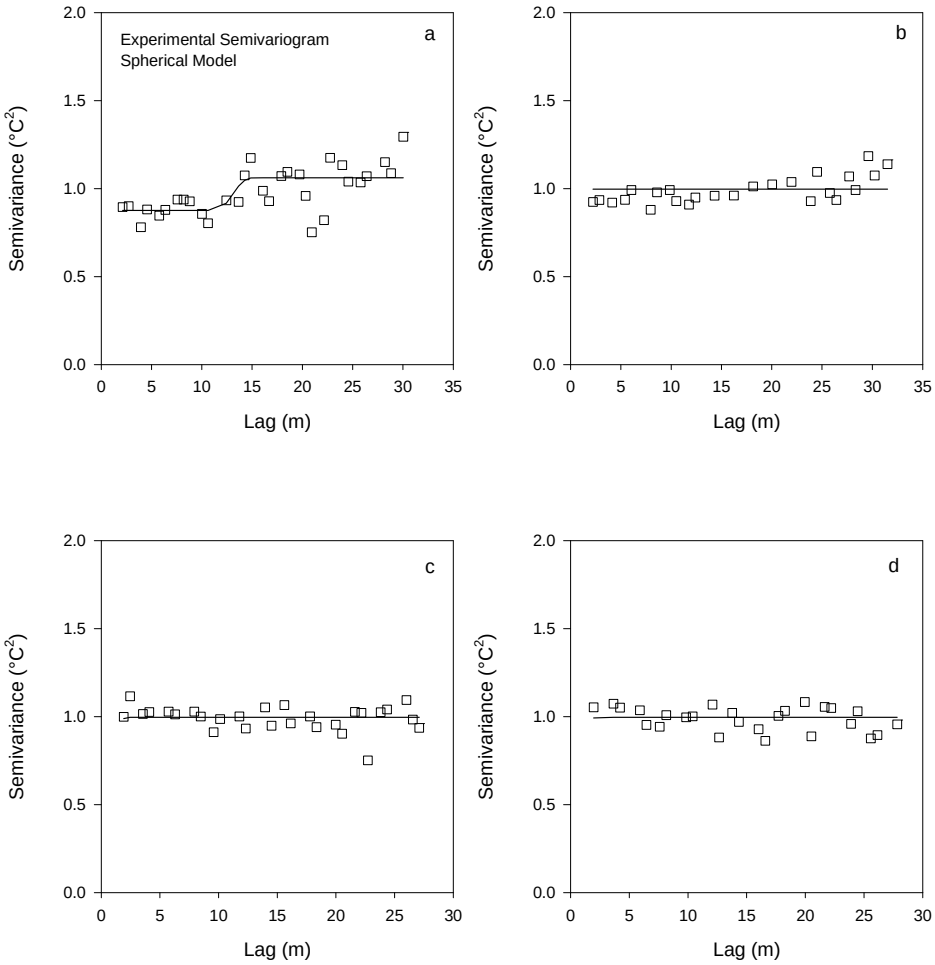


Figure 3.7. Spherical model fit of experimental semivariograms constructed from maximum spatial average temperatures for Site #1 at a) 0, b) 55, c) 65, and d) 90 cm depths.

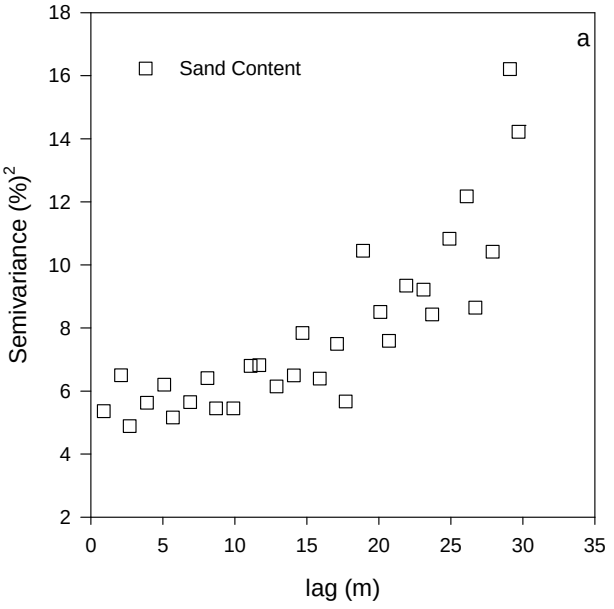


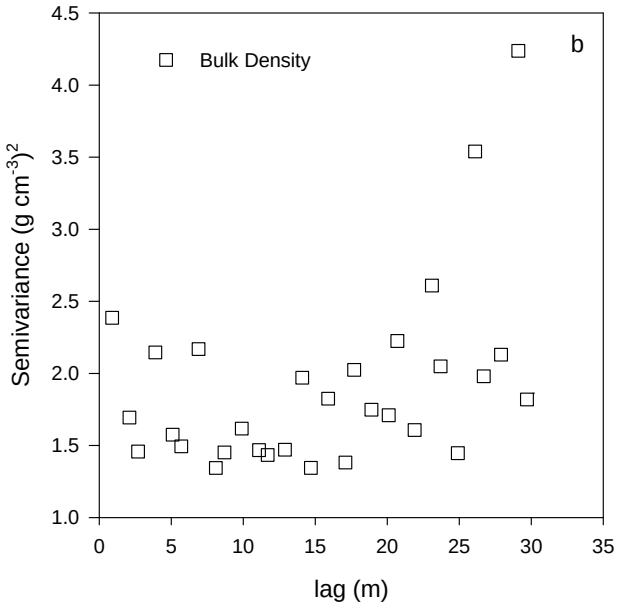


Figure 3.8. Experimental semivariograms for Site #1 a) sand content and b) bulk density

Table 3.4. Site #1 spherical model parameters.

| Depth | Min /Max | Initial Model | | | Nested Model | | Spatial Dependence | Model Fit | |
|---|---|---|---|---|---|---|---|---|---|
| | | Nugget | Sill | Range | Sill | Range | | $r^2$ | RMSE |
| cm | - | $(°C)^2$ | $(°C)^2$ | m | $(°C)^2$ | m | (%) | $(°C)^2$ | (°C) |
| 0 | Max | 0.88 | 0.88 | 2.10 | 1.06 | 16 | 100 | 0.32 | 0.13 |
| 55 | Max | 0.99 | 0.99 | 2.10 | - | - | 100 | 0.0 | 0.08 |
| 65 | Max | 0.99 | 0.99 | 2.10 | - | - | 100 | 0.0 | 0.07 |
| 90 | Max | 0.99 | 0.99 | 2.10 | - | - | 100 | 0.0 | 0.06 |

Temperatures on each day were lower at the lower slope positions from 25 to 40 m at every depth (Figure 3.6). The lower temperatures in this case could have been indicative of lower solar radiation inputs or the downslope presence of increased water contents. Evidence of this trend is suggested in the 0 cm semivariogram (Figure 3.7a) where a nested structure had a range of 16 m. The physical interpretation of the secondary structure would be that from roughly 24 to 40 m on the transect, a distance of 16 m, temperatures were responding to a certain process in a consistent fashion. Every other location on the transect behaved in a very localized manner, leading to the small ranges for the primary spherical model. A possible explanation is the development of vegetation on the transect. Temperature variability introduced by vegetation could be important for the early performance of the cover system. The cover at Site #1 was constructed the previous year and was in the first growing season. Uneven early establishment of vegetation could introduce variability in the spatial distribution of water due to the close links between the surface water and energy balances and plant modification of local microclimates (Gates, 1980; Bristow, 1988; Raich and Tufekcioglu, 2000). Unfortunately, the short transect at Site #1 renders physical interpretation of the semivariograms difficult. A sparse dataset often

leads to a noisy semivariogram that most often indicates a lack of spatial resolution (Goovaerts, 1997).

### 3.3.2 Site #2

The field experiment at Site #2 took place during late August, when average air temperatures were beginning to decrease from summer maxima (Figure 3.9). Net radiation was variable during the experiment, which was reflected in air temperature measurements, where lower radiation inputs corresponded to lower air temperatures. Average air temperature during the experiment was 15.6 °C. Two small precipitation events occurred, resulting in an accumulation of 0.8 mm on August 23, 2011, and 0.1mm on August 25, 2011. Soil temperatures recorded at the midpoint of the transect were indicative of a volume of soil that was beginning to undergo a net loss of energy at the surface, while still remaining warm at deeper depths. Temperatures averaged 13.9, 13.9, 15.7, and 14.6 °C, at the 0, 10, 50, and 90 cm depths, respectively. Average temperatures indicated that the soil surface was beginning to cool with the seasonal trend, while the midpoint of the cover was still warm from the summer radiative forcing, indicative of the lag in temperature penetration to depth. Temperature at the 90 cm depth was lower than at 50 cm, suggesting that the summer heat pulse had yet to reach its maximum at that depth. Variability of soil temperature generally decreased with depth, and was lower at the daily minimum than the daily maximum (Table 3.5). Sand content variability was low, supporting visual indications of a homogeneous texture across the cover. Bulk density variability was slightly higher, yet still low overall, which was indicative of the homogeneity of the cover, and the variability inherent in bulk density measurements.

Table 3.5. Summary statistics for Site #2 spatial temperature distributions.

| Depth (cm) | Min /Max - | Mean (°C) | Var. $(°C)^2$ | Std. Dev. (°C) |
|---|---|---|---|---|
| 0 | Max | 19.1 | 1.9 | 1.3 |
| 55 | Max | 16.9 | 0.5 | 0.7 |
| 65 | Max | 16.1 | 0.2 | 0.4 |
| 90 | Max | 15.1 | 0.2 | 0.5 |
| 0 | Min | 10.1 | 0.1 | 0.3 |
| 55 | Min | 11.6 | 0.4 | 0.6 |
| 65 | Min | 14.8 | 0.2 | 0.4 |
| 90 | Min | 14.2 | 0.2 | 0.5 |
| % Sand | - | 94.0 | 4.0 | 2.0 |
| Bulk Density | - | 1.4 | 0.1 | 0.1 |

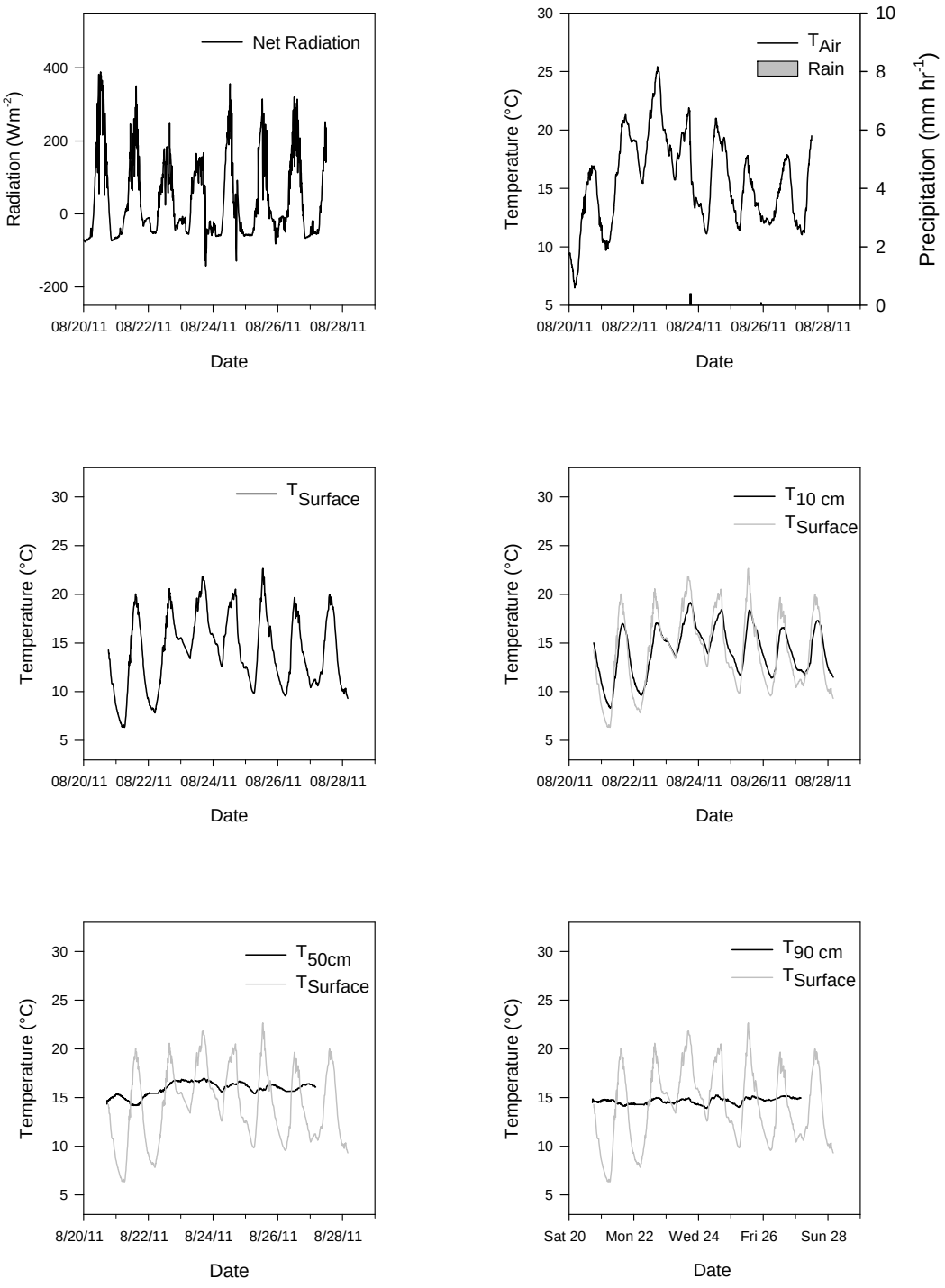


Figure 3.9. Net radiation, air temperature ($T_{air}$), rainfall (rain), and soil temperatures ($T_x$, where x = depth) measured at Site #2 during the field experiment.

Distributed temperature data at Site #2 were indicative of the homogeneity of the cover system, and the influence of aspect in diurnal temperature fluctuations (Figure 3.10). Soil temperatures were lower and displayed lower amplitudes on the north facing slope from 65 to 100 m at all depths. Temperature amplitudes decreased with depth, yet there was still evidence of diurnal fluctuations in temperature, even at the 90 cm depth. Highest soil temperatures at all depths were recorded on August 23, 2011 (Figure 3.10). It is interesting to note that the day on which highest soil temperatures were recorded did not correspond to the highest air temperature or maximum net radiation during the experiment (Figure 3.9). The previous night had low long wave radiation losses (data not shown), indicating a cloudy night that served to reduce radiative losses from the soil surface. The soil remained warmer and was thus able to commence the daily heating cycle from a higher temperature than all other nights. Even though net radiation values were lower on August 23, 2011, the input was sufficient to raise soil temperatures to their highest values.

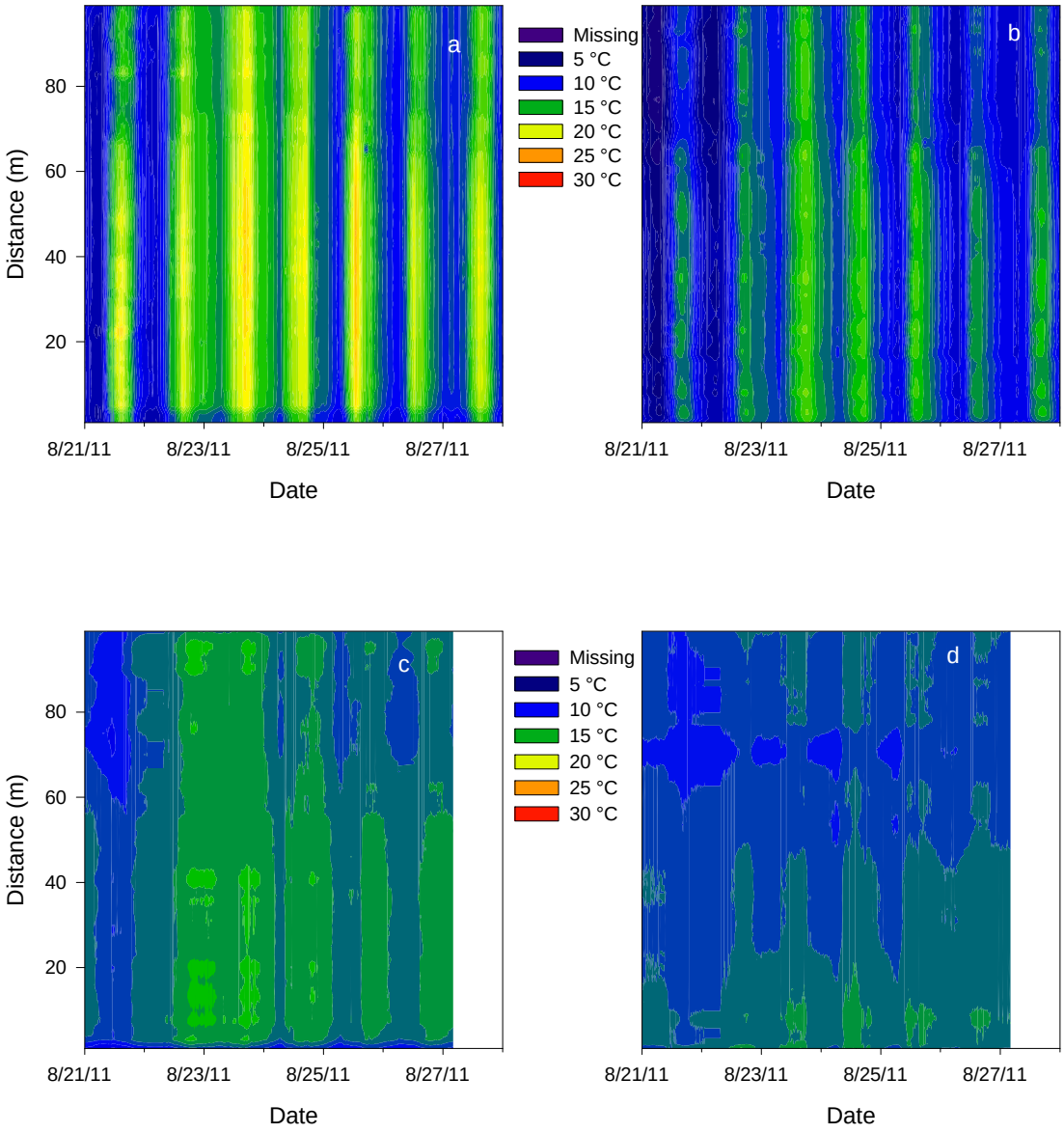


Figure 3.10. Distributed soil temperature values for Site #2 measured at a) 0, b) 10, c) 50, and d) 90 cm depths over the experimental period.

Minimum and maximum temperature semivariograms for Site #2 demonstrated a consistent nested behavior (Figures 3.11 and 3.12). Moderate spatial structure was found initially, with ranges between 2 and 28 m (Table 3.6). Secondary spatial structure was

consistently found to occur after 40 m, resulting in stronger spatial dependencies and ranges extending to 99m; the full length of the transect.

Strong temperature spatial dependence at scales from 40 to 100 m was closely mirrored by strong spatial dependence of sand content and bulk density (Figure 3.13). A model was not fit to physical property semivariograms as it was apparent that a sill had not be reached, and the shape of the experimental semivariogram was such that a spherical model would not have any physical meaning. Nevertheless, it is apparent from Figure 3.13 that spatial dependence was very strong, and measurements separated by the maximum extent of 99 m were similar.

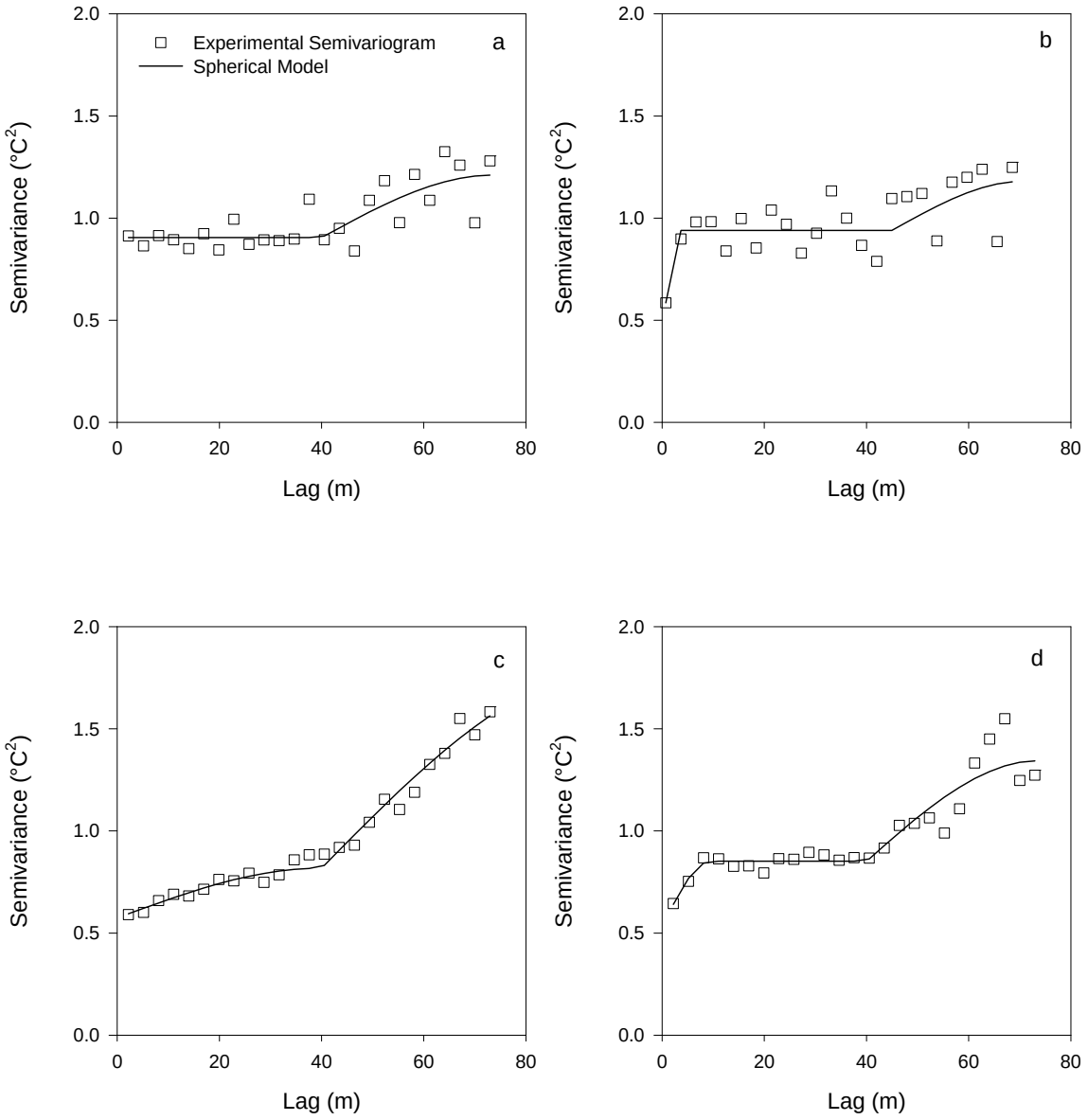


Figure 3.11. Spherical model fit of experimental semivariograms constructed from minimum spatial average temperatures for Site #2 at a) 0, b) 10, c) 50, and d) 90 cm depths.

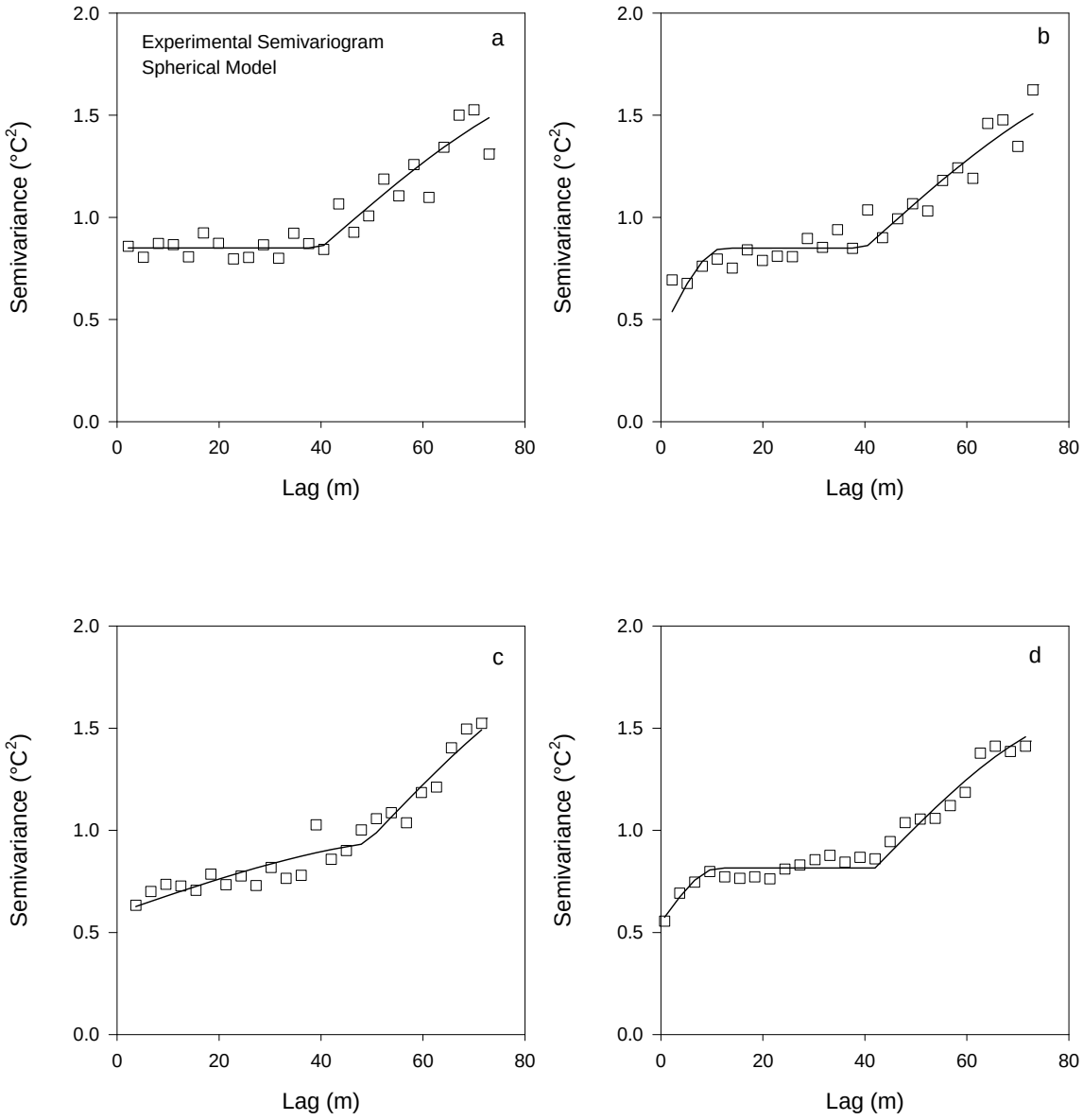


Figure 3.12. Spherical model fit of experimental semivariograms constructed from maximum spatial average temperatures for Site #2 at a) 0, b) 10, c) 50, and d) 90 cm depths.

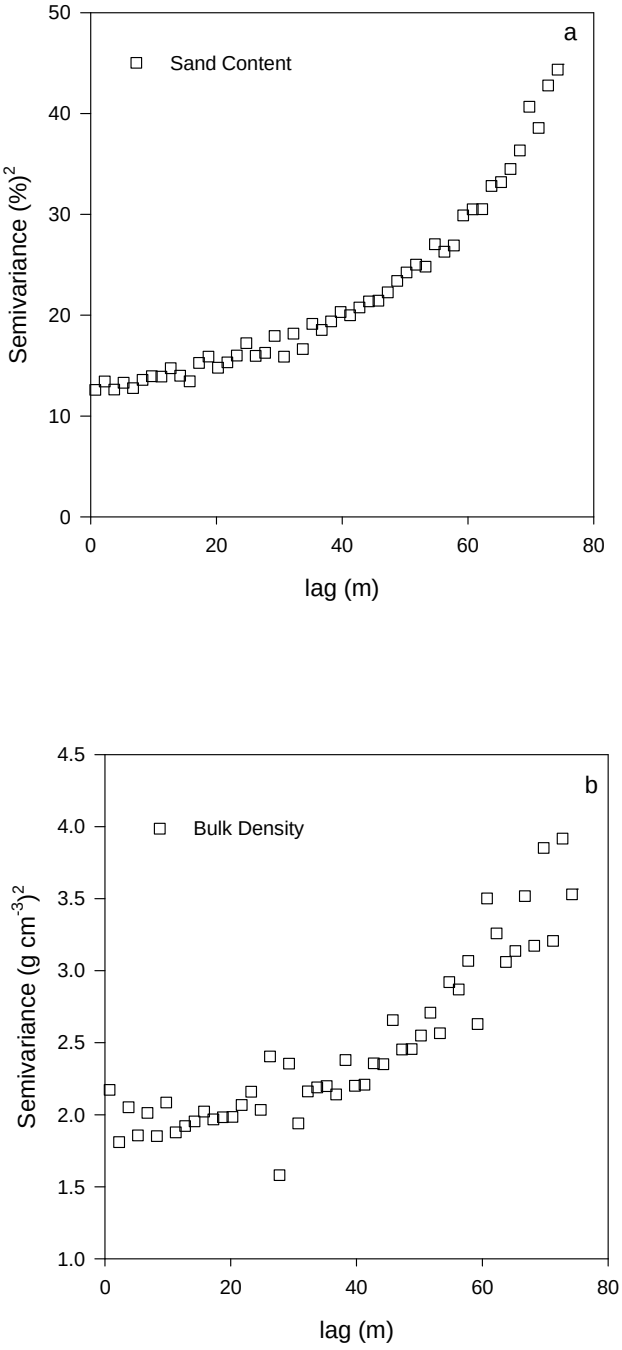


Figure 3.13. Experimental semivariograms of Site #2 a) sand content and b) bulk density.

Table 3.6. Site #2 spherical model parameters. Note the Spatial Depend. indicates spatial dependence.

| Depth | Min /Max | Initial Model | | | Spatial | Nested Model | | Spatial | Model Fit | |
|---|---|---|---|---|---|---|---|---|---|---|
| | | Nugget | Sill | Range | Depend. | Sill | Range | Depend. | $r^2$ | RMSE |
| cm | - | $(°C)^2$ | $(°C)^2$ | m | (%) | $(°C)^2$ | m | (%) | $(°C)^2$ | (°C) |
| 0 | Max | 0.85 | 0.85 | 2.17 | 100 | 1.68 | 97.2 | 51 | 0.84 | 0.07 |
| 55 | Max | 0.90 | 0.90 | 2.21 | 100 | 1.21 | 73.5 | 74 | 0.69 | 0.08 |
| 65 | Max | 0.47 | 0.77 | 16.30 | 60 | 1.67 | 97.3 | 29 | 0.90 | 0.09 |
| 90 | Max | 0.58 | 0.81 | 12.08 | 71 | 1.68 | 97.3 | 35 | 0.97 | 0.04 |
| 0 | Min | 0.42 | 0.85 | 12.30 | 50 | 1.70 | 97.3 | 25 | 0.93 | 0.07 |
| 55 | Min | 0.93 | 0.93 | 2.88 | 100 | 1.20 | 79.6 | 78 | 0.46 | 0.10 |
| 65 | Min | 0.57 | 0.82 | 39.75 | 70 | 1.79 | 97.3 | 32 | 0.98 | 0.04 |
| 90 | Min | 0.53 | 0.85 | 9.41 | 62 | 1.34 | 73.4 | 40 | 0.89 | 0.07 |

Spatial distributions of temperatures at Site #2 is suggestive of differential behavior at lag distances from 40 to 100 m. Although an exact determination of where the points are most similar cannot be determined from semivariogram analysis alone, it should be noted that the secondary structure appears to occur over a 60 lag separation. This may correspond to a division between south-facing plateau (0 to 65 m) and north-facing slope (65 to 100 m) (Figure 3.10). Each slope component behaved as a distinct unit in diurnal heating and cooling, and temporal variability in temperature was closely related to daily air temperature. Qualitative observations of temperature homogeneity were corroborated by both minimum and maximum temperature semivariograms (Figures 3.11 and 3.12). All depths for both minimum and maximum temperatures exhibited a nested structure at Site #2. In all cases the beginning of the secondary structure was around 40 m, which corresponded to the length of the north facing slope. The secondary semivariograms typically had ranges up to 100 m. This trend suggests that for distances from 40 to 100 m, roughly the distance of the plateau, minimum and maximum

temperatures showed a strong spatial similarity, and in some cases displaying strong spatial dependence below 25% (Table 3.6). Stated another way, a temperature measurement taken on the plateau would likely be similar to a measurement taken at any other location on the plateau, even if the points were separated by 60 m. Conversely, a temperature measurement taken on the cover slope near the surface would at most be similar to measurements taken within 11 m. The presence of secondary structure at 40 m was present for all depths at all times, indicating that slope aspect was the dominant control on temperature distributions within the cover system.

Spatial variations as given by the spatial dependence tended to decrease with depth and were lower at times of minimum temperatures (Table 3.6). Spatial dependency values decreased with depth, indicating that spatial similarity of soil temperature increases with depth. Temperature standard deviations (Table 3.5) decreased with depth, a finding also reported by Scharringa (1976). Decreases in temperature variability and spatial dependence are to be expected at greater depths in the profile. Soil surface temperature is a reflection of the surface energy balance and responds to high level harmonics in radiation and soil heat flux variations (Buchan, 2001). As heat is transferred through the subsurface largely by conduction, higher level harmonics associated with the radiation input are dampened and the storage of heat at preceding depths serves to decrease temperature variability (Buchan, 2001). Variability in temperature is lower for minimum temperatures due to the controlling factors of night time energy loss. During the day, microtopography, non-linear turbulent processes, and variation in radiation lead to short term variability in heat transfer processes. At night, soil cooling is largely governed by net longwave radiation from the soil surface to the sky, and soil heat flux toward the surface (Buchan, 2001). Thus for Site #2, not only is soil temperature variability decreased with depth,

but temperatures respond in a cohesive fashion, due to homogeneities in subsurface thermal properties and surface radiative forcing.

Temperature homogeneity on the plateau is explained by corresponding homogeneity in physical properties at Site #2 (Figure 3.13). The natural sandy borrow areas used as a material source for the cover were naturally lacking structure, and the process of cover construction served to eliminate any structure that may have remained. Therefore the cover material was completely homogenized, as evidenced by the physical property semivariograms. The surface of the cover was homogenized as well, with no vegetation and a final surface that was graded to arrive at a uniform surface relief. Indeed, any micro-relief was on the order of less than 10 cm at most (Figure 3.3). In the absence of any physical or biological means of introducing variability, the energy balance should remain simple and close to an idealized surface (Arya, 2001), a finding that was supported by Carey et al. (2005) at a nearby location.

### 3.3.3 Site #3

The monitoring period at Site #3 included a large precipitation event, with 2.8 mm of rain accumulating on July 1, 2012, and 38.6 mm between July 4 and July 5, 2012 (Figure 3.14). Average soil temperatures in the soil profile demonstrated the unique thermal properties of peat (Table 3.7). Temperatures throughout the cover profile demonstrated that energy tended to accumulate at the surface, resulting in large amplitude temperature fluctuations at the surface, while amplitude was greatly diminished 10 cm lower. The accumulation of energy at the surface is due to the poor thermal conductivity of an organic, high porosity soil. Interestingly, soil temperature variability was greater at night than during the day (Table 3.7). This is explained by the uniformly high temperatures during the day near the surface. Soil temperature variability decreased with depth for both minimum and maximum temperatures.

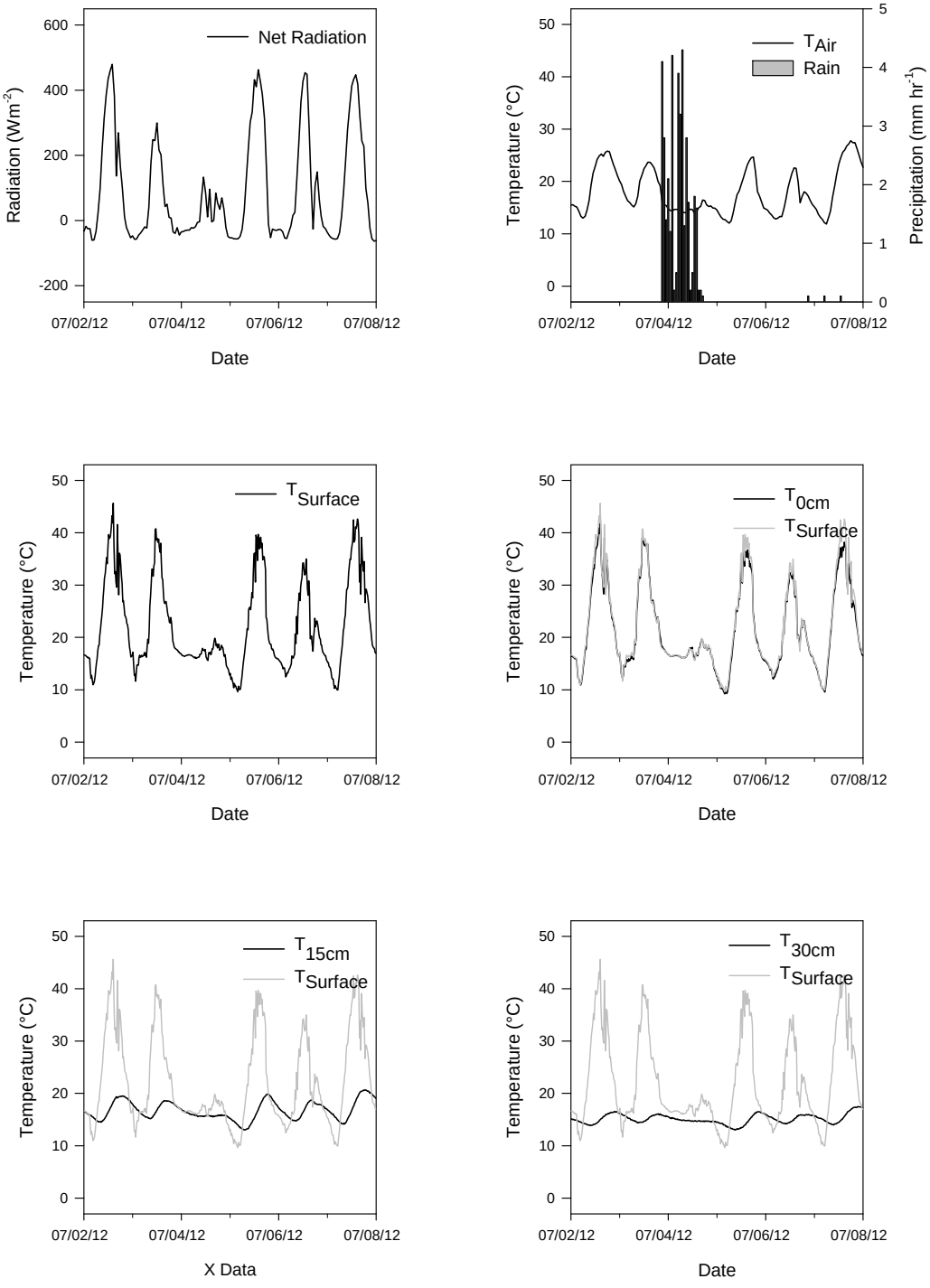


Figure 3.14. Net radiation, air temperature ($T_{air}$), rainfall (rain), and soil temperature ($T_x$, where x = depth) measured at Site #3 during the field experiment.

Table 3.7. Summary statistics for Site #2 spatial temperature distributions.

| Depth | Min /Max | Mean | Var. | Std. Dev. |
|---|---|---|---|---|
| cm | - | (°C) | $(°C)^2$ | (°C) |
| Surface | Max | 38.9 | 1.3 | 1.1 |
| 0 | Max | 35.8 | 2.8 | 1.5 |
| 10 | Max | 18.3 | 0.5 | 0.7 |
| 15 | Max | 16.1 | 0.5 | 0.7 |
| Surface | Min | 10.0 | 0.1 | 0.3 |
| 0 | Min | 10.5 | 0.1 | 0.3 |
| 10 | Min | 14.0 | 0.1 | 0.3 |
| 15 | Min | 14.2 | 0.0 | 0.1 |
| Bulk Density | - | 0.6 g $cm^{-3}$ | 0.02 $(g\ cm^{-3})^2$ | 0.1 g $cm^{-3}$ |

The unique thermal properties of peat are evident when comparing spatial distribution of temperatures at the surface and subsurface (Figure 3.15). Note that the low temperature band at 136 m in Fig. 3.15a and b represents an area where the cable needed to be buried to pass under a vehicle path. The fiber optic cable denoted in Fig. 3.15a was laid directly on the surface of the cover, and therefore exhibited the highest diurnal temperature fluctuations. Temperature fluctuations were highly dampened at the 10 and 15 cm depths in relation to the surface temperatures. The influence of the reduced radiation inputs during the storm event on July 4 was clearly seen at all depths in the profile.

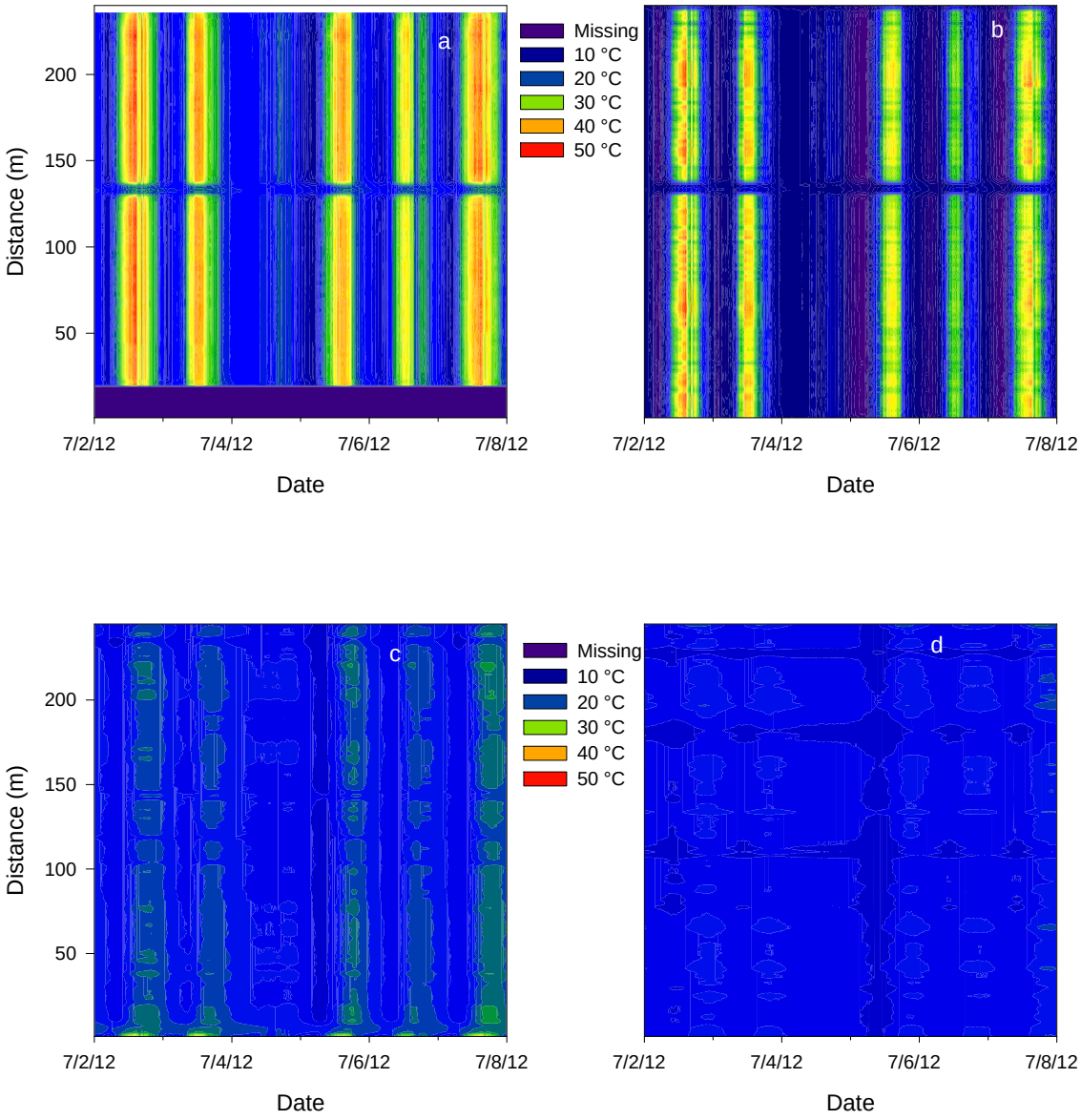


Figure 3.15. Distributed soil temperature values measured at a) cover surface, b) 0, c) 10, and d) 15 cm depths over the experimental period.

Maximum temperature spatial structure was nearly non-existent at Site #3 (Figure 3.16). Note the differences in reduced lag scale for the surface and 0 cm semivariograms (Figures 3.16a and 3.16b) as data from the portion of the cable that was buried under the vehicle access were not included in the analysis. Unlike the maximum temperature semivariograms estimated for Site

#2 (Figure 3.12) there was not any evidence of a nested structure, indicating that the thermal properties of peat lead to extensive variability at small scales. The transect at Site #3 extended for 236 m, yet in all cases for the maximum temperature the range was reached within the first 4 m or less (Table 3.8). Nested structure was only found for the Surface and 0 cm minimum temperatures (Figure 3.17). Spatial dependencies were moderate for all depths and maxima / minima, and were only slightly strengthened with the nested models. Similar to Site #2, a spherical model was not fit to Site #3 bulk density (Figure 3.18). Bulk density semivariance at Site #3 was also found to increase without reaching a sill, indicating strong spatial similarity at all locations.

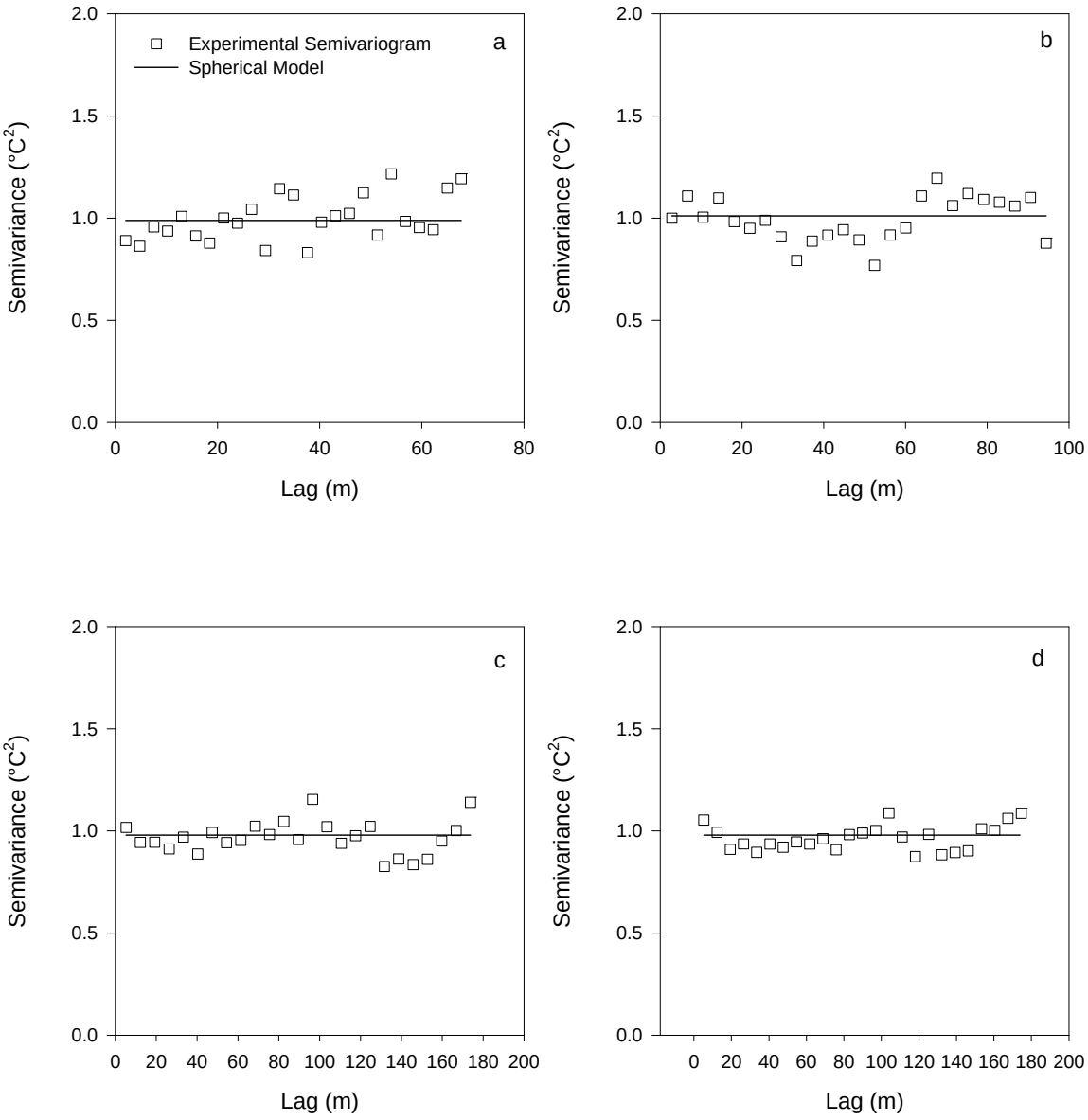


Figure 3.16. Spherical model fit of experimental semivariograms constructed from maximum spatial average temperatures for Site #3 at a) surface, b) 0, c) 10, and d) 15 cm depths.

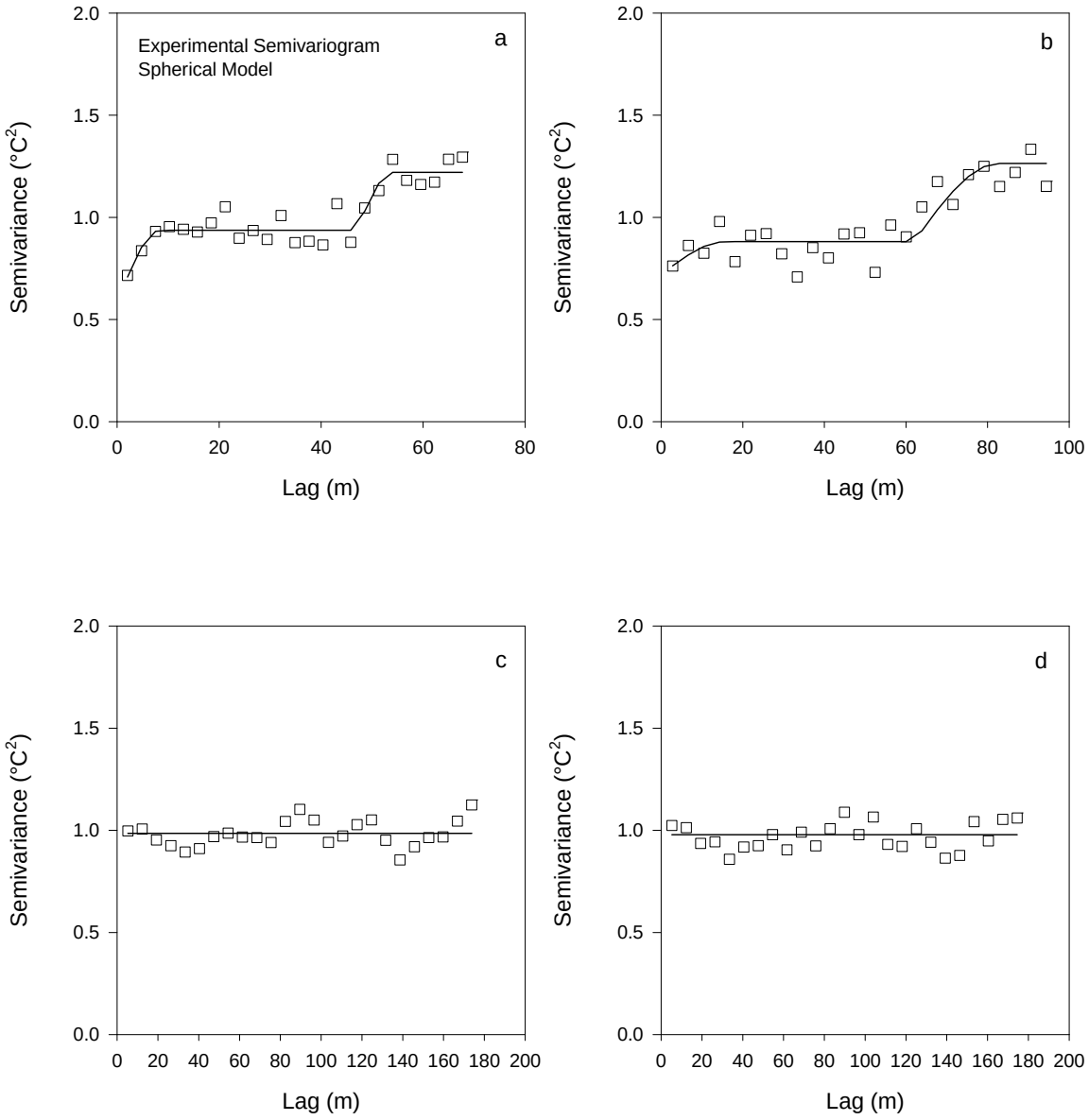


Figure 3.17. Spherical model fit of experimental semivariograms constructed from minimum spatial average temperatures for Site #3 at a) surface, b) 0, c) 10, and d) 15 cm depths.

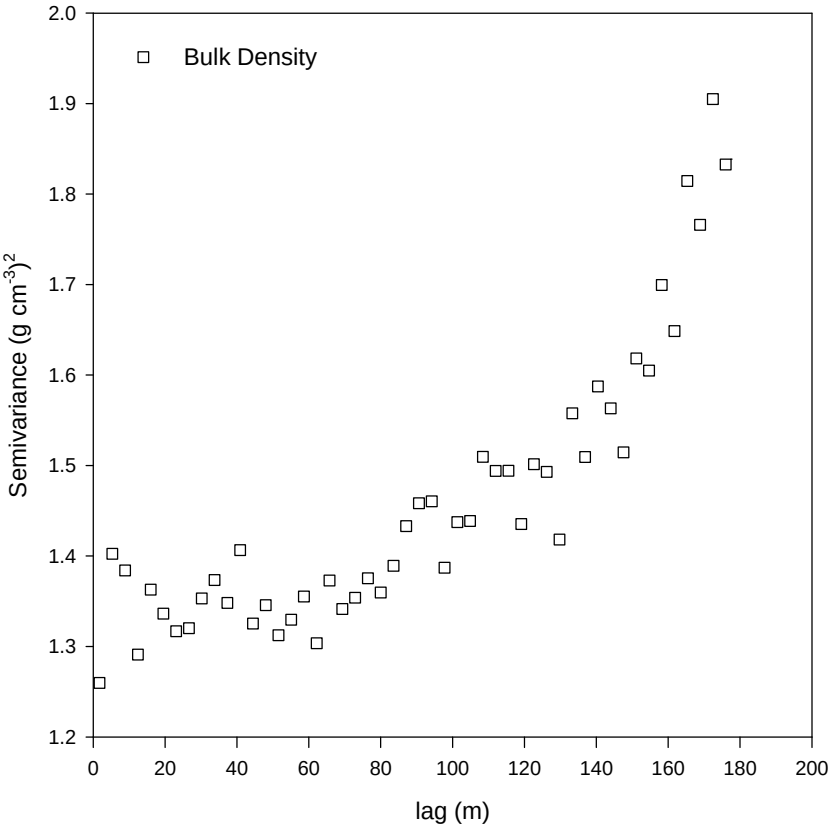


Figure 3.18. Experimental semivariogram of Site #3 bulk density.

Table 3.8. Site #3 spherical model parameters. Note that Surf. denotes surface measurement, and Spatial Depend. indicates spatial dependence.

| Depth | Min /Max | Initial Model | | | Spatial | Nested Model | | Spatial | Model Fit | |
|---|---|---|---|---|---|---|---|---|---|---|
| | | Nugget | Sill | Range | Depend. | Sill | Range | Depend. | $r^2$ | RMSE |
| (cm) | - | $(°C)^2$ | $(°C)^2$ | m | (%) | $(°C)^2$ | m | (%) | $(°C)^2$ | (°C) |
| Surf. | Max | 0.99 | 0.99 | 2.14 | 100 | | | | 0 | 0.07 |
| 0 | Max | 1.02 | 1.02 | 2.14 | 100 | | | | 0 | 0.07 |
| 15 | Max | 0.98 | 0.98 | 2.14 | 100 | | | | 0 | 0.06 |
| 30 | Max | 0.98 | 0.98 | 2.14 | 100 | | | | 0 | 0.07 |
| Surf. | Min | 0.58 | 0.94 | 8.30 | 62 | 1.22 | 53.96 | 50 | 0.87 | 0.05 |
| 0 | Min | 0.71 | 0.88 | 15.68 | 81 | 1.26 | 82.65 | 56 | 0.82 | 0.08 |
| 15 | Min | 0.98 | 0.98 | 2.14 | 100 | | | | 0 | 0.07 |
| 30 | Min | 0.98 | 0.98 | 2.14 | 100 | | | | 0 | 0.07 |

Surface temperatures at Site #3 were more variable than those at both Site #1 and Site #2 as evidenced by the greater standard deviations at 0 cm for both minimum and maximum temperatures (Table 3.7). Despite moderate spatial structure in bulk density, the only time at which spatial structure in temperature was seen at Site #3 was at the daily minimum for the Surface and 0 cm temperatures. Soil temperatures are expected to be less variable at night as temperatures are controlled by net negative longwave radiation from the surface and conduction from subsurface depths (Buchan, 2001). Therefore minimum temperatures are less affected by local scale variability in soil physical properties and heat transfer processes. Daily minimum temperatures tend to also correspond with the daily minimum variance; therefore, if any spatial structure is expected to be found, daily minimum temperatures is the most likely time (Mohanty et al. 1995).

Two possibilities exist to explain the high degree of temperature variability in a relatively shallow peat layer. For the subsurface, the thermal properties of peat, and specifically, how they manifest in the thermal property known as thermal inertia could lead to local variations. Thermal

inertia governs the amplitude of the soil heat flux density (de Vries, 1975) and depends on the thermal and physical properties of the material (Verhoef, 2004; Murray and Verhoef, 2007). Thermal inertia in peat can be up to four times greater than in mineral soils (Eggelsman, 1972). Therefore, any local differences in density or ground heat flux would be magnified relative to a mineral soil, which would be more effective at redistributing temperature (Eggelsman, 1972). Secondly, surface elevation, and specifically microtopography at Site #3 was more variable than at Site #1 and Site #2. Surface elevation coefficient of variation was 9% at Site #3, as compared to 0.3% and 0.1% at Site #1 and Site #2, respectively. The presence of variable micro-topography has been found by others to lead to spatial variations in temperatures and large differences in local ground heat flux (Kellner, 2001).

### 3.4 Summary

A DTS system has been demonstrated to have the flexibility and capability to measure soil temperature across a range of cover configurations, soil textures, and vegetation conditions. The study used semivariogram analysis to examine three different cover systems with a wide range of properties and at various depths and times.

Soil temperatures were effective in demonstrating differences in soil properties between study sites. The spatial structure of soil physical properties at Site #1 was similar to both Sites #2 and #3. However, unlike Site #2, soil temperature variability at Site #1 was higher and exhibited no spatial structure. The lack of spatial structure in soil temperature at Site #1 was attributed to the presence of vegetation. High spatial similarities in physical properties at Site #2 was reflected in the temperature measurements. The same spatial structure was found at all depths and all times, suggesting that when a cover system is constructed with a homogeneous structureless sand, the lack of variability ensures that the cover system will respond to radiation inputs as a coherent unit. Indeed, the only temperature variability seen at Site #2 may have been due to

differences in slope aspect. Bulk density variability at Site #3 was similar at all locations across the transect, yet temperature variability had very little spatial structure and was highly variable. Variability at Site #3 was attributed to the unique thermal properties of peat and the magnified effect of microtopography on the surface energy balance.

Soil temperature variability generally decreased with increasing depth. At Sites #1 and #2, not only did the variability of temperature measurements decrease with depth, but spatial similarity also increased, indicating that soil temperatures taken at depth were similar to values taken at increasingly distant locations. The exception to the trend of decreasing variability with increasing depth was at Site #3, where the spatial variability was uniformly high at all depths and we less attributed to depth as it was to time.

Finally, soil temperatures demonstrated increased spatial similarity at daily minima yet not to the degree expected. At Site #2 high spatial similarity, or low spatial dependence, was found for both daily maximum and minimum temperatures. The uniform nature of the cover system soil was entirely homogeneous, leading the cover to respond in a similar fashion at all times of the day. At Site #3, the only time secondary spatial structure with ranges greater than 5 m was found was for the Surface and 0 cm measurements at night, indicating that cooling processes are less spatially dependent than heating processes active during the day.

### 3.5 Conclusion

Spatially distributed temperature measurements were evaluated as a means of assessing the spatial structure of soil temperature in soil cover systems. The method is well suited to the mine reclamation industry, where there is a dearth of information on cover system temperature responses at scales greater than point scale. Implementation of a DTS system in soil covers has the benefit of producing temporally intensive temperature measurements at thousands of locations for multiple depths, over extended time periods. Interpretation of soil temperature

semivariograms is improved when coupled with supplemental data on physical properties. Soil temperature is an attractive variable of interest for characterizing spatial variability in soil covers due to the links that exist between soil temperature and soil water content as well as soil thermal properties. Although soil temperature is not perfectly correlated to soil water content, intensive spatial and temporal monitoring of soil temperature in reclamation cover systems nonetheless represents a promising method for characterizing their behavior at the field scale.

# 4.0 A SIMPLE METHOD FOR ASSESSING SPATIAL VARIABILITY OF THERMAL PROPERTIES IN SOIL COVER SYSTEMS

## 4.1 Preface

Installation of a DTS system and a preliminary investigation of the spatial structure of cover system temperature was discussed in the previous chapter. The spatial distributions of temperatures are of interest to the reclamation scientist, but are limited in the information that is conveyed. Estimation of thermal properties of the system is of much greater use in describing the properties and processes at work in the cover system. Current methods for estimating soil thermal properties focus on the apparent thermal diffusivity, which has the disadvantage of being highly sensitive to depth of installation and is not uniquely related to water content. Therefore, a method that improves upon the deficiencies of estimating apparent thermal diffusivity would be beneficial.

## 4.2 Introduction

The surface energy balance governs the partitioning of incoming solar radiation into separate components defined as follows (Liebethal and Foken, 2007):

$$R_n = H + LE + G_0 \quad [4.1]$$

where $R_n$ is the net radiative flux, H is the sensible heat flux to the atmosphere, LE is the latent heat of evaporation, and $G_0$ is the ground heat flux (all terms in W $m^{-2}$). Energy partitioning at the soil surface influences the transfer of mass to the atmosphere, the flux of heat in the subsurface, and the resulting temperature profile (Buchan, 2001). Soil temperature is, therefore, a critical indicator variable in the energy balance of soils and is indicative of how surface and subsurface properties are distributed within a field (Buchan, 2001).

There has been growing interest in using soil thermal properties to infer soil water content and the spatial variations of water content. Soil water content can be difficult to measure

over large areas, making soil temperature a potential proxy for soil water content, particularly given the relative ease with which soil temperature is measured (Minacapilli et al., 2009).

Knowledge of how temperature is distributed, both spatially and temporally, can provide important insights into the underlying energy balance and heat transfer processes that lead to a certain temperature state. Scharringa (1976) was a pioneer in examining the spatial distribution of temperature within a field. It was found that variances in soil temperature are highest during periods of the greatest ground heat flux (Scharringa, 1976). Soil temperature variance decreased with depth, yet it was found that point measurements in a homogeneous agricultural field had a 42% probability of incorrectly estimating the mean temperature within ±1 °C. Probabilities of incorrectly estimating mean temperature decreased to 7.5% at night (Scharringa, 1976). Spatial variability of soil temperatures in what is ostensibly a homogeneous field have been reported by others. Vauclin et al. (1982) reported anisotropy in agricultural fields and autocorrelation lengths of less than 7 m. Mohanty et al (1995; 1998) had similar findings of spatial correlations between 1.5 to 9 m in what was otherwise a homogeneous field. The strongest determinant of the spatial variability of soil temperature was determined to be soil water content (Vauclin et al., 1982; Mohanty et al., 1995; Mohanty et al., 1998).

The prospect of easily measuring soil thermal properties over large spatial extents has been made possible through the use of distributed temperature sensing (DTS). A DTS system consists of a fibre optic cable and a reader that uses a high-powered laser to measure temperatures within the fibre optic cable, accurately and precisely to within a manufacturer stated of up to 0.01 °C, at resolutions on the order of 1 m over distances of 5000 to 10,000 m (Selker et al., 2006a; Selker et al., 2006b; Tyler et al., 2009). Using a DTS system to determine water content uses one of two general methods: active heating, and passive heating. In active

heating methods, a heat pulse is generated within the stainless steel strength member of the fiber optic cable. Based on the time required to dissipate a known energy flux, the thermal conductivity and volumetric heat capacity of the soil can be estimated (Campbell et al., 1991). Passive methods measure the temperature of two or more buried cables in response to diurnal radiative forcing (Steele-Dunne et al., 2010). Given that the actual energy flux is unknown, only the apparent thermal diffusivity, α, ($m^2$ $s^{-1}$) can be estimated. In both methods, the thermal properties are then used to infer soil water content based on the following relationships:

$$\alpha = \lambda/\rho c = \lambda/C_v \quad [4.2]$$

and

$$C_v = f_s\rho_s c_s + f_w\rho_w c_w + f_a\rho_a c_a \quad [4.3]$$

where λ is thermal conductivity (W $m^{-1}$ $K^{-1}$), ρ is particle density (g $cm^{-3}$), c is specific heat (J $kg^{-1}$ $K^{-1}$), and $C_v$ is volumetric heat capacity (J $m^{-3}$ $K^{-1}$), f denotes the volume fraction of the soil (s), water (w), and air (a) components (de Vries, 1975). Note that $f_w$ is equivalent to volumetric water content, $\theta_v$, ($cm^3$ $cm^{-3}$).

A DTS system can be used to estimate water content using active heating methods to estimate thermal conductivity and heat capacity (Sayde et al., 2010). Active heating methods provide a unique determination of water content, and have been documented by others. Weiss reported that small changes in water content were difficult to resolve above water contents of 6%. Sayde et al. (2010) used a similar technique in the laboratory but also reported increasing measurement uncertainty at higher water contents, with an uncertainty of 0.046 $m^3$ $m^{-3}$ at water contents of 0.41 $m^3$ $m^{-3}$. Ciocca et al. (2012) on the other hand found the best estimates were obtained at high water contents, while water content was consistently underestimated in the dry range. A field study by Striegl et al. (2012) confirmed that active heat pulse methods were

adequate at dry field conditions, yet were insensitive to changes in water content under wet conditions. Measurement uncertainty was found to be a result of insufficient integration time (Sayde et al., 2010) and insufficient heat pulse duration to achieve asymptotic temperature rise (Ciocca et al., 2012).

Passive methods have been employed to infer the spatial distribution of water in soils. Steel-Dunne et al. (2010) used an inversion of the numerical solution to Fourier's heat diffusion equation to arrive at an estimate of apparent thermal diffusivity in order to calculate a value for soil water content. The non-unique relationship between water content and diffusivity made calculation of water content problematic. The issue stemmed from the fact that estimation of thermal diffusivity was very sensitive to cable installation depth. The uncertainty of cable depth led to estimates of diffusivity that spanned their entire measurement range of diffusivity. Rutten et al. (2010) looked to develop a numerical inversion technique that would allow for use of DTS measurements in observing spatiotemporal variability of soil-atmosphere exchange processes. Using a numerical inversion of the heat diffusion equation, it was found that heat transfer in the shallow subsurface could not be explained by conduction without accounting for phase change or vapor diffusion. Even when accounting for phase change and vapor diffusion, the technique was not able to optimize the relationship of water and temperature based on diffusivity alone (Rutten et al. 2010). Short of finding a reliable relationship between diffusivity and water content, Rutten et al. (2010) nevertheless found that passive monitoring of thermal properties with DTS could be used to provide qualitative estimates of the variation in water content. Krzeminska et al. (2011) applied passive DTS methods to describe the spatial distribution of water in a landslide. In this case, Krzeminska et al. (2011) also used temperature data to describe the spatial distribution of thermal diffusivity. It was reported that when local physical properties are taken into account,

thermal diffusivity analysis may be a viable method for elucidating fluctuations in soil water content.

However, Krzeminska et al. (2011) also summarized the limitations of using thermal diffusivity to estimate soil water content. In their study they found that diffusivity was overestimated, possibly due to not accounting for advection in the subsurface. They also found that the assumption of a uniform surface temperature was likely invalid and that diffusivity estimates were highly sensitive to the depth of the temperature measurement. Thermal diffusivity was also insensitive to water content at saturations greater than 50%. A final limitation was the requirement for a minimum time window of 24 hours, thus necessitating the use of at least a diurnal temperature series. It is clear from the summary of limitations presented by Krzeminska et al. (2011) that thermal diffusivity may not be the optimal parameter for assessing the spatial variability of soil water.

Soil thermal properties must be uniquely and directly related to water content to be useful as a measurement parameter for the investigation of the spatial variability of water content. Thermal inertia [J $m^{-2}$ $K^{-1}$ $s^{-1/2}$] is a composite thermal property that describes the resistance of the soil to temperature change for a given flux (Sabol et al., 2006; Scheidt et al., 2010; Wang et al., 2010). Thermal inertia controls the amplitude of the diurnal ground heat flux and is the key thermal property controlling the diurnal and annual surface temperature change (Buchan, 2001; Wang et al., 2010). It is defined as:

$$\mathrm{TI} = \sqrt{C_v \lambda} \qquad [4.4]$$

Thermal inertia has been extensively used in the field of remote sensing and is more precisely referred to as apparent thermal inertia (ATI) given that a surface measurement is used to estimate a property that extends with depth (Sabol et al., 2006). Apparent thermal inertia is

commonly used in remote sensing to estimate $\theta_v$ because the magnitude of changes in the thermal inertia of water and other soil components is sufficiently different to facilitate a relative comparison when sensing remotely (Minacapilli et al., 2009; Lu et al., 2009; Matsushima et al., 2012). The method was pioneered in the 1970's (Watson, 1975) and was extensively studied for large-scale mapping of $\theta_v$ (Pratt and Ellyett, 1979; Price, 1985). Apparent thermal inertia mapping has also been the subject of more recent attempts to use it as a means of retrieving $\theta_v$ from remote sensing data. Error propagation models described by Verstraeten et al. (2006) claimed that their autocorrelation method could be as accurate as 2%. Matsushima et al. (2012) developed a simpler method to estimate daily subsurface $\theta_v$ from ATI with a precision of ±3 to 4% at a 95% confidence interval. The precision reported by Matsushima et al. (2012) was thought to be sufficient for at least a qualitative classification of soil wetness into wet, medium, and dry classes using ATI estimates.

There are a number of reasons that make ATI attractive as a variable to characterize the spatial variability of water in soil cover systems. Of primary importance is that ATI will increase as soil water content increases (Price, 1985). Apparent thermal inertia also controls the amplitude of the flux of heat towards the ground surface at night, thus making it the dominant nighttime thermal property when the contributions of H and LE to the surface energy balance are diminished (Ten Berge and Stroosnijder, 1987). Steele-Dunne et al. (2010) rejected the use of thermal inertia because of challenges related to remote sensing including atmospheric opacity and the need to solve the surface energy balance. However, when ATI is measured from sunset to sunrise, when soil temperatures generally decrease, rather than incorporating diurnal temperature changes as is the case for thermal diffusivity, only the dominant source of variability is measured (Ten Berge and Stroosnijder, 1987; Verhoef, 2004). It has been shown that soil

temperature exhibits a diurnal hysteresis and reaches minimum variance at the daily minimum temperature (Mohanty et al., 1995). Therefore, measurement of the dominant soil thermal property at the point of minimum temperature variability should provide the optimal means to assessing variability in soil cover systems.

Distributed temperature sensing provides an effective means to monitor thermal properties at high spatial resolutions. Current methods to estimate thermal diffusivity have proven insufficient in elucidating spatial variations of water. Apparent thermal inertia is a lumped parameter that could be effective in assessing spatial variability of soil thermal properties related to water content, but has not been studied as a potential means of mapping water content variability in reclamation soil covers associated with the mine sector. The apparent advantages of estimating ATI using only surface temperatures are many: 1) ATI is directly related to $C_v$, which allows for at least a qualitative assessment of the distribution of water in a cover system; 2) a DTS system allows us to measure thermal properties at the high spatial and temporal resolutions required for spatial statistics; 3) measuring ATI at the surface with a DTS system does not suffer the disadvantages of remote sensing, especially atmospheric interference; and 4) measuring ATI at the surface is much easier than installing cables precisely at a known depth over large areas, thus making the technique more amenable to the mine reclamation industry. The objective of this manuscript is to assess the suitability of ATI as a means of characterizing the spatial variability of water content in unsaturated soil cover systems. The method will be compared to the currently accepted method of estimating thermal diffusivity. Each method will be assessed for repeatability and sensitivity in order to determine the method's efficacy as a means of characterizing spatial variability.

## 4.3 Theory

Thermal inertia is a key thermal parameter that modulates the ground heat flux, whether expressed at the soil surface or subsurface. In the case of vertical steady state heat flow, the soil heat flux in the subsurface, G, is proportional to the temperature gradient, and is summarized by Fourier's Law:

$$G = -\lambda \frac{dT}{dz} \quad [4.5]$$

For transient heat transfer, we must invoke the principle of energy conservation, which states that in the absence of any energy source or sink, the time rate of change in heat content of a given volume must equal the change in flux over a given distance (van Wijk and de Vries, 1963; Hillel, 1998):

$$C_v \frac{\partial T}{\partial t} = -\frac{\partial G}{\partial z} \quad [4.6]$$

Inserting Eq. 4.3

$$C_v \frac{\partial T}{\partial t} = \frac{\partial}{\partial z}\left(\lambda \frac{\partial T}{\partial z}\right) \quad [4.7]$$

Thermal inertia can be estimated from soil temperature transients by solving Eq. 4.7 with Eq. 4.1 as the surface boundary condition. Equation 4.7 can be solved numerically, but it is possible to simplify Eqs. 4.1 and 4.7 so that an analytical solution can be determined (Price, 1985). Assuming a sinusoidal variation in surface temperature with time and the following boundary conditions (Arya, 2001, Novak, 2005):

$$T(t,0) = \bar{T} + |T|_0 \sin(\omega t + \phi_0) \quad [4.8]$$

$$T(t,\infty) = \bar{T} = constant \quad [4.9]$$

where is the mean temperature, $|T|_0$ is the temperature amplitude at z = 0, $\omega = 2\pi/P$, is the angular frequency where P is the period in question (in this case a day [86,400 s]), and $\phi_0$ is the

phase at z = 0. The implicit assumption in Eq. 4.8 is that below a certain depth where temperatures remain constant, there is no net flux into the overlying volume. The solution to Eq. 4.7 then becomes (Novak, 2005):

$$T = \bar{T} + |T|_0 exp(-z/d)\sin[(\omega t + \phi_0 - z/d)] \quad [4.10]$$

where $d = \sqrt{(P\alpha/\pi)}$ is the damping depth. The phase lag relative to the surface wave increases with depth such that the depth of full phase reversal of the temperature wave is given as $z=\pi d$ (Arya, 2001). Typical values for d range from 0.1 m for a dry sandy soil, 0.07 m for a dry clay soil, and 0.05 m for a dry peat. Depths of phase reversal typically range from 0.25 to 0.22 to 0.16 m for a dry sand, clay, and peat soil, respectively.

An analytical solution for the heat flow density can also be found and when assuming uniform and constant properties and water content with depth is given as (de Vries, 1975):

$$G(t,z) = -\lambda \partial T/\partial z = |T|_0(\lambda C_v \omega)^{1/2} e^{-z/d}\cos(\omega t - z/d + \pi/4) \quad [4.11]$$

and for z = 0 we have:

$$G(t,0) = |T|_0(\lambda C_v \omega)^{1/2}\cos(\omega t + \pi/4) \quad [4.12]$$

where $(\lambda C_v \omega)^{1/2}$ is multiplied by $|T|_0\omega^{1/2}$ to obtain the amplitude of the surface heat flux density, which is equivalent to the thermal inertia.

From Eqs. 4.11 and 4.12 we see how soil temperature, TI, and G are related. Finally we arrive at a method to estimate transient surface temperature originally formulated by Brunt (1932) to calculate the drop in surface temperature on clear calm nights (van Wijk and de Vries, 1963):

$$T(t,0) = \frac{G[4\alpha(t - t_0)]^{1/2}}{\lambda \pi^{1/2}} \quad [4.13]$$

It has previously been reported by Ten Berge and Stroosnijder (1987) that daytime variations in surface temperature are dominated by properties such as albedo and roughness

length during the day, while thermal soil properties, expressed using thermal inertia, dominate surface temperature at night. Therefore, the ideal form of TI for the measurement of soil thermal property variability will be one taken at the surface that only incorporates temperature readings taken between sunset and sunrise. Assuming that on clear, calm nights that H and LE are 0, and that G is equivalent to the net radiative loss at the soil surface we can use a manipulated version of Eq. 4.13 to estimate the Apparent Thermal Inertia (ATI). The assumption of low H and LE are reasonable give the predominance of stable atmospheric profiles on calm, clear nights. As stability increases, convective heat transfer above the soil surface is diminished, and the dominant heat transfer mechanism becomes radiation (Buchan, 2005). The derivation of Eq. 4.13 used in remote sensing is given by Verhoef (2004) as:

$$ATI = \sqrt{C_v \lambda} = \frac{2|R_n| \cdot \sqrt{\Delta t}}{\Delta T_s \cdot \sqrt{\pi}} \quad [4.14]$$

where $R_n$ is the overnight net radiation measured at the soil surface, $\Delta t$ (s) is the time between sunset and sunrise taken from the point at which solar radiation readings pass through zero, and $\Delta Ts$ is the change in surface temperature between sunset and sunrise.

## 4.4 Materials and Methods

### 4.4.1 Method Development

#### 4.4.1.1 Water Content

We must first demonstrate that ATI is sensitive to changes in $\theta_v$ if ATI is to be useful as a means of qualitatively examining the distribution of water. Recall from Eq. 4.12 that diurnal variations in surface temperature are directly related to the surface soil heat flux, $G_0$, through TI (de Vries, 1975; Price, 1985; Wang and Bras, 1999). Estimation of TI from surface temperature measurements is possible when simultaneous measurements of G are made (Wang et al., 2010). In the absence of measured G an alternate expression that relates soil surface temperature to a

balance of available energy fluxes at the surface was given by Watson (1975) and in a modified linearization by Price (1985) is given as:

$$T(t,0) = T_{sky} + SV(1-a) \times \sum_{n=1}^{\infty} \frac{C_n \cos(n\omega t - \phi_n)}{\left[n\omega\left(\sqrt{C_v\lambda}\right)^2 + B^2/n + B\sqrt{C_v\lambda}(2\omega)^{1/2}\right]^{1/2}} \quad [4.15]$$

where $T_{sky}$ (°C) is the radiative temperature of the sky, S is the solar constant, V is atmospheric transmittance to solar radiation (V ~ 0.75), a is albedo, ω and φ are defined above, and B and C are linearization coefficients that are defined in Price (1985). For the purposes of this study, B and C were solved as fitting parameters. An example of how temperature is affected by ATI is demonstrated using Equation 4.15 and Figure 4.1. Given that the specific heat of water is nearly twice as large as that of mineral soil, and the negligible contribution to total heat capacity of the air components, the volumetric heat capacity, $C_v$, of a soil is largely controlled by soil water content, $\theta_v$ ($cm^3\ cm^{-3}$) (Hillel, 1998). Therefore, ATI will be largely influenced by $\theta_v$ and ρ (Matsushima et al., 2012). Soil surface temperature responses are increasingly attenuated for a given radiative as ATI increases through a reasonable range of 500 to 2000 J $m^{-2}\ K^{-1}\ s^{-1/2}$, corresponding to an increase in $\theta_v$ from 0.10 $cm^3\ cm^{-3}$ to saturation for a silty loam sand (Matsushima et al., 2012), or from 0.20 to 0.60 $cm^3\ cm^{-3}$ for a peat soil (Figure 4.1).

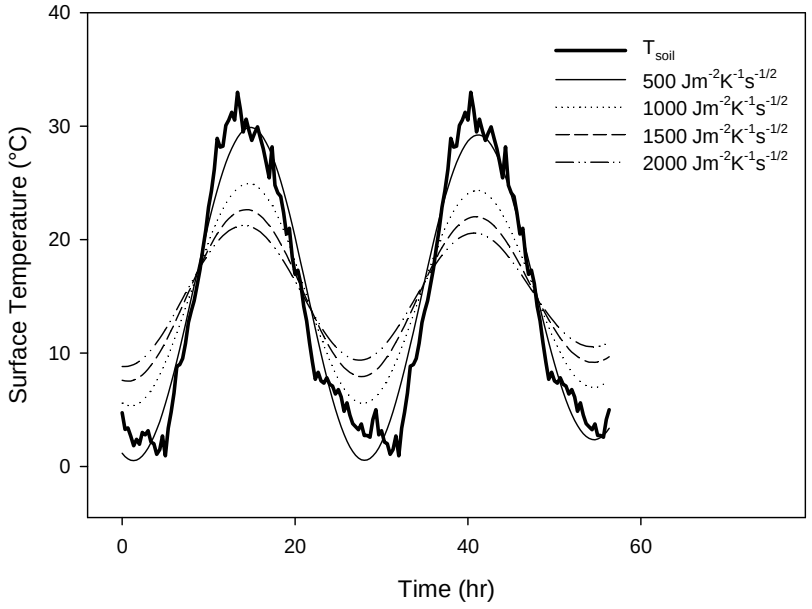


Figure 4.1. Measured and modeled (Eq. 4.15) diurnal soil surface temperature ($T_{soil}$) in response to varying thermal inertia (J $m^{-2}$ $K^{-1}$ $s^{-1/2}$).

4.4.1.2 Depth

The method for estimating ATI as presented by Verhoef (2004) represents an aggregation of subsurface soil thermal properties expressed at the soil surface. When measuring ATI at the soil surface it will be useful to know the depth over which surface ATI measurements are integrated. For diurnal measurements, the damping depth, d, will become important as this will be the depth over which daily temperature waves will penetrate. Watson (1975) suggested that damping depth would provide a reasonable estimate of the depth over which ATI was aggregated as changes in ATI were not readily detected below 10 cm. A numerical study on the depth to which changes in thermal inertia are important was given by Price (1985). It was shown graphically that for a two-layered soil with variable ATI, changes in TI below 5 cm could not be detected at the surface (Price, 1985).

Analytical solutions comparing a homogeneous soil to a two-layered system with variable subsurface ATI were given by van Wijk and Derksen (1963). For the preliminary case we assume that ground heat flux at the surface, $G_0$, is equivalent for a homogeneous and two-layered soil under equal meteorological conditions. The ratios of the amplitude of subsurface soil temperature in a homogeneous layer to that of a layered soil at depth, z, is given as (van Wijk and Derksen, 1963):

$$\frac{A_l(z)}{A_h} = \left[\frac{\lambda_2 C_{v_2}}{\lambda_1 C_{v_1}} \frac{e^{-2z/d_1}[1 + {r_l}^2 + 2r_l]}{1 + {r_l}^2 e^{-4z/d_1} - 2r_l e^{-2z/d_1}\cos(2z/d_1)}\right]^{\frac{1}{2}} \quad [4.16]$$

where the subscripts l, h, 1, and 2 refer to the layered and homogeneous soils, and the upper and lower layers in the layered soil, respectively, and z is the layer thickness (m). Van Wijk and Derksen (1963) refer to $r_l$ as an "auxiliary variable" and define it as:

$$r_l = \frac{\sqrt{\lambda_1 C_{v_1}} - \sqrt{\lambda_2 C_{v_2}}}{\sqrt{\lambda_1 C_{v_1}} + \sqrt{\lambda_2 C_{v_2}}} \quad [4.17]$$

which has also been referred to as the "thermal reflection coefficient" by Karam (2000).

The relationship given in Eq. 4.16 describes the temperature amplitude wave in the lower layer of a layered soil, relative to a homogeneous soil. For any combination of the depth of the upper layer, z, and the daily damping depth, d, the temperature amplitude will penetrate based on the disparity of the thermal inertia between the two layers. In this way, $\sqrt{(C_v \lambda)}$, or thermal inertia will act as a contact coefficient (van Wijk and Derksen, 1963). The relationship is shown graphically in Figure 4.2.

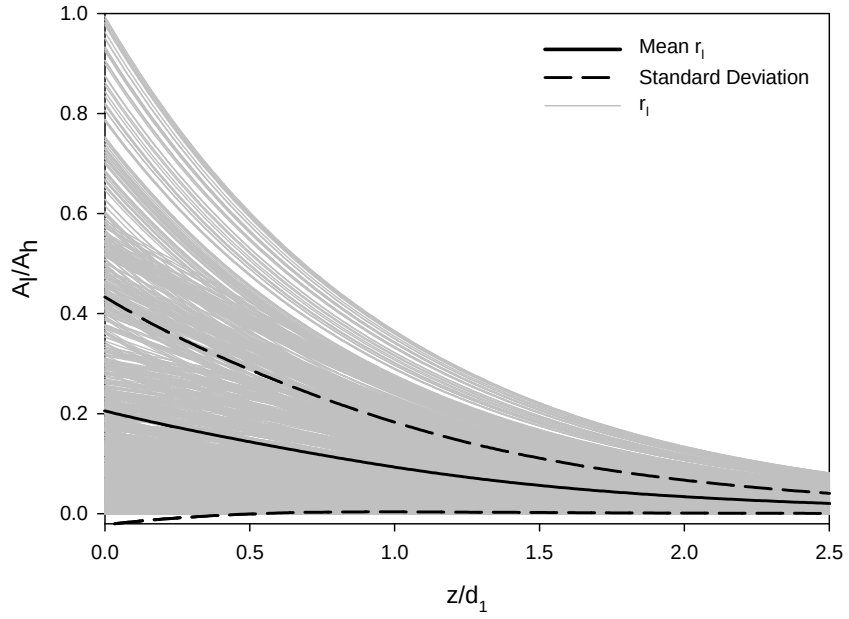


Figure 4.2. Temperature amplitude ratio in the lower layer of a layered soil as compared to a homogeneous soil. Grey lines are realizations of random combinations of $r_l$, the layer contact coefficient, and $\sqrt{((\lambda_2 [\![C_v]\!]_2)/(\lambda_1 [\![C_v]\!]_1))}$, the relative thermal inertia between two layers. The solid and dashed black lines represent the mean and one standard deviation resulting from 1000 random realizations of Eq. 4.16.

An explanation of Figure 4.2 is warranted. Two soil profiles of otherwise identical properties with the exception that one is homogenous with respect to thermal inertia and the second comprises two layers of thermal inertia due to differences in water content. The upper layer is identical to the homogeneous profile, and the lower differs from the upper layer. The difference between the upper and lower layer is described by the contact coefficient and varies from 0 to 1. When $r_l = 0$, then $\lambda_1 = \lambda_2$ and $C_{v1} = C_{v2}$ and the layered soil becomes homogeneous with respect to thermal properties. The temperature amplitude ratio then becomes 1 and the temperature wave is fully transmitted to the same depth as a homogeneous soil. When $r_l = 1$, meaning a high contact coefficient between the two layers, the upper layer is a poor conductor of heat and the temperature wave is fully contained in the upper layer. Thus $A_{l(z)} / A_h = 0$, and no

part of the temperature wave is transmitted beyond the upper layer (van Wijk and Derksen, 1963). Therefore, for soils where the majority of the daily temperature wave is restricted to a layer near the surface, we can assume that only a small portion of the temperature wave is transmitted to lower depths.

4.4.3.1 Calculation of Apparent Thermal Diffusivity

Thermal diffusivity was calculated to facilitate a comparison between thermal inertia and the current standard parameter for use in analyzing thermal properties. Several methods exist to calculate thermal inertia and are summarized by Horton and Wierenga (1983). The purpose of the present investigation is to assess the spatial variability of the thermal properties rather than the accuracy of the diffusivity estimate itself. Since the spatial variable is depth the simple Amplitude method from Horton and Wierenga (1983) was chosen as it relies on the amplitude decay between two depths and only requires that temperatures at two depths to be known. The amplitude method (Horton and Wierenga, 1983) is given by:

$$\alpha = \frac{\omega}{2}\left[\frac{z_2 - z_1}{\ln A_1/A_2}\right]^2 \qquad [4.18]$$

where ω is the radial frequency equal to 2π/P with P being the day length period (86,400 s), $A_1$ (°C) is the temperature amplitude at depth $z_1$ (m), and $A_2$ is the temperature amplitude at depth $z_2$ . Temperatures at 0 and 0.10 m were used in the calculation of apparent thermal diffusivity.

The preferred method for calculating thermal inertia is to examine the apparent thermal inertia (ATI) at the soil surface, as given by Eq. 4.14 (Verhoef, 2004). Calculation of ATI requires collocated net radiation measurements to maximize the location specific nature of DTS

measurements. Net radiation at night is equal to the balance of incoming and outgoing long wave radiation, and is given by (Arya, 2001):

$$R_n = R_L = R_{L\downarrow} + R_{L\uparrow} \quad [4.19]$$

where:

$$R_{L\downarrow} = \varepsilon_{eff} F \sigma T_{air}^4 \quad [4.20]$$

$$R_{L\uparrow} = \varepsilon_{soil} \sigma T_{soil}^4 \quad [4.21]$$

where $R_{L\downarrow}$ and $R_{L\uparrow}$ (W m$^{-2}$) are the incoming and outgoing long wave radiation, respectively $\varepsilon_{eff} = \varepsilon_{cs}F$ (-) is the effective emissivity of the sky, $\varepsilon_{soil}$ (-) is the emissivity of the soil, F is a cloud factor (always ≥1), σ the Stefan-Boltzmann constant ($5.67 \times 10^{-8}$ W m$^{-2}$ K$^{-4}$), and $T_{air}$ and $T_{soil}$ (K) the absolute temperature of the air and soil surface, respectively.

Clear sky emissivity, $\varepsilon_{cs}$, was calculated using (Brutsaert, 1975):

$$\varepsilon_{cs} = k \left( \frac{e_a}{T_{air}} \right)^{\frac{1}{m}} \quad [4.22]$$

where k and m are defined by Brutsaert (1975) as 0.642 and 7, respectively. Near surface vapour pressure (Pa) is given as:

$$e_{a\,(kPa)} = \left( \frac{RH}{100} \right) e_s \quad [4.23]$$

and the saturated vapour pressure, $e_s$ (Pa) can be found using air temperature using the Tetens (1930) formula and the coefficients provided by Buck (1981) for pure water from -20 to 50 °C (Hatfield and Baker, 2005):

$$e_{s(kPa)} = 0.61151\ exp\left( \frac{17.502 T_{air}}{T_{air} + 240.97} \right) \quad [4.24]$$

As can be seen from equations 4.22 through 4.24, net radiation at night becomes a function of the air temperature, soil surface temperature, and relative humidity. Note that because

outgoing long wave radiation requires surface temperatures, only the 215 m of the transect covered with the Surface cable could be used in the analysis. Apparent thermal inertia was then calculated using net radiation calculated using the Surface cable, and the change in soil temperature measured at 0 cm.

4.4.3.2 Calculation of Damping Depth

The utility of using a DTS system to characterize the variability of soil thermal properties in a cover system lies in taking reliable measurements that do not depend on precise depth measurements. Measurements of soil thermal properties at the surface are facilitated by using the ATI expressed at the soil surface as an aggregate of subsurface processes. The use of Eq. 4.14 is then justified by calculating a damping depth, d, and comparing the result to the depth over which it was taken, x. By then comparing the x/d to Figure 4.2, we can develop an understanding of whether a surface measurement is justified for calculating an ATI.

From Eq. 4.10 we see that the amplitude of the temperature wave, $|T|_0$, decreases exponentially with depth (Arya, 2001):

$$A = |T|_0 \exp(z/d) \quad [4.25]$$

or

$$\ln A = \ln|T|_0 - \frac{z}{d} \quad [4.26]$$

A plot of lnA as a function of z should result in a straight line with a slope of -1/d. The slope of the best fit line through the amplitude data will reveal an estimate of the damping depth (Arya, 2001).

### 4.4.2 Site Description

The field study site was an oil sands reclamation cover site 63 km north of Fort McMurray, in the oil sands region of northern Alberta, Canada (57.33°N, 111.53°W, 326 m a.s.l.). Long term climate normals for Fort McMurray (1971-2000) were classified as sub-humid continental and showed daily mean temperatures of -18.8 and 16.8 °C for January and June, respectively, while precipitation normals were 456 mm, 342 mm occurring as rainfall (Carey, 2008). The reclamation trial consisted of 36, 1 ha plots comprising 12 treatments of different cover layering configurations. The waste material consisted of a mix of mining overburden and lean oil sand that contained bitumen that was not economical for recovery. The measurement transect used in this study covered two adjoining plots with a cover that consisted of 15 cm of peat overlying at least 70 cm of clean sand (Figure 4.3). The two plots were sloped down, away from each other, at a slope of 2% such that each plot had a predominantly eastern or western facing aspect.

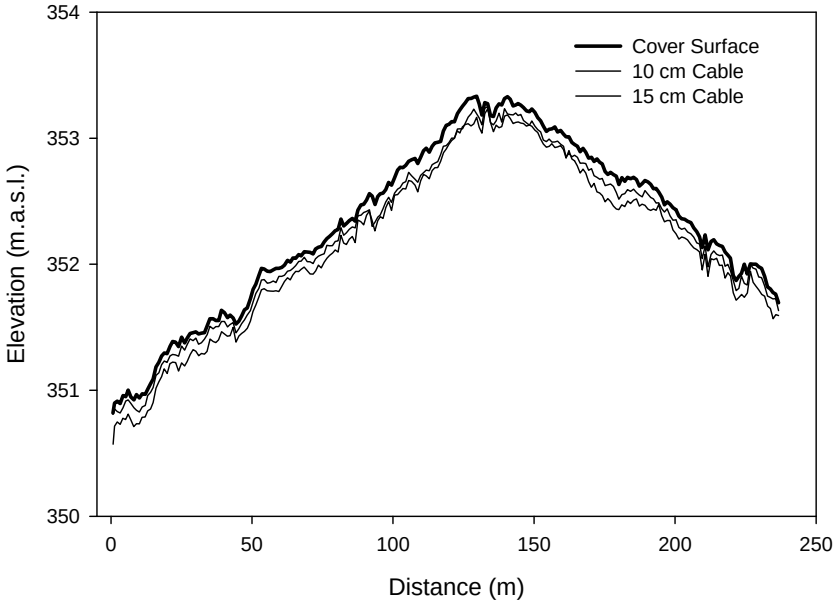


Figure 4.3. Cross section of the cover system experimental transect. Top line denotes cover surface and location of the Surface and 0 cm cable. Middle line denotes location of the 10 cm cable. Bottom line denotes location of the 15 cm cable. Note that cover material depths are exaggerated for display purposes.

### 4.4.3 Experimental Set-Up

Soil temperature in the peat layer was measured using a DTS system. An Oryx (Sensornet, United Kingdom) system was used in this study and has a manufacturer reported temperature resolution of 0.5 °C at integration times of 60 s. The system can spatially monitor fibre optic cables up to 5000 m in length with a measurement resolution of 1 m and a spatial resolution of 2 m. Measurement resolution is defined as the resolution at which the reader is capable of taking readings, while spatial resolution is defined as the distance over which the system can resolve from 10 to 90% of a step change in temperature.

A 236 m long transect was excavated to 15 cm in the surface peat layer. A single, black, 7.5 mm diameter BRUclean 150 cable (Brugg Cables, Switzerland) was laid in the base of the

trench (east to west), and the trench was backfilled to a depth of 10 cm. The cable was then laid back along the same trench in the opposite direction (west to east) and backfilled again. A third run was laid at the surface (east to west) and covered with only enough peat so as to not expose the cable directly to the atmosphere and is referred to as the 0 cm cable. Finally, the remaining cable was laid (west to east) directly on the surface of the cover. The cable laid directly on the surface was referred to as the Surface cable. The depths of the cables were taken as nominal depths, and the cable was surveyed at 1 m intervals to confirm final depth. In total, 1000 m of cable was laid, including 60 m reserved for immersion in a calibration ice bath, and 236 m for the 15, 10, and 0 cm depths, with 215 m of cable laid on the surface. The remaining 17 m was taken up in buried loops at the ends of the transect to provide a thermally distinct area to aid in data interpretation. An important point to note is that the peak of the transect was a road used for vehicle access. Each cable run was buried under the access road to avoid cable damage. Therefore, at the peak of the transect there is a 14 m zone where temperatures do not reflect the surrounding configuration.

Distributed temperature measurements were calibrated by comparing the 60 m length of cable at a constant temperature with a known temperature. It should be noted that the calibration was carried out using a single calibration bath that was not constantly mixed, as is suggested by others (Hausner et al., 2011; Van de Giesen et al., 2012), thus introducing potential sources of error and data noise. Independent temperature readings were taken with two PT-100 platinum thermistors, which provide the accuracy bias for the temperature calibration. The accuracy of the PT-100 has been reported as 0.055 °C; therefore, the absolute accuracy of the measurement cannot exceed this value (Tyler et al., 2013). The precision of the Oryx was assessed in terms of both spatial and temporal repeatability. Spatial repeatability describes the standard deviation of a

set of consecutive measurements over a length of cable at a constant temperature (Tyler et al., 2009). Temporal repeatability refers to the standard deviation of the temperature measurement for a single point over time. The spatial standard deviation was 0.17 °C, and the temporal standard deviation was 0.03 °C. The spatial standard deviation was higher than the highest value reported by Tyler et al. (2009) of 0.08 °C, yet was lower than the 0.4 °C reported by Ciocca et al. (2012). The temporal standard deviation for this study compared well with those reported by Tyler et al. (2009), which were 0.08, 0.13, and 0.31 °C. Temperature data were collected with the Oryx every 20 minutes with a 60 s integration time. Data were collected continuously over four periods in 2012: May 22 to June 6, June 18 to 22, July 2 to July 7, and July 18 to 23.

An automated meteorological station was situated nearby as part of the reclamation trial monitoring system. Air temperature (°C) and relative humidity (%) were measured jointly with an HMP45C212 temperature and humidity probe (Vaisala, Finland), net radiation ($Wm^{-2}$) was measured with an NRLITE2 net radiometer (Kipp & Zonen, The Netherlands), incoming and outgoing short wave radiation ($Wm^{-2}$) were measured with a CMP3 pyranometer (Kipp & Zonen, The Netherlands) , wind speed and direction were monitored with a 05103-10 Wind Monitor (R.M. Young, United States), and precipitation (mm) was measured with a TE525 Rain Gage (Texas Electronics, United States). Data were output every 20 minutes and rainfall was recorded as a unique event for every 0.25 mm bucket tip.

A vertically instrumented cover system profile was monitored to provide point source measurements of volumetric water content, temperature, and matric potential during the experiment. Volumetric water content was measured with CS 616 water content reflectometers (Campbell Scientific, Canada). Soil temperature and matric potential were measured jointly using CS 229 heat dissipation water matric potential sensors (Campbell Scientific, Canada).

Sensors were placed in pairs at depths of 5, 15, 25, 35, 55, 85, 115, and 145 cm. Only the measurements taken in the 30 cm peat layer at 5 and 15 cm were of interest for the purposes of this experiment. Measurements were collected every 4 hours for a total of 6 measurements daily.

Bulk density and thermal properties of the peat were measured every metre along the DTS transect. Bulk density was measured using by carefully inserting a steel ring of known volume into the surface of the soil to minimize compaction. The soil core was trimmed at the open end of the ring and then transferred to a sample bag. The samples were then oven dried to determine gravimetric water content, and bulk density. Thermal diffusivity, $\alpha$ ($m^2\ s^{-1}$), and volumetric heat capacity, $C_v$ (MJ $m^{-3}\ K^{-1}$) were measured using dual probe heat pulse methods described by Bristow (2002). Thermal conductivity (W $m^{-1}\ K^{-1}$) was then calculated from the product of $\alpha$ and $C_v$.

### 4.4.4 Evaluation of Thermal Property Estimation Methods

The objective of the field experiment was to compare the suitability of using ATI as a means of describing spatial variability as opposed to the more generally accepted method of using $\alpha$. It must be stressed again that the experiment was an examination of spatial uncertainty, and not an examination of the accuracy with which the true value of either ATI or $\alpha$ is calculated. Two questions were then asked of the estimations to address the spatial uncertainty: a) is the property repeatable? and; b) is the property spatially sensitive? In terms of repeatability, we must know whether estimation of the parameter can reliably and repeatedly reproduce a known feature (Goovaerts, 1997). In the case of the current field experiment, the test section was the zone in which the cables were buried under the access road for protection for vehicular traffic. In terms of sensitivity, an error propagation analysis was conducted using sequential perturbation to assess the uncertainty in the overall (ASME, 2005).

## 4.5 Results and Discussion

### 4.5.1 Damping Depth

The utility of using surface temperature measurements to estimate ATI is increased if it is determined that temperature fluctuations are confined to near-surface soil layers. Surface-normalized temperatures measured in the subsurface were never greater than 40% of those measured at the surface (Figure 4.4). Temperature fluctuations were largely confined to a layer near the surface. Damping depths were estimated using Eq. 4.26 and averaged 0.07 m (Figure 4.5). While there was some variability in installation depth of the 10 cm cable, the majority of the cable was installed below the daily average damping depth. When comparing average layer depth of 0.095 m and an estimated damping depth of 0.07 m, and conferring with Figure 4.2 we would expect to find a maximum temperature amplitude ratio of approximately 0.3 and an average of approximately 0.075. Recall that temperature amplitude ratios close to zero indicate rl values approaching 1. An $r_l$ value approaching 1 is indicative of a surface layer that is a poor conductor, in which the majority of the daily temperature change takes place. It is thus reasonable to expect that only a small portion of the temperature wave would be transmitted to the lower layer. Therefore, for the purposes of this study, we will assume that the bulk of the daily heat transfer processes occurred above the subsurface cables, and can be adequately captured by the 0 cm cable through an estimate of ATI.

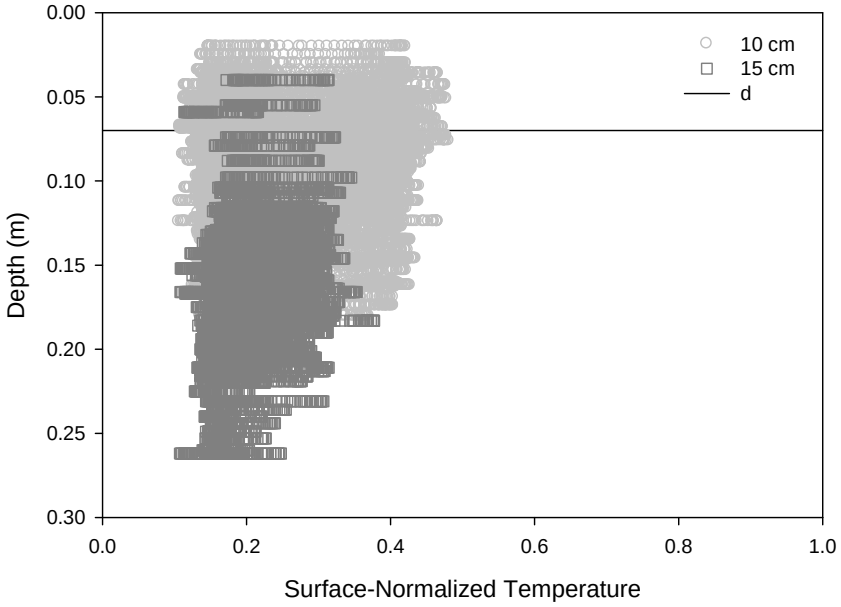


Figure 4.4. Temperature amplitude as a function of depth for all measurement locations on July 20, 2012.

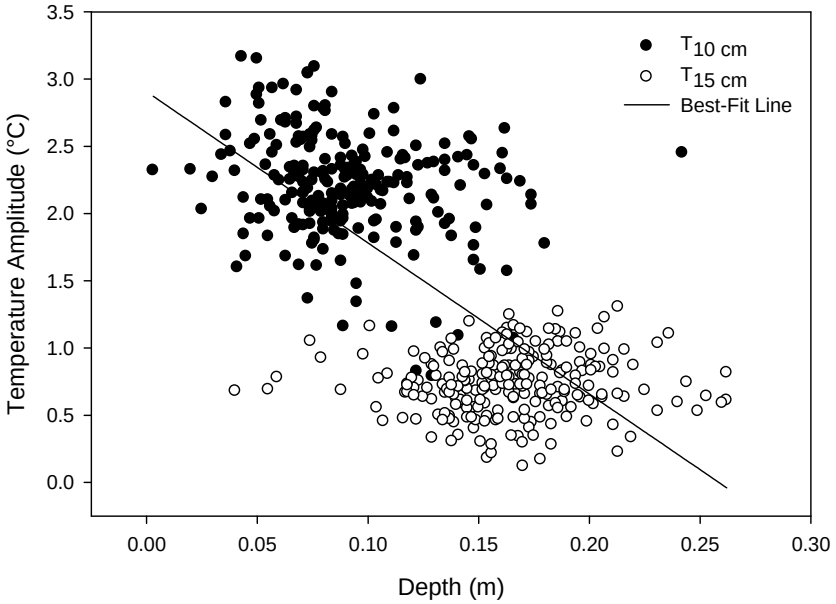


Figure 4.5. Temperature amplitude as a function of depth showing the best-fit line used to calculate damping depth from Equation 4.26.

#### 4.5.1.1 Initial Screening

Selection of candidate days suitable for thermal inertia analysis underwent initial screening based on soil temperatures and climatic conditions. Distributed soil cover temperatures were monitored from May to July, 2012 (Figure 4.6). Corresponding air and soil temperatures measured at the 200 m point are shown in Fig. 4.7. Although air and soil temperatures in late May were similar to those measured in June and July, the relationship between air temperature and relative humidity showed a clear distinction between spring and summer periods (Figure 4.8). The two periods were distinctly different in terms of their response to near surface meteorological conditions. In order to best facilitate a consistent comparison between days, only measurements taken after 1 Jun. 2012 will be considered.

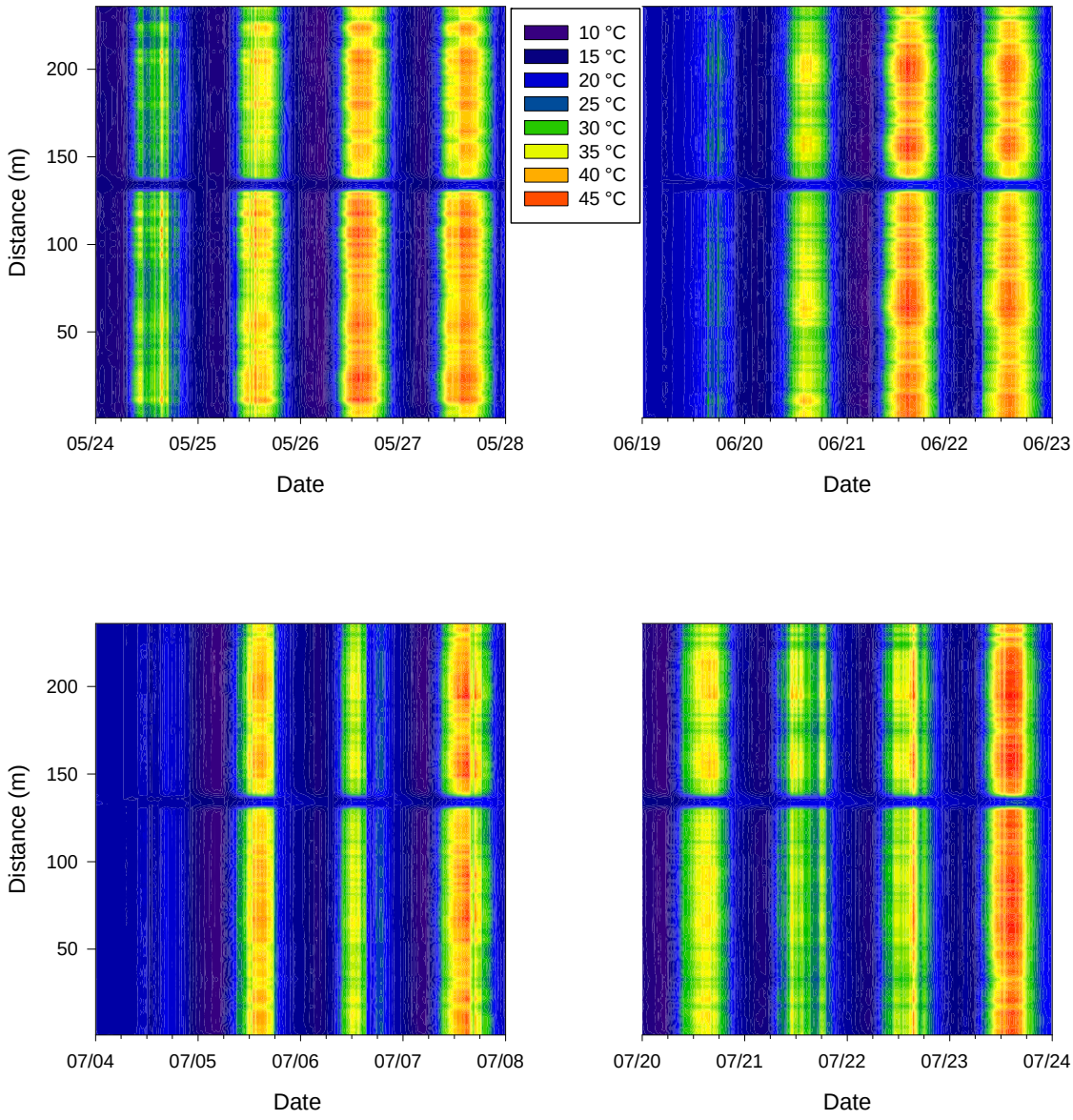


Figure 4.6. Temperature contour measured at 0 and 10 cm on a) 24 to 28 May; b) 19 to 22 Jun.; c) 4 to 7 Jul. and; d) 19 to 23 Jul. 2012.

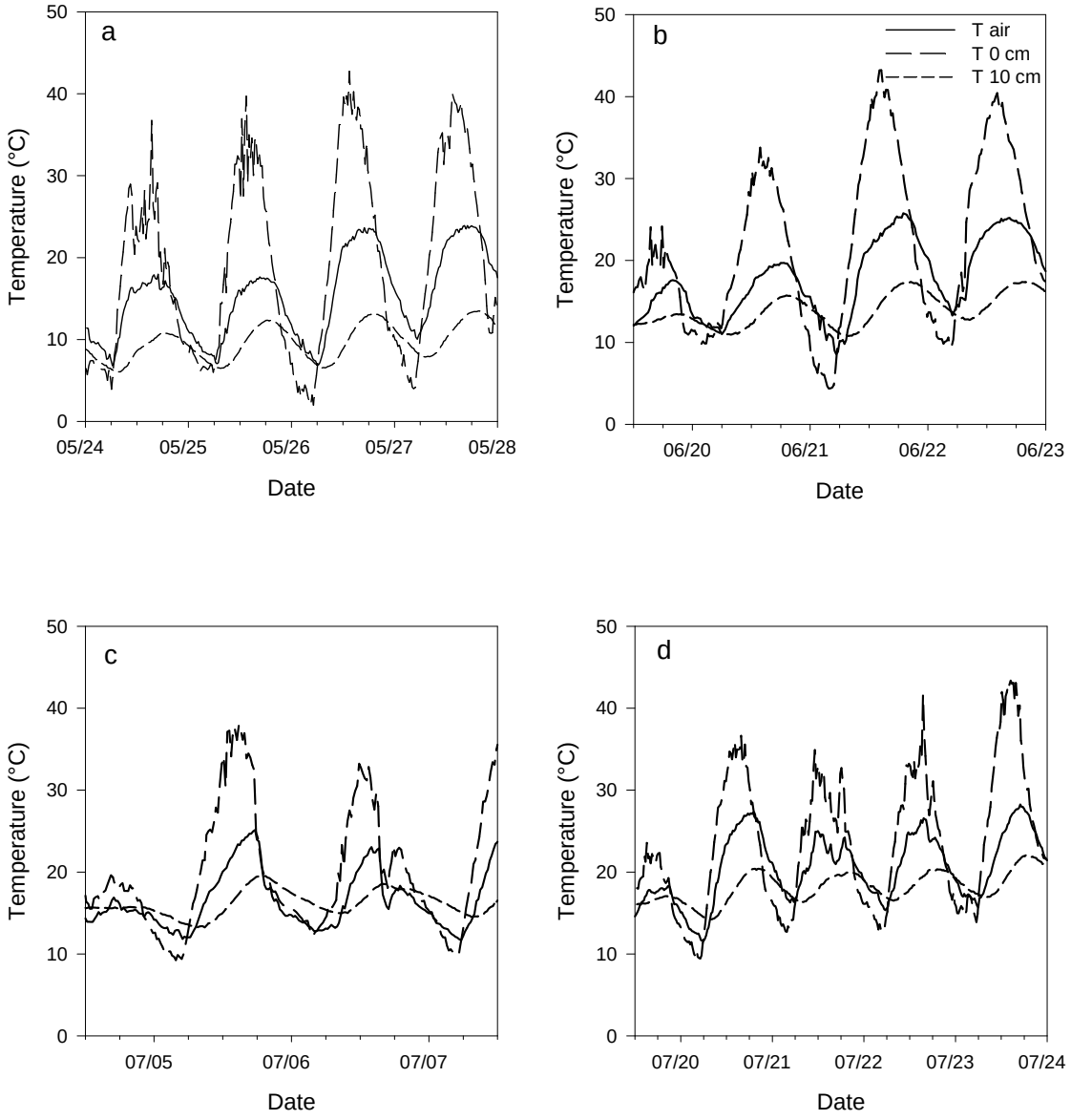


Figure 4.7. Air temperature and soil temperature measured at 0 and 10 cm on a) 24 to 28 May; b) 19 to 22 Jun.; c) 4 to 7 Jul. and; d) 19 to 23 Jul. 2012.

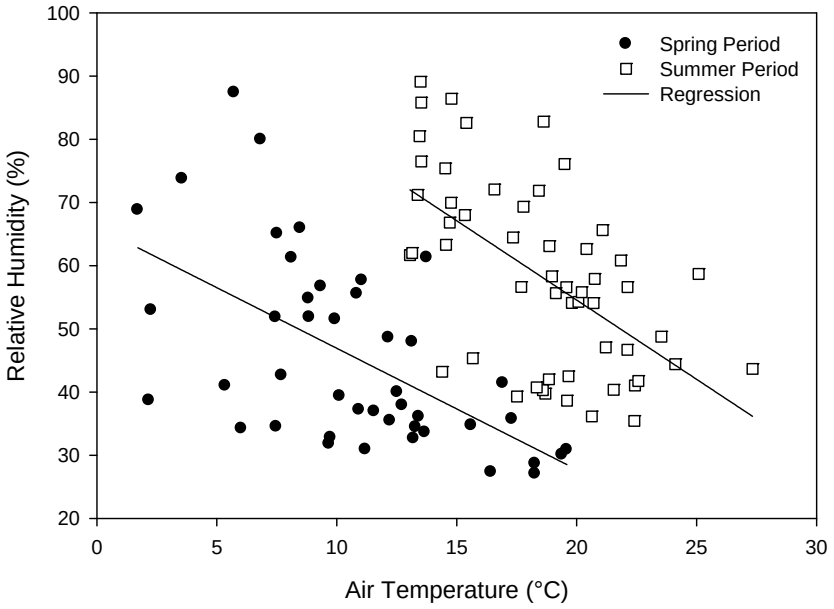


Figure 4.8. Relationship between air temperature and relative humidity for the spring period (1 Apr. to 31 May) and the summer period (1 Jun. to 31 Jul.).

According to Eq. 4.14, a certain set of meteorological criteria must be satisfied. The process for selection of candidate days from the full data set is outlined below. The July 19 to July 24, 2012 measurement period was used as an example.

Cloud cover was not monitored at the meteorological station. Whether a night was clear or not was determined semi-qualitatively using two means. The first was to examine the net radiation profile as measured at the meteorological station. Net radiation on nights beginning on July 20 and 23, 2012 exhibited smooth profiles, while $R_n$ profiles on the remaining days were noisy, indicating periodic cloud cover (Figure 4.9). Nights beginning on July 21 and 22 were reserved for possible inclusion due to the high radiative input during the day and smooth nighttime $R_n$ profile. July 19 and 24 were rejected at this point due to high variability in $R_n$ profiles, and low overall radiative input, indicating cloud cover. The overnight temperature difference between the Surface and 0 cm cable at the 200 m point were then calculated (Figure

4.9). Overnight temperature differences were negative, indicating a lower Surface temperature, as would be expected. Temperature differences on nights beginning on July 20 through 23, 2012 reached a distinct minimum, suggesting that the soil cover was radiating energy into a clear sky, while the 0 cm cable was still receiving energy from the soil below.

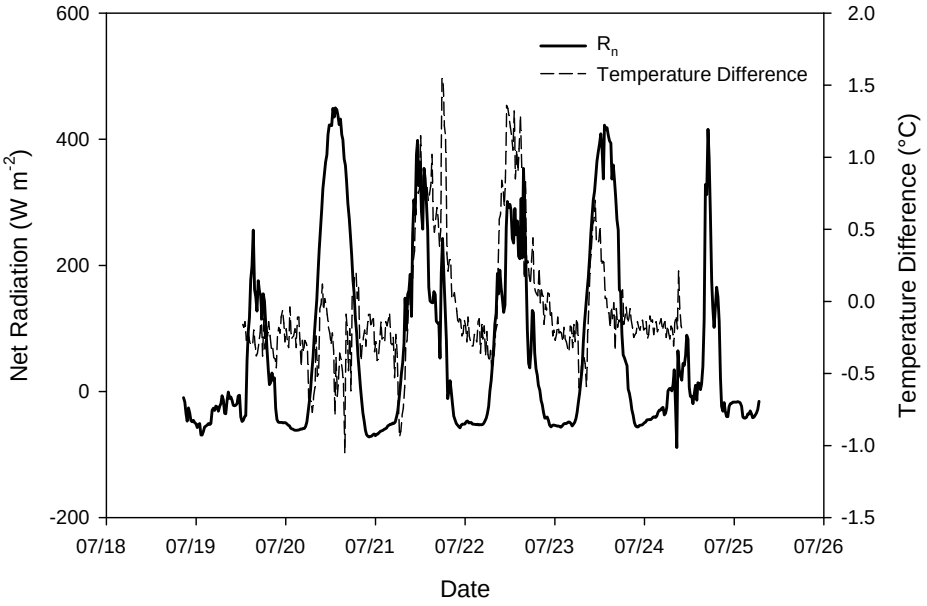


Figure 4.9. Net radiation ($R_n$) measured at the meteorological station and temperature differences between the Surface and 0 cm cable for the July 19 to July 24 period.

Once potential candidate days were screened for cloud cover, their further suitability was assessed based on overnight temperature time series and overnight wind speed (Figure 4.10). Calculation of ATI is based on overnight temperature differences; as such the temperature time series must exhibit a clear and definite minimum. Using the temperature time series at the 200 m point in the cover system, it is clear that July 22 and 23 were rejected. Overnight wind speeds on the potential remaining candidate days were then considered. Overnight wind speeds on nights beginning on July 20 and 21 averaged 1.9 and 1.4 $ms^{-1}$, respectively, and both reached minima of 0.7 $ms^{-1}$. Average overnight wind speed for the night beginning on July 24 was 6.9 $ms^{-1}$;

therefore, it was rejected. This process of elimination left July 20 and 21 as the candidate days for estimation of ATI from this measurement period.

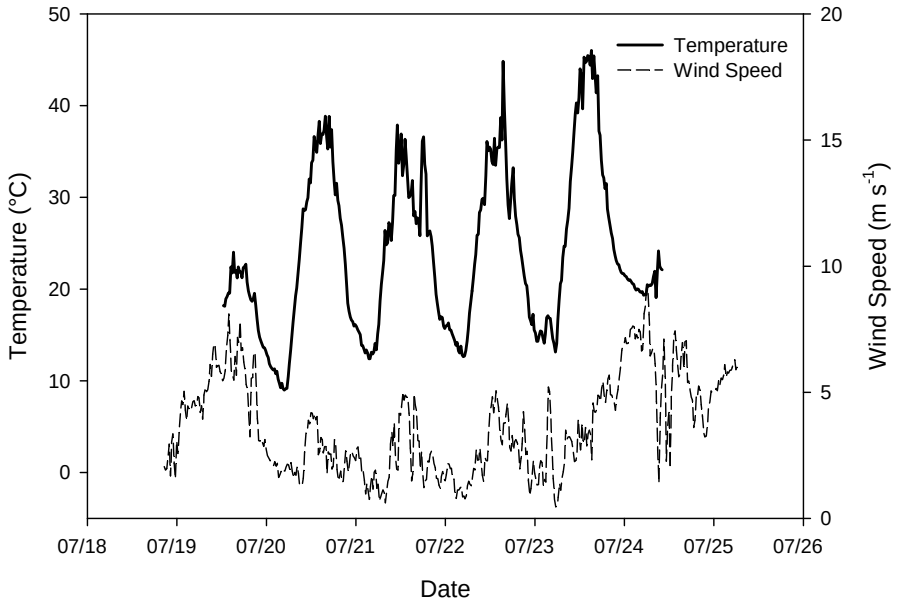


Figure 4.10. Surface temperature and wind speed time series measured from July 19 to July 24.

The following dates were chosen as candidates for estimation of ATI from the original dataset: June 20 and 21, July 5 and 6, and July 20 and 21, 2012. The three sets of candidate days could then be grouped according to the average matric potential measured for that day at the point source monitoring station (Table 4.1). Volumetric water content was not used to group the candidate days because the measurements showed variation of less than 0.01 $cm^3$ $cm^{-3}$ between days. Although differences in matric potential also appear to be small, it is important to recall the unique properties of peat, where 10 kPa represents an irreversible threshold for plant establishment (Thompson and Waddington, 2013). Examination of the field-derived soil water characteristic curve demonstrates that the range of water contents in which the peat experiences wetting and drying is low, thus making relatively small changes in matric potential of 1 kPa of

greater importance (Figure 4.11). Note that the field-derived soil water characteristic curve was developed by plotting the responses of a matric potential sensor and a water content sensor that were collocated at the same depth.

Table 4.1. Average daily matric potential for each candidate day

| Date | Average Matric Potential (kPa) |
|---|---|
| 20 Jun. 2012 | -7 |
| 21 Jun. 2012 | -9 |
| 5 Jul. 2012 | -1 |
| 6 Jul. 2012 | -3 |
| 20 Jul. 2012 | -2 |
| 21 Jul. 2012 | -4 |

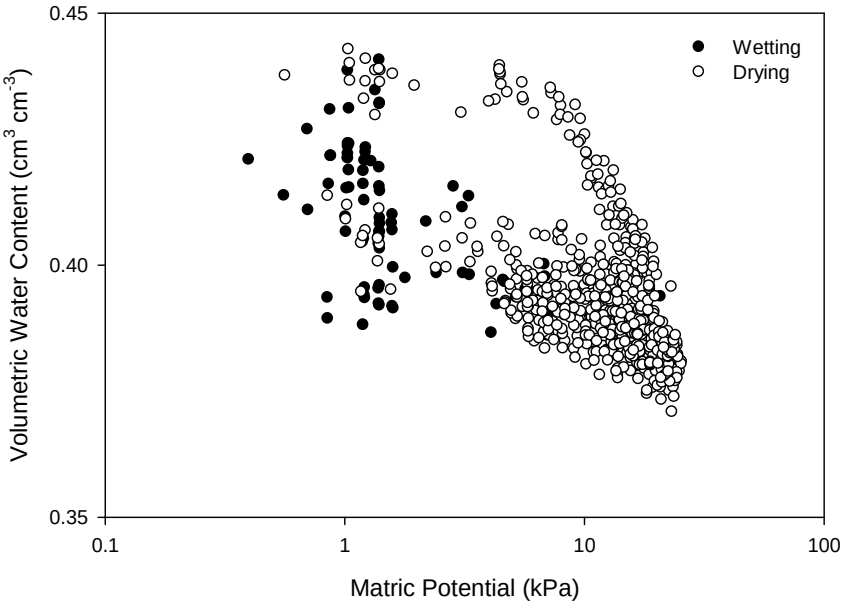


Figure 4.11. Field-derived soil water characteristic curve for the cover system peat material.

### 4.5.2 Thermal Inertia

Spatially distributed ATI was calculated for the two wetted periods and the two dry periods (Figure 4.12). The most prominent feature occurs at 126 to 140 m, and represented the portion of the transect where both the Surface and 0 cm cable passed underneath the access road. The feature is repeatedly and reliably estimated using ATI, which is unsurprising, given the large change in thermal regimes between the surface and depth. Although not a stringent test, the ability to represent known features within a field provides confidence that less obvious features will be reliably represented (Goovaerts, 1997). Put another way, if the 126 to 140 m feature was not always represented in a similar fashion, we would not be able to have any confidence at all that the method would be sensitive enough to assess actual variability.

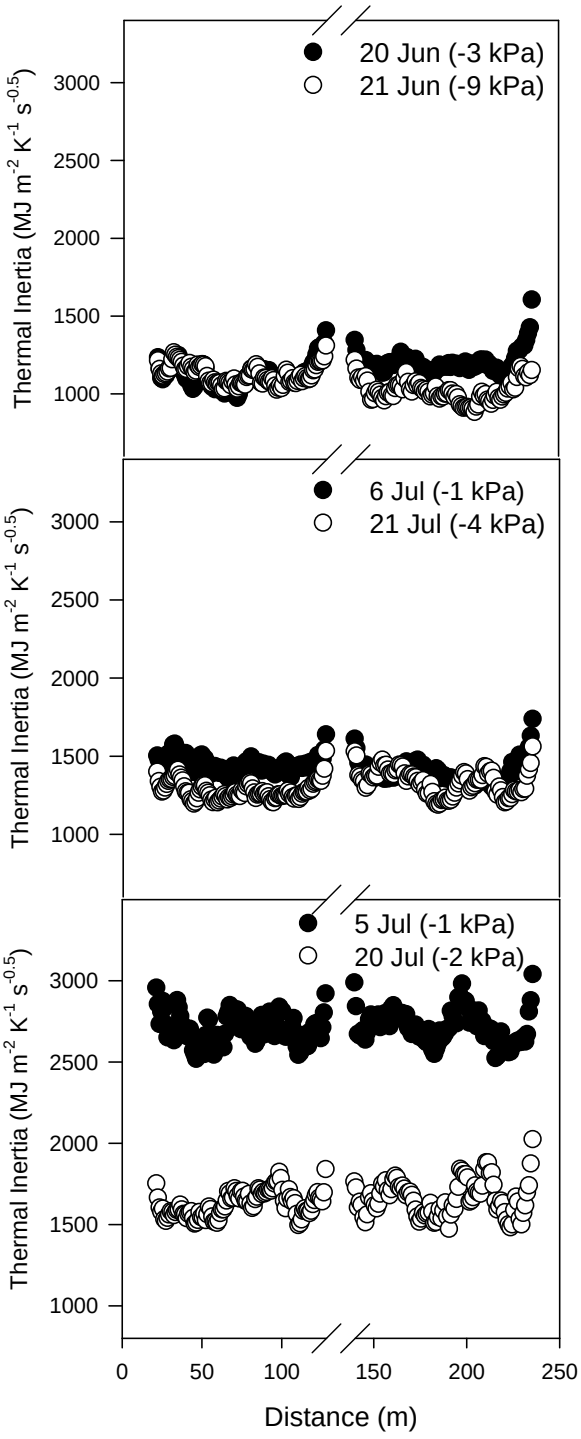


Figure 4.12. Apparent thermal inertia arranged in order of decreasing matric potential. Note that high values between 130 and 140 m have been omitted for clarity.

The largest precipitation event of the monitoring period occurred on July 3 and 4, when 38.6 mm of rain accumulated. The next day, 5 Jul. 2012, had both the lowest matric potential and the greatest spatially averaged value of ATI during the monitoring period (2701.89 MJ $m^{-2}$ $K^{-1}$ $s^{1/2}$) (Figure 4.12). The remaining days followed the same rank order, with increasing matric potential corresponding to decreasing ATI. It is important to note that while matric potential was used at parameter of interest for expressing the wetness of the soil, volumetric water content displayed a similar relationship to ATI. However, the range in water content corresponding to the range in matric potential was small, and only encompassed volumetric water contents of 0.39 to 0.41 $m^3$ $m^{-3}$. Therefore, while not a perfect reflection of soil water content, the range in matric potential facilitates an easier examination of the relationship between ATI and the overall wetness of a soil.

### 4.5.3 Sensitivity

The uncertainty in estimations of ATI must be estimated in order to be acceptable as a method for characterizing the spatial variability of soil cover systems. The new method was also compared to the accepted method using apparent thermal diffusivity to characterize the spatial distribution of water and energy. To this end, an error propagation analysis was conducted to determine the primary sensitivities in the estimation of both methods. The uncertainties used in the error propagation analysis were taken from manufacturer's published literature where possible (Table 4.2). Depth uncertainty used the standard deviation of the mean depth measurement as the uncertainty input. In some cases, such as that for $R_n$ only the final uncertainty is given, and not the error propagation from the intermediate calculations used to arrive at the final value.

Table 4.2. Ranges of parameter values used in the uncertainty analysis.

| Parameter | Uncertainty Range | Unit | Affected Thermal Property | Equation Reference |
|---|---|---|---|---|
| z | ± 0.04 | m | α | 4.18 |
| $R_n$ | ± 5.3 | $Wm^{-2}$ | ATI | 4.14 |
| $T_{soil}$ | ± 0.16 | °C | ATI, α | 4.14, 4.18 |
| t | ± 2400 | s | ATI | 4.14 |
| $E_{soil}$ | ± 0.01 | - | $R_n$ | 4.19 |

Final uncertainties were estimated to be ± $1.5\times10^{-7}$ $m^2$ $s^{-1}$ for thermal diffusivity and ± 267 MJ $m^{-2}$ $K^{-1}$ $s^{-0.5}$ for ATI. To illustrate the effect of uncertainty, estimates of diffusivity and ATI on 5 Jul. 2012 and 20 Jul. 2012 were made, along with 90, 95, and 99% confidence intervals (CI). Diffusivity estimates were subject to a wide range of uncertainty, and were not able to detect any substantial differences between a wet and dry day (Figure 4.13). Conversely, ATI estimates were well outside the range of uncertainty (Figure 4.14).

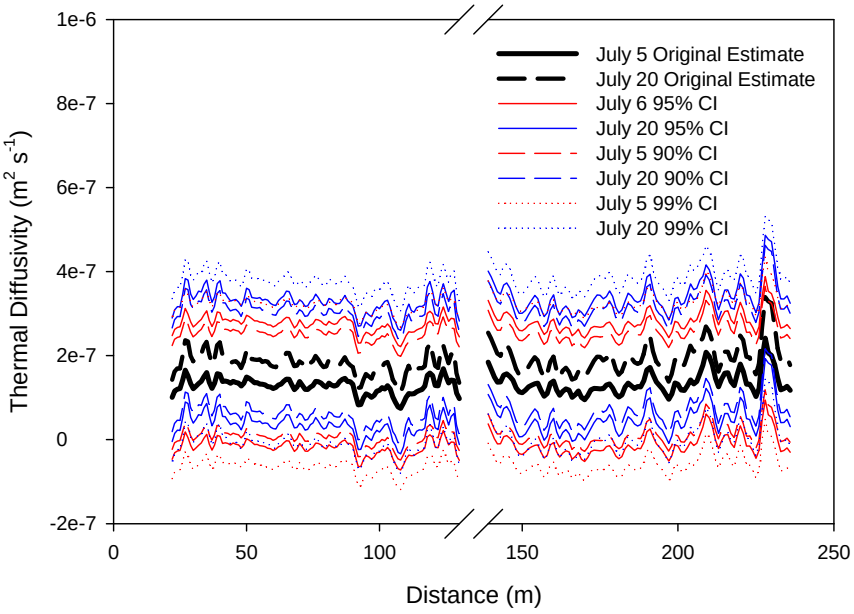


Figure 4.13. Uncertainty surrounding estimation of thermal diffusivity on 5 Jul. and 20 Jul. 2012 expressed in terms of confidence intervals (CI).

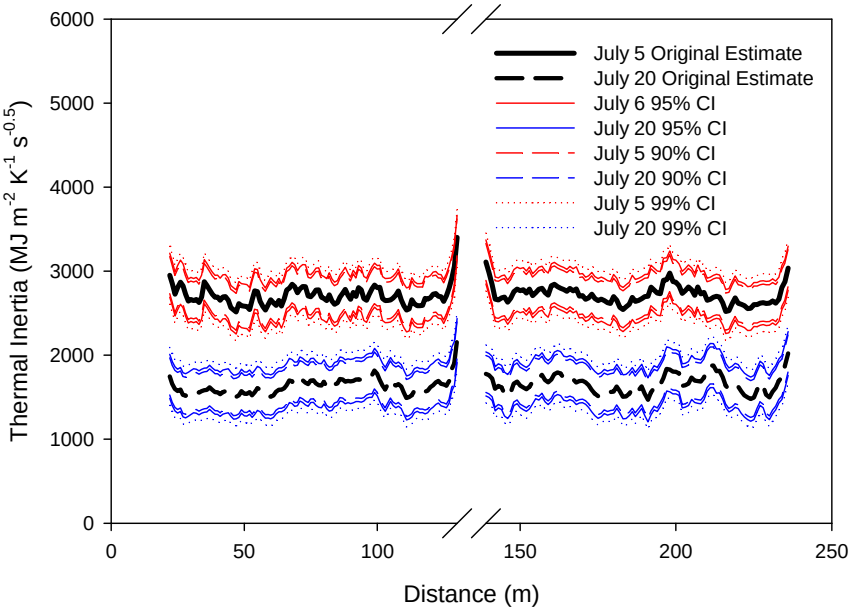


Figure 4.14. Uncertainty surrounding estimation of thermal inertia on 5 Jul. and 20 Jul. 2012 expressed in terms of confidence intervals (CI).

Error propagation analysis highlighted the importance of uncertainty when choosing a thermal property to estimate for use in characterizing spatial variability. Thermal diffusivity is highly sensitive to changes in measurement depth. Although great care was taken in the installation of the cable, depth is a difficult variable to control with precision, especially over large spatial extents. This is especially true in mining applications where cover systems are often constructed with stony material. The importance of carefully controlling depth in spatial estimation of thermal diffusivity was also highlighted as a major source of uncertainty by Steele-Dunne et al. (2010). In the uncertainty analysis conducted by Steele-Dunne et al. (2010) a depth uncertainty error standard deviation of 0.5 cm led to diffusivity estimates that covered their entire dynamic range of plausible measurements.

Uncertainty in ATI was much smaller, and was primarily due to the uncertainty involved in estimating $R_n$ at each location. The effect of uncertainty in the calculation of ATI is magnified in the overall estimation because $R_n$ is doubled (cf. Eq. 4.14). Uncertainty in $R_n$, in turn, is primarily a function of uncertainty in emissivity. The researcher may choose to use $R_n$ measured by the meteorological station. While the precision of modern radiometers is very good, it defeats the purpose of a spatial analysis to have $R_n$ anchored to one spatial location. Accepting that $R_n$ is the major source of uncertainty in estimating ATI the spatially variable parameter, $T_{soil}$, is still far more precise than depth for diffusivity estimates.

**4.6 Conclusions**

The present study looked to examine the suitability of estimating apparent thermal inertia, ATI, using distributed temperature sensing as a means of assessing spatial variability in unsaturated soil cover systems. Estimation of apparent thermal diffusivity using temperature measurements at two or more depths over the course of a day has been the most commonly used method for inferring soil wetness. There are two issues in estimating thermal diffusivity that

diminish its effectiveness. The first is that regardless of the estimation technique, diffusivity is very sensitive to measurement depth. The precision required, likely within ± 0.5 cm, precludes the use of the technique over large spatial extents in mine reclamation. The accuracy of the diffusivity estimate at a single point can be improved with more sophisticated analyses, but a more sophisticated technique, such as harmonic analysis (Horton and Wierenga, 1983) or a numerical solution (Steele-Dunne et al., 2010) will not change the salient fact that diffusivity is sensitive to depth, and spatial control of measurement depth is imprecise. Second, estimation of diffusivity requires the full diurnal range of soil temperatures for calculation. Controls on daytime near-surface soil temperature are highly non-linear, and depend on myriad factors (van Wijk and de Vries, 1963, Ten Berge and Stroosnijder, 1987). Uncertainty resulting from non-linear, turbulent processes is then incorporated into the diffusivity estimate.

Apparent thermal inertia, ATI, a measure of a soil's resistance to temperature change, was proposed as an improved method for characterizing the spatial variability of a soil thermal property that is directly related to soil water content. Apparent thermal inertia was proposed to counter the major shortcomings of estimating thermal diffusivity. First, the primary spatial variable in estimating ATI is temperature, which is easily and precisely measured using a DTS system. Second, the need to know a precise measurement depth is eliminated as the surface temperature is the only variable of interest. Third, ATI is a lumped variable that integrates subsurface heat transfer into one variable, negating the need to explicitly account for latent heat exchange below the surface. Finally, estimation of ATI is ideal for characterizing spatial variability as it is estimated when soil temperatures are at their daily minimal variance. Therefore, any true variations in thermal properties are less likely to be obscured by temperature changes in response to turbulent processes.

Typical analyses estimate thermal properties as an intermediate step in estimating ground heat flux or soil water content. However additional estimations only increase the overall uncertainty as errors are propagated through subsequent estimations. Estimated values quickly become meaningless as estimated properties are further removed from the original measured parameter. If the objective of the experiment is to characterize spatial variability, then the goal should be to optimize the use of the most precise parameters. In this case, it is not the absolute value of ATI that is of primary interest; it is the spatially distributed value measured on the same day. The precision of temperature measurements as opposed to the imprecision of depth measurements makes ATI an ideal parameter for characterizing spatial variability using temperature.

# 5.0 CHARACTERIZING SPATIAL VARIABILITY OF THERMAL PROPERTIES IN SOIL COVER SYSTEMS USING HIGH RESOLUTION TEMPERATURE MONITORING

## 5.1 Preface

Rigorous studies on the spatial variability of thermal properties in cover systems do not exist. In the previous chapters the utility of a DTS system in reclamation cover systems was explored, and a method was developed to estimate the change in thermal properties of the cover system. The distribution of thermal properties and the dominant spatial scales are not known. In this final research chapter, the methods developed in the previous two chapters will be applied to investigating the spatial scaling properties of apparent thermal inertia. Information on the spatial variability of thermal properties in cover systems will improve our understanding of how the systems behave at the field scale and can lead to more sustainable designs.

## 5.2 Introduction

Soil cover systems are an essential component in mine reclamation and closure operations. Performance of the cover system will be affected by soil water and energy dynamics at a range of spatial and temporal scales. Typically the distribution of water is the primary parameter of interest in studies investigating spatial variability as the volume of water in the cover system will control evaporation, infiltration, runoff, and vegetation growth. Scaling point source measurements to areal performance is difficult and subject to uncertainty (Robinson et al., 2008), while intensively measuring soil water content at a range of spatial and temporal scales is difficult and expensive (Minacapilli et al., 2009). Fortunately, soil water content also controls the extent to which energy is partitioned at the soil surface into latent, sensible, and ground heat fluxes (Hillel, 1998). The distribution of energy in a cover system will control performance by determining the exchange of heat and mass to the atmosphere as well as the temperature profile with depth (Buchan, 2001). Spatial variations in the surface energy balance will be influenced by

the distribution of soil thermal properties. Although often overlooked, the distribution of soil thermal properties may be an effective means of assessing the spatial variability of physical properties, energy, and indirectly, soil water content in a cover system.

Net radiation, evaporation, air temperature, and wind speed interact in a complex manner to determine daily soil temperatures. Despite the complex interactions, it has been shown previously that spatial distributions of temperature can be used to assess spatial variability of thermal properties, physical properties, and soil water content. Spatial variability of temperature and thermal properties has been found to be inversely related to soil water content (Usowicz et al., 1996; Bond-Lamberty et al., 2006). Spatial dependence of thermal properties has been shown to be similar to bulk density, due to the important effects that the volume of air, particles, and water in a given soil volume will have on determining soil temperature (Usowicz et al., 1996). Similarly, Lipiec et al. (2007) found that in sloping vineyard soils, spatial variations in thermal conductivity and volumetric heat capacity were found to be most similar to those of water content, while the distribution of thermal diffusivity was most closely related to bulk density, although reasons for the relationship were not given.

Other research has focused more closely on the link between the distribution of water and temperature in the soil. Vauclin et al. (1982) reported that the spatial structure of soil temperature agreed well with the spatial structure of water content. Bond-Lamberty et al. (2006) reported negative correlations between soil temperature and water content and similar spatial structures between the two, suggesting that soil water content was having an effect on the distribution of temperatures in the soil. Mohanty et al. (1998) found spatial relationships between soil temperature and water content, although not at all times. Furthermore, Usowicz et al. (2006) reported that the interaction of bulk density and air filled porosity is a better predictor of thermal

properties than water content alone, which is not surprising, given that bulk density will determine the volume of water that a soil is capable of storing.

Measurements of soil thermal properties can provide important insight into the performance of a cover system. However, methods other than point source measurements of soil temperature are required if the spatial structure of soil thermal properties in cover systems are to be characterized at large scales. Distributed temperature sensing is a recently available technique that optimizes the spatial scale triplet by taking many measurements at a small scale over large spatial extents (Western et al. 2002). A DTS system is capable of measuring temperatures distributed along fibre optic cables up to 10 km in length at measurements resolutions of 1 m at high temporal frequencies (Selker et al., 2006; Tyler et al., 2009; Suarez et al., 2011). The technique has been readily adopted by researchers for a wide range of applications related to streams (Selker et al, 2006; Westhoff et al., 2007; Vogt et al., 2010), aquifers (Henderson et al., 2009), municipal sewers (Schilperoort et al, 2009; Hoes et al., 2010), and atmospheric boundary layers (Thomas et al., 2011) among others. Distributed temperature sensing has also been applied to soils for examining the spatial variability of thermal properties. Soil water content and apparent thermal diffusivity have been reported to be generally spatially correlated when using passive monitoring of diurnal temperature histories (Steele-Dunne et al., 2010; Krzeminska et al., 2011). A major deficiency of using passive methods to infer soil water content is the high sensitivity of thermal diffusivity to cable installation depth. Sensitivity analyses conducted by Steele-Dunne et al. (2010) demonstrated that by simulating an standard error uncertainty of ±0.5 cm in cable installation depth was sufficient to vary thermal diffusivity across the entire operating range. A more accurate determination of the spatial distribution of water content can be determined using active heat pulse methods (Weiss, 2003; Striegl and Loheide, 2012). Active

methods can be used to provide a unique determination of water content as was shown by Sayde et al. (2010). However, inaccuracies are commonly reported, even with the more accurate active heat-pulse methods for determining water content from soil temperature, especially at water contents close to saturation (Sayde et al., 2010; Striegl and Loheide, 2012). In all cases, whether using passive or active methods, the non-unique relationship between thermal diffusivity and soil water content has precluded an accurate and unique determination of water content.

An ideal soil thermal property of interest for investigation of spatial variability studies would be one that is directly related to water content. Thermal inertia is a soil thermal property that governs the amplitude of daily temperature changes in response to changes in soil heat flux (Wang et al., 2010). Thermal inertia is the square root of the product of volumetric heat capacity and thermal conductivity and is described as a measurement of the resistance of the soil to temperature change (Matsushima et al., 2012). Given that thermal inertia is a product of volumetric heat capacity and thermal conductivity, it has a direct relationship with soil water content, unlike thermal diffusivity, which has a non-unique relationship with the amount of water in the soil.

When using surface properties or remote sensing to estimate thermal inertia, the property becomes an integration of subsurface thermal inertia and is expressed at the surface as an apparent thermal inertia (ATI) (Sabol, 2006). The relationship between ATI and soil water content has attracted considerable interest in remote sensing studies in describing the spatial distribution of water in a landscape using thermal properties alone. Using remotely sensed ATI was first introduced in the 1970's (Watson, 1975) and was subsequently developed to map soil water content over large areas (Pratt and Ellyett, 1979; Price, 1985). More recently the technique has been shown to accurately map soil water content over large areas (Verstraeten et al., 2006;

Wang et al., 2010). Estimating ATI may be particularly useful for classifying field distribution of water into qualitative levels, such as wet, medium, and dry (Matsushima et al., 2012).

The drawbacks related to estimating ATI using satellite remote sensing including atmospheric attenuation and vegetation opacity have precluded the widespread adoption of using ATI to characterize the spatial variability of soil thermal properties (Steele-Dunne et al., 2010). In addition, using traditional methods to estimate ATI require satellite observations of daily minimum and maximum temperatures, surface reflectance, and accounting for the surface energy balance and lower boundary water content (Verstraeten et al., 2006; Steele-Dunne et al., 2010). However, a technique developed by Verhoef (2004) circumvents these issues by only requiring measurements of surface temperature and net radiation on calm, clear nights. The formulation is uniquely suited to application with a DTS system as it avoids complications due to depth uncertainty and atmospheric opacity. The Verhoef (2004) method is also well suited to applications in the mining industry where installing fiber optic cable over large distances at precise depths is a challenge.

The performance of a soil cover will be controlled in large part by its ability to store and then release water to the atmosphere. These water storage dynamics will be reflected in the distribution of thermal properties and how incoming radiation energy is partitioned within the soil. Traditional point source monitoring of a cover system does not provide any information as to the behavior of the system at the field scale. The distribution of thermal properties in cover systems could provide valuable insight into the performance of these systems, yet has not been previously investigated. The objective of this study was to characterize the spatial variability of thermal properties in a cover system using a distributed temperature sensing system.

Investigating the inherent spatial scales of variability of thermal properties could lead to a better understanding of the performance of these systems at the field scale.

## 5.3 Theory

### 5.3.1 Apparent Thermal Inertia

Soil temperature will change in response to the partitioning of incoming solar radiation at the soil surface:

$$R_n = H + LE + G_0 \quad [5.1]$$

where $R_n$ is the net radiative flux, H is the sensible heat flux to the atmosphere, LE is the latent heat of evaporation, and $G_0$ is the ground heat flux at the surface (all terms in W $m^{-2}$).

Heat transfer in an elementary volume of soil can be described using Fourier's Law, assuming homogeneity and thermal equilibrium (Novak, 2005):

$$C_v \frac{\partial T}{\partial t} = -\frac{\partial G}{\partial z} = \frac{\partial}{\partial z}\left(\lambda \frac{\partial T}{\partial z}\right) \quad [5.2]$$

where t is time, T is soil temperature, z is depth below the soil surface, G is the soil heat flux density, $C_v$ is the volumetric heat capacity (J $m^{-3}$ $K^{-1}$) and λ is thermal conductivity (W $m^{-1}$ $K^{-1}$). Volumetric heat capacity is further defined as:

$$C_v = f_s\rho_s c_s + f_w\rho_w c_w + f_a\rho_a c_a \quad [5.3]$$

where f denotes the volume fraction of the soil (s), water (w), and air (a) components (de Vries, 1975). Note that $f_w$ is equivalent to volumetric water content, $\theta_v$, ($cm^3$ $cm^{-3}$).

Transient ground heat flux can be expressed as a periodic function of time, t, and depth, z: (de Vries, 1975):

$$G(t,z) = |T|_0(\lambda C_v \omega)^{1/2} e^{-z/d} \cos(\omega t - z/d + \pi/4) \quad [5.4]$$

where $|T|_0$ is the amplitude of the diurnal surface temperature wave, ω is the radial frequency equal to $2\pi/P$, where P is the period, and d is the damping depth, $d = (P\alpha/\pi)^{1/2}$ and

$(\lambda C_v\,\omega)^{1/2}$ is thermal inertia, which, when multiplied by $|T|_0\,\omega^{1/2}$ describes a soil's resistance to temperature change by governing the amplitudes of both ground heat flux and surface temperature (Buchan, 2001; Wang et al., 2010).

Damping depth is considered to be the depth over which daily thermal inertia is integrated. Rearranging Eq. 3 to express G at the soil surface, z = 0, we have:

$$G(t,0) = |T|_0(\lambda C_v \omega)^{1/2}\cos(\omega t + \pi/4) \quad [5.5]$$

A method to estimate surface temperature transients from G was developed by Brunt (1932) to calculate the drop in surface temperature for calm, clear nights (van Wijk and de Vries, 1963):

$$T(t,0) = \frac{G[4\alpha(t-t_0)]^{1/2}}{\lambda\pi^{1/2}} \quad [5.6]$$

Verhoef (2004) expanded the method developed by Brunt (1932) to estimate thermal inertia on calm, clear nights by using the drop in soil surface temperature and net radiation from sunset to sunrise.

$$TI = \sqrt{C_v\lambda} = \frac{2|\overline{R_n}|\sqrt{\Delta t}}{\Delta T_s\sqrt{\pi}} \quad [5.7]$$

where, where $|R_n|$ (W $m^{-2}$) is the absolute value of the average nighttime net radiation between sunset and sunrise, $\Delta t$ (s) is the length of time between sunset and sunrise, and $\Delta T_s$ (K) is the change in soil surface temperature over the same time period. The point at which short wave solar radiation passed through zero was used to determine the timing for sunset and sunrise.

Soil surface temperatures are the only soil temperature required for estimating thermal inertia using the Verhoef (2004) method. The method does not measure thermal inertia as a function of depth, and assumes that thermal inertia expressed at the surface is an integration of

thermal inertia above the daily damping depth, weighted more heavily to surface temperatures (Sabol, 2006). Therefore, for the purposes of this study, it is assumed that thermal inertia estimated at the soil surface is an apparent value, and is referred to as Apparent Thermal Inertia (ATI).

Net radiation at night was calculated using (Arya, 2001):

$$R_n = R_{nL} = R_{L\downarrow} - R_{L\uparrow} \quad [5.8]$$

where:

$$R_{L\downarrow} = \varepsilon_{eff} F \sigma T_{air}^4 \quad [5.9]$$

$$R_{L\uparrow} = \varepsilon_{soil} \sigma T_{soil}^4 \quad [5.10]$$

where $R_{L\downarrow}$ and $R_{L\uparrow}$ (W m$^{-2}$) are the incoming and outgoing long wave radiation, respectively; $\varepsilon_{eff} = \varepsilon_{cs}F$ (-)is the effective emissivity of the sky, $\varepsilon_{soil}$ (-) is the bare soil emissivity taken as 0.95, F is a cloud factor (always ≥1), σ the Stefan-Boltzmann constant ($5.67 \times 10^{-8}$ W m$^{-2}$ K$^{-4}$), and $T_{air}$ and $T_{soil}$ (K) the absolute temperature of the air and soil surface, respectively.

Clear sky emissivity, $\varepsilon_{cs}$, was calculated using (Brutsaert, 1975):

$$\varepsilon_{cs} = k\left(\frac{e_a}{T_{air}}\right)^{\frac{1}{m}} \quad [5.11]$$

where k and m are defined by Brutsaert (1975) as 0.642 and 7, respectively. Near surface vapour pressure (Pa) was calculated using:

$$e_{a\,(kPa)} = RHe_s \quad [5.12]$$

and the saturated vapour pressure, $e_s$ (Pa) was found using air temperature and coefficients provided by for pure water from -20 to 50 °C (Tetens, 1930; Buck 1981; Hatfield and Baker, 2005):

$$e_{s(kPa)} = 0.61151\ exp\left(\frac{17.502T_{air}}{T_{air} + 240.97}\right) \quad [5.13]$$

### 5.3.2 Empirical Mode Decomposition

Empirical mode decomposition (EMD) is a spatial analysis technique that has recently been applied in soil science investigations of spatial variability. The EMD method separates the variation in the spatial series into discrete component characteristic scales. Empirical mode decomposition is unlike other methods used in spatial analysis in that it works directly in the spatial domain, rather than transforming the data series into the spectral domain as is done with spectral and wavelet analysis (Biswas and Si, 2011c). The underlying assumption in EMD is that a variable signal, whether spatial or temporal, is composed of multiple oscillatory modes of differing frequencies that superimpose to form the initial signal at the measurement scale (Huang et al., 1998; Sang et al., 2012). Empirical mode decomposition is a tool used to sift out the component scales of variation and determine their overall contribution to the total variance (Biswas et al., 2009). For a more complete discussion of EMD in comparison to wavelet analysis, the reader is directed to the work of Biswas et al. (2013), who demonstrated that EMD scale components retain more physical meaning than wavelet based methods, and were more accurate in identifying the spatial scales contributing to the measurement variance.

Empirical mode decomposition decomposes the measurement signal into separate components called an intrinsic mode function (IMF). According to Huang et al. (1998), an IMF is a function that must satisfy two conditions: 1) the number of extrema and zero crossings in the dataset must either equal, or differ at most by one; and 2) the mean value of the envelope defined by the local extrema must equal zero. The extrema envelope is created by joining all local maxima and minima through spline interpolation to form an upper and lower envelope, respectively (Biswas et al., 2009; Biswas and Si, 2011c).

The EMD method is adaptive and works directly with the data, without the need to rely on a mathematical function to transform the data, as is the case with wavelet analysis (Biswas and Si, 2011c). For a complete treatment of the EMD process used to separate out the component IMFs the reader is referred to the examples shown by others (Huang et al., 1998; Biswas and Si, 2011c; and Sang et al., 2012). The process is briefly summarized below for an example spatial series Y(x):

1. Determine all local maxima and local minima and define an upper envelope (UE) and lower envelope (LE) by joining the local extrema through spline interpolation. The resultant envelopes encompass all data points. The local mean of the envelope, $m_1 = (UE + LE)/2$ is subtracted from the data Y(x), leaving the first prototype, $h_1(x) = Y(x) - m_1(x)$.

2. The prototype is then used as the input data for the next k iterations until the local envelope symmetry condition is satisfied. When satisfied, the prototype $h_{1k}(x)$ becomes the first IMF, $C_1 = h_{1k}(x)$.

3. A convergence test is applied to the local envelope sifting process to ensure that the resultant IMF retains enough physical meaning in both frequency and amplitude.

4. The first IMF sifted from the input data contains the highest frequency, or shortest scale components, and is removed from the input data, leaving a residue function, $r_1(x) = Y(x) - C_1$. The residue is then used as the input data for the subsequent sifting of larger scales.

5. The sifting continues for n iterations until the residue $r_n(x)$ contains only one extremum or a monotonic function.

6. Finally, the original input signal is the sum of all IMFs and can be written as (Biswas and Si, 2011):

$$Y(x) = \sum_{j=1}^{n} C_j(x) + r_n(x) \qquad [5.14]$$

The total variance of the original spatial series ($\sigma^2$) is represented by the summation of each IMF and is given as (Biswas and Si, 2011):

$$\sigma^2 = \frac{1}{N}\sum_{i=1}^{N}(x_i - \mu)^2 \quad [5.15]$$

where:

$$\mu = \frac{1}{N}\sum_{i=1}^{N} x_i \quad [5.16]$$

and N is the number of points in the spatial series. Finally, the percent contribution to the total variance of each individual IMF can be calculated as:

$$\%\ Contribution = \left(\frac{Variance\ of\ IMF_i}{\sum Variance\ of\ all\ IMFs}\right) \times 100 \quad [5.17]$$

Examination of the amount of contribution of a particular IMF to the total variance allows for an estimation of the relative dominance of a particular spatial scale. The average scale of an IMF is calculated by counting the number of oscillations present in the IMF in question. For example, if over a 100 m transect a particular IMF exhibits 5 oscillations, then the average spatial scale of that IMF will be 100 / 5 = 20 m. This was the method used for reporting average spatial scales in the subsequent analysis. Oscillations of the IMFs can vary locally, and as such, reporting of spatial scales represents an average range for the particular scale. Therefore, the spatial scales of each IMF will be reported as a range, rather than a discrete value.

## 5.4 Materials and Methods

### 5.4.1 Site Description

The field experiment was situated in the oil sands region of northern Alberta, Canada (57.33°N, 111.53°W, 326 m a.s.l.). The climate at the site is classified as continental sub humid. Long term climate normals at the Fort McMurray airport, 63 km to the south indicated daily

mean temperatures of -18.8 and 16.8 °C for January and June, respectively, while precipitation normals were 456 mm, with 342 mm occurring as rainfall (Carey, 2008).

The field experiment was part of a 36 ha reclamation trial consisting of 12 alternate cover treatments, each 1 ha in area, arranged randomly in triplicate over a lean oil sands waste dump. A 236 m experimental transect was located along two adjoining plots that sloped at 2% to meet at a crest at the midpoint (Figure 5.1). The transect ran east to west, with the origin of the transect (0 m in Figure 5.1) representing the eastern end. The cover soils consisted of nominally 30 cm of peat overlying at least 70 cm of fine textured sand.

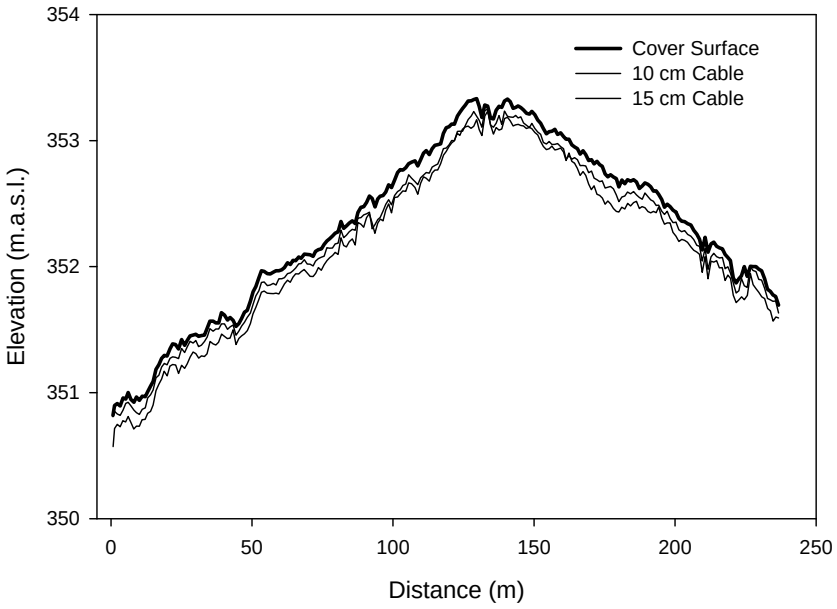


Figure 5.1. Cross section of the cover system experimental transect. Top line denotes cover surface and location of the Surface and 0 cm cable. Middle line denotes location of the 10 cm cable. Bottom line denotes location of the 15 cm cable. Note that cover material depths are exaggerated for display purposes.

A distributed temperature sensing (DTS) system was installed to measure the spatial distribution of temperatures within the cover. A Sensornet Oryx (Sensornet, United Kingdom) system was used, and had manufacturer stated temperature resolutions less than 0.5 °C at integration times of 60s. Spatial and temporal repeatability was verified during calibration. The Oryx DTS system was capable of a 1 m sampling resolution and 2 m spatial resolution. Differences in the sampling and spatial resolution arise due to the fact that while the Oryx returns a measurement every 1 m, a distance of 2 m is required to resolve from 80% of a step change in temperature.

A 1000 m BruClean 150 fiber optic cable (Brugg Cables, Switzerland) was installed in the peat layer of the cover system to monitor temperatures at the surface, 0, 10, and 15 cm over the 236 m transect (Figure 5.1). The midpoint crest of the transect was used as a path for

vehicular access. Therefore, all four cable runs were buried at the midpoint of the transect for protection. Cable elevation was measured every meter using a Trimble R8 GNSS (Trimble, United States). The only temperatures required to estimate ATI using the method developed by Verhoef (2004) are the 0 cm temperature to act as a skin temperature, and the Surface temperature, with which to calculate $R_n$. The 0 cm cable was placed at the soil surface and covered with sufficient material so as to not be directly exposed to the atmosphere. The Surface cable was laid directly on the soil surface immediately adjacent to the 0 cm cable and was left exposed. The entire 236 m transect was traversed with the 0 cm cable; however, only 215 m of the transect was covered with the Surface cable. Only the 215 m that was covered by both the 0 cm and Surface cable was used in the data analysis. Distributed temperature data were recorded every 20 minutes using a 60 s integration time. Data were collected from May 22 to July 23, 2012.

The Oryx DTS was calibrated by comparing a 60 m calibration section of cable with independent temperature readings. The calibration section of cable and two PT-100 platinum thermistors were immersed in a large cooler that filled with ice and topped with water. It should be noted that the mixture was not continuously mixed, leading to possible stratification of temperatures in the bath. The possibility of temperature stratification in the calibration bath is a source of error that could have led to noise in the temperature readings. Instrument precision is reported as spatial and temporal repeatability. Spatial repeatability is the standard deviation of a section of cable over successive measurements. Temporal repeatability is the standard deviation of a single point over time. Spatial and temporal repeatability for this study were found to be ±0.17 °C and ±0.03 °C, respectively. The spatial and temporal repeatability values are slightly

higher than those reported by Tyler et al. (2009), and compare well with those of Ciocca et al. (2009).

Soil water content, matric potential, and temperature at 5 and 15 cm depths were measured at a nearby point source monitoring station during the field experiment. The point-source monitoring station was installed into a plot consisting of the same peat-over-sand configuration as the experimental transect. Monitoring data were collected every four hours using CS 616 (Campbell Scientific, Canada) sensors for water content ($cm^3\ cm^{-3}$) and CS 229 (Campbell Scientific, Canada) sensors for soil temperature (°C) and matric potential (kPa).

Meteorological conditions during the field experiment were recorded at a nearby meteorological station. The following parameters were measured every 20 minutes: air temperature (°C) and relative humidity (%) (HMP45C212 temperature and humidity probe, Vaisala, Finland); net radiation ($Wm^{-2}$) (NRLITE2 net radiometer, Kipp & Zonen, The Netherlands); incoming and outgoing short wave radiation ($Wm^{-2}$) (CMP3 pyranometer, Kipp & Zonen, The Netherlands); wind speed and direction (05103-10 Wind Monitor, R.M. Young, United States); and precipitation (mm) (TE525 Rain Gage, Texas Electronics, United States). Rainfall was recorded as a unique event for every 0.25 mm bucket tip.

Surface bulk density was measured every meter along the transect using a 6.4 cm diameter, 3.1 cm high steel ring. The ring was pressed into the surface soil, taking care to minimize compaction. The sample was then excavated and trimmed to be even with the ring (Hao et al., 2006). Laboratory thermal property analyses were conducted on air dried peat samples for every transect location using dual-probe heat pulse methods (Bristow et al., 1994). Samples were placed in a sample vessel and a 10 s heat pulse was applied to determine thermal diffusivity, heat capacity, and thermal conductivity. Additional physical properties were

measured on bulk peat samples taken from the study area. Particle size distribution was measured according to ASTM D422 (2007). Soil water characteristic curves were measured according to ASTM D6836 (2008).

A standardized means of comparing meteorological conditions between days was required. Vapor pressure deficit (VPD) incorporates air temperature and relative humidity in a way that describes the drying power of the prevailing conditions for that day (Ashcroft and Gollan, 2013). Maximum daily VPD in Pascals was calculated as:

$$VPD = \frac{SVP \times (100 - RH)}{100} \quad [5.18]$$

where RH is the minimum daily relative humidity, and SVP is the saturated vapor pressure:

$$SVP = \frac{610.7 \times 107.5T}{273.3 + T} \quad [5.19]$$

where T is the maximum daily air temperature (°C).

Apparent thermal inertia, elevation, and surface bulk density were analyzed with EMD to determine the dominant scales of spatial variation. Apparent thermal inertia values exhibited a distinct peak at the transect midpoint where the cable passed under the vehicle access path, which lead to a highly skewed data distribution. Spatial analysis required a continuous dataset and a distinct spurious data feature had the potential to leak artificial noise into the analysis. Therefore, the 14 m portion of data representing the area where the cable passed under the vehicle path was excised and then backfilled by linear interpolation. Removing that portion of the data was felt to be valid given that the spike in ATI was a known consistent artifact of the data. All input data used in the EMD analysis were log-transformed for normality if the skewness of their distribution exceeded 0.5 (Webster and Oliver, 2007).

## 5.5 Results and Discussion

Field average peat bulk density was 0.57 g $cm^{-3}$ with a resultant estimated porosity of 0.57, assuming an organic particle density of 1.35 g $cm^{-3}$ (Redding and Devito, 2006). Field measured SWCC showed the possibility of hysteresis, although this was not verified with separate wetting and drying curves (Figure 5.2). The field measured air entry value appeared to have occurred at 8 kPa.

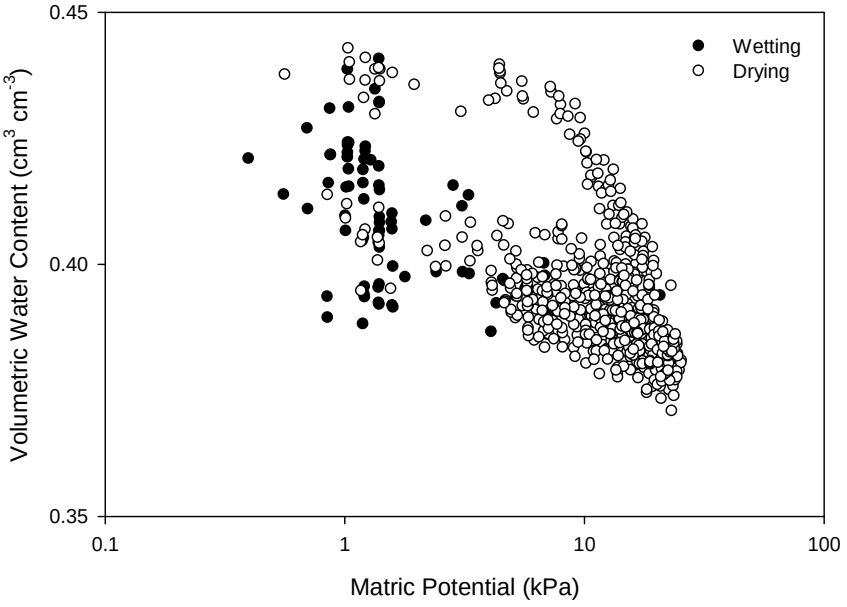


Figure 5.2. Field measured soil water characteristic curve developed using matric potential and volumetric water content data measured at the point source monitoring station. Symbols indicate wetting and drying portions of the relationship.

Air temperatures averaged 16.2 °C for roughly the first half of the experiment and increased to an average of 20.2 °C for the second half (Figure 5.3). Major rainfall accumulations occurred on 3 Jun. 2012 (16.3 mm), from 16 Jun. to 18 Jun. 2012 (15 mm), and from 3 Jul. to 4 Jul. 2012 (38.3 mm). Volumetric water content measured at 5 cm increased following the major rainfall events (Figure 5.4). Soil temperatures measured at 5 cm demonstrated both strong

diurnal patterns and a steady increase over the duration of the experiment (Figure 5.4). Matric potential measured with CS229 sensors responded to precipitation inputs and demonstrated that a minor event on 18 and 19 Jul. 2012 was sufficient to decrease matric potential to near-saturated levels (Figure 5.4). A comparison of volumetric water content and matric potential demonstrates that while the two sensors respond to the same precipitation inputs there is a greater response seen with the CS 229 matric potential sensors than the CS 616 sensors. From Figure 5.2, it is possible that water contents could be near saturation while still maintaining a small amount of tension. Changes in water content may also be a reflection of volume changes of the peat material. In addition, the response of the CS 229 sensor during wet periods may also be as a result of the instrument resolution at matric potentials greater than -10 kPa. It is clear that neither measurement provides a clear picture in isolation. Therefore, the degree of soil wetness will need to be interpreted using both matric potential and volumetric water content as a variable of interest.

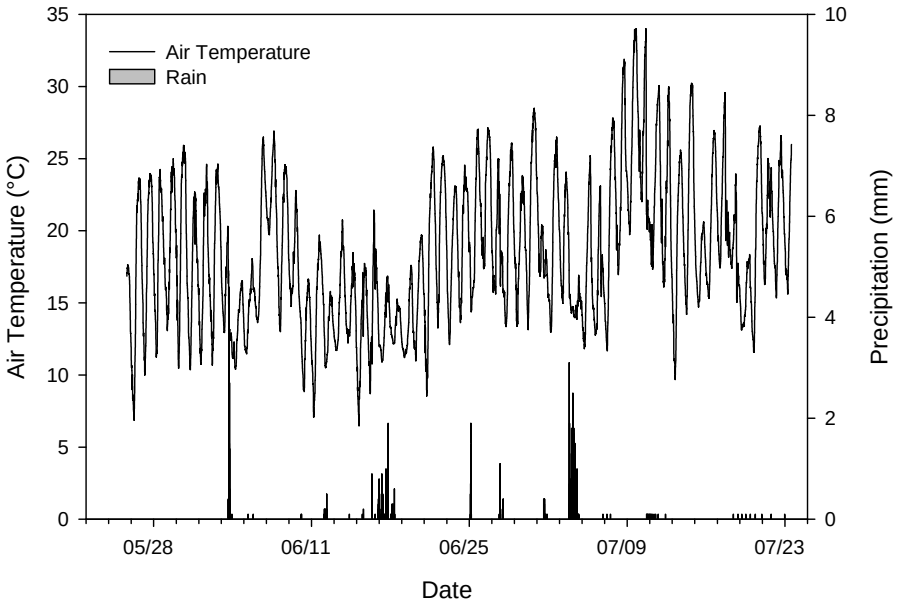


Figure 5.3. Air temperature and rainfall recorded during the field experiment.

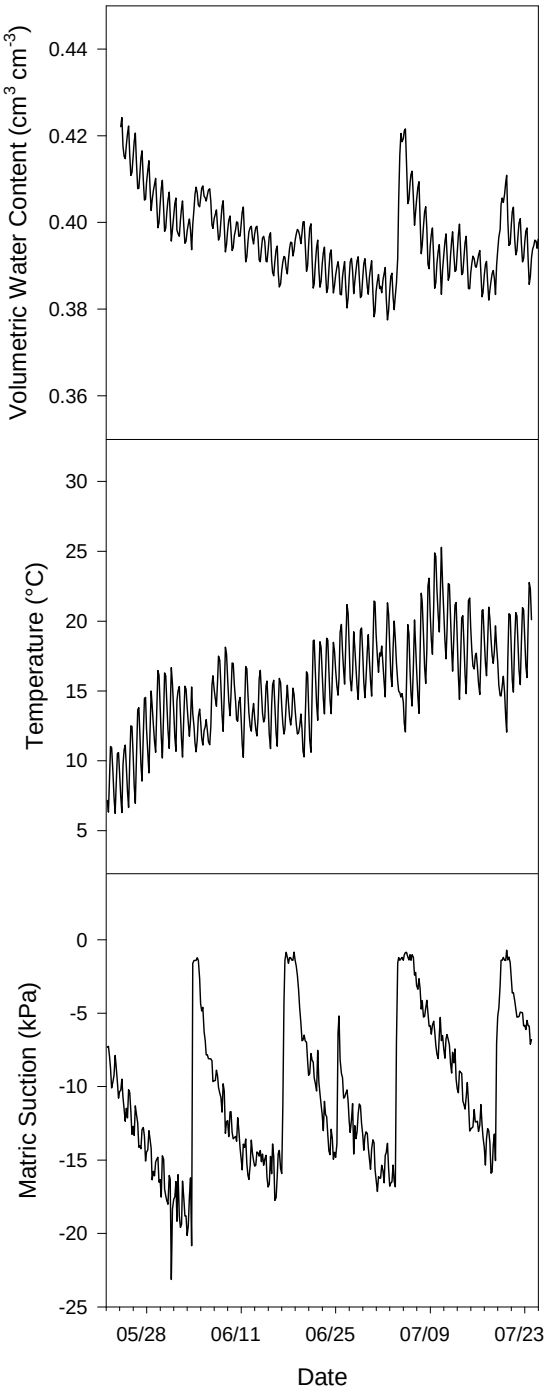


Figure 5.4. Volumetric soil water content (top), soil temperature (middle) and matric potential (bottom) measured at 5 cm depth at the point source monitoring station during the field experiment.

The Verhoef (2004) method used for estimating ATI assumes negligible latent and sensible heat transfer, thus requiring overnight periods to have calm winds and cloudless skies. Six days out of the entire May through July dataset met the criteria for thermal inertia analysis and will be the focus of this study. The days that conformed to the criteria of cloudless nights with low wind speeds and smooth radiation profiles were June 20 and 21, July 5 and 6, and July 20 and 21, 2012 (Figure 5.5). Soil surface temperature variability was expected to be at a minimum at the point of daily minimum temperatures that occur just prior to sunrise. Therefore, any spatial variability and its relationship to physical properties should be most apparent at the minimum overnight temperature.

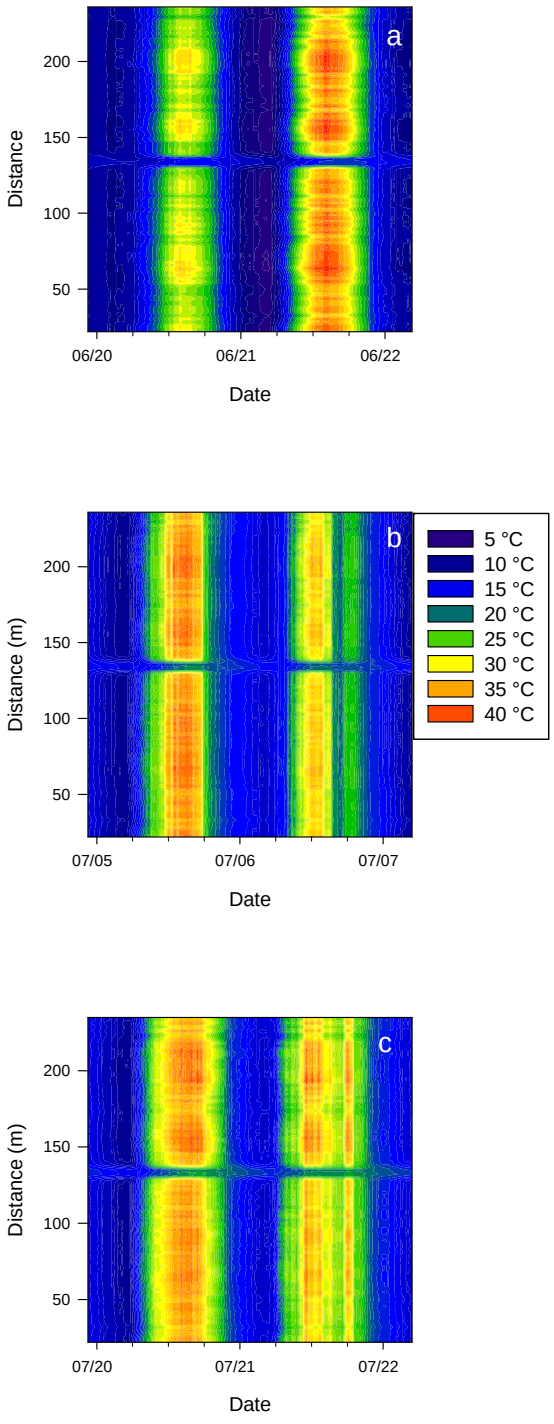


Figure 5.5. Soil surface temperatures as a function of distance and time measured on a) 20 and 21 Jun.; b) 5 and 6 Jul.; and c) 20 and 21 Jul. 2012.

Spatial variability of the daily minimum temperature occurring just prior to sunrise appeared to decrease with increasing minimum temperatures (Figure 5.6). That is, lower spatial mean temperatures corresponded to greater spatial variability as denoted by the standard deviation (Table 5.1). Spatial mean temperatures at the 0 cm cable had no correlation to bulk density and were not well correlated to elevation (Table 5.1).

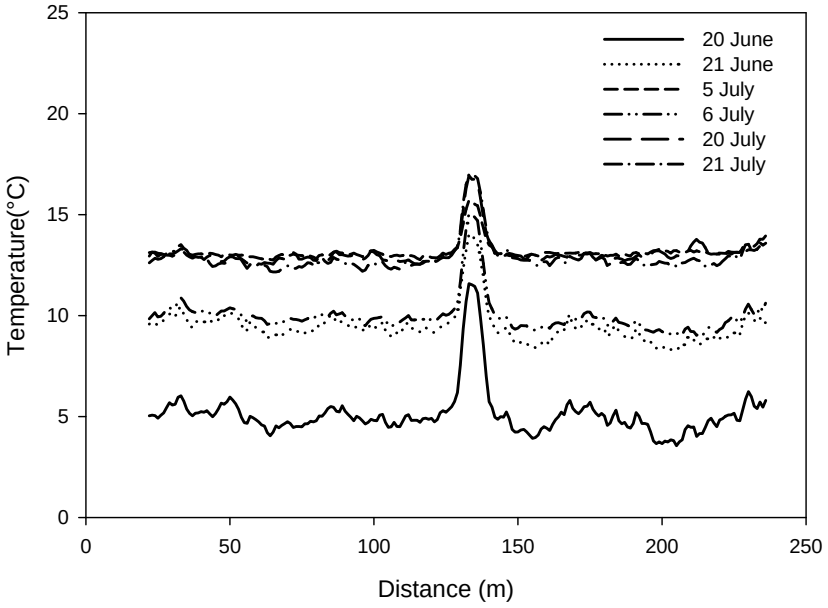


Figure 5.6. Daily minimum soil temperatures as a function of distance measured at the 0 cm cable.

Table 5.1. Spatial mean temperature and standard deviation (SD) of the daily minimum surface soil temperature for the eight candidate days.

| Day | Mean (°C) | SD (%) | Spatial Correlation | |
|---|---|---|---|---|
| | | | Bulk Density | Elevation |
| June 20 | 4.9 | 0.5 | -0.04 | 0.21 |
| June 21 | 9.3 | 0.4 | 0.02 | 0.14 |
| July 5 | 13.1 | 0.9 | -0.10 | 0.26 |
| July 6 | 9.8 | 0.4 | -0.032 | 0.19 |
| July 20 | 13.0 | 0.2 | -0.10 | 0.24 |
| July 21 | 12.7 | 0.3 | -0.11 | 0.28 |

Spatial representations of the variability of daily minimum surface temperature do not reveal meaningful trends, as temperature merely represents the state of the local energy balance at that particular instant (Scott, 2000). Apparent thermal inertia was then examined as a means of revealing the true scales of variability within the cover system. Apparent thermal inertia was estimated for the six candidate days using Equation 5.15 (Figure 5.7). Spatial distribution of ATI across the transect was not correlated with measured physical properties at the measurement scale (Table 5.2).

Table 5.2. Spatial mean and standard deviation (SD) of ATI and spatial correlations to: bulk density (BD), elevation (Elev.), volumetric heat capacity ($C_v$), and thermal conductivity ($\lambda$)

| Day | Mean ATI ($MJ\ m^{-2}\ K^{-1}\ s^{-0.5}$) | SD (%) | Correlation | | | |
|---|---|---|---|---|---|---|
| | | | D | Elev. | $C_v$ | $\lambda$ |
| June 20 | 1150.85 | 80.74 | 0.06 | 0.20 | -0.19 | -0.05 |
| June 21 | 1065.15 | 80.53 | 0.01 | 0.22 | 0.17 | 0.08 |
| July 5 | 2701.89 | 93.97 | 0.06 | 0.02 | -0.06 | -0.03 |
| July 6 | 1418.86 | 64.56 | 0.16 | 0.18 | 0.13 | 0.12 |
| July 20 | 1634.12 | 92.72 | 0.02 | 0.02 | 0 | 0 |
| July 21 | 1299.70 | 73.11 | -0.12 | 0.22 | -0.1 | -0.03 |

The dominant feature in Figure 5.7 is the peak in ATI that corresponded to the central vehicle access path. The ability to represent the change in thermal properties corresponding to the vehicle access path confers a level of confidence in the repeatability of the ATI estimation method (Goovaerts, 1997). The central peak in ATI was removed from subsequent analyses.

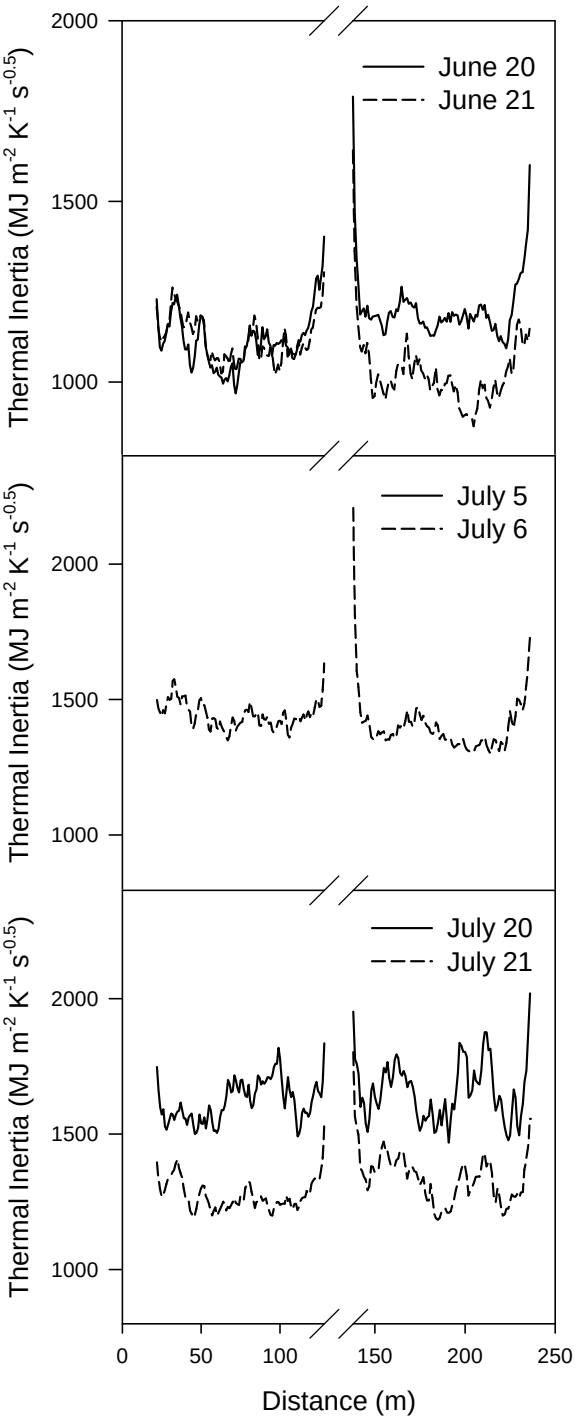


Figure 5.7. Apparent thermal inertia as a function of transect distance for three sets of candidate days.

Two elements were of interest when describing the distribution of ATI in the field: the temporal patterns and the spatial distribution. Describing temporal patterns is important in describing why a certain ATI was estimated on a given day. Characterizing the spatial distribution of ATI will begin to describe relationships to measured physical properties and the spatial scales of variation within field-scale ATI measurements.

### 5.5.1 Temporal Distribution

Average ATI values of all spatial data varied temporally between successive days and between pairs of days. The most plausible explanation for the transient nature of the scale shifts would most likely be soil water content. Daily average ATI and soil water content measured at 5 cm at the central monitoring location were correlated ($R^2 = 0.66$) (Figure 5.8). However, the strength of the relationship was not strong enough to preclude examining other factors that could lead to changes in ATI. Bond-Lamberty et al. (2005) found that 90 to 95% of shallow soil temperature variability could be explained using a weighted sum of air temperature ($\bar{T}_w$ ). The correlation between an 11 day weighted sum air temperature and ATI was not as strong as that between ATI and $\theta_v$ ($R^2 = 0.44$). The lower correlation was not surprising, given that ATI is a composite thermal property and not a direct reflection of soil surface temperature. Near surface atmospheric boundary layers are sensitive to soil water content (McCumber and Pielke, 1981; Pan and Mahrt, 1987) and daily maximum vapor pressure deficit was previously used by Ashcroft and Gollan (2013) to provide a qualitative assessment of ATI. In our case daily maximum vapor pressure deficit was poorly correlated with ATI ($R^2 = 0.10$). Soil matric potential was the best predictor of ATI ($R^2 = 0.76$). Strong correlations between ATI and both $\theta_v$ and matric potential provide greater confidence that estimates of daily mean ATI are reflections of at least the general wetness of the soil, if not the water content directly.

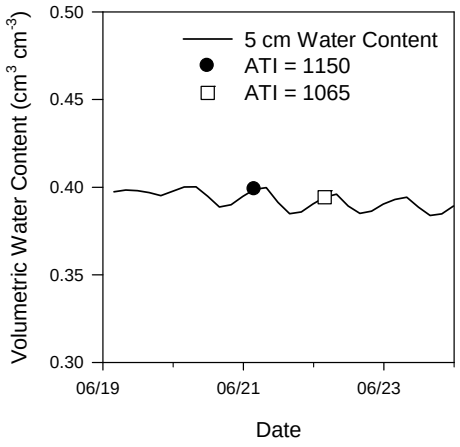


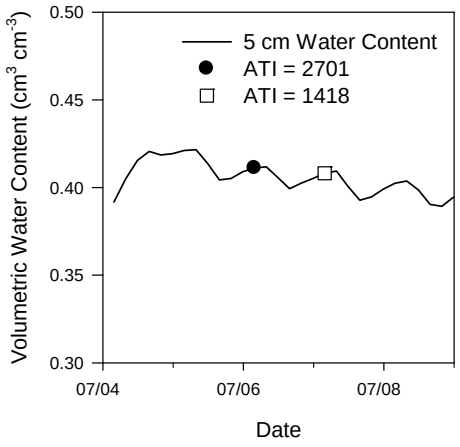


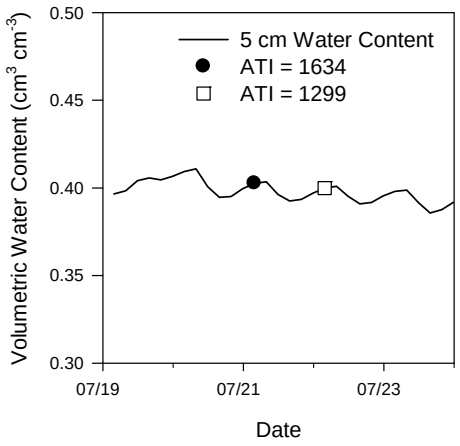


Figure 5.8. Daily spatial-averaged ATI in relation to volumetric water content measured at 5 cm during the experiment.

### 5.5.2 Spatial Distribution

The magnitude of ATI is related to the amount of water in the soil as given by the matric potential and volumetric water content. Although transient in nature, the amount of water in the soil is influenced by spatially static physical and thermal properties. The spatial scaling of bulk density, air-dried volumetric heat capacity, air-dried thermal conductivity, and elevation did not reveal any consistent trends (Figure 5.9). The total variance in volumetric heat capacity and elevation skewed towards scales that were greater than half the transect at 108 m. Variance in air-dried thermal conductivity and bulk density was dominated by the small scale of less than 3 m.

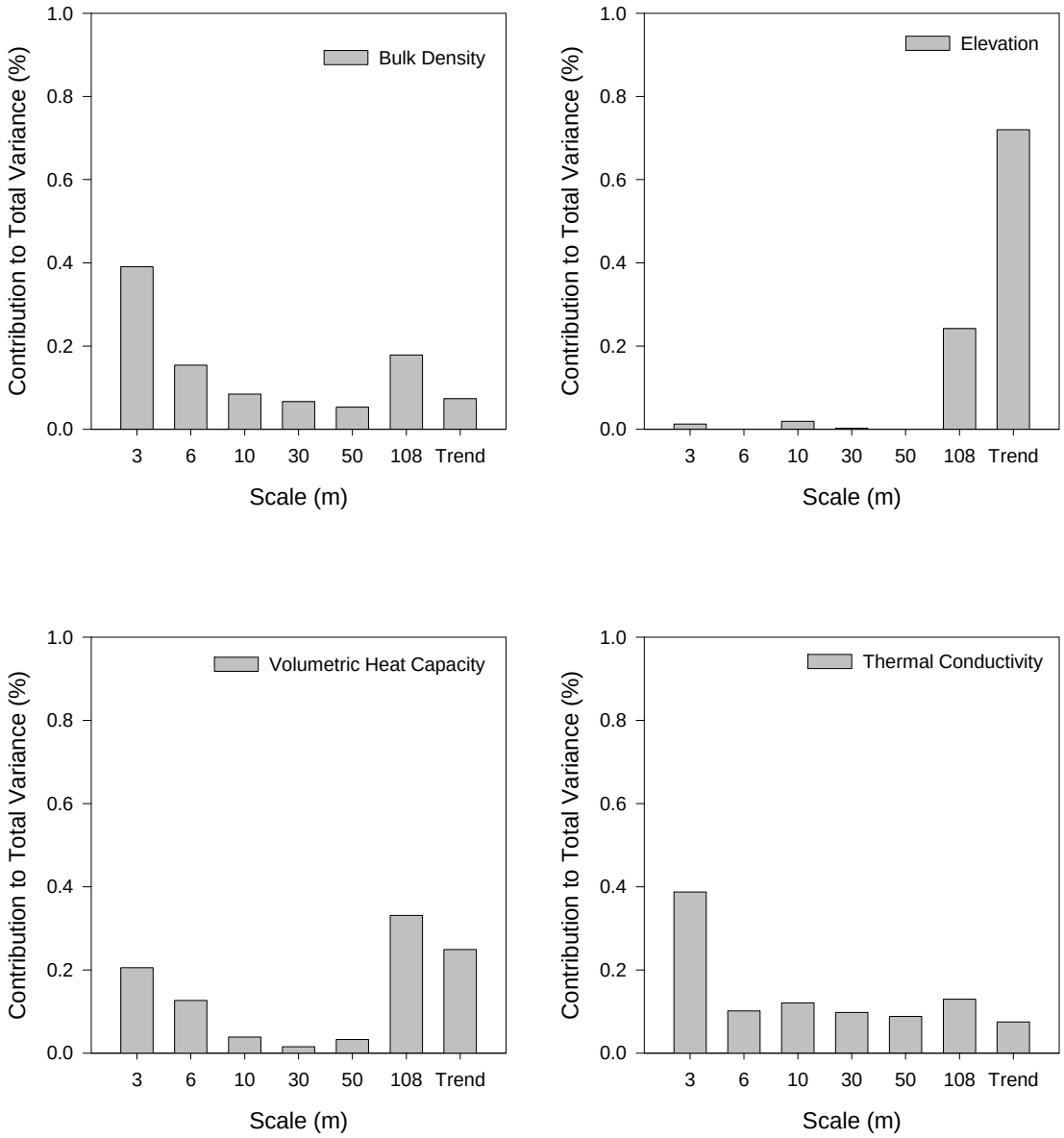


Figure 5.9. Intrinsic spatial scales and their relative dominance of measured physical properties on the experimental transect.

Spatial variance in ATI was dominated by either the 30 m scale or the large scale trend (Figure 5.10). Scale dominance was transient and was variable between days, suggesting that static physical and thermal properties of the air-dried peat were not controlling the distribution of ATI within the transect. Dominant-scale correlations between ATI and physical properties were

not consistent. For example, the field scale trend in ATI on 20 Jun. 2013 was highly positively correlated with all physical and thermal properties and had $R^2$ values of ≥0.71. Conversely, the next day, 21 Jun. 2012 was highly negatively correlated only with elevation with $R^2$ = -0.91 and no other physical properties. Given that physical properties are unlikely to change so dramatically within 24 hours, it is most likely that a transient parameter is leading to transient scale shifts in ATI.

When compared with matric potential and volumetric water content, it is clear that a wet transect is dominated by the 30 m scale, while drying leads to a scale shift to the field-scale trend (Figure 5.10). Both laboratory measured and field SWCCs indicated an AEV of 7 to 8 kPa. Average daily matric potential for 20 Jun. and 21 Jun. 2012 were 7 and 9 kPa, respectively, which corresponded to the shift away from being dominated by the 30 m scale, to being dominated by the field scale trend. Apparent thermal inertia was also correlated to volumetric water content ($r^2$ = 0.66), providing further evidence that, while a unique estimation of water content cannot be made, the property is related to the general wetness of the soil.

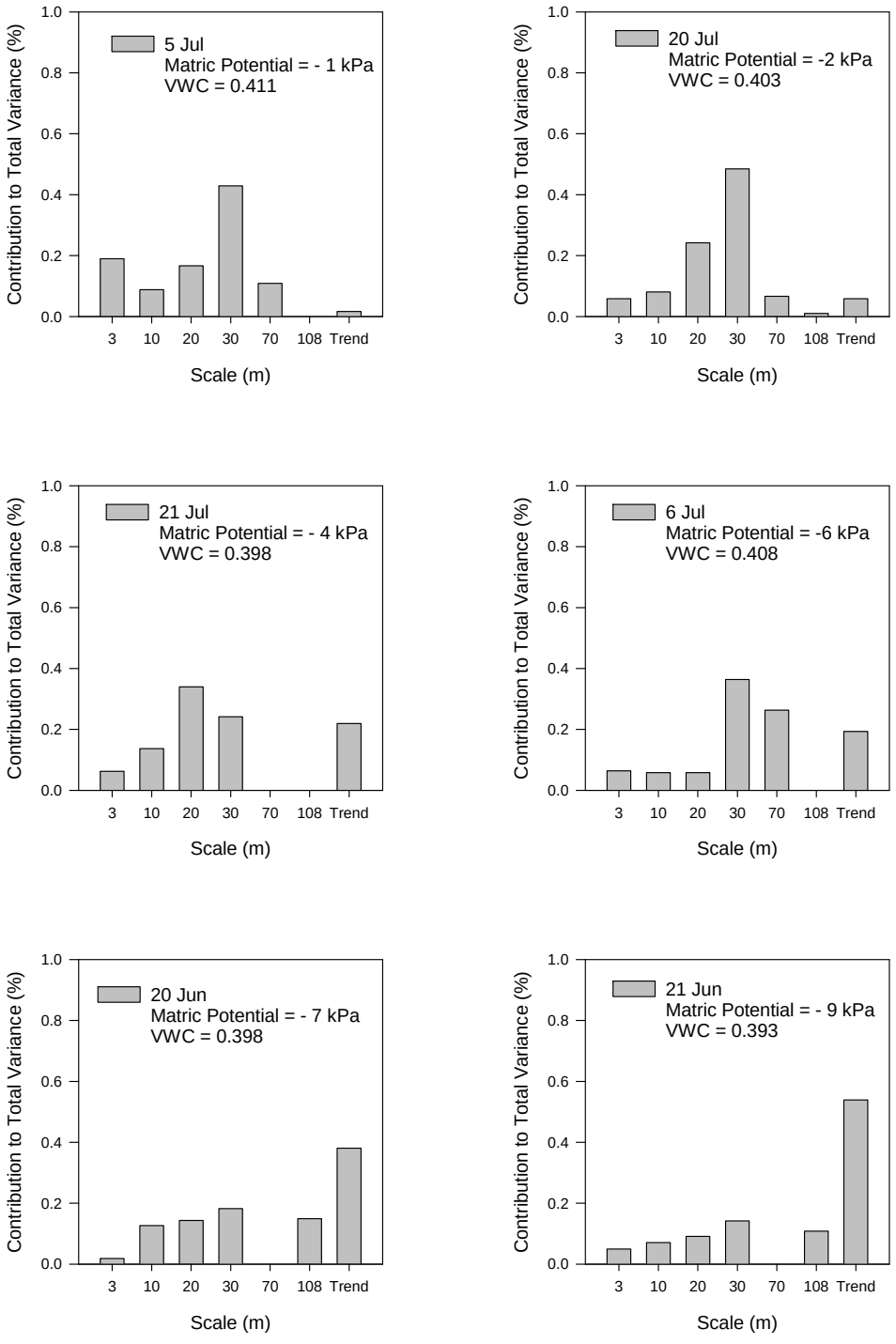


Figure 5.10. Intrinsic spatial scales and their relative dominance of ATI with respect to daily average matric potential. Note that VWC indicates volumetric water content ($cm^3\ cm^{-3}$)

Temporal shifts in spatial scales of variability in ATI are not surprising. An extensive body of research exists that highlights the interrelations of physical and environmental controls on the distribution of water in a landscape. Topography is often cited as a dominant non-local control of the distribution of water in a field (Grayson et al., 1997; Vanderlinden et al., 2011). Indeed topography has been found to be a dominant control on water distribution in reclamation cover systems (Kelln et al., 2008) and in steeply sloping systems (Gómez-Plaza et al., 2000). However, in relatively flat areas, such as the transect in our study, topography does not exert any substantial control (Kaleita et al., 2004).

Comparison of the results of the current study with existing reports in the literature underlines the fact that no two locations are alike, and that spatial controls on water distribution combine in non-linear fashion (Western et al., 2004). Spatial variability has been found to exhibit hysteresis in response to water content, with decreasing variability during wetting periods and increasing variability as the soil dries (Ivanov et al., 2010). The spatial characteristics of water content distribution were unique to the particular domain and the combined effects of topography, soil depth, and antecedent water content. Decreasing spatial variability with increasing water content has been reported elsewhere (Brocca et al., 2007), while the opposite has also been reported (Brocca et al., 2010). Western et al. (1998) found wet periods increased variability in soil water content due to lateral redistribution of water during wet periods as compared to locally controlled homogeneity during dry periods. During wet winter periods spatial correlation lengths were between 35 and 50 m, and increased to 50 to 60 m during dry summer periods.

The current field study represented a completely new landscape that was constructed in such a manner as to limit variability as evidenced by the planar surfaces and homogeneous

material. It would seem from reports in the literature that variability of soil properties in the cover system are often what contribute to variability in the distribution of water. Spatial variability of available soil water in a cover system did not respond to the total amount of water available in the soil, and was universally variable irrespective of the level of wetness or dryness (Mapfumo et al., 2006). The total lack of spatial dependence was attributed to heterogeneity of the topsoil material, which was comprised of a mixture of peat and clay loam material. A reclamation cover system studied by Leatherdale et al. (2012) increased in spatial variability with a decrease in water content. The variability during dry periods was attributed to spatial variations in textural properties and vegetation densities. Conversely, no distinct spatial pattern in $CO_2$ flux was found on a spatially homogeneous cover system comprised of a uniform fine to medium grained sand (Kabwe et al., 2005).

The shift in spatial scales found in the current study could be related to the peat material that comprised the cover system. Spatial variability of soil water content in organic soils with no topographical relief was studied by Anctil et al. (2002). Spatial measurements of water content were not correlated with organic matter, suggesting that near-surface water content variability was controlled by other unreported factors. Correlation lengths for two sampling days with high water contents were reported to be 37 and 31 m with ranges greater than 100 m for a 755 m transect. The change in spatial structure with changes in water content were not discussed. Petrone et al. (2004) noted that spatial patterns of water content in a cutover peatland differed between wetting and drying periods, although the differences were not further explored. Szatylowicz et al. (2007) observed that spatial variability of peat water content increased as the peat dried. It was postulated that the variability was due to increases in bulk density and hydrophobicity, both of which increased as the soil dried.

The transect used in the current study was comprised of a homogenous peat material and was characterized by near uniformity in physical properties and very little variability in elevation. Drying periods tended to homogenize the soil surface and led to ATI estimates that were dominated by the field scale trend. Inputs of precipitation were organized in a consistent fashion and revealed a consistent shift to the 30 m scale during wet periods. It is interesting to note that the 30 m scale was one of the lowest contributors to total variance for physical and thermal properties, yet was consistently found to be important for ATI. The importance of the 30 m scale is not fully understood, and should be the subject of further investigation.

Remote sensing scientists have frequently cited the benefits of measuring soil water content remotely from surface soil properties (Gillies and Carlson, 1995; Verstraeten et al., 2006). However, due to complications inherent to remote sensing such as atmospheric transmissivity, vegetation, and surface micro-variations, estimates of water content are generally only reflective of water contents at the immediate soil surface. A DTS system such as the one employed in this study should be an advance over remote sensing techniques because of the depth of measurement influence and the high spatial resolution. However, it was shown in the current study that physical and certain thermal properties could not be readily detected by DTS. A possible explanation is the scale difference in the measurement support; that is, physical and air-dried thermal properties were taken from soil cores tens of cubic centimeters in volume, whereas the DTS measures temperatures immediately surrounding the cable. Using a DTS system to estimate thermal properties or soil water content presents an interesting challenge with great potential. Future studies of this kind should investigate systems with greater topographical or textural variations, so as to clearly delineate areas where differential behavior would be expected. In addition, active heating DTS methods may be preferable to passive methods,

irrespective of whether thermal diffusivity or thermal inertia is the parameter of interest. Active heating methods release a known flux of energy into the soil, allowing for a determination of thermal conductivity, based on the temperature change with time. Active heating methods have the potential to accurately measure soil water content with a much higher level of precision than passive methods (Sayde et al., 2010; Ciocca et al., 2012). Research into this area is underway and should be the subject of future investigations in the mining industry.

The salient point arising from this discussion is that the distribution of water in both natural and reclaimed systems is not controlled by one dominant factor, but is highly site-specific. The interaction of physical properties and near-surface meteorological conditions lead to dominant spatial scales of variability that change with time and are unique to each site. In the case of our field study, wetter conditions led ATI variability to shift scale dominance toward the 30 m scale. Drying conditions tended to homogenize near surface conditions leading to a dominance of the field-scale trend. Days with intermediate water contents showed components of both the smaller 30 m scale, as well as an increasing contribution from the field-scale trend.

### 5.6 Summary and Conclusions

The combination of measuring apparent thermal inertia with a DTS system was found to be effective in investigating the spatial scaling of thermal properties as a proxy for water content in soil cover systems. A DTS system measures at small scales and large extents, and in doing so avoids a major drawback commonly found with measuring water content over large areas. Use of ATI as a variable of interest is appealing because the parameter responds to changes in water content and only requires measurement of temperatures at the soil surface, thus avoiding depth sensitivity issues prevalent with estimating thermal diffusivity. Results of this study also highlight the need for an investigation of spatial scales other than just the measurement scale. An

investigation of the intrinsic spatial scales revealed increased dominance of smaller scales during wetter periods; a finding that is not apparent at the measurement scale.

# 6.0 SYNTHESIS AND CONCLUSIONS

Soil cover systems are a critical component of a mine's reclamation program. Understanding how these systems are responding to climatic inputs is critical for judging the performance of the systems. Typically, performance of a cover system is monitored at a small number of vertically intensive monitoring locations. Monitoring at a small number of isolated locations may have been appropriate for small pilot scale systems of a few hundred square meters in area. However, soil cover systems are increasing in size and can cover tens or even hundreds of hectares. Investigating the spatial variability of the critical properties and processes that govern cover system performance is imperative if we are to improve our understanding of how the systems function at the field scale.

Very few studies have been conducted on the spatial variability inherent in covers systems, and have only focused on soil water content. Water content is difficult and expensive to measure intensively over large areas and has likely precluded further investigation. A recent technique being applied in the earth sciences uses distributed temperature sensing (DTS) to measure temperatures at spatial resolutions down to a meter over thousands of meters. Extensive, high resolution datasets are the ideal for investigating spatial variability, yet spatial variability of soil temperatures and thermal properties has received little attention, especially in the reclamation industry. Soil temperatures and thermal properties are important in and of themselves, as the data can provide insight into local variations in the surface energy balance and are reflective of soil physical properties. In addition, soil temperatures and thermal properties are also reflective of subsurface water content and can at least provide qualitative information as to the general wetness of the soil.

The purpose of this research was to investigate the spatial variability of temperature and thermal properties that exist in soil cover systems. A DTS system was used to do so as it

provides an unprecedented opportunity to generate the ideal spatial dataset of high spatial resolutions over large extents. The research in this dissertation describe the methods used for achieve the research goal.

### 6.1 Applications to the Mining Industry

A DTS system has not been previously been used in the mine reclamation industry for use in instrumenting cover systems. Given the novelty of using a DTS system in a mining application a case study of installations in a range of cover system textures and configurations was needed. Chapter 3 detailed the commissioning of a DTS system in three cover systems. The three cover systems encompassed a wide range of textures and configurations, and represented a broad cross-section of what may be encountered in the reclamation industry. Soil temperatures measured in the cover systems were used to provide preliminary indications of the spatial variability through the use of semivariograms. Semivariogram analysis was able to distinguish the major features found at each site by demonstrating the spatial structure of the temperature spatial series. Spatial variability of soil temperatures has been investigated previously, but never for the mining industry and not when using the unique dataset that is obtained with a DTS system. The study found in Chapter 3 demonstrated that a DTS system could be employed in a mining context and the data were useful for investigating the spatial variability that exists in the cover systems.

### 6.2 Method Development

Chapter 3 investigated the spatial variability of soil temperatures within the cover systems. While soil temperature is an important variable of interest, it is often more useful to use the temperature data to estimate a property of the system. Current methods using apparent thermal diffusivity to infer local variations in water content have met with limited success, due to the non-unique relationship between thermal diffusivity and water content, as well as high

sensitivities to installation depth. The purpose of Chapter 4 was to develop a method that could be readily applied to studies in the mining industry that both minimized estimation uncertainties and was at least qualitatively related to water content. Apparent thermal inertia was adapted from remote sensing for use in cover system investigations. Apparent thermal inertia was found to be sensitive to changes in water content and subject to less uncertainty than apparent thermal diffusivity. The results of Chapter 4 represent a novel application for spatial variability studies and would be the main parameter of interest when used to investigate the scaling properties of cover systems.

### 6.3 Spatial Scaling

The ultimate goal of the research program was to investigate the spatial scaling properties of a cover system at the field scale. Chapter 5 applied the installation techniques from Chapter 3, and used the method developed in Chapter 4 to finally determine the dominant scales of variation that exist at the field scale. Apparent thermal inertia was found to be a transient property that did not have similar scaling properties to the measured physical and thermal properties. It was found that the spatial scaling depended on the the water content of the system. The findings from Chapter 5 represent a critical development in our understanding of how cover systems behave on the field scale. It can no longer be assumed that the cover system will respond uniformly to changes in climatic conditions. The results of Chapter 5 highlight the need to understand cover system performance at all spatial scales to develop a true picture of the performance of the system.

### 6.4 Implications for Future Research

The spatial scaling of soil thermal properties provides important insights into the performance of soil cover systems at the field scale. Knowledge of how cover systems behave at the field scale will allow the designer to better plan the layout of monitoring systems. A

systematic monitoring plan can then be based on data that are representative of the entire cover system across all spatial scales, as opposed to the current method of assuming homogeneity and monitoring at a point source. Information regarding the spatial scaling of cover systems will also be useful when modelling the system. Understanding the dominant scale of variation will provide useful input into numerical models when trying to understand how the system will behave under varying climatic scenarios.

A DTS system has proven to be remarkably useful for applications in the mining industry. The system is robust and stand-alone; two important criteria when instrumenting a remote site. Construction of cover systems lends itself to ease of instrumentation with fiber optic cables, as the cables are easily laid as subsequent cover layers are added. Instrumenting into existing cover systems can be laborious, yet no more so than traditional monitoring sensors. Difficulties can arise in cover systems that incorporate stony materials in the cover borrow material, and care must be taken so as to not damage the cable. Precise depth discrimination is also difficult in stony materials used in the construction of many cover systems.

Like all measurement variables, apparent thermal inertia represents a compromise between ease of application, utility of the results, and quality of the output. Apparent thermal inertia was chosen for use in this research because the concept is easily understood, is more directly related to water content than thermal diffusivity, and does not require precise depth measurements. In that way, the use of apparent thermal inertia represents an improvement over the existing methods. However, direct measurements of soil water content will likely continue to be the preferred measurement variable as some researchers may not see the utility in estimating thermal properties when investigating the distribution of water. Until such as time as water

content can be more directly measured with a system that enjoys the measurement resolution of a DTS system, estimating thermal properties will remain an important variable of interest.

The possibilities for expanding future research from the initial steps taken in this dissertation are myriad. The most obvious avenue involves the use of active heat pulse methods combined with a DTS for direct measurement of water content over the entire length of the fiber optic cable. Direct measurements of water content using heat pulse methods would be a critical link between point source measurements and remotely sensed areal measurements. Active heat pulse measurements in a cable installed throughout the entire cover system would provide an unprecedented level of detail in characterizing large spatial areas. Furthermore, using heat pulse methods and DTS could also allow for spatially distributed water content measurements at any selected depth. Adding a depth component could thus provide calculations of soil water storage over unprecedented spatial extents, which is currently prohibitive with existing water content sensor technology. At larger spatial scales, current remote sensing techniques have very limited depth discrimination, and a heat pulse / DTS measurement system that is able to measure water content at various depths would be a substantial advancement in measurement techniques.

Estimation of thermal properties remains a viable and necessary research goal. The apparent thermal inertia method developed in this dissertation is an improvement over the existing method in that it is readily measured and is not subject to depth uncertainty. To improve estimates of thermal inertia, greater depth discrimination would be useful. The method assumes that measurements are integrated over the daily damping depth. Greater spatial coverage at multiple depths would increase our confidence in the estimate and provide insights into the spatial distribution of damping depth. Finally, characterizing the spatial variability of cover systems, whether measuring water content, physical, or thermal properties, should remain a

research priority. Reclamation projects represent a large capital investment for a mine site. It is imperative to understand how that cover system is performing and verify that the investment is functioning as designed. Furthermore, a good understanding of how the cover system is functioning provides further confidence to stakeholders and can lead to more sustainable mine reclamation programs.

## LIST OF REFERENCES


Albrecht, B. and C.H. Benson. 2001. Effect of desiccation on compacted natural clays, J. Geotech. and Geoenv. Eng. 127:67-76.

Albright, W.H., C.H. Benson, G.W. Gee, A.C. Roesler, T. Abichou, P. Apiwantragoon, B.F. Lyles, and S.A. Rock, 2004. Field water balance of landfill final covers. J. Environ. Qual. 33:2317-2332.

Albright, W. H., C.H. Benson, G.W. Gee, T. Abichou, S.W. Tyler and S.A. Rock. 2006a. Field performance of three compacted clay landfill covers. Vadose Zone J. 5:1157-1171.

Albright, W. H., C.H. Benson, G.W. Gee, T. Abichou, E. McDonald, S.W. Tyler and S.A. Rock. 2006b. Field performance of a compacted clay landfill final cover at a humid site. J. Geotech. Geoenviron. Eng. 132:1393-1403.

Al-Kayssi, A.W. 2002. Spatial variability of soil temperature under greenhouse conditions. Renew. Energ. 27:453-462.

ASME. 2005. PTC 19.1-2005: Test Uncertainty. ASME, New York, NY.

ASTM. 2007. ASTM D422: Standard test method for particle-size analysis of soils. ASTM Int'l. West Conshohocken, PA.

ASTM. 2008. ASTM D6836: Standard test methods for determination of the soil water characteristic curve for desorption using a hanging column, pressure extractor, chilled mirror hygrometer, and/or centrifuge. ASTM Int'l. West Conshohocken, PA.

Anctil, F., R. Mathieu, L.E. Parent, A.A. Viau, M. Sbih, and M. Hessami. 2002. Geostatistics of near-surface moisture in bare cultivated organic soils. J. Hydrol. 260: 30-37.

Arya, S.P. 2001. Introduction to micrometeorology. Academic Press, New York, NY.

Ashcroft, M.B. and J.R. Gollan. 2013. Moisture, thermal inertia, and the spatial distribution of near-surface soil and air temperatures: Understanding factors that promote microrefugia. Agr. Forest. Meteorol. 176: 7-89.

Aubertin, M., E. Cifuentes, S.A. Apithy, B. Bussière, J. Molson, and R.P. Chapuis. 2009. Analyses of water diversion along inclined covers with capillary barrier effects. Can. Geotech. J. 46:1146-1164.

Baskan, O., Y. Kosker, and G. Erpul. 2013. Spatial and temporal variation of moisture content in the soil profiles of two different agricultural fields of semi-arid region. Environ. Monit. Assess. doi: 10.1007/s10661-013-3343-8.

Bhumralkar, C.M. 1975. Numerical experiments on the computation of ground surface temperature in an atmospheric general circulation model. J. Appl. Meteorol. 14:1246-1258.

Biswas A. and B.C. Si. 2011a. Identifying scale specific controls of soil water storage in a hummocky landscape using wavelet coherency. Geoderma, 165:50–59.

Biswas, A. and B.C. Si. 2011b. Scales and locations of time stability of soil water storage in a hummocky landscape. J. Hydrol. 408:100-112.

Biswas, A. and B.C. Si. 2011c. Revealing the controls of soil water storage at different scales in a hummocky landscape. Soil Sci. Soc. Am. J. 75: 1295-1306.

Biswas, A., and B.C. Si. 2011d. Depth persistence of the spatial pattern of soil water storage in a hummocky landscape. Soil Sci. Soc. Am. J. 75:1099-1109.

Biswas, A., L.K. Tallon, and B.C. Si. 2009. Scale-specific relationships between soil properties: Hilbert-Huang Transform. Paedometron. 28:17-20.

Biswas, A., H.P. Cresswell, H.W. Chau, R.A. Viscarra Rossel, and B.C. Si. 2013. Separating scale-specific soil spatial variability: A comparison of multi-resolution analysis and empirical mode decomposition. Geoderma. 209-210:57-64.
Blight, G.E., and A.B. Fourie. 2005. Experimental landfill caps for semi-arid and arid climates. Waste Manage. Res. 23:113-125.
Blöschl, G. and R. Grayson. 2000. Spatial observations and interpolation. In: Grayson, R. and G. Blöschl (eds.), Spatial patterns in catchment hydrology: Observations and modeling. Cambridge University Press, United Kingdom. p. 17-50.
Bohnhoff, G.L., A.D. Ogorzalek, C.H. Benson, C.D. Shackleford, and P. Apiwantragoon. 2009. Field data and water-balance predictions for a monolithic cover in a semi-arid climate. J. Geotech. Geoenviron. Eng. 135:333-348.
Bond-Lamberty, B., K.M. Brown, C. Goranson, and S.T. Gower. 2006. Spatial dynamics of soil moisture and temperature in a black spruce boreal chronosequence. Can. J. For. Res. 36:2794-2802.
Brady, N.C. and R.R. Weil. 2007. The natured and properties of soils. 14th Ed. Prentice Hall, Upper Saddle River, NJ.
Bristow, K.L. 1988. The role of mulch and its architecture in modifying soil temperature. Aust. J. Soil. Res. 26:269-280.
Bristow, K.L. 2002. Thermal conductivity. In: Dane, J.H. and G.C. Topp (eds.) Methods of soil analysis. Part 4 Physical methods. Soil Science society of America, Inc., Madison, WI. p. 1209-1226.
Brocca, L., R. Morbidelli, F. Melone, and T. Moramarco. 2007. Soil moisture spatial variability in experimental areas of central Italy. J. Hydrol. 333:356-373. doi:10.1016/j.hydrol.2006.09.004.
Brocca, L., F. Melone, T. Moramarco, and R. Morbidelli. 2010. Spatial-temporal variability of soil moisture and its estimation across scales. Water Resour. Res. 46:W02516. doi:10.1029/2009WR008016
Brunt, D. 1932. Notes on radiation in the atmosphere. I. Quart. J. R. Meteorol. Soc. 58, 389-420.
Brutsaert, W. 1975. On a derivable formula for long-wave radiation from clear skies. Water Resour. Res. 11:742–744.
Buchan, G.D. 2001. Soil temperature regime. In: Smith, K.A. and Mullins, C.E. (Eds). Soil and environmental analysis. Physical methods, 2nd Ed. Marcel Dekker, Inc. New York, NY. p. 539-594.
Buck, A.L. 1981. New equations for computing vapor pressure and enhancement factor. J. Appl. Meteorol. 20:1527-1532.
Campbell, G.S. 1977. An introduction to environmental biophysics. Springer-Verlag, New York, NY.
Campbell, G.S., K. Calissendorff, and J.H. Williams. 1991. Probe for measuring soil specific heat using a heat pulse method. Soil Sci. Soc. Am. J. 55:291-293.
Campbell, G.S., J.D. Jungbauer, Jr., W.R. Bidlake, and R.D. Hungerford. 1994. Predicting the effect of temperature on soil thermal conductivity. Soil Sci. 158:307-313.
Carey, S.K. 2008. Growing season energy and water exchange from an oil sands overburden reclamation soil cover, Fort McMurray, Alberta, Canada. Hydrol. Processes. 22:2847-2857.
Carey, S.K., S.L. Barbour, and M.J. Hendry. 2005. Evaporation from a waste-rock surface, Key Lake, Saskatchewan. Can. Geotech. J. 42:1189-1199.

Carslaw, H.S. and J.C. Jaeger. 1959. Conduction of heat in solids. 2nd ed. Oxford University Press, London.
Ciocca, F., I. Lunati, N. Van de Giessen, and M. B. Parlange. 2012. Heated optical fiber for distributed soil moisture measurements: a lysimeter experiment. Vadose Zone J. 11. doi: 10.2136/vzj2011.0199.
Costa, S. and M. Scoble. 2006. An interdisciplinary approach to integrating sustainability into mining engineering education and research. J. Clean. Prod. 14:366-373.
Cressie, N.A.C. 1991. Statistics for spatial data. John Wiley & Sons, Inc. Toronto.
de Vries, D.A. 1963. Thermal properties of soils. In: W.R. van Wijk, (ed). Physics of plant environment. North Holland. p. 210-235.
De Vries, D.A. 1975. Heat transfer in soils. In: de Vries, D.A. and N.H. Afgan (Eds.) Heat and mass transfer in the biosphere. Part I: Transfer processes in the plant environment. John Wiley and Sons, New York, NY. p. 4-28
Eggelsman, R. 1972. The thermal constants of different high-bogs and sandy soil. Proc. 4th Int. Peat Congr. 3:371-382.
Foken, T. 2008. The energy balance closure problem: an overview. Ecol. Appl. 18:1351-1367.
Freifeld, B.M., S. Finsterle, T.C. Onstott, P. Toole, and L.M. Pratt. 2008. Ground surface temperature reconstructions: Using in situ estimates for thermal conductivity acquired with a fiber-optic distributed thermal perturbation sensor. Geophys. Res. Lett. 35, L14309, doi:10.1029/2008GL034762.
Fuchs, M., and A. Hadas. 1972. The heat flux density in a non-homogeneous bare loessial soil. Boundary Layer Meteorol. 3:191-200.
Gao, Z., R. Horton, L. Wang, H. Liu, and J. Wen. 2008. An improved force-restore method for soil temperature prediction. 59:972-981.
Garrido, F., M. Ghodrati, and M. Chendorain. 1999.Small-scale measurement of soil water content using a fiber optic sensor. Soil Sci. Soc. Am. J. 63:1505-1512.
Gates D.M. 1980. Biophysical ecology. Springer-Verlag, New York.
Gee, G.W., W.H. Albright, and C.H. Benson. 2006. Comment on "Evaluation of evapotranspirative covers for waste containment in arid and semiarid regions in the southwestern USA". Vadose Zone J. 5:809:812.
Gillies, R.R. and T.N. Carlson. 1995. Thermal remote sensing of suface soil water content with partial vegetation cover for incorporatlion into climate models. J. Appl. Meteor. 34:745-756.
Gómez-Plaza, A., M. Martínez-Mena, J. Albaladejo, and V.M. Castillo. 2001. Factors regulating spatial distribution of soil water content in small semi-arid catchments. J. Hydrol. 253:1261–1277.
Goovaerts, P. 1997. Geostatistics for natural resources evaluation. Oxford University Press, Oxford.
Grayson, R.B., A.W. Western, F.H.S. Chiew and G. Blöschl. 1997. Preferred states in spatial soil moisture patterns: Local and nonlocal controls. Water Resour. Res. 33:2897-2908.
Hao, X., B.C. Ball, J.L.B. Culley, M.R. Carter, and G.W. Parkin. 2006. Soil density and porosity. In: Carter, M.R. and E.G. Gregorich (Eds.) Soil samping and methods of analysis. 2nd Ed. CRC Press, Boca Raton, FL. p. 749-750.
Hatfield, J.L. and J.M. Baker (Eds.) 2005. Micrometeorology in agricultural systems. ASA, Madison, WI.

Hauser, V. L., Weand, B. L., and Gill, M. D. 2001. Natural covers for landfills and buried waste. J. Envir. Engrg. 127:768-775.
Hausner, M.B., F. Suárez, K.E. Glander, N. Van de Giesen, J.S. Selker, and S.W. Tyler. 2011. Calibrating single-ended fiber-optic Raman spectra distributed temperature sensing data. Sensors. 11:10859-10879.
Henderson, R.D., F.D. Day-Lewis, and C. F. Harvey. 2009. Investigation of aquifer-estuary interaction using wavelet analysis of fiber-optic temperature data. Geophys. Res. Lett. 36, L06403, doi: 10.1029/2008GL036926.
Heusinkveld, B.G., A.F.G. Jacobs, A.A.M. Holtslag, and S.M. Berkowicz. 2004. Surface energy balance closure in an arid region: role of soil heat flux. Agric. For. Meteorol. 122:21-37.
Hillel, D. 1998. Environmental soil physics. Academic Press, San Diego, CA.
Hoes, O.A.C., R.P.S. Schilperoort, W.M.J. Luxemburg, F.H.L.R. Clemens, N.C. van de Giesen. 2009. Locating illicit connections in storm water sewers using fiber-optic distributed temperature sensing. Water Res. 43:5187-5197.
Hopmans, J. W. and J. H. Dane. 1986a. Thermal conductivity of two porous media as a function of water content, temperature, and density. Soil Science 142:187-195.
Hopmans, J. W. and J. H. Dane. 1986b. Temperature dependence of soil hydraulic properties. Soil Sci. Soc. Am. J. 50:4-9.
Hopmans, J.W., J. Šimunek, and K.L. Bristow. 2002. Indirect estimation of soil thermal properties and water flux using heat pulse probe measurements: Geometry and dispersion effects. Water Resour. Res. 38:10.1029/2000WR000071, 2002.
Horton, R. and P.J. Wierenga. 1983. Estimating the soil heat flux from observations of soil temperature near the surface. Soil Sci. Soc. Am. J. 47:14-20.
Horton, R. 2002. Soil thermal diffusivity. In: Dane, J.H. and G.C. Topp (eds.) Methods of soil analysis. Part 4 Physical methods. Soil Science society of America, Inc., Madison, WI. p. 1227-1232.
Hu, W. and B.C. Si. 2013. Soil water prediction based on its scale-specific control using multivariate empirical mode decomposition. Geoderma. 193-194:180-188.
Huang, N.E., Z. Shen, S.R. Long, M.L.C. Wu, H.H. Shih, Q.N. Zheng, N.C. Yen, C.C. Tung, and H.H. Liu. 1998. The empirical mode decomposition method and the Hilbert spectrum for non-stationary time series analysis. Proc. R. Soc. Lond. Ser. A – Math. Phys. Eng. Sci. 454A, 903-995.
Incropera, F.P. and D.P. DeWitt. 1996. Introduction to heat transfer. 3rd ed. John Wiley and Sons. New York, NY.
Isaaks, E.H. and R.M. Srivastava. 1989. An introduction to applied geostatistics. Oxford University Press. New York, NY.
Ivanov, V.Y., S. Fatichi, G.D. Jenerette, J.F. Espeleta, P.A. Troch, and T.E. Huxman. 2010. Hysteresis of soil moisture spatial heterogeneity and the "homogenizing" effect of vegetation. Water Resour. Res. 46: W09521, doi:10.1029/2009WR008611, 2010.
Jury, W.A., W.R. Gardner, and W.H. Gardner. 1991. Soil physics. 5th ed. John Wiley & Sons, Inc. Toronto, ON.
Kabwe, L.K., R.E. Farrell, S.K. Carey, M.J. Hendry, and G.W. Wilson. 2005. Characterizing spatial and temporal variations in CO2 fluxes from ground surface using three complimentary measurement techniques. J. Hydrol. 311:80-90.
Kachanoski, R.G., and E. de Jong. 1988. Scale dependence and the temporal persistence of spatial patterns of soil water storage. Water Resour. Res. 24:85-91.

Kahle, A.B., A.R. Gillespie, A.F.H. Goetz, and J.D. Addington. 1975. Thermal inertia mapping. In: Proceedings of the 10th International Symposium on Remote Sensing of Environment, 175, Environmental Research Institute of Michigan, Ann Arbor, MI, October, p. 985-994.
Kahle, A.B., A.R. Gillespie, A.F.H. Goetz, and J.D. Addington. 1976. Thermal inertia imaging as a geologic mapping tool. Geophys. Res. Lett. 3: 26-28.
Kaleita, A.L., L.F. Tian, and M.C. Hirschi. 2004. Identifcation of optimal sampling locations and grid size for soil moisture mapping. ASAE Paper No. 041146.
Karam, M.A. 2000. A thermal wave approach for heat transfer in a nonuniform soil. Soil Sci. Soc. Am. 64: 1219-1225.
Kelln, C., Barbour, L. and Qualizza, C. 2008. Controls on the spatial distribution of soil moisture and solute transport in a sloping reclamation cover. Can. Geotech. J. 45:351-366.
Kellner, E. 2001. Surface energy fluxes and control of evapotranspiration form a Swedish Sphagnum mire. Ag. For. Met. 110:101-123.
Khire, M. V., Benson, C. H., and Bosscher, P. J. 1997. Water balance modeling of earthen final covers. J. Geotech. Geoenvir. Engrg. 123:744-754.
Kluitenberg, G. J., J. M. Ham, and K. L. Bristow 1993. Error analysis of the heat pulse method for measuring soil volumetric heat capacity. Soil Sci. Soc. Am. J. 57:1444–1451.
Kluitenberg, G.J. 2002. Heat capacity and specific heat. In: Dane, J.H. and G.C. Topp (eds.) Methods of soil analysis. Part 4 Physical methods. Soil Science society of America, Inc., Madison, WI. p. 1201-1208.
Krzeminska, D.M., S.C. Steele-Dunne, T.A. Bogaard, M.M. Rutten, P. Sailhac, and Y. Geraud. 2011. High-resolution temperature observations to monitor soil thermal properties as a proxy for soil moisture condition in clay-shale landslide. Hydrol. Process. doi: 10.1002/hyp.7980.
Kustas, W.P., J.H. Prueger, J.L. Hatfield, K. Ramalingam, and L.E. Hipps. 2000. Variability in soil heat flux from a mesquite dune site. Agric. For. Meteorol. 103:249-264.
Lauzon, N., F. Anctil, and J. Petrinovic. 2004. Characterization of soil moisture conditions at temporal scales from a few days to annual. Hydrol. Process. 18:3235-3254.
Leatherdale, J., D.S. Chanasyk, and S. Quideau. 2012. Soil water regimes of reclaimed upland slopes in the oil sands region of Alberta. Can. J. Soil Sci. 92: 117-129.
Liebethal, C. and T. Foken. 2007. Evaluatin of six parameterization approaches for the ground heat flux. Theor. Appl. Climatol. 88:43-56.
Lipiec, J., B. Usowicz, and A. Ferrero. 2007. Impact of soil compaction and wetness on thermal properties of sloping vineyard soil. Int. J. Heat Mass Tran. 50:3837-3847.
Liu and Si. 2008. Dual-probe heat pulse method for snow density and thermal properties measurement. Geophys. Res. Lett. 35: L16404, doi:10.1029/2008GL034897, 2008.
Liu, G., B. Lu, T. Ren, R. Horton, and B.C. Si. 2008. Analytical solution of heat pulse method in a parallelepiped sample space with inclined needles. Soil Sci. Soc. Am. J. 72: 1208-1216.
Lu, N., B.S. Kaya, and J.W. Godt. 2011. Direction of unsaturated flow in a homogeneous and isotropic hillslope. Water Resour. Res. 47, W02519, doi:10.1029/2010WR010003,2011.
Mapfumo, E., D.S. Chanasyk, and C.L.A. Chaikowsky. 2006. Stochastic simulation of soil water status on reclaimed land in Northern Alberta. JOSH. 6:34-44.
Matsushima, D., R. Kimura, and M. Shinoda. 2012. Soil moisture estimation using thermal inertia: potential and sensitivity to data conditions. J. Hydrometeorol. 13:638-648.

McCumber, M.C. and R.A. Pielke. 1981. Simulation of the effects of surface fluxes of heat and moisture in a mesoscale numerical model: 1. Soil layer. J. Geophys. Res., C.10: 9929-9938.
McGuire, P.E., B.J. Andraski, and R.E. Archibald. 2009. Case study of a full-scale evapotranspiration cover. J. Geotech. Geoenviron. Eng. 135: 316-332.
Minacapilli, M., M Iovino, and I.F. Blanda. 2009. High resolution remote estimation of soil surface water content by a thermal inertia approach. J. Hydrol. 379: 229-238.
Mohanty, B.P., W.M. Klittich, R. Horton, and M.Th. van Genuchten. 1995. Spatio-temporal variability of soil temperature within three land areas exposed to different tillage systems. Soil Sci. Soc. Am. J. 59:752-759.
Mohanty, B.P., P.J. Shouse, and M.T. van Genuchten. 1998. Spatio-temporal dynamics of water and heat in a field soil. Soil Till. Res. 47:133-143.
Mori, Y., J.W. Hopmans, A.P. Mortensen, and G.J. Kluitenberg. 2003. Multi-functional heat pulse probes for the simultaneous measurement of soil water content, solute concentration, and heat transport properties. Vadose Zone J. 2: 561-571.
Mori, Y., J.W. Hopmans, A.P. Mortensen, and G.J. Kluitenberg. 2005. Estimation of vadose zone water flux from multi-functional heat pulse probe measurements. Soil Sci. Soc. Am. J. 69: 599-606.
Murray, T., and A. Verhoef. 2007. Moving towards a more mechanistic approach in the determination of soil heat flux from remote measurements 1. A Universal approach to calculate thermal inertia. 2007. Agric. For. Meteorol. 147:80-87.
Nassar, I.N. and R. Horton. 2002. Coupled heat and water transfer. In: Dane, J.H. and G.C. Topp (eds.) Methods of soil analysis. Part 4 Physical methods. Soil Science society of America, Inc., Madison, WI. p. 1249-1252.
Nicholson, R.V., R.W. Gillham, J.A. Cherry, and E.J. Reardon. 1989. Reduction of acid generation in mine tailings through the use of moisture-retaining cover layers as oxygen barriers. Can. Geotech. J. 26:1-8.
Nielsen, D.R., J.W. Biggar, and K.T. Erh. 1973. Spatial variability of field measured soil water properties. Hilgardia. 42:214-259.
Novak, M.D. 2005. Soil temperature. In: Hatfield, J.L. and J.M. Baker (Eds.) 2005. Micrometeorology in agricultural systems. ASA, Madison, WI. p. 105-129.
Ogorzalek, A.S., Bohnhoff, G. L., Shackelford, C. D., Benson, C. H., and Apiwantragoon, P. 2008. Comparison of field data and water-balance predictions for a capillary barrier cover. J. Geotech. Geoeng. 134:470-486.
O'Kane, M., G.W. Wilson, and S.L. Barbour. 1998. Instrumentation and monitoring of an engineered soil cover system for mine waste rock. Can. J. Geotech. 35:828-846.
O'Kane, M. and L. Barbour. 2003. Predicting field performance of lysimeters used to evaluate cover systems for mine wastes. Proceedings of 6th International Conference for Acid Rock Drainage. Cairns, Australia. July, 2003.
Oliver, S.A., H.R. Oliver, J.S. Wallace, and A.M. Roberts. 1987. Soil heat flux and temperature variation with vegetation, soil type and climate. Agric. For. Meteorol. 39:257-269.
Ochsner, T. E., T. J. Sauer, and R. Horton, 2007. Soil heat storage measurements in energy balance studies. Agron. J., 99:311–319.
Pan, H.-L. and L. Mahrt. 1987. Interaction between soil hydrology and boundary-layer development. Boundary-Layer Meteorol. 38:185-202.

Parent, A.C., F. Anctil, and L.E. Parent. 2006. Characterization of temporal variability in near-surface soil moisture at scales from 1h to 2 weeks. J. Hydrol. 325:56-66.
Paul, E.A. 2007. Soil microbiology, ecology and biochemistry. 3rd Ed. Academic Press, New York, NY.
Perfect, E., and J. Caron, 2002. Spectral analysis of tillage-induced differences in soil spatial variation. Soil Sci. Soc. Am. J. 66:1587–1595.
Petrone, R.M., J.D. Price, S.K. Carey, and J.M. Waddington. 2004. Statistical characterization of the spatial variability of soil moisture in a cutover peatland. Hydrol. Processes. 18:41-52.
Pohn, H.A., T.W. Offield, and K. Watson. 1974. Thermal inertia mapping from satellite-discrimination of geologic units in Oman. J. Res. US Geol. Surv. 2, 147-158.
Pratt, D.A. 1980. Two-dimensional model variability in thermal inertia surveys. Remote Sens. Environ. 9: 325-338.
Pratt, D.A. and C.D. Ellyett. 1979. The thermal inertia approach to mapping of soil moisture and geology. Remote Sens. Environ. 8:151-168.
Price, J.C. 1985. On the analysis of thermal infrared imagery: the limited utility of apparent thermal inertia. Remote Sensing of Environment. 18:59-73.
Raich, J.W. and A. Tufekcioglu. 2000. Vegetation and soil respiration: correlations and controls. Biogeochemistry. 48:71-90.
Redding, T.E. and K.J. Devito. 2006. Particle densities of wetland soils in northern Alberta, Canada. Can. J. Soil Sci. 86:57-60.
Robinson, D.A., C.S. Campbell, J.W. Hopmans, B.K. Hornbuckle, S.B. Jones, R. Knight, F. Ogden, J. Selker, and O. Wendroth. 2008. Soil moisture measurement for ecological and hydrological watershed-scale observatories: A review. Vadose Zone J. 7:358-389.
Rutten, M.M., S.C. Steele-Dunne, J. Judge, and N. van de Giesen. 2010. Understanding heat transfer in the shallow subsurface using temperature observations. Vadose Zone J. 9: 1034-1045.
Sabol, D.E., A.R. Gillespie, E. McDonald, and I. Danilina. 2006. Differential thermal inertia of geological surfaces. 2nd Annual international symposium of recent advances in quantitative remote sensing. University of Valencia, Torrent, Spain. 25-29 Jul. 2006.
Sang, Y.F., Z. Wang, and C. Liu. 2012. Period identification in hydrologic time series using empirical mode decomposition and maximum entropy spectral analysis. J. Hydrol. 424-425:154-164.
Santanello, J.A., and Friedl, M.A. 2003. Diurnal covariation in soil heat flux and net radiation. J. Appl. Meteorol. 42:851-862.
Sauer, T.J. 2002. Heat flux density. In: Dane, J.H. and G.C. Topp (eds.) Methods of soil analysis. Part 4 Physical methods. Soil Science society of America, Inc., Madison, WI. p. 1233-1248.
Sayde, C., C. Gregory, M. Gil-Rodriquez, N. Tufillaro, S. Tyler, N. van de Giesen, M. English, R. Cuenca, and J.S. Selker. 2010. Feasibility of soil moisture monitoring with heated fiber optics. Water Resour. Res. 46: W06201, doi:10.1029/2009WR007846.
Scanlon, B.R., R.C. Reedy, K.E. Keese, and S.F. Dwyer. 2005. Evaluation of evapotranspirative covers for waste containment in arid and semi-arid regions in the Southwestern USA. Vadoze Zone J. 4:55-71.
Scanlon, B.R. 2006. Response to “Comments on evaluation of evapotranspirative covers for waste containment in arid and semiarid regions in the Southwestern USA.” Vadose Zone J. 5:813-814.

Schabenberger, O. and C.A. Gotway. 2005. Statistical methods for spatial data analysis. Chapman & Hall/CRC. New York.
Scharringa, M. 1976. On the representativeness of soil temperature measurements. Agric. Meteorol. 16:263-276.
Scheidt, S., M. Ramsey, and N. Lancaster. 2010. Determining soil moisture and sediment availability at White Sands Dune Field, New Mexico, from apparent thermal inertia data. J. Geophys. Res., 115, F02019, doi:10.1029/2009JF001378.
Schilperoort, R.P.S. and F.H.L.R. Clemens. 2009. Fibre-optic distributed temperature sensing in combined sewer systems. Water Sci. Technol. 60.5: 1127-1134.
Scott, H.D. 2000. Soil physics: Agricultural and environmental applications. Iowa State University Press, Ames, IA.
Selker, J.S., C.K. Keller, and J.T. McCord. 1999. Vadose zone processes. Lewis Publishers, New York, NY.
Selker, J.S., N. Van De Giesen, M. Westhoff, W. Luxemburg, and M. B. Parlange. 2006a. Fiber optics opens window on stream dynamics. Geophys. Res. Lett. 33. doi:10.1029/2006GL027979.
Selker, J.S., L. Thévenaz, H. Huwald, A. Mallet, W. Luxemburg, N. Van De Giesen, M. Stejskal, J. Zeman, M. Westhoff, and M. B. Parlange. 2006b. Distributed fiber-optic temperature sensing for hydrologic systems. Water Resour. Res. 42. doi:10.1029/2006WR005326
Shahraeeni, E. and D. Or. 2010. Thermo-evaporative fluxes from heterogeneous porous surfaces resolved by infrared thermography. Water Resour. Res. 46, W09511, doi: 10.1029/2009WR008455.
Shahraeeni, E. and D. Or. 2011. Quantification of subsurface thermal regimes beneath evaporating porous surfaces. Int. J. Heat Mass Tran. 54:4193-4202.
Si, B.C., and R.E. Farrell. 2004. Scale dependent relationships between wheat yield and topographic indices: A wavelet approach. Soil Sci. Soc. Am. J. 68:577–588.
Si, B.C. 2008. Spatial scaling analyses of soil physical properties: a review of spectral and wavelet methods. Vadose Zone J. 7:547-562.
Si, B.C., R.G. Kachanoski, and W.D. Reynolds. 2008. Analysis of soil variability. p. 1163-1192. In Soil sampling and methods of analysis. 2nd ed. Carter, M.R. and E.G. Gregorich (eds.) CRC Press, Boca Raton, FL.
Steele-Dunne, S.C., M.M. Rutten, D.M. Krzeminska, M. Hauser, S.W. Tyler, J.S. Selker, T.A. Bogaard, N.C. van de Giesen. 2009. Feasibility of soil moisture estimation using passive distributed temperature sensing. Water Resour. Res. doi:10.1029/2009WR008272.
Striegl, A.M., and S.P. Loheide. 2012. Heated distributed temperature sensing for field scale soil moisture monitoring. Ground Water. 50: 340-347.
Szatylowicz, J., T. Gnatowski, D. Szejba, R. Oleszczuk, T. Brandyk, and C. Kechavarzi. 2007. Moisture content variability in drained fen soil. In Okruszko, T., E. Maltby, J. Szatylowicz, D.M. Swiatek, and W. Kotowski. Wetlands: Monitoring, Modelling and Management. Taylor and Francis Group, London. pp. 113-120.
Tallon, L.K. and B.C. Si. 2004. Representative soil water benchmarking for environmental monitoring. J. Environmental Informatics. 4:31-39.
Tallon, L.K., M.A. O'Kane, D.E. Chapman, M.A. Phillip, R.E. Shurniak, and R.L. Strunk. 2011. Unsaturated sloping layered cover system: Field investigation. Can. J. Soil Sci. 91:161-168.

Ten Berge, H.F.M. and L. Stroosnijder. 1987. Sensitivity of surface variables to changes in physical soil properties: imitations to thermal remote sensing of bare soils. IEEE Trans. Geosci. Remote Sensing GE-25:702-708.
Tetens, O. 1930. Uber einige meteorologische Begriffe. Z. Geophys. 6:297-309.
Thomas, C.K., A.M. Kennedy, J. S. Selker, A. Moretti, M. H. Schroth, A. R. Smoot, N. B. Tufillaro and M. J. Zeeman. 2011. High-resolution fibre-optic temperature sensing: A new tool to study the two-dimensional structure of atmospheric surface layer flow. doi 10.1007/s10546-011-9672-7. Boundary-Layer Meteorology
Thompson, D.K. and J.M. Waddington. 2013. Peat properties and water retention in boreal forested peatlands subject to wildfire. Water Resour. Res. 49:3651-3658.
Torrence, C. and G.P. Compo. 1997. A practical guide to wavelet analysis. Bull. Am. Meteorol. Soc. 79:61-78.
Tyler, S.W., J.S. Selker, M.B. Hausner, C.E. Hatch, T. Torgersen, C.E. Thodal, and S.G. Schladow. 2009. Environmental temperature sensing using Raman spectra DTS fiber-optic methods. Water Resour. Res. 45, W00D23, doi:10.1029/2008WR007052.
Tyler, S.W., D.M. Holland, V. Zagorodnov, A.A. Stern, C. Sladek, S. Kobs, S. White, F. Suárez, and J. Bryenton. 2013. J. Glaciol. 59:583-591.
Usowicz, B., J. Kossowski, and P. Baranowski. 1996. Spatial variability of soil thermal properties in cultivated fields. Soil Till. Res. 39:85-100.
Usowicz, B. and J.B. Usowicz. 2004. Spatial and temporal variation of selected physical and chemical properties of soil. Institute of Agrophysics, Polish Academy of Sciences, Lublin. ISBN 83-87385-96-4.
Usowicz, B., J. Lipiec, and A. Ferrero. 2006. Prediction of soil thermal conductivity based on penetration resistance and water content or air-filled porosity. Int. J. Heat Mass Transfer. 49:5010-5017.
Vachaud, G., A.P. Desilans, P. Balabanis, and M. Vauclin. 1985. Temporal stability of spatially measured soil-water probability density function. Soil Sci. Soc. Am. J. 49:822-828.
Van de Giesen, N., S.C. Steele-Dunne, J. Jansen, O. Hoes, M.B. Hausner, S. Tyler, and J. Selker. 2012. Double-ended calibration of fiber-optic Raman spectra distributed temperature sensing data. Sensors (Basel). 12(5):5471-5485.
Van de Griend, A.A., P.J. Camillo, and R.J. Gurney. 1985. Discrimination of soil physical parameters, thermal inertia, and soil moisture from diurnal surface temperature fluctuations. Water Resour. Res. 21: 997-1009.
Vanderlinden, K., H. Vereecken, H. Hardelauf, M. Herbst, G. Martínez, M.H. Cosh, and Y.A. Pachepsky. 2011. Temporal stability of soil water contents: a review of data and analyses. Vadose Zone J. doi:10.2136/vzj2011.0178.
Van Wijk, W.R., and W.J. Derkesen. 1963. Sinusoidal temperature variation in a layered soi. In: Van Wijk, W.R. (Ed.) Physics of plant environment. Norht-Holland, Amsterdam. p. 171-209.
Van Wijk, W.R., and D.A. de Vries. 1963. Periodic temperature variations in a homogeneous soil. In: Van Wijk, W.R. (Ed.) Physics of plant environment. Norht-Holland, Amsterdam. p. 103-143.
Vauclin, M. S.R. Vieira, R. Bernard, and J.L. Hatfield. 1982. Spatial variability of surface temperature along two transects of a bare soil. Water Resour. Res. 18:1677-1686.

Vereecken, H., J.A. Hopmans, H. Bogema, J. Vanderbought, J.A. Vrugt, and J.W. Hopmans. 2008. On the value of soil moisture measurements in vadose zone hydrology: A review. Water Resour. Res. 44. W00D06, doi: 10.1029/2008WR006829.

Verhoef, A. Remote estimation of thermal inertia and soil heat flux for bare soil. Agric. For. Meteorol. 123:221-236.

Verstraeten, W.W., F. Veroustraete, C.J. van der Sande, I. Grootaers, and J. Feyen. 2006. Soil moisture retrieval using thermal inertia, determined with visible and thermal spaceborne data, validated for European forests. Remote Sens. Environ. 101:299-314.

Vogt, T.; P. Schneider, L. Hahn-Woernle, O.A. Cirpka, Estimation of seepage rates in a losing stream by means of fiber-optic high-resolution vertical temperature profiling, J. Hydrol. 380: 154-164.

Wang, J., and R.L. Bras. 1999. Ground heat flux estimated from surface soil temperatures. J. Hydrol. 216: 214-226.

Wang, J., R.L. Bras, G. Sivandran, and R.G. Knox. 2010. A simple method for the estimation of thermal inertia. Geophys. Res. Lett. 37, L05404, doi:10.1029/2009GL041851.

Watson, K. 1975. Geologic applications of thermal infrared images. P. IEEE. 128-135.

Webster, R., and M.A. Oliver. 2001. Geostatistics for environmental scientists. John Wiley and Sons, New York, NY.

Weeks, B. and G.W. Wilson. 2005. Variations in moisture content for a soil cover over a 10 year period. Can. Geotech. J. 42: 1615-1630.

Weiss, J.D. 2003. Using fiber optics to detect moisture intrusion into a landfill cap consisting of a vegetative soil barrier. J. Air & Waste Manage. Assoc. 53:1130-1148.

Western, A. W. and Blöschl, G. 1999. On the spatial scaling of soil moisture. J. Hydrol. 217:203-224.

Western, A.W., G. Blöschl, and R.B. Grayson. 1998. Geostatistical characterization of soil moisture patterns in the Tarrawarra catchment. J. Hydrol. 205:20-37.

Western, A., S.L. Zhou, R.B. Grayson, T.A. McMahon, G. Blöschl, and D.J. Wilson. 2004. Spatial correlation of soil moisture in small catchments and its relationship to dominant spatial hydrological processes. J. Hydrol. 286:113-134.

Westhoff, M.C., H. H. G. Savenije, W. M. J. Luxemburg, G. S. Stelling, N. C. van de Giesen, J. S. Selker, L. Pfister, and S. Uhlenbrook. 2007. A distributed stream temperature model using high resolution temperature observations, Hydrol. Earth Syst. Sci., 11: 1469-1480.

Wu, W., M.A. Geller, and R.E. Dickinson. 2002. The response of soil moisture to long-term variability of precipitation. J. Hydromet. 3:604-613.

Yan, R. and R.X. Gao. 2007. A tour of the Hilbert-Huang transform: and empirical tool for signal analysis. IEEE Instrum. Meas. Mag. 1094-6969:40-45.

Yanful, E.K. 1993. Oxygen diffusion through soil covers on sulphidic mine tailings. J. Geotech. Eng. 119:1207-1228.

Yates, T.T., B.C. Si, R.E. Farrell, and D.J. Pennock. 2006. Wavelet spectra of nitrous oxide emission from hummocky terrain during spring snowmelt. Soil Sci. Soc. Am. J. 70:1110–1120.

Xu, M., J. Chen, and Y. Qi. 2002. Growing-season temperature and soil moisture along a 10 km transect across a forested landscape. Clim. Res. 22:57-72.

## Appendix 1. Example Data

Table A1. Example of DTS temperature data collected at Site #1 on July 17, 2011.

| Distance | 9:35 | 9:45 | 9:55 | 10:05 | 10:15 | 10:25 | 10:35 | 10:45 | 10:55 |
|---|---|---|---|---|---|---|---|---|---|
| 1 | 0.27 | 0.27 | 0.27 | 0.27 | 0.27 | 0.27 | 0.27 | 0.27 | 0.27 |
| 2 | 1.0146 | 1.0146 | 1.0146 | 1.0146 | 1.0146 | 1.0146 | 1.0146 | 1.0146 | 1.0146 |
| 3 | 7.53 | 8.17 | 8.74 | 9.01 | 9.32 | 9.79 | 9.81 | 9.83 | 10.87 |
| 4 | 8.34 | 8.96 | 9.46 | 9.69 | 9.97 | 10.36 | 10.35 | 10.3 | 11.3 |
| 5 | 9.64 | 10.17 | 10.62 | 10.68 | 10.95 | 11.25 | 11.25 | 11.1 | 12.04 |
| 6 | 12.82 | 13.34 | 13.86 | 14.01 | 14.44 | 14.74 | 14.9 | 14.69 | 15.67 |
| 7 | 10.69 | 11.44 | 12.01 | 12.13 | 12.65 | 13.32 | 13.47 | 13.28 | 14.53 |
| 8 | 10.01 | 10.57 | 11.16 | 11.46 | 11.59 | 12.13 | 12.06 | 12.12 | 13.15 |
| 9 | 10.97 | 11.59 | 11.94 | 11.94 | 12.56 | 12.93 | 12.77 | 12.77 | 13.62 |
| 10 | 13.81 | 14.07 | 14.59 | 14.59 | 14.84 | 15.06 | 15.09 | 14.94 | 15.75 |
| 11 | 18.36 | 19.24 | 19.51 | 19.77 | 20.01 | 20.03 | 20.32 | 20.35 | 21.09 |
| 12 | 13.88 | 14.07 | 15.54 | 15.03 | 15.03 | 15.27 | 15.39 | 15.07 | 16.81 |
| 13 | 15.96 | 16.27 | 16.89 | 16.8 | 16.54 | 17.36 | 17.08 | 17.76 | 18.16 |
| 14 | 16.06 | 16.63 | 15.96 | 16.84 | 16.94 | 17.49 | 16.71 | 17.12 | 17.51 |
| 15 | 20.07 | 20.58 | 20.59 | 20.32 | 20.02 | 20.6 | 21.92 | 21.05 | 21.4 |
| 16 | 18.18 | 18.35 | 19.19 | 18.72 | 19.35 | 20.2 | 19.87 | 20.62 | 18.88 |
| 17 | 17.73 | 18.28 | 17.53 | 17.7 | 17.71 | 18.18 | 17.33 | 17.49 | 16.35 |
| 18 | 18.06 | 17.52 | 18.48 | 17.21 | 17.45 | 18.12 | 16.75 | 16.62 | 17.77 |
| 19 | 18.45 | 16.55 | 17.97 | 16.13 | 18.24 | 18.85 | 18.42 | 17.78 | 16.4 |
| 20 | 18.48 | 17.8 | 18.73 | 18.97 | 17.63 | 19.48 | 16.86 | 17.52 | 17.08 |
| 21 | 18.85 | 17.86 | 19.88 | 17.76 | 18.99 | 18.31 | 17.4 | 17.53 | 17.05 |
| 22 | 18.37 | 17.4 | 18.06 | 18.33 | 16.57 | 18.5 | 17.59 | 18.09 | 16.79 |
| 23 | 18.33 | 16.89 | 17.91 | 17.14 | 18.18 | 17.02 | 18.64 | 17.48 | 18.17 |
| 24 | 16.36 | 18.9 | 17.64 | 18.78 | 17.29 | 17.29 | 17.4 | 16.45 | 19.08 |
| 25 | 17.58 | 17.61 | 17.09 | 18.17 | 19.38 | 17.79 | 18.23 | 18.91 | 18.25 |
| 26 | 17.55 | 18.82 | 17.67 | 18.46 | 17.06 | 18.15 | 17.64 | 18.38 | 19.75 |
| 27 | 18.34 | 18.15 | 17.34 | 17.38 | 17.73 | 17.69 | 18.53 | 18.17 | 18.15 |
| 28 | 17.86 | 19.22 | 17.88 | 17.17 | 19.22 | 18.65 | 17.44 | 18.48 | 16.69 |
| 29 | 20.71 | 16.95 | 18.26 | 18.28 | 17.92 | 18.44 | 18.87 | 18.52 | 16.13 |
| 30 | 17.17 | 16.74 | 17.87 | 18.03 | 19.67 | 18.47 | 18.34 | 18.63 | 17.36 |
| 31 | 19.24 | 17.92 | 18.42 | 18.57 | 18.1 | 18.76 | 18.89 | 18.09 | 18.77 |
| 32 | 17.23 | 17.25 | 17.92 | 18.05 | 18.62 | 18.44 | 17.68 | 17.98 | 17.6 |
| 33 | 19.12 | 17.85 | 17.08 | 17.45 | 17.25 | 19.2 | 19.02 | 17.2 | 16.84 |
| 34 | 18.62 | 17.56 | 17.69 | 18.81 | 17.42 | 19.33 | 17.92 | 17.75 | 18.51 |
| 35 | 18.97 | 16.66 | 18.1 | 18.85 | 17.17 | 18.4 | 17.95 | 18.78 | 18.91 |
| 36 | 19.8 | 17.97 | 17.9 | 18.07 | 19.07 | 16.66 | 16.71 | 19.37 | 16.99 |
| 37 | 18.23 | 18.43 | 17.28 | 18.51 | 18.2 | 19.23 | 16.99 | 17.63 | 18.05 |
| 38 | 16.4 | 18.3 | 17.99 | 17.47 | 18.81 | 17.02 | 18.74 | 18.97 | 18.19 |
| 39 | 18.53 | 18.12 | 18.55 | 18.4 | 17.53 | 18.39 | 17.83 | 18.53 | 18.66 |
| 40 | 19.01 | 18.66 | 18.54 | 17.72 | 18.35 | 16.53 | 17.77 | 17.31 | 19.06 |

Table A1 continued.

| Distance | 9:35 | 9:45 | 9:55 | 10:05 | 10:15 | 10:25 | 10:35 | 10:45 | 10:55 |
|---|---|---|---|---|---|---|---|---|---|
| 41 | 17.26 | 18.81 | 18.36 | 17.78 | 18.3 | 17.24 | 17.43 | 18.25 | 18.33 |
| 42 | 17.11 | 17.86 | 18.09 | 17.27 | 17.21 | 17.12 | 17.96 | 16.72 | 16.17 |
| 43 | 17.45 | 18.76 | 18.77 | 18.21 | 17.84 | 18.29 | 17.19 | 17.86 | 17.59 |
| 44 | 16.98 | 18.9 | 18.98 | 17.06 | 18.7 | 18.64 | 17.81 | 16.94 | 17.89 |
| 45 | 18.57 | 17.69 | 17.59 | 18.5 | 17.2 | 18.53 | 18.71 | 18.38 | 18.66 |
| 46 | 18.8 | 19.41 | 19.72 | 17.92 | 17.34 | 17 | 18.24 | 17.88 | 18.01 |
| 47 | 15.61 | 16.83 | 17.45 | 18.02 | 16.99 | 17.72 | 18.35 | 17.86 | 18.5 |
| 48 | 17.43 | 16.99 | 17.54 | 18.47 | 16.99 | 18.91 | 18.77 | 18.86 | 18.47 |
| 49 | 18.28 | 17.86 | 18.8 | 18.38 | 19.02 | 18.03 | 19.04 | 18.92 | 18.66 |
| 50 | 19.91 | 20.09 | 19.07 | 20.69 | 21.32 | 20.36 | 20.47 | 20.38 | 19.53 |
| 51 | 19.6 | 21.21 | 20.83 | 21.08 | 22.05 | 21.2 | 20.57 | 21.48 | 21.86 |
| 52 | 19.36 | 21.19 | 19.59 | 18.77 | 21.21 | 21.61 | 19.85 | 21.36 | 21.01 |
| 53 | 20.46 | 21.29 | 22.73 | 21.28 | 21.62 | 24.09 | 21.91 | 22.57 | 24.68 |
| 54 | 21.56 | 21.59 | 23 | 21.64 | 23.41 | 24.49 | 24.65 | 26.87 | 26.42 |
| 55 | 20.17 | 20.98 | 21.51 | 21.94 | 21.85 | 23.06 | 23.39 | 26.01 | 24.08 |
| 56 | 18.61 | 20.79 | 19.88 | 20.08 | 21.73 | 22.52 | 22.68 | 22.21 | 23.82 |
| 57 | 18.91 | 18.36 | 18.78 | 19.06 | 20.34 | 20.74 | 21.43 | 22.01 | 21.52 |
| 58 | 19.42 | 19.83 | 20.09 | 20.52 | 21.14 | 21.66 | 21.59 | 22.71 | 21.92 |
| 59 | 20.3 | 21.03 | 20.67 | 20.46 | 21.57 | 22.77 | 21.98 | 22.45 | 22.1 |
| 60 | 21.5 | 18.6 | 22.68 | 21.35 | 21.87 | 22.25 | 22.93 | 25.02 | 24.79 |
| 61 | 21.47 | 20.86 | 23.1 | 23.39 | 25.02 | 25.11 | 25.28 | 26.3 | 26.03 |
| 62 | 21.63 | 21.5 | 23.12 | 23.42 | 24 | 24.38 | 23.04 | 25.46 | 28.05 |
| 63 | 21.92 | 22.17 | 20.77 | 22.95 | 23.09 | 24.33 | 24.12 | 25.04 | 25.33 |
| 64 | 20.93 | 21.97 | 22.55 | 23.44 | 22.59 | 25.13 | 24.14 | 24.62 | 26 |
| 65 | 21.62 | 20.49 | 22.93 | 21.76 | 22.02 | 25.57 | 24.86 | 25.45 | 26.8 |
| 66 | 19.69 | 20.32 | 21.43 | 22.37 | 22.78 | 23.94 | 23.56 | 23.82 | 24.58 |
| 67 | 19.88 | 23.05 | 21.42 | 23.1 | 23.05 | 23 | 23.94 | 25.1 | 24.89 |
| 68 | 20.72 | 21.26 | 21.25 | 21.85 | 23.63 | 23.36 | 23.92 | 26.59 | 25.59 |
| 69 | 19.21 | 20.75 | 19.72 | 19.93 | 19.62 | 22.91 | 19.57 | 21.42 | 23.31 |
| 70 | 18.36 | 21.08 | 20.51 | 19.43 | 21.23 | 21.72 | 21.99 | 21.78 | 23.36 |
| 71 | 19.63 | 20.82 | 19.94 | 20.81 | 20.9 | 23.39 | 21.99 | 23.43 | 24.77 |
| 72 | 20.71 | 20.5 | 22.23 | 22.92 | 22.57 | 26.46 | 24.7 | 24.29 | 26.53 |
| 73 | 19.8 | 20.59 | 21.76 | 22.04 | 22.34 | 23.64 | 22.97 | 25.25 | 22.89 |
| 74 | 18.13 | 18.92 | 18.86 | 21.07 | 20.54 | 20.7 | 22.16 | 21.88 | 22.05 |
| 75 | 19.54 | 20.62 | 20.86 | 19.42 | 21.95 | 21.51 | 23.98 | 22.5 | 24.39 |
| 76 | 20.23 | 20.74 | 21.3 | 20.98 | 24.68 | 23.69 | 24.81 | 25.56 | 23.64 |
| 77 | 20.31 | 20.89 | 21.05 | 22.65 | 21.75 | 21.72 | 23.51 | 23.05 | 23.85 |
| 78 | 19.5 | 20.1 | 20.92 | 19.8 | 19.81 | 21.02 | 22.52 | 22.54 | 22.45 |
| 79 | 17.5 | 18.57 | 17.05 | 20.06 | 19.81 | 20.76 | 20.08 | 20.01 | 22.44 |
| 80 | 16.7 | 18.76 | 18.42 | 18.5 | 18.44 | 19.63 | 20.41 | 22.06 | 21.1 |

Table A1 continued.

| Distance | 9:35 | 9:45 | 9:55 | 10:05 | 10:15 | 10:25 | 10:35 | 10:45 | 10:55 |
|---|---|---|---|---|---|---|---|---|---|
| 81 | 19.01 | 18.56 | 18.73 | 19.86 | 20.83 | 20.79 | 21.3 | 22.56 | 21.34 |
| 82 | 18.47 | 19.5 | 19.98 | 20.45 | 21.73 | 21.69 | 21 | 21.7 | 22.62 |
| 83 | 18.15 | 19.4 | 20.65 | 19.51 | 20.2 | 22.99 | 22.28 | 21.28 | 20.73 |
| 84 | 18.99 | 19.86 | 20.05 | 20.05 | 21.4 | 20.67 | 20.65 | 20.98 | 21.02 |
| 85 | 18.88 | 19.81 | 18.55 | 18.94 | 20.14 | 21.48 | 20.62 | 20.2 | 23.09 |
| 86 | 18.4 | 19.07 | 18.84 | 18.65 | 20.19 | 20.68 | 20.88 | 21.53 | 20.71 |
| 87 | 18.36 | 20.1 | 20.06 | 19.81 | 20.63 | 21.52 | 22.56 | 23.79 | 23.79 |
| 88 | 19.46 | 19.64 | 18.9 | 21.37 | 19.31 | 22.27 | 20.69 | 19.2 | 21.28 |
| 89 | 19.75 | 18.12 | 19.86 | 19.16 | 21.09 | 21.36 | 21.13 | 19.15 | 21.35 |
| 90 | 16.8 | 18.51 | 17.5 | 18.11 | 18.6 | 19.93 | 19.41 | 18.44 | 18.92 |
| 91 | 16.54 | 15.86 | 15 | 15.61 | 15.11 | 15.39 | 16.94 | 16.83 | 16.77 |
| 92 | 15.73 | 14.35 | 15.03 | 15.02 | 13.42 | 14.37 | 14.48 | 15.12 | 16.58 |
| 93 | 13.31 | 15.35 | 15.5 | 14.84 | 15.35 | 14.56 | 14.52 | 16.45 | 15.86 |
| 94 | 14.55 | 14.38 | 16.58 | 14.91 | 15.39 | 15.55 | 16.09 | 15.43 | 16.4 |
| 95 | 14.28 | 15.81 | 15.43 | 14.26 | 15.57 | 15.73 | 15.04 | 16.78 | 16.12 |
| 96 | 13.5 | 15.35 | 14.99 | 15.29 | 14.7 | 15.14 | 15.14 | 15.25 | 15.03 |
| 97 | 13.04 | 14.27 | 13.95 | 15.7 | 15 | 14.69 | 13.99 | 15.61 | 15.47 |
| 98 | 13.03 | 15.88 | 14.94 | 15.94 | 13.78 | 14.62 | 15.56 | 17.44 | 15.35 |
| 99 | 13.69 | 15.05 | 15.76 | 15.29 | 15.09 | 15.41 | 15.15 | 15.26 | 15.98 |
| 100 | 13.26 | 14.48 | 14.23 | 14.87 | 15.15 | 15.24 | 16.52 | 14.52 | 15.14 |
| 101 | 16.53 | 13.81 | 15.32 | 15.42 | 15.63 | 15.44 | 14.92 | 15.52 | 15.91 |
| 102 | 14.82 | 16.62 | 14.85 | 15.64 | 15.02 | 14.81 | 14.97 | 16.4 | 15.94 |
| 103 | 16.41 | 15.25 | 15.85 | 15.44 | 14.72 | 16.16 | 15.99 | 16.22 | 17.21 |
| 104 | 15.23 | 15.61 | 15.61 | 16.1 | 17.45 | 17.17 | 17.2 | 16.93 | 17.75 |
| 105 | 16.65 | 15.65 | 16 | 15.43 | 18.53 | 17.06 | 15.84 | 16.77 | 16.42 |
| 106 | 16.88 | 16.43 | 16.02 | 15.67 | 17.66 | 15.79 | 15.79 | 14.86 | 14.71 |
| 107 | 14.79 | 16.67 | 15.99 | 16.1 | 17.2 | 16.38 | 16.04 | 16.7 | 17.27 |
| 108 | 16.17 | 16.55 | 16.01 | 17.68 | 15.93 | 16.1 | 15.92 | 16.65 | 16.42 |
| 109 | 17.26 | 17.23 | 16.74 | 17.25 | 16.42 | 16.7 | 17.54 | 17.84 | 15.86 |
| 110 | 17.18 | 16.81 | 16.37 | 14.55 | 15.22 | 16.43 | 16.96 | 17.97 | 16.46 |
| 111 | 16.73 | 17.26 | 17.13 | 15.63 | 17.97 | 17.9 | 16.08 | 17.46 | 16.61 |
| 112 | 16.13 | 18.11 | 17.51 | 17.13 | 16.51 | 18.42 | 17.02 | 16.09 | 17.84 |
| 113 | 17.66 | 17.81 | 17.33 | 16.84 | 17.03 | 17.58 | 17.97 | 17.17 | 16.49 |
| 114 | 16.97 | 17.91 | 17.22 | 17.66 | 16.57 | 18.36 | 18.38 | 17.79 | 17.69 |
| 115 | 16.68 | 18.46 | 16.21 | 16.74 | 17.74 | 18.8 | 17.86 | 17.49 | 17.72 |
| 116 | 17.96 | 16.97 | 18.91 | 18.1 | 17.86 | 19.19 | 18.1 | 16.15 | 20 |
| 117 | 17.24 | 18.13 | 18.09 | 17.83 | 19.24 | 17.01 | 16.45 | 17.9 | 17.73 |
| 118 | 17.67 | 18.08 | 18.19 | 18.37 | 16.88 | 18.05 | 18.84 | 18.22 | 18.82 |
| 119 | 17.65 | 18.6 | 18.11 | 18.39 | 17.05 | 18.51 | 18.71 | 17.29 | 17.62 |
| 120 | 16.85 | 17.96 | 17.35 | 17.09 | 17.37 | 17.31 | 17.71 | 16.86 | 16.63 |

Table A1 continued.

| Distance | 9:35 | 9:45 | 9:55 | 10:05 | 10:15 | 10:25 | 10:35 | 10:45 | 10:55 |
|---|---|---|---|---|---|---|---|---|---|
| 121 | 16.8 | 17.04 | 17.18 | 16.53 | 17.04 | 16.72 | 17.43 | 17.28 | 19.07 |
| 122 | 17.6 | 17.98 | 17.92 | 17.68 | 17.49 | 17.31 | 16.57 | 16.62 | 16.45 |
| 123 | 16.9 | 17.26 | 18.13 | 17.03 | 16.08 | 16.46 | 16.86 | 16.54 | 16.06 |
| 124 | 16.86 | 17.06 | 16.3 | 16.74 | 17.98 | 17.57 | 17.2 | 16.86 | 18.01 |
| 125 | 15.6 | 18.03 | 15.38 | 16.77 | 17.27 | 17.91 | 15.81 | 16.92 | 16.76 |
| 126 | 16.39 | 18.07 | 16.26 | 16.88 | 17.69 | 16.61 | 17.27 | 17.76 | 18.18 |
| 127 | 17.72 | 17.2 | 16.29 | 18.52 | 18.63 | 17.49 | 17.44 | 17.91 | 19.15 |
| 128 | 19.26 | 17.07 | 18.39 | 18.54 | 16.74 | 18.8 | 17.76 | 17.58 | 18.19 |
| 129 | 17.65 | 18.29 | 17.87 | 18.5 | 16.91 | 17.41 | 15.95 | 15.54 | 16.34 |
| 130 | 17.3 | 17.93 | 17.1 | 17.96 | 17.64 | 18.16 | 17.16 | 16.11 | 17.72 |
| 131 | 17.09 | 17.27 | 16.2 | 16.05 | 17.55 | 18.29 | 16.69 | 17.42 | 16.77 |
| 132 | 18.14 | 16.67 | 16.72 | 16.36 | 18.27 | 17.75 | 16.94 | 16.29 | 17.03 |
| 133 | 16.02 | 16.24 | 16.69 | 18.96 | 16.64 | 16.77 | 16.26 | 17.48 | 17.71 |
| 134 | 16.27 | 17.81 | 17.11 | 17.99 | 17.15 | 15.64 | 17.19 | 18.52 | 16.3 |
| 135 | 17.43 | 16.59 | 17.91 | 17.57 | 16.03 | 17.26 | 16.38 | 17.79 | 17.98 |
| 136 | 16.69 | 17.14 | 17.05 | 17.03 | 18.51 | 17.86 | 17.64 | 18.84 | 17.89 |
| 137 | 15.76 | 17 | 15.96 | 17.33 | 17.5 | 16.79 | 16.02 | 15.55 | 17.81 |
| 138 | 16.64 | 16.62 | 17.15 | 15.89 | 15.87 | 18.77 | 16.97 | 16.05 | 15.47 |
| 139 | 15.13 | 16.44 | 15.3 | 16.42 | 16.44 | 16.93 | 14.71 | 17.17 | 16.37 |
| 140 | 15.72 | 15.99 | 16.13 | 17.07 | 15.88 | 15.02 | 15.37 | 15.76 | 16.57 |
| 141 | 17.32 | 15.81 | 16.31 | 15.13 | 16.56 | 17.07 | 15.49 | 15.97 | 16.26 |
| 142 | 15.77 | 16.05 | 16.33 | 17.29 | 14.17 | 15.72 | 17.16 | 15.53 | 16.85 |
| 143 | 16.13 | 16 | 16.8 | 16.63 | 16.65 | 16.77 | 18.26 | 17.93 | 16.07 |
| 144 | 16.98 | 16.62 | 16.41 | 15.95 | 17.53 | 16.81 | 17.36 | 16.17 | 17.51 |
| 145 | 16.54 | 18.42 | 16.41 | 17.45 | 18.29 | 17.6 | 16.43 | 16.88 | 17.05 |
| 146 | 16.88 | 17.86 | 18.45 | 16.93 | 17.34 | 16.59 | 15.63 | 16.3 | 17.93 |
| 147 | 17.47 | 17.5 | 17.09 | 17.05 | 16.61 | 17.35 | 17.46 | 17.16 | 17.19 |
| 148 | 18.39 | 17.89 | 17.07 | 17.13 | 16.91 | 15.95 | 18.43 | 16.71 | 16.14 |
| 149 | 19.88 | 17.85 | 16.62 | 18.55 | 16.72 | 17.82 | 16.76 | 17.58 | 17.32 |
| 150 | 16.59 | 15.79 | 16.48 | 17.36 | 17.02 | 16.35 | 17.07 | 18.5 | 17.7 |
| 151 | 18.33 | 16.91 | 16.75 | 17.51 | 15.29 | 15.61 | 17.04 | 16.92 | 17.19 |
| 152 | 16.78 | 15.73 | 18.11 | 15.91 | 16.61 | 17.9 | 14.73 | 16.2 | 15.11 |
| 153 | 16.38 | 16.58 | 15.53 | 15.69 | 16.71 | 16.38 | 16.89 | 17.32 | 16.39 |
| 154 | 15.81 | 16.52 | 15.67 | 15.41 | 16.42 | 16.48 | 16.27 | 16.41 | 15.37 |
| 155 | 15.37 | 16.08 | 15.38 | 15.85 | 15.69 | 16.68 | 17.19 | 15.26 | 14.5 |
| 156 | 16.62 | 15.32 | 17.04 | 16.33 | 15.15 | 16.64 | 16.09 | 17.13 | 15.39 |
| 157 | 16.45 | 15.62 | 17.24 | 17.55 | 15.74 | 16.36 | 15.95 | 15.09 | 16.49 |
| 158 | 16.93 | 16.55 | 16.75 | 17.31 | 16.93 | 16.15 | 16.5 | 15.83 | 16.38 |
| 159 | 16.83 | 16.36 | 15.45 | 16.36 | 15.42 | 15.78 | 14.38 | 15.22 | 16.39 |
| 160 | 15.88 | 15.43 | 16.27 | 14.49 | 15.93 | 15.37 | 15.85 | 16.26 | 15.79 |

Table A1 continued.

| Distance | 9:35 | 9:45 | 9:55 | 10:05 | 10:15 | 10:25 | 10:35 | 10:45 | 10:55 |
|---|---|---|---|---|---|---|---|---|---|
| 161 | 15.73 | 13.17 | 14.86 | 16.72 | 15.12 | 14.44 | 13.6 | 16.96 | 14.78 |
| 162 | 15.63 | 14.13 | 15.21 | 14.11 | 15.72 | 15.45 | 15.18 | 15.84 | 14.37 |
| 163 | 13.67 | 16.18 | 15.35 | 15.06 | 15.48 | 15.38 | 15.61 | 14.66 | 14.91 |
| 164 | 13.49 | 14.92 | 14.59 | 14.61 | 13.7 | 14.63 | 13.26 | 16.91 | 14.85 |
| 165 | 14.47 | 13.33 | 13.33 | 14.65 | 15.24 | 13.44 | 14.83 | 15.1 | 14.84 |
| 166 | 14.71 | 15.14 | 14.2 | 14.62 | 14.8 | 13.75 | 14.99 | 14.6 | 14.46 |
| 167 | 14.5 | 14.51 | 12.92 | 12.35 | 14.39 | 14.11 | 12.91 | 13.62 | 12.17 |
| 168 | 14.45 | 13.31 | 12.97 | 14.75 | 13.81 | 13.8 | 12.93 | 13.64 | 14.64 |
| 169 | 11.63 | 11.49 | 12.96 | 14.52 | 12.92 | 14.27 | 12.74 | 12.45 | 12.91 |
| 170 | 12.3 | 11.13 | 12.16 | 13.5 | 12.36 | 12.31 | 13.87 | 13.11 | 12.95 |
| 171 | 14.47 | 11.64 | 12.8 | 12.49 | 14.02 | 12.94 | 11.93 | 12.43 | 12.57 |
| 172 | 10.74 | 12.63 | 12.89 | 12.26 | 12.55 | 13.83 | 11.86 | 14.06 | 12.44 |
| 173 | 12.41 | 14.19 | 12.56 | 11.8 | 12.8 | 13.2 | 11.47 | 12.5 | 13.88 |
| 174 | 11.92 | 13.47 | 13.21 | 11.97 | 11.64 | 12.22 | 12.4 | 12.1 | 13.87 |
| 175 | 13.21 | 10.92 | 14.46 | 13.42 | 14.7 | 12.96 | 13.48 | 12.59 | 13.49 |
| 176 | 13.64 | 12.85 | 13.24 | 13.89 | 12.58 | 13.99 | 13.08 | 13.54 | 12.77 |
| 177 | 12.61 | 12.87 | 14.48 | 12.38 | 12.23 | 14.27 | 13.78 | 12.85 | 12.98 |
| 178 | 12.77 | 13.73 | 12.81 | 13.33 | 13.31 | 13.75 | 12.56 | 12.83 | 12.48 |
| 179 | 12.73 | 12.69 | 14.74 | 13.95 | 14.76 | 13.98 | 12.26 | 12.48 | 13.6 |
| 180 | 12.14 | 12.53 | 13.86 | 12.64 | 14.4 | 13.95 | 13.19 | 13.59 | 12.97 |
| 181 | 12.25 | 14.93 | 14.28 | 13.31 | 13.42 | 13.36 | 12.73 | 13.83 | 13.65 |
| 182 | 13.86 | 13.48 | 14.74 | 13.94 | 13.59 | 14.67 | 12.92 | 13.16 | 14.76 |
| 183 | 12.65 | 14.95 | 15.48 | 13.71 | 14.76 | 15.14 | 14.11 | 13.89 | 13.81 |
| 184 | 14.28 | 14.22 | 14.58 | 14.68 | 15.64 | 15.28 | 12.92 | 15.68 | 17.09 |
| 185 | 13.9 | 13.32 | 15.57 | 13.97 | 13.5 | 15.05 | 14.84 | 15.2 | 15.93 |
| 186 | 14.11 | 15.54 | 15.19 | 14.06 | 13.87 | 15.64 | 14.75 | 15.39 | 13.91 |
| 187 | 15.51 | 15.03 | 15.69 | 14.89 | 14.6 | 17.3 | 15.31 | 16.2 | 14.94 |
| 188 | 14.48 | 16.34 | 14.17 | 16.03 | 15.03 | 15.87 | 14.54 | 16.03 | 13.93 |
| 189 | 14.77 | 15.63 | 14.55 | 16.92 | 14.74 | 14.68 | 14.44 | 15.23 | 14.42 |
| 190 | 14.58 | 14.73 | 14.9 | 14.38 | 16.38 | 13.98 | 15.63 | 16.27 | 15.01 |
| 191 | 15.72 | 15.1 | 15.74 | 16.64 | 16.62 | 16.95 | 17.79 | 15.75 | 16.53 |
| 192 | 15.6 | 13.81 | 15.47 | 16.32 | 14.75 | 16.61 | 16.28 | 16.85 | 15.05 |
| 193 | 15.01 | 15.87 | 16.62 | 16.61 | 16.96 | 17.62 | 16.01 | 16.8 | 15.59 |
| 194 | 15.13 | 14.58 | 16.35 | 16.03 | 15.58 | 15.62 | 16.47 | 17.96 | 16.03 |
| 195 | 14.88 | 15.28 | 16.75 | 16.76 | 17.01 | 15.76 | 15.38 | 14.63 | 16.95 |
| 196 | 16.41 | 16.74 | 16.06 | 14.54 | 14.36 | 17.57 | 16.23 | 15.36 | 17.22 |
| 197 | 14.54 | 14.87 | 15.54 | 15.39 | 15.62 | 15.76 | 15.76 | 16.63 | 15.82 |
| 198 | 15.02 | 16.04 | 13.64 | 15.71 | 15.63 | 15.47 | 16.61 | 14.71 | 15.49 |
| 199 | 15.95 | 15.89 | 16.04 | 14.01 | 14.52 | 15.24 | 15.63 | 16.57 | 16.13 |
| 200 | 15.45 | 15.65 | 14.45 | 15.44 | 16.14 | 15.35 | 14.58 | 15.81 | 15.87 |

Table A1 continued.

| Distance | 9:35 | 9:45 | 9:55 | 10:05 | 10:15 | 10:25 | 10:35 | 10:45 | 10:55 |
|---|---|---|---|---|---|---|---|---|---|
| 201 | 16.39 | 15.14 | 16.43 | 16.3 | 16.29 | 15.36 | 15.44 | 14.76 | 14.47 |
| 202 | 15.58 | 15.58 | 15.54 | 14.34 | 16.96 | 15.24 | 14.6 | 14.06 | 15.13 |
| 203 | 15.31 | 16.47 | 15.72 | 14.79 | 15.5 | 17.25 | 17.07 | 13.83 | 14.54 |
| 204 | 15.14 | 15.19 | 15.99 | 15.37 | 14.89 | 14.33 | 16.46 | 15.51 | 14.78 |
| 205 | 14.67 | 15.14 | 15.9 | 15.5 | 15.61 | 15.91 | 15.75 | 14.87 | 16.27 |
| 206 | 16.28 | 15.3 | 16.29 | 15.3 | 15.68 | 16.57 | 15.73 | 16.72 | 14.86 |
| 207 | 16.59 | 15.39 | 14.86 | 16.13 | 16.48 | 15.88 | 17.37 | 17.46 | 16.85 |
| 208 | 15.69 | 16.03 | 15.93 | 15.11 | 14.98 | 17.54 | 15.46 | 16.04 | 14.79 |

Table A2. Example of DTS temperature data collected at Site #2 on Aug 22, 2011.

| Distance | 00:05 | 00:15 | 00:25 | 00:35 | 00:45 | 00:55 | 01:05 | 01:15 | 01:25 |
|---|---|---|---|---|---|---|---|---|---|
| 1 | 0.27 | 0.27 | 0.27 | 0.27 | 0.27 | 0.27 | 0.27 | 0.27 | 0.27 |
| 2 | 1.0146 | 1.0146 | 1.0146 | 1.0146 | 1.0146 | 1.0146 | 1.0146 | 1.0146 | 1.0146 |
| 3 | 23.78 | 23.81 | 23.85 | 23.8 | 23.82 | 23.85 | 23.84 | 23.78 | 23.82 |
| 4 | 22.65 | 22.67 | 22.75 | 22.68 | 22.63 | 22.76 | 22.68 | 22.66 | 22.72 |
| 5 | 20.92 | 20.94 | 20.98 | 20.89 | 20.95 | 20.94 | 20.88 | 20.91 | 20.85 |
| 6 | 19.59 | 19.62 | 19.55 | 19.67 | 19.54 | 19.53 | 19.54 | 19.43 | 19.42 |
| 7 | 18.43 | 18.42 | 18.41 | 18.41 | 18.32 | 18.3 | 18.24 | 18.2 | 18.2 |
| 8 | 13.71 | 13.73 | 13.75 | 13.74 | 13.72 | 13.75 | 13.7 | 13.68 | 13.67 |
| 9 | 7.16 | 7.17 | 7.14 | 7.18 | 7.17 | 7.13 | 7.2 | 7.2 | 7.18 |
| 10 | 5.01 | 5.1 | 5.1 | 5.1 | 5.12 | 5.12 | 5.12 | 5.14 | 5.1 |
| 11 | 5.55 | 5.58 | 5.58 | 5.59 | 5.56 | 5.6 | 5.53 | 5.49 | 5.54 |
| 12 | 5.79 | 5.81 | 5.79 | 5.77 | 5.76 | 5.84 | 5.78 | 5.77 | 5.72 |
| 13 | 4.18 | 4.24 | 4.18 | 4.19 | 4.12 | 4.21 | 4.2 | 4.26 | 4.24 |
| 14 | 2.84 | 2.94 | 2.93 | 2.9 | 2.91 | 2.93 | 2.88 | 2.92 | 2.94 |
| 15 | 2.81 | 2.83 | 2.81 | 2.86 | 2.85 | 2.8 | 2.87 | 2.85 | 2.85 |
| 16 | 3.02 | 3.04 | 3.1 | 3.07 | 3.02 | 3.02 | 3.04 | 3.05 | 3.09 |
| 17 | 2.83 | 2.83 | 2.81 | 2.88 | 2.85 | 2.87 | 2.84 | 2.84 | 2.85 |
| 18 | 2.29 | 2.42 | 2.33 | 2.36 | 2.31 | 2.4 | 2.39 | 2.4 | 2.38 |
| 19 | 2.34 | 2.28 | 2.35 | 2.36 | 2.38 | 2.42 | 2.45 | 2.37 | 2.45 |
| 20 | 2.54 | 2.57 | 2.58 | 2.59 | 2.57 | 2.67 | 2.62 | 2.64 | 2.66 |
| 21 | 2.65 | 2.67 | 2.68 | 2.68 | 2.64 | 2.74 | 2.72 | 2.7 | 2.71 |
| 22 | 2.47 | 2.53 | 2.53 | 2.55 | 2.5 | 2.56 | 2.49 | 2.57 | 2.53 |
| 23 | 2.42 | 2.4 | 2.43 | 2.43 | 2.44 | 2.48 | 2.5 | 2.38 | 2.47 |
| 24 | 2.46 | 2.41 | 2.47 | 2.55 | 2.49 | 2.46 | 2.5 | 2.47 | 2.54 |
| 25 | 2.5 | 2.44 | 2.5 | 2.47 | 2.48 | 2.49 | 2.54 | 2.56 | 2.5 |
| 26 | 2.51 | 2.45 | 2.51 | 2.49 | 2.51 | 2.55 | 2.55 | 2.49 | 2.59 |
| 27 | 2.41 | 2.44 | 2.44 | 2.4 | 2.42 | 2.51 | 2.47 | 2.42 | 2.49 |
| 28 | 2.32 | 2.28 | 2.3 | 2.36 | 2.33 | 2.35 | 2.36 | 2.35 | 2.34 |
| 29 | 2.21 | 2.22 | 2.22 | 2.2 | 2.25 | 2.29 | 2.26 | 2.29 | 2.28 |
| 30 | 2.22 | 2.19 | 2.24 | 2.21 | 2.23 | 2.28 | 2.29 | 2.25 | 2.27 |
| 31 | 2.43 | 2.4 | 2.36 | 2.41 | 2.45 | 2.44 | 2.43 | 2.47 | 2.44 |
| 32 | 2.59 | 2.56 | 2.56 | 2.56 | 2.58 | 2.62 | 2.62 | 2.57 | 2.57 |
| 33 | 2.49 | 2.51 | 2.51 | 2.55 | 2.52 | 2.56 | 2.48 | 2.56 | 2.54 |
| 34 | 2.5 | 2.5 | 2.46 | 2.56 | 2.53 | 2.58 | 2.5 | 2.56 | 2.56 |
| 35 | 2.24 | 2.32 | 2.31 | 2.37 | 2.27 | 2.38 | 2.36 | 2.36 | 2.41 |
| 36 | 2.32 | 2.33 | 2.35 | 2.36 | 2.3 | 2.35 | 2.32 | 2.4 | 2.37 |
| 37 | 2.26 | 2.28 | 2.29 | 2.25 | 2.26 | 2.29 | 2.26 | 2.33 | 2.32 |
| 38 | 2.14 | 2.17 | 2.12 | 2.2 | 2.17 | 2.15 | 2.2 | 2.15 | 2.2 |
| 39 | 2.09 | 2.07 | 2.1 | 2.12 | 2.16 | 2.2 | 2.21 | 2.12 | 2.19 |
| 40 | 2.02 | 2.06 | 2.02 | 2.04 | 2.07 | 2.13 | 2.16 | 2.1 | 2.09 |

Table A2 continued.

| Distance | 00:05 | 00:15 | 00:25 | 00:35 | 00:45 | 00:55 | 01:05 | 01:15 | 01:25 |
|---|---|---|---|---|---|---|---|---|---|
| 41 | 1.98 | 2 | 1.98 | 1.94 | 1.98 | 2 | 2.08 | 2.01 | 2.04 |
| 42 | 1.89 | 1.91 | 1.99 | 1.93 | 1.98 | 1.95 | 1.93 | 2.04 | 1.94 |
| 43 | 2.03 | 2.03 | 2.06 | 2.07 | 2.02 | 2.04 | 2.09 | 2.12 | 2.05 |
| 44 | 2.23 | 2.22 | 2.24 | 2.2 | 2.27 | 2.21 | 2.3 | 2.28 | 2.31 |
| 45 | 2.3 | 2.33 | 2.36 | 2.35 | 2.34 | 2.32 | 2.4 | 2.36 | 2.33 |
| 46 | 2.13 | 2.19 | 2.21 | 2.19 | 2.23 | 2.23 | 2.22 | 2.22 | 2.15 |
| 47 | 1.95 | 2.01 | 2.04 | 2.04 | 2 | 2.06 | 2.06 | 1.99 | 2.01 |
| 48 | 1.98 | 2.03 | 2.01 | 2.06 | 2.07 | 2.06 | 2.05 | 2.05 | 2.04 |
| 49 | 2.02 | 2.01 | 1.96 | 2.05 | 2.05 | 2.04 | 2.06 | 2.08 | 2.1 |
| 50 | 1.99 | 2.05 | 2 | 2.03 | 2.02 | 2.03 | 2.07 | 2.03 | 2.11 |
| 51 | 2.09 | 2.21 | 2.2 | 2.11 | 2.17 | 2.19 | 2.16 | 2.22 | 2.18 |
| 52 | 2.08 | 2.16 | 2.12 | 2.12 | 2.13 | 2.16 | 2.15 | 2.21 | 2.15 |
| 53 | 2.19 | 2.19 | 2.2 | 2.24 | 2.19 | 2.28 | 2.29 | 2.21 | 2.23 |
| 54 | 2.36 | 2.34 | 2.35 | 2.33 | 2.36 | 2.44 | 2.39 | 2.36 | 2.37 |
| 55 | 2.05 | 2.1 | 2.03 | 2.05 | 2.12 | 2.09 | 2.11 | 2.06 | 2.1 |
| 56 | 1.87 | 1.93 | 1.87 | 1.89 | 1.91 | 1.93 | 1.87 | 1.97 | 1.88 |
| 57 | 2.13 | 2.18 | 2.08 | 2.13 | 2.18 | 2.21 | 2.19 | 2.17 | 2.21 |
| 58 | 2.27 | 2.3 | 2.28 | 2.23 | 2.29 | 2.29 | 2.28 | 2.29 | 2.28 |
| 59 | 2.32 | 2.28 | 2.27 | 2.29 | 2.2 | 2.32 | 2.32 | 2.34 | 2.28 |
| 60 | 2.32 | 2.4 | 2.37 | 2.38 | 2.4 | 2.41 | 2.41 | 2.37 | 2.41 |
| 61 | 2.34 | 2.32 | 2.34 | 2.37 | 2.38 | 2.36 | 2.4 | 2.38 | 2.4 |
| 62 | 2.23 | 2.31 | 2.21 | 2.28 | 2.31 | 2.31 | 2.3 | 2.29 | 2.22 |
| 63 | 1.98 | 2.04 | 1.94 | 2.02 | 1.98 | 2.04 | 1.99 | 2.02 | 2.07 |
| 64 | 2.06 | 2.12 | 2.11 | 2.11 | 2.13 | 2.19 | 2.16 | 2.14 | 2.14 |
| 65 | 2.27 | 2.25 | 2.27 | 2.29 | 2.33 | 2.32 | 2.32 | 2.32 | 2.36 |
| 66 | 2.19 | 2.22 | 2.17 | 2.24 | 2.24 | 2.26 | 2.24 | 2.21 | 2.16 |
| 67 | 2.17 | 2.17 | 2.16 | 2.17 | 2.23 | 2.25 | 2.26 | 2.19 | 2.21 |
| 68 | 2.25 | 2.31 | 2.25 | 2.28 | 2.3 | 2.32 | 2.3 | 2.3 | 2.29 |
| 69 | 2.39 | 2.4 | 2.39 | 2.45 | 2.44 | 2.47 | 2.4 | 2.5 | 2.49 |
| 70 | 2.32 | 2.3 | 2.31 | 2.29 | 2.32 | 2.38 | 2.39 | 2.4 | 2.41 |
| 71 | 1.99 | 2.02 | 1.98 | 2.01 | 2.06 | 2.12 | 2.06 | 2.06 | 2.04 |
| 72 | 2.1 | 2.09 | 2.16 | 2.14 | 2.1 | 2.13 | 2.17 | 2.19 | 2.16 |
| 73 | 2.16 | 2.19 | 2.22 | 2.22 | 2.18 | 2.23 | 2.25 | 2.24 | 2.25 |
| 74 | 2.04 | 2.12 | 2.07 | 2.15 | 2.11 | 2.11 | 2.13 | 2.18 | 2.14 |
| 75 | 2.15 | 2.19 | 2.12 | 2.17 | 2.18 | 2.21 | 2.23 | 2.22 | 2.22 |
| 76 | 2.37 | 2.29 | 2.34 | 2.35 | 2.31 | 2.39 | 2.45 | 2.39 | 2.37 |
| 77 | 2.45 | 2.54 | 2.49 | 2.51 | 2.56 | 2.51 | 2.63 | 2.55 | 2.51 |
| 78 | 2.47 | 2.54 | 2.52 | 2.57 | 2.53 | 2.56 | 2.59 | 2.53 | 2.53 |
| 79 | 2.47 | 2.43 | 2.47 | 2.51 | 2.53 | 2.5 | 2.53 | 2.54 | 2.51 |
| 80 | 2.52 | 2.54 | 2.5 | 2.51 | 2.53 | 2.61 | 2.56 | 2.55 | 2.58 |

Table A2 continued.

| Distance | 00:05 | 00:15 | 00:25 | 00:35 | 00:45 | 00:55 | 01:05 | 01:15 | 01:25 |
|---|---|---|---|---|---|---|---|---|---|
| 81 | 2.54 | 2.59 | 2.57 | 2.58 | 2.65 | 2.66 | 2.63 | 2.64 | 2.62 |
| 82 | 2.52 | 2.56 | 2.57 | 2.56 | 2.58 | 2.59 | 2.66 | 2.6 | 2.63 |
| 83 | 2.51 | 2.55 | 2.52 | 2.52 | 2.51 | 2.58 | 2.6 | 2.63 | 2.61 |
| 84 | 2.57 | 2.57 | 2.59 | 2.62 | 2.63 | 2.62 | 2.62 | 2.7 | 2.61 |
| 85 | 3.03 | 3.07 | 3.1 | 3.08 | 3.06 | 3.13 | 3.16 | 3.17 | 3.14 |
| 86 | 6.46 | 6.49 | 6.46 | 6.5 | 6.42 | 6.46 | 6.44 | 6.45 | 6.38 |
| 87 | 11.21 | 11.26 | 11.22 | 11.24 | 11.15 | 11.18 | 11.11 | 11.08 | 11.03 |
| 88 | 12.61 | 12.7 | 12.65 | 12.64 | 12.63 | 12.55 | 12.55 | 12.47 | 12.42 |
| 89 | 12.72 | 12.75 | 12.72 | 12.75 | 12.7 | 12.72 | 12.66 | 12.63 | 12.51 |
| 90 | 12.99 | 13 | 12.94 | 12.97 | 12.9 | 12.95 | 12.83 | 12.75 | 12.8 |
| 91 | 13.96 | 13.94 | 13.91 | 13.91 | 13.82 | 13.88 | 13.81 | 13.74 | 13.65 |
| 92 | 14.93 | 14.96 | 14.95 | 14.92 | 14.85 | 14.91 | 14.76 | 14.7 | 14.6 |
| 93 | 15.05 | 15.1 | 15.05 | 15.02 | 15.02 | 14.97 | 14.87 | 14.85 | 14.71 |
| 94 | 14.97 | 14.99 | 14.97 | 14.97 | 14.92 | 14.93 | 14.81 | 14.75 | 14.75 |
| 95 | 15.05 | 15.07 | 15.07 | 15 | 14.97 | 14.91 | 14.95 | 14.75 | 14.73 |
| 96 | 15.33 | 15.29 | 15.28 | 15.26 | 15.28 | 15.17 | 15.12 | 15.03 | 14.88 |
| 97 | 15.32 | 15.33 | 15.28 | 15.31 | 15.22 | 15.23 | 15.15 | 15.04 | 14.96 |
| 98 | 15.32 | 15.31 | 15.35 | 15.31 | 15.21 | 15.28 | 15.16 | 15.02 | 15.03 |
| 99 | 15.33 | 15.37 | 15.34 | 15.27 | 15.22 | 15.24 | 15.14 | 15.06 | 15.03 |
| 100 | 15.28 | 15.27 | 15.22 | 15.28 | 15.21 | 15.18 | 15.13 | 15 | 15.03 |
| 101 | 15.25 | 15.29 | 15.28 | 15.2 | 15.11 | 15.14 | 15.04 | 14.99 | 14.99 |
| 102 | 15.18 | 15.18 | 15.2 | 15.16 | 15.11 | 15.06 | 15.02 | 14.95 | 14.92 |
| 103 | 15.16 | 15.17 | 15.16 | 15.12 | 15.12 | 15.07 | 14.99 | 15 | 14.93 |
| 104 | 15.18 | 15.16 | 15.16 | 15.1 | 15.1 | 15.06 | 14.96 | 14.86 | 14.82 |
| 105 | 15.14 | 15.19 | 15.13 | 15.13 | 15.07 | 15.07 | 14.99 | 14.96 | 14.88 |
| 106 | 15.05 | 15.07 | 15.05 | 15.07 | 15.02 | 15.02 | 14.96 | 14.89 | 14.87 |
| 107 | 15.05 | 14.99 | 15.09 | 14.98 | 14.98 | 15 | 14.85 | 14.77 | 14.79 |
| 108 | 15.15 | 15.14 | 15.12 | 15.12 | 15.06 | 15.01 | 14.98 | 14.86 | 14.84 |
| 109 | 15.16 | 15.19 | 15.17 | 15.14 | 15.07 | 15.05 | 15.02 | 14.88 | 14.9 |
| 110 | 15.3 | 15.25 | 15.24 | 15.26 | 15.21 | 15.22 | 15.08 | 15.05 | 14.97 |
| 111 | 15.21 | 15.22 | 15.21 | 15.21 | 15.11 | 15.11 | 15.08 | 15.03 | 14.93 |
| 112 | 15.14 | 15.17 | 15.12 | 15.09 | 15.07 | 15 | 14.98 | 14.87 | 14.87 |
| 113 | 15.17 | 15.12 | 15.07 | 15.08 | 15.12 | 15.07 | 15.04 | 14.92 | 14.88 |
| 114 | 15.17 | 15.13 | 15.15 | 15.2 | 15.16 | 15.06 | 15.03 | 14.92 | 14.91 |
| 115 | 15.2 | 15.17 | 15.13 | 15.16 | 15.07 | 15.11 | 15.05 | 14.91 | 14.89 |
| 116 | 15.25 | 15.24 | 15.15 | 15.17 | 15.09 | 15.15 | 15.04 | 14.95 | 14.89 |
| 117 | 15.25 | 15.39 | 15.22 | 15.35 | 15.2 | 15.22 | 15.21 | 15.12 | 15.01 |
| 118 | 15.39 | 15.36 | 15.43 | 15.34 | 15.32 | 15.35 | 15.28 | 15.19 | 15.11 |
| 119 | 15.57 | 15.49 | 15.36 | 15.42 | 15.39 | 15.38 | 15.29 | 15.25 | 15.21 |
| 120 | 15.41 | 15.46 | 15.41 | 15.43 | 15.37 | 15.36 | 15.25 | 15.22 | 15.14 |

Table A2 continued.

| Distance | 00:05 | 00:15 | 00:25 | 00:35 | 00:45 | 00:55 | 01:05 | 01:15 | 01:25 |
|---|---|---|---|---|---|---|---|---|---|
| 121 | 15.36 | 15.33 | 15.37 | 15.28 | 15.3 | 15.26 | 15.23 | 15.14 | 15.02 |
| 122 | 15.27 | 15.3 | 15.29 | 15.27 | 15.25 | 15.23 | 15.17 | 15.13 | 15.06 |
| 123 | 15.49 | 15.49 | 15.49 | 15.48 | 15.44 | 15.43 | 15.31 | 15.25 | 15.2 |
| 124 | 15.68 | 15.54 | 15.59 | 15.59 | 15.52 | 15.49 | 15.42 | 15.35 | 15.26 |
| 125 | 15.54 | 15.56 | 15.47 | 15.5 | 15.4 | 15.42 | 15.36 | 15.22 | 15.18 |
| 126 | 15.38 | 15.37 | 15.42 | 15.32 | 15.31 | 15.33 | 15.22 | 15.1 | 15.08 |
| 127 | 15.31 | 15.36 | 15.31 | 15.27 | 15.2 | 15.24 | 15.13 | 15.11 | 14.96 |
| 128 | 15.47 | 15.43 | 15.46 | 15.41 | 15.32 | 15.3 | 15.28 | 15.18 | 15.17 |
| 129 | 15.36 | 15.34 | 15.35 | 15.36 | 15.3 | 15.27 | 15.29 | 15.12 | 15.07 |
| 130 | 15.26 | 15.32 | 15.31 | 15.25 | 15.22 | 15.27 | 15.24 | 15.1 | 14.97 |
| 131 | 15.32 | 15.31 | 15.34 | 15.32 | 15.14 | 15.22 | 15.17 | 15.14 | 15.03 |
| 132 | 15.5 | 15.46 | 15.43 | 15.42 | 15.4 | 15.37 | 15.3 | 15.21 | 15.16 |
| 133 | 15.57 | 15.57 | 15.52 | 15.51 | 15.43 | 15.4 | 15.33 | 15.33 | 15.22 |
| 134 | 15.37 | 15.4 | 15.43 | 15.46 | 15.34 | 15.36 | 15.23 | 15.21 | 15.11 |
| 135 | 15.32 | 15.32 | 15.29 | 15.33 | 15.25 | 15.22 | 15.18 | 15.09 | 15.1 |
| 136 | 15.41 | 15.42 | 15.41 | 15.39 | 15.32 | 15.23 | 15.23 | 15.15 | 15.06 |
| 137 | 15.47 | 15.54 | 15.41 | 15.47 | 15.39 | 15.37 | 15.29 | 15.18 | 15.14 |
| 138 | 15.52 | 15.48 | 15.49 | 15.51 | 15.45 | 15.35 | 15.28 | 15.23 | 15.17 |
| 139 | 15.47 | 15.46 | 15.42 | 15.35 | 15.37 | 15.34 | 15.3 | 15.19 | 15.2 |
| 140 | 15.39 | 15.4 | 15.33 | 15.34 | 15.34 | 15.38 | 15.19 | 15.17 | 15.14 |
| 141 | 15.37 | 15.46 | 15.36 | 15.32 | 15.29 | 15.31 | 15.26 | 15.14 | 15.06 |
| 142 | 15.43 | 15.49 | 15.47 | 15.42 | 15.37 | 15.42 | 15.32 | 15.16 | 15.19 |
| 143 | 15.48 | 15.52 | 15.47 | 15.39 | 15.39 | 15.36 | 15.28 | 15.19 | 15.14 |
| 144 | 15.4 | 15.42 | 15.38 | 15.38 | 15.35 | 15.32 | 15.24 | 15.13 | 15.08 |
| 145 | 15.34 | 15.35 | 15.29 | 15.29 | 15.24 | 15.31 | 15.18 | 15.12 | 14.99 |
| 146 | 15.28 | 15.24 | 15.28 | 15.22 | 15.18 | 15.22 | 15.17 | 15.1 | 15 |
| 147 | 15.34 | 15.31 | 15.32 | 15.28 | 15.24 | 15.2 | 15.16 | 15.08 | 15.05 |
| 148 | 15.31 | 15.4 | 15.4 | 15.32 | 15.27 | 15.29 | 15.28 | 15.14 | 15.11 |
| 149 | 15.32 | 15.38 | 15.37 | 15.31 | 15.26 | 15.26 | 15.22 | 15.13 | 15.06 |
| 150 | 15.25 | 15.31 | 15.28 | 15.23 | 15.23 | 15.21 | 15.12 | 15.04 | 15.01 |
| 151 | 15.36 | 15.31 | 15.3 | 15.3 | 15.26 | 15.28 | 15.14 | 15.12 | 15.05 |
| 152 | 15.42 | 15.45 | 15.34 | 15.37 | 15.35 | 15.35 | 15.28 | 15.19 | 15.2 |
| 153 | 15.41 | 15.43 | 15.31 | 15.38 | 15.37 | 15.29 | 15.18 | 15.2 | 15.16 |
| 154 | 15.26 | 15.27 | 15.25 | 15.27 | 15.2 | 15.17 | 15.1 | 15.01 | 15.02 |
| 155 | 15.15 | 15.15 | 15.1 | 15.11 | 15.05 | 15.03 | 15.05 | 14.96 | 14.88 |
| 156 | 15.33 | 15.31 | 15.27 | 15.27 | 15.23 | 15.25 | 15.09 | 15.05 | 14.94 |
| 157 | 15.46 | 15.44 | 15.34 | 15.4 | 15.33 | 15.26 | 15.23 | 15.16 | 15.12 |
| 158 | 15.39 | 15.39 | 15.29 | 15.33 | 15.29 | 15.23 | 15.17 | 15.09 | 14.98 |
| 159 | 15.36 | 15.32 | 15.27 | 15.28 | 15.26 | 15.17 | 15.14 | 15.08 | 15.01 |
| 160 | 15.19 | 15.19 | 15.15 | 15.15 | 15.1 | 15.09 | 15.03 | 14.86 | 14.85 |

Table A2 continued.

| Distance | 00:05 | 00:15 | 00:25 | 00:35 | 00:45 | 00:55 | 01:05 | 01:15 | 01:25 |
|---|---|---|---|---|---|---|---|---|---|
| 161 | 15 | 14.96 | 14.89 | 14.92 | 14.87 | 14.85 | 14.83 | 14.74 | 14.69 |
| 162 | 14.83 | 14.76 | 14.76 | 14.79 | 14.76 | 14.77 | 14.67 | 14.57 | 14.6 |
| 163 | 14.77 | 14.78 | 14.68 | 14.65 | 14.75 | 14.68 | 14.67 | 14.54 | 14.51 |
| 164 | 14.73 | 14.74 | 14.72 | 14.73 | 14.66 | 14.67 | 14.65 | 14.51 | 14.49 |
| 165 | 14.69 | 14.7 | 14.65 | 14.69 | 14.63 | 14.57 | 14.56 | 14.48 | 14.45 |
| 166 | 14.57 | 14.63 | 14.59 | 14.59 | 14.56 | 14.6 | 14.51 | 14.45 | 14.4 |
| 167 | 14.65 | 14.6 | 14.65 | 14.62 | 14.63 | 14.62 | 14.54 | 14.43 | 14.42 |
| 168 | 14.61 | 14.67 | 14.62 | 14.65 | 14.61 | 14.62 | 14.57 | 14.47 | 14.42 |
| 169 | 14.77 | 14.66 | 14.71 | 14.71 | 14.67 | 14.66 | 14.62 | 14.48 | 14.45 |
| 170 | 14.85 | 14.85 | 14.83 | 14.83 | 14.82 | 14.8 | 14.81 | 14.68 | 14.62 |
| 171 | 14.69 | 14.75 | 14.68 | 14.7 | 14.68 | 14.74 | 14.7 | 14.58 | 14.52 |
| 172 | 14.66 | 14.74 | 14.67 | 14.68 | 14.64 | 14.64 | 14.6 | 14.6 | 14.51 |
| 173 | 14.65 | 14.71 | 14.65 | 14.71 | 14.66 | 14.64 | 14.57 | 14.52 | 14.53 |
| 174 | 14.58 | 14.57 | 14.54 | 14.55 | 14.5 | 14.6 | 14.55 | 14.45 | 14.36 |
| 175 | 14.46 | 14.45 | 14.42 | 14.49 | 14.42 | 14.52 | 14.37 | 14.38 | 14.35 |
| 176 | 14.48 | 14.51 | 14.49 | 14.53 | 14.46 | 14.55 | 14.48 | 14.4 | 14.35 |
| 177 | 14.52 | 14.58 | 14.52 | 14.63 | 14.59 | 14.57 | 14.51 | 14.55 | 14.48 |
| 178 | 14.52 | 14.57 | 14.56 | 14.63 | 14.55 | 14.58 | 14.53 | 14.48 | 14.48 |
| 179 | 14.53 | 14.62 | 14.58 | 14.57 | 14.57 | 14.54 | 14.5 | 14.4 | 14.39 |
| 180 | 14.59 | 14.58 | 14.57 | 14.62 | 14.6 | 14.6 | 14.52 | 14.46 | 14.43 |
| 181 | 14.49 | 14.57 | 14.51 | 14.56 | 14.54 | 14.55 | 14.46 | 14.41 | 14.42 |
| 182 | 14.48 | 14.45 | 14.47 | 14.52 | 14.48 | 14.46 | 14.45 | 14.33 | 14.3 |
| 183 | 14.48 | 14.52 | 14.5 | 14.54 | 14.49 | 14.46 | 14.47 | 14.4 | 14.34 |
| 184 | 14.41 | 14.33 | 14.36 | 14.39 | 14.32 | 14.42 | 14.29 | 14.26 | 14.23 |
| 185 | 14.19 | 14.23 | 14.19 | 14.21 | 14.17 | 14.23 | 14.15 | 14.14 | 14.04 |
| 186 | 14.12 | 14.09 | 14.1 | 14.05 | 14.09 | 14.12 | 14.13 | 14.05 | 14.04 |
| 187 | 13.98 | 14.04 | 14.05 | 14.06 | 13.99 | 14.01 | 14.06 | 14.03 | 14.02 |
| 188 | 14.2 | 14.18 | 14.25 | 14.15 | 14.16 | 14.18 | 14.15 | 14.15 | 14.14 |
| 189 | 14.08 | 14.12 | 14.11 | 14.12 | 14.06 | 14.04 | 14.12 | 14.07 | 14.07 |
| 190 | 14.11 | 14.13 | 14.14 | 14.09 | 14.14 | 14.13 | 14.11 | 14.08 | 14.03 |
| 191 | 14.26 | 14.27 | 14.23 | 14.22 | 14.29 | 14.33 | 14.21 | 14.2 | 14.19 |
| 192 | 14.31 | 14.38 | 14.34 | 14.36 | 14.35 | 14.36 | 14.27 | 14.26 | 14.24 |
| 193 | 14.32 | 14.35 | 14.3 | 14.37 | 14.33 | 14.39 | 14.33 | 14.34 | 14.25 |
| 194 | 14.23 | 14.22 | 14.26 | 14.25 | 14.24 | 14.24 | 14.23 | 14.21 | 14.12 |
| 195 | 14.16 | 14.17 | 14.15 | 14.26 | 14.23 | 14.24 | 14.16 | 14.17 | 14.2 |
| 196 | 14.15 | 14.23 | 14.26 | 14.24 | 14.2 | 14.17 | 14.24 | 14.18 | 14.16 |
| 197 | 14.25 | 14.31 | 14.26 | 14.32 | 14.33 | 14.32 | 14.33 | 14.25 | 14.2 |
| 198 | 14.34 | 14.4 | 14.37 | 14.38 | 14.41 | 14.47 | 14.41 | 14.35 | 14.31 |
| 199 | 14.41 | 14.43 | 14.34 | 14.37 | 14.38 | 14.41 | 14.36 | 14.39 | 14.36 |
| 200 | 14.39 | 14.43 | 14.34 | 14.4 | 14.38 | 14.39 | 14.32 | 14.32 | 14.27 |

Table A2 continued.

| Distance | 00:05 | 00:15 | 00:25 | 00:35 | 00:45 | 00:55 | 01:05 | 01:15 | 01:25 |
|---|---|---|---|---|---|---|---|---|---|
| 201 | 14.44 | 14.45 | 14.4 | 14.48 | 14.43 | 14.43 | 14.43 | 14.34 | 14.36 |
| 202 | 14.46 | 14.41 | 14.4 | 14.4 | 14.41 | 14.45 | 14.48 | 14.35 | 14.4 |
| 203 | 14.41 | 14.41 | 14.4 | 14.39 | 14.41 | 14.39 | 14.43 | 14.37 | 14.33 |
| 204 | 14.36 | 14.35 | 14.37 | 14.38 | 14.38 | 14.42 | 14.36 | 14.29 | 14.35 |
| 205 | 14.39 | 14.39 | 14.39 | 14.37 | 14.39 | 14.4 | 14.34 | 14.36 | 14.32 |
| 206 | 14.39 | 14.45 | 14.43 | 14.44 | 14.39 | 14.43 | 14.4 | 14.4 | 14.32 |
| 207 | 14.32 | 14.37 | 14.37 | 14.38 | 14.39 | 14.32 | 14.37 | 14.25 | 14.27 |
| 208 | 14.38 | 14.34 | 14.41 | 14.38 | 14.33 | 14.39 | 14.38 | 14.34 | 14.28 |
| 209 | 14.43 | 14.52 | 14.47 | 14.49 | 14.5 | 14.5 | 14.49 | 14.45 | 14.42 |
| 210 | 14.53 | 14.51 | 14.56 | 14.58 | 14.5 | 14.53 | 14.51 | 14.45 | 14.4 |
| 211 | 14.48 | 14.43 | 14.5 | 14.5 | 14.46 | 14.52 | 14.42 | 14.42 | 14.41 |
| 212 | 14.55 | 14.53 | 14.5 | 14.47 | 14.52 | 14.55 | 14.57 | 14.45 | 14.45 |
| 213 | 14.51 | 14.52 | 14.52 | 14.56 | 14.5 | 14.46 | 14.47 | 14.43 | 14.42 |
| 214 | 14.4 | 14.42 | 14.47 | 14.42 | 14.36 | 14.49 | 14.46 | 14.41 | 14.44 |
| 215 | 14.35 | 14.39 | 14.39 | 14.47 | 14.4 | 14.44 | 14.4 | 14.45 | 14.32 |
| 216 | 14.52 | 14.43 | 14.44 | 14.5 | 14.44 | 14.44 | 14.45 | 14.47 | 14.46 |
| 217 | 14.41 | 14.41 | 14.43 | 14.47 | 14.45 | 14.42 | 14.47 | 14.45 | 14.44 |
| 218 | 14.4 | 14.52 | 14.44 | 14.5 | 14.45 | 14.45 | 14.48 | 14.42 | 14.4 |
| 219 | 14.66 | 14.66 | 14.72 | 14.67 | 14.75 | 14.68 | 14.74 | 14.67 | 14.65 |
| 220 | 14.88 | 14.84 | 14.86 | 14.95 | 14.92 | 14.94 | 14.89 | 14.86 | 14.85 |
| 221 | 14.94 | 14.98 | 14.9 | 15.01 | 15 | 14.95 | 14.98 | 14.95 | 14.88 |
| 222 | 14.97 | 15.05 | 15.02 | 15 | 14.95 | 15 | 15.02 | 14.96 | 14.93 |
| 223 | 15 | 15.01 | 15.07 | 15.06 | 15.09 | 15.04 | 15.01 | 15.06 | 14.92 |
| 224 | 14.97 | 15.02 | 14.98 | 14.97 | 14.96 | 14.97 | 14.98 | 14.97 | 14.94 |
| 225 | 14.82 | 14.84 | 14.82 | 14.82 | 14.83 | 14.86 | 14.86 | 14.76 | 14.77 |
| 226 | 14.84 | 14.86 | 14.83 | 14.88 | 14.79 | 14.86 | 14.84 | 14.86 | 14.81 |
| 227 | 14.93 | 14.96 | 15.02 | 14.99 | 14.95 | 15.01 | 14.96 | 14.98 | 14.87 |
| 228 | 14.99 | 15.01 | 15.01 | 14.98 | 15.02 | 15.03 | 15.05 | 14.99 | 14.98 |
| 229 | 15.03 | 14.96 | 14.97 | 14.93 | 14.99 | 15 | 14.99 | 14.94 | 14.95 |
| 230 | 14.96 | 15.08 | 15.06 | 15.02 | 14.97 | 15.01 | 15.02 | 14.96 | 14.98 |
| 231 | 15.04 | 15.14 | 15.1 | 15.15 | 15.09 | 15.17 | 15.14 | 15.06 | 15.12 |
| 232 | 15.2 | 15.13 | 15.2 | 15.15 | 15.12 | 15.16 | 15.15 | 15.16 | 15.2 |
| 233 | 15.19 | 15.26 | 15.24 | 15.13 | 15.16 | 15.18 | 15.17 | 15.16 | 15.15 |
| 234 | 15.09 | 15.2 | 15.15 | 15.08 | 15.11 | 15.2 | 15.16 | 15.21 | 15.09 |
| 235 | 15.1 | 15.25 | 15.17 | 15.14 | 15.16 | 15.13 | 15.17 | 15.07 | 15.15 |
| 236 | 15.14 | 15.21 | 15.16 | 15.18 | 15.19 | 15.14 | 15.21 | 15.16 | 15.13 |
| 237 | 15.18 | 15.15 | 15.14 | 15.17 | 15.23 | 15.17 | 15.15 | 15.16 | 15.15 |
| 238 | 15.17 | 15.21 | 15.19 | 15.18 | 15.2 | 15.22 | 15.16 | 15.15 | 15.1 |
| 239 | 15.16 | 15.17 | 15.14 | 15.18 | 15.13 | 15.12 | 15.21 | 15.07 | 15.09 |
| 240 | 14.97 | 15.04 | 15.03 | 15.07 | 15 | 15.06 | 14.98 | 15.05 | 14.99 |

Table A2 continued.

| Distance | 00:05 | 00:15 | 00:25 | 00:35 | 00:45 | 00:55 | 01:05 | 01:15 | 01:25 |
|---|---|---|---|---|---|---|---|---|---|
| 241 | 14.95 | 14.95 | 14.99 | 14.94 | 14.9 | 14.99 | 14.97 | 14.93 | 14.9 |
| 242 | 14.94 | 14.95 | 14.89 | 14.95 | 14.94 | 14.96 | 14.94 | 14.92 | 14.93 |
| 243 | 15.01 | 15.01 | 15.01 | 15.03 | 15.02 | 14.93 | 14.98 | 14.99 | 15.03 |
| 244 | 14.97 | 15.02 | 15 | 15.03 | 15.04 | 14.96 | 15.03 | 14.99 | 14.99 |
| 245 | 14.9 | 14.95 | 14.92 | 14.98 | 14.92 | 14.98 | 14.93 | 14.86 | 14.88 |
| 246 | 15.08 | 15.07 | 15.1 | 15.05 | 15.03 | 15.08 | 15.01 | 14.99 | 14.98 |
| 247 | 15.19 | 15.21 | 15.19 | 15.22 | 15.2 | 15.24 | 15.19 | 15.23 | 15.21 |
| 248 | 15.23 | 15.24 | 15.24 | 15.19 | 15.19 | 15.23 | 15.25 | 15.22 | 15.2 |
| 249 | 15.25 | 15.14 | 15.11 | 15.19 | 15.17 | 15.25 | 15.19 | 15.2 | 15.14 |
| 250 | 15.17 | 15.22 | 15.18 | 15.19 | 15.15 | 15.2 | 15.18 | 15.12 | 15.11 |
| 251 | 15.25 | 15.26 | 15.3 | 15.29 | 15.25 | 15.26 | 15.23 | 15.15 | 15.22 |
| 252 | 15.37 | 15.33 | 15.32 | 15.32 | 15.31 | 15.35 | 15.27 | 15.28 | 15.22 |
| 253 | 15.2 | 15.18 | 15.15 | 15.14 | 15.2 | 15.23 | 15.19 | 15.24 | 15.14 |
| 254 | 15.17 | 15.18 | 15.17 | 15.14 | 15.23 | 15.14 | 15.23 | 15.17 | 15.1 |
| 255 | 15.18 | 15.21 | 15.15 | 15.18 | 15.19 | 15.15 | 15.18 | 15.15 | 15.17 |
| 256 | 15.12 | 15.09 | 15.03 | 15.02 | 15.11 | 15.11 | 15.04 | 15.06 | 15.05 |
| 257 | 15.08 | 15.06 | 15 | 15.04 | 15.05 | 15.08 | 15 | 15.05 | 15.05 |
| 258 | 15.16 | 15.03 | 15.08 | 15.04 | 15.03 | 15.11 | 15.1 | 15.09 | 15.05 |
| 259 | 15.07 | 15.07 | 15.03 | 14.99 | 14.94 | 15.03 | 15.04 | 15 | 15 |
| 260 | 15.02 | 15 | 15.02 | 14.99 | 15.01 | 14.99 | 15.01 | 14.97 | 14.93 |
| 261 | 15.03 | 15.02 | 15.06 | 15.08 | 15.02 | 15.07 | 15.06 | 15.05 | 15.04 |
| 262 | 15.13 | 15.11 | 15.15 | 15.13 | 15.13 | 15.12 | 15.16 | 15.12 | 15.03 |
| 263 | 15.1 | 15.1 | 15.16 | 15.15 | 15.1 | 15.13 | 15.15 | 15.1 | 15.09 |
| 264 | 15.11 | 15.13 | 15.12 | 15.16 | 15.13 | 15.19 | 15.1 | 15.08 | 15.06 |
| 265 | 15.1 | 15.14 | 15.02 | 15.1 | 15.08 | 15.08 | 15.11 | 14.98 | 15 |
| 266 | 15.05 | 15.06 | 15.04 | 15.05 | 15.05 | 15.02 | 15.09 | 14.93 | 14.97 |
| 267 | 15.04 | 15.11 | 15.04 | 15.02 | 15.01 | 15.11 | 15.03 | 15.05 | 15 |
| 268 | 15.02 | 15.12 | 15.06 | 15.11 | 15.09 | 15.1 | 15 | 15.09 | 15.06 |
| 269 | 15.06 | 15.06 | 15.05 | 15.08 | 15.07 | 15.1 | 15 | 15.03 | 15.01 |
| 270 | 15.04 | 15.05 | 15.03 | 15.03 | 14.99 | 14.98 | 15.01 | 15.01 | 14.98 |
| 271 | 15 | 15.08 | 15.06 | 15.04 | 15 | 14.98 | 15.02 | 14.94 | 14.99 |
| 272 | 14.99 | 14.92 | 14.99 | 14.96 | 15.02 | 15.09 | 15.01 | 14.96 | 14.94 |
| 273 | 15.03 | 15.01 | 15.11 | 15.09 | 14.99 | 15.07 | 15 | 14.97 | 14.97 |
| 274 | 15.09 | 15.14 | 15.12 | 15.14 | 15.11 | 15.13 | 15.02 | 15.05 | 15.05 |
| 275 | 15.14 | 15.18 | 15.21 | 15.21 | 15.14 | 15.2 | 15.1 | 15.14 | 15.14 |
| 276 | 15.23 | 15.26 | 15.32 | 15.33 | 15.24 | 15.23 | 15.22 | 15.27 | 15.23 |
| 277 | 15.38 | 15.34 | 15.3 | 15.39 | 15.31 | 15.3 | 15.33 | 15.28 | 15.29 |
| 278 | 15.42 | 15.42 | 15.46 | 15.43 | 15.38 | 15.46 | 15.47 | 15.38 | 15.35 |
| 279 | 15.33 | 15.35 | 15.3 | 15.27 | 15.36 | 15.4 | 15.39 | 15.26 | 15.21 |
| 280 | 15.25 | 15.25 | 15.2 | 15.28 | 15.25 | 15.24 | 15.24 | 15.15 | 15.23 |

Table A2 continued.

| Distance | 00:05 | 00:15 | 00:25 | 00:35 | 00:45 | 00:55 | 01:05 | 01:15 | 01:25 |
|---|---|---|---|---|---|---|---|---|---|
| 281 | 15.34 | 15.32 | 15.34 | 15.39 | 15.29 | 15.39 | 15.32 | 15.28 | 15.28 |
| 282 | 15.48 | 15.48 | 15.5 | 15.5 | 15.41 | 15.52 | 15.39 | 15.49 | 15.44 |
| 283 | 15.52 | 15.55 | 15.49 | 15.44 | 15.51 | 15.5 | 15.48 | 15.4 | 15.37 |
| 284 | 15.31 | 15.31 | 15.34 | 15.29 | 15.29 | 15.26 | 15.24 | 15.25 | 15.2 |
| 285 | 14.96 | 15.08 | 15.01 | 15.01 | 14.93 | 14.99 | 15.02 | 15.02 | 14.96 |
| 286 | 11.44 | 11.5 | 11.38 | 11.49 | 11.42 | 11.48 | 11.45 | 11.5 | 11.44 |
| 287 | 6.64 | 6.64 | 6.57 | 6.57 | 6.61 | 6.67 | 6.68 | 6.65 | 6.66 |
| 288 | 5.57 | 5.58 | 5.59 | 5.6 | 5.63 | 5.63 | 5.69 | 5.63 | 5.67 |
| 289 | 5.96 | 5.93 | 5.95 | 5.92 | 5.92 | 5.96 | 5.95 | 5.88 | 5.94 |
| 290 | 6.56 | 6.54 | 6.52 | 6.47 | 6.48 | 6.44 | 6.48 | 6.39 | 6.44 |
| 291 | 4.82 | 4.78 | 4.75 | 4.79 | 4.75 | 4.81 | 4.78 | 4.77 | 4.73 |
| 292 | 3.79 | 3.82 | 3.8 | 3.74 | 3.82 | 3.75 | 3.82 | 3.78 | 3.82 |
| 293 | 4.28 | 4.34 | 4.37 | 4.3 | 4.33 | 4.26 | 4.21 | 4.18 | 4.22 |
| 294 | 4.44 | 4.47 | 4.42 | 4.39 | 4.42 | 4.46 | 4.39 | 4.36 | 4.28 |
| 295 | 3.81 | 3.84 | 3.84 | 3.8 | 3.77 | 3.8 | 3.81 | 3.81 | 3.85 |
| 296 | 2.92 | 2.95 | 2.91 | 2.95 | 2.96 | 3 | 2.97 | 2.98 | 2.95 |
| 297 | 3.27 | 3.27 | 3.17 | 3.19 | 3.19 | 3.24 | 3.18 | 3.16 | 3.22 |
| 298 | 3.31 | 3.2 | 3.22 | 3.23 | 3.23 | 3.23 | 3.19 | 3.21 | 3.22 |
| 299 | 3.13 | 3.12 | 3.09 | 3.11 | 3.05 | 3.08 | 3.13 | 3.03 | 3.04 |
| 300 | 3.23 | 3.21 | 3.22 | 3.25 | 3.2 | 3.22 | 3.11 | 3.22 | 3.18 |
| 301 | 3.67 | 3.72 | 3.66 | 3.69 | 3.64 | 3.65 | 3.6 | 3.61 | 3.56 |
| 302 | 3.59 | 3.54 | 3.5 | 3.49 | 3.48 | 3.51 | 3.48 | 3.45 | 3.47 |
| 303 | 3.42 | 3.45 | 3.36 | 3.42 | 3.35 | 3.31 | 3.37 | 3.34 | 3.35 |
| 304 | 3.27 | 3.35 | 3.27 | 3.27 | 3.28 | 3.31 | 3.25 | 3.2 | 3.19 |
| 305 | 3.32 | 3.39 | 3.36 | 3.4 | 3.31 | 3.32 | 3.31 | 3.33 | 3.27 |
| 306 | 3.58 | 3.54 | 3.52 | 3.55 | 3.54 | 3.47 | 3.52 | 3.53 | 3.52 |
| 307 | 3.38 | 3.32 | 3.37 | 3.41 | 3.31 | 3.33 | 3.34 | 3.38 | 3.3 |
| 308 | 3.66 | 3.53 | 3.65 | 3.63 | 3.53 | 3.58 | 3.56 | 3.56 | 3.55 |
| 309 | 3.73 | 3.7 | 3.65 | 3.71 | 3.7 | 3.65 | 3.62 | 3.63 | 3.62 |
| 310 | 3.47 | 3.5 | 3.43 | 3.49 | 3.46 | 3.5 | 3.47 | 3.44 | 3.47 |
| 311 | 3.44 | 3.47 | 3.39 | 3.48 | 3.42 | 3.45 | 3.39 | 3.47 | 3.4 |
| 312 | 3.92 | 3.92 | 3.84 | 3.9 | 3.85 | 3.83 | 3.86 | 3.87 | 3.81 |
| 313 | 4.33 | 4.34 | 4.29 | 4.28 | 4.26 | 4.2 | 4.22 | 4.16 | 4.19 |
| 314 | 3.59 | 3.57 | 3.62 | 3.56 | 3.5 | 3.58 | 3.52 | 3.51 | 3.51 |
| 315 | 2.77 | 2.75 | 2.79 | 2.78 | 2.77 | 2.75 | 2.74 | 2.79 | 2.74 |
| 316 | 2.87 | 2.94 | 2.9 | 2.9 | 2.94 | 2.96 | 2.92 | 2.99 | 3 |
| 317 | 3.71 | 3.76 | 3.67 | 3.7 | 3.78 | 3.75 | 3.78 | 3.81 | 3.73 |
| 318 | 11.13 | 11.16 | 11.11 | 11.15 | 11.05 | 11.14 | 11.18 | 11.16 | 11.13 |
| 319 | 10.74 | 10.71 | 10.53 | 10.69 | 10.68 | 10.66 | 10.58 | 10.65 | 10.64 |
| 320 | -0.49 | -0.52 | -0.64 | -0.66 | -0.49 | -0.75 | -0.55 | -0.51 | -0.39 |

Table A3. Example of DTS temperature data collected at Site #3 on July 5, 2012.

| Distance | 00:10 | 00:30 | 00:50 | '01:10 | 01:30 | 01:50 | 02:10 | 02:30 | 02:50 |
|---|---|---|---|---|---|---|---|---|---|
| 1 | 0.27 | 0.27 | 0.27 | 0.27 | 0.27 | 0.27 | 0.27 | 0.27 | 0.27 |
| 2 | 1.0146 | 1.0146 | 1.0146 | 1.0146 | 1.0146 | 1.0146 | 1.0146 | 1.0146 | 1.0146 |
| 3 | 18.27 | 17.99 | 17.69 | 17.33 | 17.1 | 16.85 | 16.59 | 16.33 | 16.33 |
| 4 | 17.77 | 17.5 | 17.19 | 16.85 | 16.64 | 16.3 | 16.2 | 15.94 | 15.94 |
| 5 | 16.25 | 15.92 | 15.77 | 15.54 | 15.23 | 14.73 | 14.83 | 14.54 | 14.54 |
| 6 | 14.84 | 14.46 | 14.37 | 14.1 | 13.76 | 13.3 | 13.36 | 13.15 | 13.15 |
| 7 | 14.03 | 13.55 | 13.45 | 13.21 | 12.92 | 12.57 | 12.52 | 12.32 | 12.32 |
| 8 | 14.25 | 13.95 | 13.79 | 13.65 | 13.3 | 13.15 | 13.01 | 12.79 | 12.79 |
| 9 | 14.43 | 14.21 | 14.1 | 14.01 | 13.67 | 13.52 | 13.35 | 13.26 | 13.26 |
| 10 | 14.3 | 14.11 | 13.97 | 13.85 | 13.57 | 13.51 | 13.37 | 13.24 | 13.24 |
| 11 | 14.28 | 14.17 | 13.94 | 13.83 | 13.63 | 13.57 | 13.36 | 13.29 | 13.29 |
| 12 | 14.36 | 14.12 | 14.03 | 13.9 | 13.76 | 13.73 | 13.46 | 13.38 | 13.38 |
| 13 | 14.45 | 14.17 | 14.09 | 13.99 | 13.78 | 13.82 | 13.58 | 13.46 | 13.46 |
| 14 | 14.44 | 14.26 | 14.03 | 13.97 | 13.73 | 13.7 | 13.62 | 13.4 | 13.4 |
| 15 | 14.38 | 14.22 | 14.03 | 13.87 | 13.8 | 13.58 | 13.57 | 13.46 | 13.46 |
| 16 | 14.4 | 14.25 | 14.06 | 13.88 | 13.82 | 13.71 | 13.5 | 13.48 | 13.48 |
| 17 | 14.36 | 14.19 | 14.07 | 13.88 | 13.75 | 13.74 | 13.56 | 13.36 | 13.36 |
| 18 | 14.34 | 14.19 | 14.02 | 13.82 | 13.82 | 13.76 | 13.55 | 13.41 | 13.41 |
| 19 | 14.42 | 14.17 | 13.96 | 13.85 | 13.85 | 13.71 | 13.45 | 13.32 | 13.32 |
| 20 | 14.32 | 14.1 | 13.96 | 13.86 | 13.78 | 13.74 | 13.49 | 13.32 | 13.32 |
| 21 | 14.24 | 14.15 | 14.01 | 13.92 | 13.64 | 13.64 | 13.59 | 13.36 | 13.36 |
| 22 | 14.29 | 14.18 | 14.05 | 14 | 13.65 | 13.66 | 13.49 | 13.37 | 13.37 |
| 23 | 14.32 | 14.19 | 14 | 14.04 | 13.67 | 13.62 | 13.46 | 13.33 | 13.33 |
| 24 | 14.3 | 14.22 | 14.07 | 14.01 | 13.76 | 13.65 | 13.54 | 13.31 | 13.31 |
| 25 | 14.42 | 14.28 | 14.07 | 14.03 | 13.95 | 13.76 | 13.71 | 13.48 | 13.48 |
| 26 | 14.43 | 14.25 | 14.06 | 14.03 | 13.89 | 13.72 | 13.74 | 13.46 | 13.46 |
| 27 | 14.51 | 14.32 | 14.1 | 14.04 | 13.93 | 13.79 | 13.75 | 13.48 | 13.48 |
| 28 | 14.47 | 14.35 | 14.14 | 14.07 | 13.96 | 13.75 | 13.69 | 13.55 | 13.55 |
| 29 | 14.42 | 14.25 | 14.1 | 14.01 | 13.89 | 13.75 | 13.65 | 13.55 | 13.55 |
| 30 | 14.43 | 14.28 | 14.13 | 13.96 | 13.84 | 13.73 | 13.62 | 13.44 | 13.44 |
| 31 | 14.45 | 14.32 | 14.15 | 13.95 | 13.92 | 13.72 | 13.58 | 13.44 | 13.44 |
| 32 | 14.51 | 14.35 | 14.09 | 14.06 | 13.91 | 13.82 | 13.59 | 13.54 | 13.54 |
| 33 | 14.49 | 14.36 | 14.12 | 14.09 | 13.98 | 13.76 | 13.61 | 13.54 | 13.54 |
| 34 | 14.46 | 14.39 | 14.21 | 14.11 | 13.93 | 13.78 | 13.7 | 13.64 | 13.64 |
| 35 | 14.5 | 14.35 | 14.2 | 14.1 | 13.98 | 13.91 | 13.8 | 13.64 | 13.64 |
| 36 | 14.46 | 14.34 | 14.16 | 14.11 | 13.95 | 13.92 | 13.77 | 13.66 | 13.66 |
| 37 | 14.46 | 14.33 | 14.29 | 14.13 | 13.89 | 13.95 | 13.77 | 13.68 | 13.68 |
| 38 | 14.5 | 14.41 | 14.31 | 14.21 | 13.9 | 13.97 | 13.83 | 13.64 | 13.64 |
| 39 | 14.58 | 14.42 | 14.32 | 14.23 | 14.02 | 14.06 | 13.88 | 13.73 | 13.73 |
| 40 | 14.53 | 14.33 | 14.23 | 14.15 | 14 | 13.96 | 13.71 | 13.71 | 13.71 |

Table A3 continued.

| Distance | 00:10 | 00:30 | 00:50 | '01:10 | 01:30 | 01:50 | 02:10 | 02:30 | 02:50 |
|---|---|---|---|---|---|---|---|---|---|
| 41 | 14.55 | 14.33 | 14.23 | 14.08 | 14 | 13.94 | 13.76 | 13.64 | 13.64 |
| 42 | 14.52 | 14.41 | 14.23 | 14.15 | 14.02 | 14.06 | 13.79 | 13.63 | 13.63 |
| 43 | 14.55 | 14.42 | 14.31 | 14.32 | 14.08 | 14.06 | 13.87 | 13.69 | 13.69 |
| 44 | 14.67 | 14.4 | 14.35 | 14.34 | 14.19 | 14 | 13.92 | 13.67 | 13.67 |
| 45 | 14.68 | 14.45 | 14.27 | 14.34 | 14.03 | 13.99 | 13.91 | 13.67 | 13.67 |
| 46 | 14.72 | 14.45 | 14.33 | 14.27 | 14.08 | 14.01 | 13.87 | 13.76 | 13.76 |
| 47 | 14.69 | 14.48 | 14.45 | 14.24 | 14.1 | 14.02 | 13.87 | 13.76 | 13.76 |
| 48 | 14.62 | 14.5 | 14.35 | 14.2 | 14.06 | 13.97 | 13.81 | 13.66 | 13.66 |
| 49 | 14.6 | 14.5 | 14.38 | 14.23 | 14.06 | 13.98 | 13.86 | 13.67 | 13.67 |
| 50 | 14.69 | 14.52 | 14.4 | 14.32 | 14.09 | 14.06 | 13.93 | 13.74 | 13.74 |
| 51 | 14.67 | 14.31 | 14.29 | 14.25 | 13.99 | 13.89 | 13.79 | 13.67 | 13.67 |
| 52 | 14.97 | 14.5 | 14.59 | 14.44 | 14.15 | 14.07 | 14 | 13.82 | 13.82 |
| 53 | 15.38 | 14.95 | 15.05 | 14.85 | 14.52 | 14.54 | 14.49 | 14.35 | 14.35 |
| 54 | 15.57 | 15.23 | 15.25 | 15.06 | 14.91 | 14.95 | 14.81 | 14.76 | 14.76 |
| 55 | 15.52 | 15.43 | 15.3 | 15.26 | 15.14 | 15.13 | 15.03 | 14.97 | 14.97 |
| 56 | 15.34 | 15.23 | 15.02 | 15.06 | 14.91 | 14.85 | 14.76 | 14.74 | 14.74 |
| 57 | 15.23 | 15.13 | 15.03 | 14.99 | 14.75 | 14.85 | 14.7 | 14.63 | 14.63 |
| 58 | 15.19 | 15.02 | 14.98 | 14.87 | 14.72 | 14.8 | 14.77 | 14.54 | 14.54 |
| 59 | 15 | 15.01 | 14.81 | 14.74 | 14.72 | 14.77 | 14.72 | 14.49 | 14.49 |
| 60 | 14.99 | 14.99 | 14.64 | 14.78 | 14.77 | 14.74 | 14.69 | 14.58 | 14.58 |
| 61 | 14.99 | 14.84 | 14.71 | 14.7 | 14.67 | 14.67 | 14.65 | 14.46 | 14.46 |
| 62 | 14.92 | 14.74 | 14.83 | 14.7 | 14.69 | 14.7 | 14.72 | 14.42 | 14.42 |
| 63 | 14.9 | 14.74 | 14.9 | 14.75 | 14.74 | 14.78 | 14.64 | 14.59 | 14.59 |
| 64 | 14.97 | 14.81 | 14.83 | 14.78 | 14.76 | 14.78 | 14.64 | 14.62 | 14.62 |
| 65 | 14.89 | 14.75 | 14.77 | 14.67 | 14.66 | 14.67 | 14.62 | 14.57 | 14.57 |
| 66 | 14.61 | 14.67 | 14.61 | 14.57 | 14.47 | 14.53 | 14.49 | 14.33 | 14.33 |
| 67 | 14.46 | 14.42 | 14.37 | 14.46 | 14.31 | 14.35 | 14.36 | 14.2 | 14.2 |
| 68 | 14.36 | 14.21 | 14.22 | 14.26 | 14.16 | 14.15 | 14.21 | 14.11 | 14.11 |
| 69 | 14.31 | 14.23 | 14.26 | 14.25 | 14.15 | 14.28 | 14.18 | 14.13 | 14.13 |
| 70 | 14.37 | 14.32 | 14.34 | 14.29 | 14.33 | 14.38 | 14.22 | 14.2 | 14.2 |
| 71 | 14.53 | 14.35 | 14.41 | 14.33 | 14.38 | 14.3 | 14.32 | 14.23 | 14.23 |
| 72 | 14.57 | 14.4 | 14.46 | 14.45 | 14.3 | 14.36 | 14.3 | 14.28 | 14.28 |
| 73 | 14.47 | 14.29 | 14.34 | 14.29 | 14.2 | 14.22 | 14.22 | 14.17 | 14.17 |
| 74 | 14.46 | 14.3 | 14.3 | 14.28 | 14.22 | 14.24 | 14.23 | 14.09 | 14.09 |
| 75 | 14.47 | 14.39 | 14.27 | 14.34 | 14.28 | 14.3 | 14.36 | 14.07 | 14.07 |
| 76 | 14.51 | 14.46 | 14.45 | 14.42 | 14.33 | 14.41 | 14.37 | 14.24 | 14.24 |
| 77 | 14.41 | 14.33 | 14.43 | 14.33 | 14.23 | 14.37 | 14.22 | 14.24 | 14.24 |
| 78 | 14.44 | 14.42 | 14.43 | 14.3 | 14.33 | 14.33 | 14.24 | 14.27 | 14.27 |
| 79 | 14.68 | 14.65 | 14.61 | 14.5 | 14.55 | 14.51 | 14.47 | 14.37 | 14.37 |
| 80 | 14.66 | 14.67 | 14.62 | 14.56 | 14.58 | 14.55 | 14.52 | 14.45 | 14.45 |

Table A3 continued.

| Distance | 00:10 | 00:30 | 00:50 | '01:10 | 01:30 | 01:50 | 02:10 | 02:30 | 02:50 |
|---|---|---|---|---|---|---|---|---|---|
| 81 | 14.75 | 14.67 | 14.71 | 14.6 | 14.68 | 14.72 | 14.6 | 14.61 | 14.61 |
| 82 | 14.8 | 14.74 | 14.72 | 14.74 | 14.73 | 14.71 | 14.73 | 14.6 | 14.6 |
| 83 | 14.9 | 14.85 | 14.78 | 14.78 | 14.87 | 14.7 | 14.77 | 14.68 | 14.68 |
| 84 | 14.92 | 14.84 | 14.74 | 14.74 | 14.78 | 14.71 | 14.7 | 14.66 | 14.66 |
| 85 | 14.66 | 14.56 | 14.52 | 14.56 | 14.53 | 14.47 | 14.58 | 14.45 | 14.45 |
| 86 | 14.4 | 14.32 | 14.42 | 14.34 | 14.42 | 14.29 | 14.33 | 14.26 | 14.26 |
| 87 | 14.36 | 14.23 | 14.2 | 14.13 | 14.23 | 14.2 | 14.1 | 14.16 | 14.16 |
| 88 | 14.27 | 14.19 | 14.1 | 14.06 | 14.11 | 14.19 | 14.01 | 14.03 | 14.03 |
| 89 | 14.43 | 14.41 | 14.32 | 14.3 | 14.32 | 14.44 | 14.28 | 14.25 | 14.25 |
| 90 | 14.7 | 14.7 | 14.64 | 14.63 | 14.53 | 14.71 | 14.51 | 14.47 | 14.47 |
| 91 | 14.83 | 14.85 | 14.73 | 14.75 | 14.48 | 14.69 | 14.61 | 14.52 | 14.52 |
| 92 | 14.78 | 14.65 | 14.58 | 14.63 | 14.5 | 14.65 | 14.6 | 14.49 | 14.49 |
| 93 | 14.78 | 14.67 | 14.6 | 14.69 | 14.58 | 14.74 | 14.59 | 14.56 | 14.56 |
| 94 | 14.92 | 14.87 | 14.86 | 14.85 | 14.76 | 14.85 | 14.73 | 14.7 | 14.7 |
| 95 | 14.95 | 14.81 | 14.81 | 14.84 | 14.73 | 14.87 | 14.7 | 14.66 | 14.66 |
| 96 | 14.84 | 14.77 | 14.77 | 14.63 | 14.63 | 14.69 | 14.68 | 14.68 | 14.68 |
| 97 | 14.88 | 14.97 | 14.83 | 14.71 | 14.69 | 14.81 | 14.72 | 14.73 | 14.73 |
| 98 | 15.1 | 15.01 | 14.97 | 14.9 | 14.87 | 14.92 | 14.83 | 14.85 | 14.85 |
| 99 | 15.16 | 15.11 | 14.98 | 14.94 | 14.96 | 14.95 | 14.89 | 14.91 | 14.91 |
| 100 | 15.11 | 15.01 | 14.91 | 14.92 | 14.91 | 14.92 | 14.87 | 14.72 | 14.72 |
| 101 | 14.93 | 15.01 | 14.89 | 14.82 | 14.8 | 14.8 | 14.78 | 14.61 | 14.61 |
| 102 | 14.84 | 14.9 | 14.76 | 14.76 | 14.67 | 14.78 | 14.69 | 14.63 | 14.63 |
| 103 | 14.74 | 14.75 | 14.65 | 14.67 | 14.54 | 14.65 | 14.54 | 14.52 | 14.52 |
| 104 | 14.62 | 14.6 | 14.57 | 14.51 | 14.48 | 14.46 | 14.35 | 14.33 | 14.33 |
| 105 | 14.62 | 14.59 | 14.55 | 14.55 | 14.52 | 14.51 | 14.38 | 14.31 | 14.31 |
| 106 | 14.64 | 14.63 | 14.51 | 14.58 | 14.46 | 14.56 | 14.43 | 14.43 | 14.43 |
| 107 | 14.68 | 14.7 | 14.63 | 14.65 | 14.52 | 14.61 | 14.57 | 14.59 | 14.59 |
| 108 | 14.8 | 14.72 | 14.81 | 14.74 | 14.65 | 14.75 | 14.67 | 14.59 | 14.59 |
| 109 | 14.86 | 14.73 | 14.78 | 14.68 | 14.63 | 14.8 | 14.71 | 14.55 | 14.55 |
| 110 | 14.83 | 14.71 | 14.74 | 14.84 | 14.65 | 14.76 | 14.59 | 14.56 | 14.56 |
| 111 | 14.79 | 14.72 | 14.69 | 14.76 | 14.7 | 14.7 | 14.64 | 14.6 | 14.6 |
| 112 | 14.78 | 14.75 | 14.66 | 14.61 | 14.7 | 14.69 | 14.57 | 14.59 | 14.59 |
| 113 | 14.76 | 14.75 | 14.64 | 14.58 | 14.62 | 14.64 | 14.48 | 14.49 | 14.49 |
| 114 | 14.48 | 14.48 | 14.45 | 14.39 | 14.35 | 14.42 | 14.3 | 14.28 | 14.28 |
| 115 | 14.29 | 14.31 | 14.34 | 14.35 | 14.31 | 14.28 | 14.19 | 14.17 | 14.17 |
| 116 | 14.38 | 14.29 | 14.34 | 14.35 | 14.29 | 14.32 | 14.26 | 14.25 | 14.25 |
| 117 | 14.45 | 14.35 | 14.46 | 14.44 | 14.31 | 14.41 | 14.3 | 14.27 | 14.27 |
| 118 | 14.57 | 14.42 | 14.45 | 14.46 | 14.41 | 14.48 | 14.32 | 14.23 | 14.23 |
| 119 | 14.65 | 14.58 | 14.5 | 14.51 | 14.46 | 14.45 | 14.29 | 14.22 | 14.22 |
| 120 | 14.86 | 14.64 | 14.6 | 14.62 | 14.58 | 14.6 | 14.51 | 14.48 | 14.48 |

Table A3 continued.

| Distance | 00:10 | 00:30 | 00:50 | '01:10 | 01:30 | 01:50 | 02:10 | 02:30 | 02:50 |
|---|---|---|---|---|---|---|---|---|---|
| 121 | 14.98 | 14.83 | 14.78 | 14.81 | 14.72 | 14.81 | 14.83 | 14.56 | 14.56 |
| 122 | 15.11 | 15.06 | 14.9 | 15 | 14.87 | 14.9 | 14.86 | 14.71 | 14.71 |
| 123 | 15.05 | 15.11 | 14.96 | 14.97 | 14.93 | 14.93 | 14.86 | 14.7 | 14.7 |
| 124 | 15.03 | 15.03 | 14.93 | 14.9 | 14.83 | 14.8 | 14.8 | 14.67 | 14.67 |
| 125 | 14.92 | 14.92 | 14.85 | 14.79 | 14.74 | 14.84 | 14.65 | 14.6 | 14.6 |
| 126 | 14.79 | 14.83 | 14.65 | 14.68 | 14.64 | 14.67 | 14.59 | 14.62 | 14.62 |
| 127 | 14.75 | 14.72 | 14.69 | 14.75 | 14.54 | 14.56 | 14.58 | 14.45 | 14.45 |
| 128 | 14.73 | 14.52 | 14.6 | 14.56 | 14.46 | 14.51 | 14.51 | 14.34 | 14.34 |
| 129 | 14.58 | 14.44 | 14.48 | 14.3 | 14.4 | 14.39 | 14.42 | 14.34 | 14.34 |
| 130 | 14.45 | 14.38 | 14.42 | 14.32 | 14.33 | 14.37 | 14.34 | 14.18 | 14.18 |
| 131 | 14.35 | 14.29 | 14.29 | 14.26 | 14.15 | 14.27 | 14.16 | 14.03 | 14.03 |
| 132 | 14.2 | 14.25 | 14.16 | 14.22 | 14.03 | 14.19 | 14.04 | 13.97 | 13.97 |
| 133 | 14.15 | 14.09 | 14.02 | 14.13 | 13.96 | 14.03 | 13.97 | 13.85 | 13.85 |
| 134 | 13.97 | 13.93 | 13.85 | 13.89 | 13.76 | 13.84 | 13.78 | 13.66 | 13.66 |
| 135 | 14.01 | 13.97 | 13.95 | 13.9 | 13.82 | 13.93 | 13.87 | 13.77 | 13.77 |
| 136 | 14.25 | 14.17 | 14.21 | 14.13 | 14.09 | 14.14 | 14 | 14.03 | 14.03 |
| 137 | 14.17 | 14.18 | 14.09 | 14.13 | 14.11 | 14.16 | 14.02 | 14.03 | 14.03 |
| 138 | 14.03 | 14.06 | 13.89 | 14.11 | 14.06 | 14.04 | 13.9 | 13.87 | 13.87 |
| 139 | 14.12 | 14.14 | 13.94 | 14.08 | 14.06 | 14.01 | 13.87 | 13.83 | 13.83 |
| 140 | 14.17 | 14.17 | 14.15 | 14.14 | 14.02 | 13.96 | 13.98 | 14.03 | 14.03 |
| 141 | 14.24 | 14.18 | 14.19 | 14.25 | 14.09 | 14.12 | 14.11 | 13.99 | 13.99 |
| 142 | 14.3 | 14.27 | 14.29 | 14.27 | 14.25 | 14.18 | 14.14 | 13.96 | 13.96 |
| 143 | 14.46 | 14.46 | 14.41 | 14.38 | 14.34 | 14.32 | 14.3 | 14.17 | 14.17 |
| 144 | 14.56 | 14.5 | 14.41 | 14.43 | 14.4 | 14.38 | 14.39 | 14.27 | 14.27 |
| 145 | 14.62 | 14.54 | 14.48 | 14.51 | 14.45 | 14.53 | 14.4 | 14.36 | 14.36 |
| 146 | 14.72 | 14.72 | 14.59 | 14.6 | 14.51 | 14.67 | 14.45 | 14.39 | 14.39 |
| 147 | 14.55 | 14.61 | 14.47 | 14.54 | 14.43 | 14.48 | 14.37 | 14.31 | 14.31 |
| 148 | 14.28 | 14.22 | 14.21 | 14.22 | 14.19 | 14.1 | 14.11 | 14.06 | 14.06 |
| 149 | 14.12 | 14.05 | 14.07 | 13.97 | 14 | 14.04 | 14.01 | 13.97 | 13.97 |
| 150 | 14.07 | 14.08 | 14.08 | 14 | 13.94 | 14.15 | 13.95 | 13.95 | 13.95 |
| 151 | 14.08 | 14.1 | 14.04 | 14.04 | 14 | 14.04 | 13.98 | 13.9 | 13.9 |
| 152 | 14.08 | 14.01 | 13.99 | 13.95 | 13.93 | 13.95 | 13.91 | 13.85 | 13.85 |
| 153 | 14.24 | 14.11 | 14.22 | 14.12 | 14.11 | 14.07 | 14.02 | 13.9 | 13.9 |
| 154 | 14.28 | 14.26 | 14.2 | 14.19 | 14.14 | 14.13 | 14.04 | 13.93 | 13.93 |
| 155 | 14.26 | 14.19 | 14.1 | 14.2 | 14.21 | 14.16 | 14.08 | 14.02 | 14.02 |
| 156 | 14.34 | 14.2 | 14.14 | 14.18 | 14.2 | 14.16 | 14.11 | 14.07 | 14.07 |
| 157 | 14.33 | 14.25 | 14.16 | 14.21 | 14.24 | 14.19 | 14.14 | 14.13 | 14.13 |
| 158 | 14.46 | 14.45 | 14.35 | 14.31 | 14.28 | 14.29 | 14.26 | 14.22 | 14.22 |
| 159 | 14.29 | 14.23 | 14.26 | 14.25 | 14.03 | 14.17 | 14.06 | 14.09 | 14.09 |
| 160 | 14.16 | 14.12 | 14.16 | 14.2 | 13.98 | 14.09 | 14.06 | 13.98 | 13.98 |

Table A3 continued.

| Distance | 00:10 | 00:30 | 00:50 | '01:10 | 01:30 | 01:50 | 02:10 | 02:30 | 02:50 |
|---|---|---|---|---|---|---|---|---|---|
| 161 | 14.32 | 14.21 | 14.23 | 14.26 | 14.16 | 14.1 | 14.21 | 14.14 | 14.14 |
| 162 | 14.08 | 14.17 | 14.02 | 14.09 | 13.88 | 13.97 | 14.05 | 13.95 | 13.95 |
| 163 | 13.51 | 13.6 | 13.47 | 13.52 | 13.37 | 13.55 | 13.49 | 13.32 | 13.32 |
| 164 | 13.29 | 13.3 | 13.24 | 13.28 | 13.24 | 13.29 | 13.17 | 13.16 | 13.16 |
| 165 | 13.61 | 13.46 | 13.48 | 13.42 | 13.43 | 13.53 | 13.5 | 13.37 | 13.37 |
| 166 | 13.92 | 13.77 | 13.7 | 13.67 | 13.64 | 13.79 | 13.73 | 13.56 | 13.56 |
| 167 | 13.64 | 13.55 | 13.55 | 13.57 | 13.59 | 13.59 | 13.52 | 13.44 | 13.44 |
| 168 | 13.52 | 13.42 | 13.4 | 13.44 | 13.44 | 13.42 | 13.34 | 13.35 | 13.35 |
| 169 | 13.67 | 13.57 | 13.59 | 13.57 | 13.52 | 13.57 | 13.53 | 13.56 | 13.56 |
| 170 | 13.89 | 13.79 | 13.77 | 13.75 | 13.78 | 13.74 | 13.73 | 13.72 | 13.72 |
| 171 | 13.92 | 13.84 | 13.91 | 13.78 | 13.76 | 13.81 | 13.72 | 13.67 | 13.67 |
| 172 | 13.85 | 13.87 | 13.84 | 13.78 | 13.79 | 13.8 | 13.6 | 13.68 | 13.68 |
| 173 | 14.1 | 14.15 | 14.05 | 14.08 | 14.01 | 14.02 | 13.85 | 13.92 | 13.92 |
| 174 | 14.35 | 14.32 | 14.09 | 14.21 | 14.14 | 14.14 | 14.03 | 13.97 | 13.97 |
| 175 | 14.45 | 14.38 | 14.33 | 14.33 | 14.25 | 14.31 | 14.16 | 14.01 | 14.01 |
| 176 | 14.44 | 14.38 | 14.37 | 14.43 | 14.32 | 14.32 | 14.25 | 14.19 | 14.19 |
| 177 | 14.53 | 14.48 | 14.36 | 14.39 | 14.28 | 14.29 | 14.32 | 14.23 | 14.23 |
| 178 | 14.46 | 14.47 | 14.37 | 14.38 | 14.25 | 14.25 | 14.21 | 14.2 | 14.2 |
| 179 | 14.5 | 14.38 | 14.34 | 14.39 | 14.28 | 14.24 | 14.23 | 14.22 | 14.22 |
| 180 | 14.52 | 14.4 | 14.33 | 14.31 | 14.25 | 14.36 | 14.21 | 14.22 | 14.22 |
| 181 | 14.57 | 14.55 | 14.48 | 14.5 | 14.31 | 14.48 | 14.4 | 14.17 | 14.17 |
| 182 | 14.54 | 14.5 | 14.49 | 14.46 | 14.36 | 14.49 | 14.42 | 14.19 | 14.19 |
| 183 | 14.46 | 14.5 | 14.42 | 14.43 | 14.3 | 14.44 | 14.36 | 14.29 | 14.29 |
| 184 | 14.61 | 14.57 | 14.5 | 14.49 | 14.44 | 14.53 | 14.5 | 14.42 | 14.42 |
| 185 | 14.68 | 14.7 | 14.61 | 14.52 | 14.43 | 14.61 | 14.6 | 14.34 | 14.34 |
| 186 | 14.61 | 14.58 | 14.53 | 14.52 | 14.36 | 14.54 | 14.5 | 14.28 | 14.28 |
| 187 | 14.79 | 14.61 | 14.63 | 14.63 | 14.55 | 14.67 | 14.54 | 14.54 | 14.54 |
| 188 | 15.07 | 14.9 | 14.92 | 14.94 | 14.9 | 14.94 | 14.9 | 14.88 | 14.88 |
| 189 | 15.14 | 15.06 | 15.05 | 15.09 | 15.09 | 15 | 15.03 | 14.92 | 14.92 |
| 190 | 14.88 | 14.8 | 14.85 | 14.86 | 14.77 | 14.8 | 14.69 | 14.64 | 14.64 |
| 191 | 14.63 | 14.59 | 14.6 | 14.63 | 14.56 | 14.59 | 14.54 | 14.43 | 14.43 |
| 192 | 14.71 | 14.66 | 14.7 | 14.64 | 14.55 | 14.63 | 14.66 | 14.42 | 14.42 |
| 193 | 14.61 | 14.59 | 14.62 | 14.55 | 14.44 | 14.47 | 14.55 | 14.32 | 14.32 |
| 194 | 14.46 | 14.53 | 14.42 | 14.43 | 14.36 | 14.43 | 14.39 | 14.2 | 14.2 |
| 195 | 14.4 | 14.47 | 14.33 | 14.28 | 14.29 | 14.33 | 14.28 | 14.13 | 14.13 |
| 196 | 14.49 | 14.46 | 14.33 | 14.35 | 14.23 | 14.37 | 14.24 | 14.17 | 14.17 |
| 197 | 14.61 | 14.56 | 14.47 | 14.42 | 14.37 | 14.43 | 14.32 | 14.21 | 14.21 |
| 198 | 14.58 | 14.43 | 14.36 | 14.4 | 14.33 | 14.36 | 14.32 | 14.25 | 14.25 |
| 199 | 14.69 | 14.58 | 14.49 | 14.54 | 14.41 | 14.55 | 14.47 | 14.44 | 14.44 |
| 200 | 14.79 | 14.77 | 14.71 | 14.61 | 14.52 | 14.58 | 14.58 | 14.48 | 14.48 |

Table A3 continued.

| Distance | 00:10 | 00:30 | 00:50 | 01:10 | 01:30 | 01:50 | 02:10 | 02:30 | 02:50 |
|---|---|---|---|---|---|---|---|---|---|
| 201 | 14.77 | 14.71 | 14.74 | 14.65 | 14.62 | 14.54 | 14.67 | 14.41 | 14.41 |
| 202 | 14.78 | 14.65 | 14.63 | 14.57 | 14.63 | 14.54 | 14.55 | 14.4 | 14.4 |
| 203 | 14.78 | 14.64 | 14.64 | 14.56 | 14.47 | 14.52 | 14.49 | 14.49 | 14.49 |
| 204 | 14.82 | 14.7 | 14.65 | 14.64 | 14.52 | 14.63 | 14.56 | 14.47 | 14.47 |
| 205 | 14.74 | 14.7 | 14.64 | 14.58 | 14.5 | 14.64 | 14.56 | 14.45 | 14.45 |
| 206 | 14.8 | 14.61 | 14.66 | 14.59 | 14.53 | 14.6 | 14.58 | 14.48 | 14.48 |
| 207 | 14.9 | 14.77 | 14.74 | 14.75 | 14.65 | 14.69 | 14.65 | 14.58 | 14.58 |
| 208 | 14.99 | 14.88 | 14.9 | 14.84 | 14.73 | 14.81 | 14.74 | 14.67 | 14.67 |
| 209 | 15.02 | 14.99 | 14.94 | 14.88 | 14.82 | 14.9 | 14.8 | 14.76 | 14.76 |
| 210 | 15.01 | 15.04 | 14.9 | 14.89 | 14.8 | 14.88 | 14.85 | 14.77 | 14.77 |
| 211 | 15.06 | 15 | 14.95 | 14.96 | 14.89 | 14.89 | 14.88 | 14.74 | 14.74 |
| 212 | 15 | 14.98 | 14.95 | 14.95 | 14.91 | 14.88 | 14.89 | 14.78 | 14.78 |
| 213 | 15.01 | 14.97 | 14.91 | 14.92 | 14.87 | 14.85 | 14.86 | 14.75 | 14.75 |
| 214 | 15.02 | 14.97 | 15 | 14.87 | 14.88 | 14.9 | 14.84 | 14.74 | 14.74 |
| 215 | 15.15 | 15.02 | 15.08 | 15.01 | 15.02 | 15 | 14.96 | 14.87 | 14.87 |
| 216 | 15.23 | 15.07 | 15.13 | 15.15 | 15.03 | 15.12 | 14.94 | 14.99 | 14.99 |
| 217 | 15.17 | 15.09 | 15.12 | 15.02 | 14.95 | 15.08 | 14.97 | 14.97 | 14.97 |
| 218 | 15.14 | 15 | 14.97 | 14.93 | 14.87 | 15 | 14.92 | 14.9 | 14.9 |
| 219 | 15.16 | 14.87 | 14.91 | 14.99 | 14.88 | 14.93 | 14.89 | 14.92 | 14.92 |
| 220 | 15.04 | 14.87 | 14.97 | 14.97 | 14.98 | 14.9 | 14.83 | 14.83 | 14.83 |
| 221 | 14.81 | 14.72 | 14.75 | 14.69 | 14.72 | 14.69 | 14.61 | 14.59 | 14.59 |
| 222 | 14.57 | 14.54 | 14.48 | 14.48 | 14.45 | 14.48 | 14.46 | 14.37 | 14.37 |
| 223 | 14.51 | 14.46 | 14.46 | 14.47 | 14.46 | 14.46 | 14.37 | 14.4 | 14.4 |
| 224 | 14.41 | 14.39 | 14.44 | 14.37 | 14.36 | 14.42 | 14.32 | 14.24 | 14.24 |
| 225 | 14.33 | 14.31 | 14.29 | 14.26 | 14.18 | 14.29 | 14.19 | 14.08 | 14.08 |
| 226 | 14.18 | 14.17 | 14.11 | 14.09 | 14.02 | 14.19 | 14.05 | 14 | 14 |
| 227 | 14.04 | 13.99 | 13.99 | 13.93 | 13.86 | 14.1 | 13.92 | 13.93 | 13.93 |
| 228 | 13.98 | 13.96 | 13.96 | 13.93 | 13.85 | 14.04 | 13.98 | 13.85 | 13.85 |
| 229 | 13.94 | 13.99 | 13.8 | 13.88 | 13.83 | 13.9 | 13.83 | 13.77 | 13.77 |
| 230 | 13.75 | 13.79 | 13.62 | 13.69 | 13.66 | 13.75 | 13.67 | 13.54 | 13.54 |
| 231 | 13.67 | 13.64 | 13.56 | 13.51 | 13.51 | 13.69 | 13.59 | 13.48 | 13.48 |
| 232 | 13.68 | 13.65 | 13.57 | 13.57 | 13.61 | 13.57 | 13.61 | 13.52 | 13.52 |
| 233 | 13.68 | 13.67 | 13.57 | 13.69 | 13.63 | 13.69 | 13.67 | 13.5 | 13.5 |
| 234 | 13.65 | 13.54 | 13.52 | 13.58 | 13.51 | 13.67 | 13.58 | 13.42 | 13.42 |
| 235 | 13.53 | 13.44 | 13.4 | 13.42 | 13.42 | 13.52 | 13.48 | 13.43 | 13.43 |
| 236 | 13.47 | 13.4 | 13.3 | 13.42 | 13.41 | 13.37 | 13.42 | 13.39 | 13.39 |
| 237 | 13.52 | 13.59 | 13.42 | 13.57 | 13.45 | 13.46 | 13.52 | 13.47 | 13.47 |
| 238 | 13.63 | 13.74 | 13.56 | 13.67 | 13.66 | 13.58 | 13.62 | 13.57 | 13.57 |
| 239 | 13.85 | 13.81 | 13.72 | 13.74 | 13.77 | 13.75 | 13.77 | 13.72 | 13.72 |
| 240 | 13.94 | 13.93 | 13.76 | 13.91 | 13.84 | 13.85 | 13.79 | 13.84 | 13.84 |